SNR Maximizing Linear Filters with Interference Suppression Capabilities for DS-CDMA

Young C. Yoon

Department of Electrical Engineering
McGill University
Montreal, Canada

January 1998

A thesis submitted to the Faculty of the Graduate Studies and Research in partial fulfillment of the requirements for the degree of Doctor of Philosophy

0-612-44637-9

Abstract

This thesis considers the design of receivers for multi-user communication systems based on asynchronous direct-sequence code-division multiple-access (DS-CDMA). Its primary aim is to improve current receiver designs which exhibit shortcomings in systems using long sequence spreading (where the spreading sequence changes with each consecutive bit). The conventional matched filter (MF) and noise-whitening MF (NWMF) receivers incur a degradation in performance under power-imbalance (near-far like) conditions. Similar to that of the conventional MF (CMF), the near-far resistance of the NWMF is shown to be zero. Other receivers, including multi-user receivers, suffer from either incompatibility or excessive complexity under long sequence spreading.

Motivated by the need for low-complexity receivers compatible with long sequence spreading, the thesis investigates the design of linear time-invariant (LTI) filters which maximize the signal-to-noise ratio (SNR) for bit symbol detection. It develops the chip-delay locked MF (CLMF) which requires the knowledge of interferer chip delays and signal powers; knowledge of their spreading sequences is unnecessary. Moreover, it takes advantage of the observation that multiple-access interference (MAI) is generally neither white nor stationary, but cyclostationary. Analysis of the CLMF demonstrates that it can deliver non-zero near-far resistance along with performance beyond that of the CMF and NWMF. Furthermore, the computation of the filter response is required only when an interferer signal parameter changes. The complexity of the computation grows linearly with the number of interferers. In addition, insight and directions are presented for the development of adaptive versions of the CLMF which eliminate the need for interferer signal parameters altogether.

Based on the same approach used to develop the CLMF, the thesis presents a general framework from which other one-shot linear detectors can be derived. With increasing knowledge of interferer signal parameters, this approach can synthesize the NWMF, the one-shot linear minimum mean squared error (MMSE) detector and the one-shot decorrelator. Furthermore, the limiting forms of the NWMF and CLMF in the absence of background additive white Gaussian noise (AWGN) are shown to be, respectively, an inverse chip filter followed by a despreading filter (or correlator) and a decorrelator-type CLMF. The thesis also examines how additional knowledge of interferer phase-offsets, the presence of intersymbol interference (ISI) and the presence of both unlocked and chip-delay locked interferers affect filter design.

Sommaire

Cette thèse porte sur la conception de récepteurs pour les systèmes de communications asynchrones à usagers-multiples utilisant l'accès multiple à répartition par code (AMRC) à séquences directes. Son but principal est d'améliorer la conception des récepteurs actuels possédant les faiblesses inhérantes aux systèmes utilisant de longues séquences pseudo-aléatoires (où l'étalement spectral pour chaque bit consécutif n'est pas fait par la même séquence). Les récepteurs basés sur le filtre adapté conventionel (CMF) et sur le filtre adapté qui rend le bruit blanc (NWMF) ont une dégradation en performance causée par les différences entre les puissances des signaux (le problème proximité-éloignement). Il est démontré que, comme celle du CMF, la résistance au problème proximité-éloignement du NWMF est égale à zéro. Les autres récepteurs, incluant les récepteurs à usagers-multiples, sont soit trop complexes ou incompatibles lorsque de longues séquences sont utilisées.

Motivé par le besoin de récepteurs de faible-complexité compatibles avec de longues séquences, cette thèse étudie la conception des filtres linéaires invariant dans le temps qui maximisent le rapport signal-à-bruit (RSB) pour la détection de bits. Le filtre, qui maximise le RSB avec la connaissance des délais de "chips" et des puissances des signaux des autres usagers, est développé et présenté; la connaissance des séquences pseudo-aléatoires des autres usagers n'est pas nécessaire. Ce filtre, dénommé CLMF, profite du fait que l'interférence d'accès multiple n'est générallement ni blanche ni stationnaire, mais stationnaire-cyclique. L'analyse du CLMF démontre que sa résistance au problème proximité-éloignement peut être différente de zéro et que sa performance est meilleure que celles du CMF et du NWMF. De plus, le calcul de la réponse impulsionnelle du filtre est requis seulement quand l'un des paramètres du signal d'un des autres usagers change. La complexité de ce calcul augmente de façon linéaire avec le nombre d'usagers. Des suggestions et des commentaires fondamentaux utiles pour le développement de versions adaptives du CLMF qui éliminent complètement le besoin des paramètres des signaux des autres usagers sont presentés.

En se basant sur la même approche de développement du CLMF, cette thèse offre un cadre général de travail pour la conception d'autres détecteurs linéaires symbole par symbole. Lorsqu'un plus grand nombre de paramètres de signaux sont connus, il est possible de concevoir par cette méthode le NWMF, le détecteur linéaire symbole par symbole qui minimise le carré de la moyenne de l'erreur et le décorrelateur symbole par symbole. Il est montré que la forme asymptotique du NWMF et du CLMF, en absence de bruit blanc Gaussien additif, deviennent, respectivement, un filtre dont la réponse fréquentielle est l'inverse de celle du chip suivi par un filtre compresseur (ou corrélateur) et un filtre CLMF de type décorrelateur. Cette thèse examine aussi l'impact de la connaissance des phases-relatives des autres usagers, la présence de l'interférence entre-symboles et la présence des autres usagers avec ou sans la connaissance de leurs délais de chips, sur la conception des filtres.

Acknowledgments

My Ph.D. studies were supported by the Natural Sciences and Engineering Research Council of Canada (NSERC), McGill University (the David Stewart Memorial Fellowship) and the Canadian Institute of Telecommunications Research (CITR). I acknowledge with gratitude the financial support of these institutions.

Over the past four years, I have benefited immensely from the careful guidance of Dr. Harry Leib, my Ph.D. supervisor. Dr. Leib gave generously of his time to oversee the progress of my research and thesis. I would like to thank him for his advice, critical insight and constant support.

I also wish to express my appreciation to Dr. Peter Kabal and Dr. Tomas J.F. Pavlasek, members of my Ph.D. committee, for their encouragement, support and kind counsel.

My research has also profited from many discussions with fellow graduate students including Jean-Paul Chaib, Florence Danilo, Marc Kimpe, Rami Mehio, Nader Sheikholeslami, Dr. Jacek Stachurski and other fellow members of the Telecommunications and Signal Processing (TSP) Lab. I thank them for making my experience at McGill enjoyable and memorable.

In closing, I wish to express my gratitude to my wife Jinnie and our respective families and friends for their loving support and encouragement.

Contents

List of Figures

List of Tables

Chapter 1

Introduction

The vision of personal communication services (PCS) is to offer an individual the means to communicate with anyone anywhere anytime. Among the many difficulties imposed by this vision is the challenge of offering to consumers the freedom of untethered mobility through wireless technology. The growing demand for wireless communication services is reflected in the emergence and proliferation of cordless phones, cellular communication services and wireless data services [3].

This thesis is concerned with the study of one particular system for realizing this vision — multi-user communication systems based on direct-sequence code-division multiple-access (DS-CDMA). The first section of this chapter introduces multi-user communication systems and three basic multiple-access techniques. The second section focusses on DS-CDMA. The third section formulates the overall objective of the research while the final section outlines the organization of the thesis.

1.1 Multiple-Access Techniques for Multi-User Wireless Communications

In multi-user communication systems such as the one depicted in Fig. 1.1, many users transmit to a single point over a limited and shared region of spectrum. One example is the uplink of a cellular communication system in which a number of mobile terminals transmit to a common base station receiver. Another is the uplink of a satellite communication system where a number of ground terminals transmit to a common receiver orbiting the earth. The task of multiple-access techniques is to manage the sharing of the spectrum and to enable the separation of users' signals at the receiver.

There are three basic multiple-access techniques: Frequency-Division Multiple-

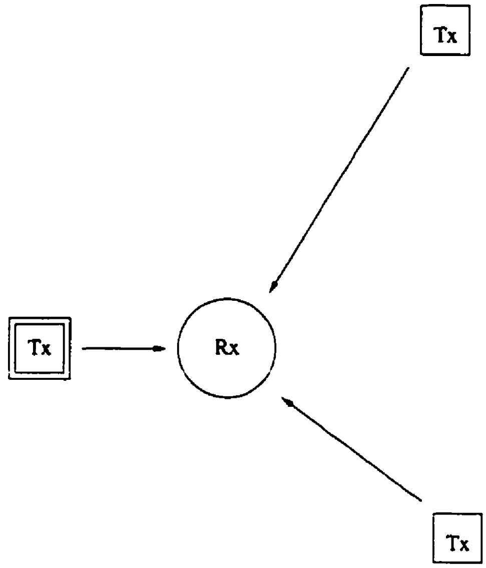

Fig. 1.1 An example of a multiple-access system: the uplink of a cellular communication system.

Access (FDMA), Time-Division Multiple-Access (TDMA) and Code-Division Multiple-Access (CDMA). The organization of the multiple-access techniques is given in Fig. 1.2. The following description of the various techniques proceeds from the top of Fig. 1.2 down towards the subject of the thesis — asynchronous DS-CDMA.

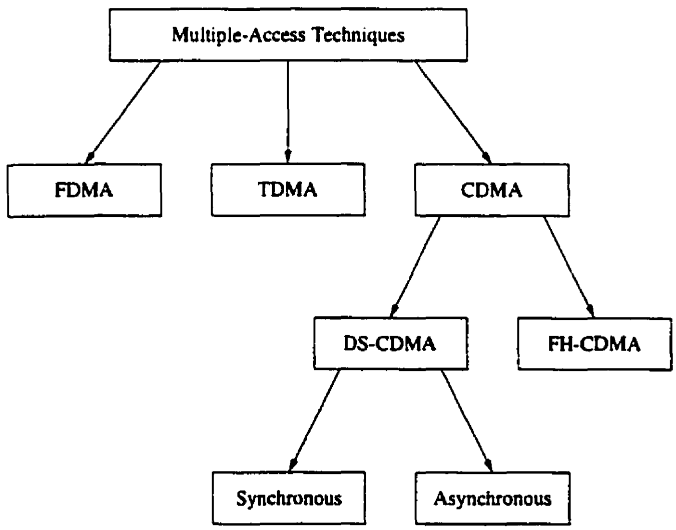

Fig. 1.2 Organization of multiple-access techniques.

In FDMA, the spectrum is partitioned into disjoint frequency bands or frequency slots. Each user is assigned a particular band for signal transmission. An example of an FDMA system is the Advanced Mobile Phone System (AMPS) [4, pp. 483–

491]. In TDMA, each user is assigned, instead, a particular time slot for signal transmission. This requires synchronization among the users to ensure that only a single user transmits while the other users wait in silence for their turn to transmit. In practice, TDMA, is combined with FDMA so that, in effect, a number of users share a particular frequency band through TDMA. An example of a TDMA system is the Global System for Mobile Communication (GSM) originally known as Groupe Speciale Mobile [4, pp. 500–506]. Since the signals of each user are orthogonal (as can be immediately deduced in either the frequency or time domain), FDMA and TDMA are also known as orthogonal multiple-access techniques.

1.1.1 CDMA

In CDMA, known also as spread spectrum multiple-access (SSMA), all users employ the same spectral band. Moreover, CDMA is often referred to as a wideband multiple-access technique since the ratio of the available bandwidth for transmission to the minimum required bandwidth for bit transmission (information bandwidth) can be quite large. In contrast, FDMA and hybrid TDMA/FDMA are often referred to as narrowband multiple-access techniques since the transmission bandwidth is not much larger than the information bandwidth. There are two principal categories of CDMA techniques distinguished according to how the spectrum is utilized: frequency-hopping CDMA (FH-CDMA) and direct-sequence CDMA (DS-CDMA). Since the latter is the subject of the thesis, the description of the former is brief while that of the latter is more detailed.

FH-CDMA

In FH-CDMA, the spectrum is again partitioned into small frequency bands as in FDMA; however, each user is permitted to transmit in any one of the many frequency bands. The users are distinguished by assigning unique frequency hopping patterns to each of the transmitters. These patterns are known to the receiver as well. Further information on FH-CDMA can be found in [5, 6].

DS-CDMA

In DS-CDMA, all users transmit over the entire spectrum simultaneously. As depicted in Fig. 1.3, transmission in DS-CDMA is, in general, accomplished in four stages. Information bits generated at the bit rate are input to a channel encoder to produce a sequence of coded bits. Next, the coded bits are passed through a second stage

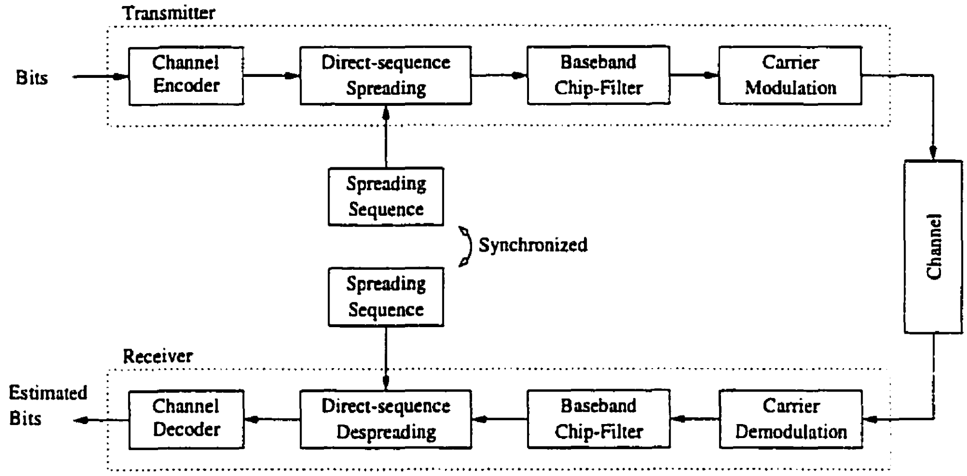

Fig. 1.3 Block diagram of a transmitter and receiver in DS-CDMA.

of encoding referred to as direct-sequence spreading. Each coded bit is encoded (or spread) by a *spreading sequence* which is also referred to as a signature sequence or pseudo-noise (PN) sequence. A spreading sequence consists of elements known as *chips* which are generated at a rate known as the chip rate. Similar to the bit symbols, the chips can be constructed from binary symbols, 0 and 1, which are mapped to -1 and 1, respectively. In contrast, however, the chip rate is typically much higher than the bit rate; the ratio of the chip rate to the bit rate is often loosely referred to as the *processing gain* or *bandwidth expansion factor*. In contrast to FDMA or TDMA where each user is identified by a particular frequency slot or time slot, in DS-CDMA, it is the spreading sequence which identifies and distinguishes each user from other users. Thus, conceptually, the spreading sequence furnishes the addressing capability in DS-CDMA.

DS-CDMA can be further subdivided into either synchronous or asynchronous DS-CDMA as follows.

Synchronous DS-CDMA

In synchronous DS-CDMA, signal transmissions among all users are synchronized. The synchronization of users permits the construction of spreading sequences with zero cross-correlation thereby making the signals of all users orthogonal. This is another example of an orthogonal multiple-access technique.

Asynchronous DS-CDMA

Asynchronous DS-CDMA differs from synchronous DS-CDMA in that signal transmissions among the users are uncoordinated. This removes the difficulty of synchronizing the transmitting instants of remote users. However, this simplification and added flexibility comes at a cost. Since the relative timing of bit symbol transmissions among any two users can change, the orthogonality of users' signals can no longer be guaranteed. Although it is possible to design spreading sequences with low cross-correlations at any relative delay, it is impossible, however, to design spreading sequences that maintain orthogonality over all relative delays [7].

1.2 Asynchronous Direct-Sequence Code-Division Multiple-Access

This section provides a further description of asynchronous DS-CDMA — the subject of this thesis. Henceforth, the term asynchronous shall be dropped and DS-CDMA shall refer to asynchronous DS-CDMA for the remainder of the thesis. First, many important properties associated with DS-CDMA systems are reviewed. Second, a brief overview of several applications based on DS-CDMA is presented along with examples of real systems either in service or under development. And third, methods for resolving the major weakness of DS-CDMA known as the near-far problem are discussed. Further information on the fundamentals of DS-CDMA can be found in the tutorial papers of [5, 7, 8] and the textbooks of [6, 9, 10, 11]. A mathematical description of DS-CDMA systems is presented later in Chapter 2.

1.2.1 Properties of DS-CDMA systems

This section describes a number of important properties associated with DS-CDMA systems. A comprehensive summary of these properties and others of lesser significance can be found in [12].

Improved Capacity

Capacity refers to the number of users that can be accommodated by a multiple-access system. The following discussion on capacity deals with single-cell and multiple-cell (or cellular) communication systems. In the former, all users are located in a confined geographical region known as a *cell* and communicate with a single common point as illustrated in Fig. 1.1. In the latter, the users may be distributed over a large area, divided into a large number of cells, as illustrated in Fig. 1.4 where each hexagon represents a cell [4, pp. 25-30][12]. Users located in a particular cell communicate with the central receiver of that cell.

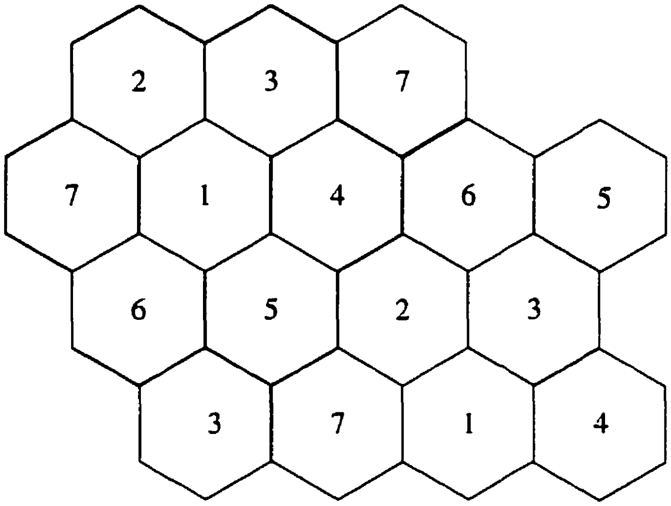

Fig. 1.4 A multiple-cell system employing frequency re-use.

In DS-CDMA, capacity is highly dependent on the application [13]. In single-cell systems, capacity can be markedly less than that of orthogonal multiple-access schemes [7, 14] whose capacity is determined by the number of orthogonal channels (approximately equal to the processing gain of the system [7]). In DS-CDMA systems, capacity may be reduced since users' signals are no longer orthogonal and each user acts as a source of interference to other users. However, the loss in capacity can be recovered depending on the application when other factors such as periods of voice silence in voice services, to be explained later, are taken into consideration.

In multiple-cell systems, DS-CDMA has the potential of delivering a significant increase in capacity [13, 15, 12]. This can be attributed to primarily two properties peculiar to DS-CDMA. These are its ability to exploit periods of voice or transmission silence as mentioned earlier and its frequency re-use factor of 1 to be explained shortly. From a business perspective, increased capacity can translate to a decrease in the number of costly cell sites to be constructed and maintained. Indeed, this is the major reason for the considerable interest in DS-CDMA cellular systems. Situations where DS-CDMA is or is not beneficial in terms of capacity with respect to orthogonal multiple-access schemes are summarized in [13].

Robustness in Multipath Channels

Signals used in DS-CDMA tend to be well suited to cope with multipath channels in which delayed replicas of the originally transmitted signal arrive at the receiver. For example, in an urban environment, the delay between the first signal to arrive and its last replica is typically less than 5 μs [16]. The resolvability of any two paths (or two replicas) is possible as long as the time delay between them exceeds the inverse of the bandwidth of the signals [16]. In FDMA and TDMA/FDMA systems using narrowband signals, the replicas can result in the severe distortion of transmitted signals. For example, in GSM where the signal bandwidth is 200 kHz [4, p. 505], time delay differences less than 5 μs cannot be resolved. On the other hand, in DS-CDMA systems using wideband signals, the effect of delayed replicas can be mitigated. For example, in the cellular DS-CDMA system commonly referred to as *IS-95* [1, 17] [4, pp. 519-533], where the signal bandwidth is 1.25 MHz, time delay differences greater than 0.8 μs can be resolved. Moreover, delayed replicas can be coherently or non-coherently combined by implementing RAKE receivers [16] to improve further the quality of signal reception.

Reduced Network Management

No need to synchronize users

In TDMA and synchronous DS-CDMA systems, signal transmissions among all the users must be rigidly coordinated to maintain orthogonality among users' signals. This incurs a significant overhead in the management of the network to coordinate the signal transmissions of remote users. These difficulties are eliminated in DS-CDMA as well as in FDMA.

No intra-cell frequency coordination

In FDMA where the spectrum is divided into frequency slots, the slot in which each user transmits must be carefully coordinated to prevent two or more users from transmitting over the same slot. In DS-CDMA, such coordination is unnecessary since all users transmit across the entire allocated spectrum.

Uncoordinated Signal Multiplexing

Depending on the application, signal transmissions from a user may be bursty in nature. For example, in voice applications, periods of silence, where signal transmission is unnecessary, occupy more than half the time in a typical telephone conversation [15, p. 305]. In TDMA or FDMA systems, where each time or frequency slot is reserved to a particular user, the silent periods cannot be easily shared with or allocated to other users to increase capacity. In DS-CDMA, however, these periods of silence can be exploited naturally to increase capacity since the users do not reserve any particular frequency slot or time slot and, instead, share the resources. Signal transmissions can be suppressed or transmitted signal powers can be reduced (as in the IS-95 system [1]) to lower the level of MAI perceived by other users. This technique alone can translate into a twofold increase in capacity for cellular voice services [15, p. 305].

No Need for Frequency Re-use

Cellular systems based on FDMA or TDMA/FDMA require *frequency re-use* to prevent or reduce co-channel interference [4, pp. 26-30] [18, pp. 792-794]. Frequency re-use is implemented by partitioning a given spectrum into regions as shown in the example in Fig. 1.5. The regions, numbered from 1 to 7, are assigned to cells in a

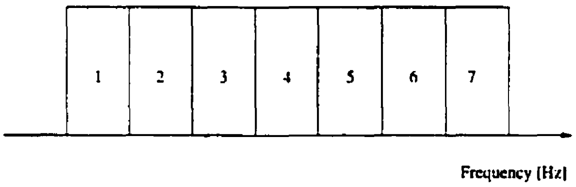

Fig. 1.5 Partitioning of the spectrum for frequency re-use.

manner which maximizes the distance between cells sharing (or re-using) the same frequency bands. This is illustrated in Fig. 1.4. The physical distance separating cells sharing common frequency bands ensures the attenuation of signals from remote users transmitting in the same frequency band. This technique is characterized by the *frequency re-use factor* representing the ratio of the bandwidth used by one cell to the entire bandwidth shared by all cells. In Fig. 1.4, the frequency re-use factor is 1/7 similar to that of AMPS [4, Table 8.3 p. 422]. In GSM, the factor can be either 1/3 or 1/4. The need for frequency re-use in FDMA and TDMA/FDMA cellular systems reduces their spectral efficiency [bits/Hz] and capacity by the frequency re-use factor (compared to their single cell counterpart where the frequency re-use factor is 1). In contrast, in cellular DS-CDMA applications, where all transmissions share the entire spectrum, the frequency re-use factor is 1.

Power-Imbalance Problem

All the properties described so far have highlighted the many attractive features of DS-CDMA. It, however, does possess a serious weakness which occurs under *power-imbalance* conditions. Power-imbalance refers to the situation when the received signal powers among users are non-uniform. For instance, this can occur when transmitted signal powers are uncontrolled. The received signal power of a user physically *near* the receiver can be much stronger than those of other users *far* away from the receiver.

This example is portrayed in Fig. 1.1 where the doubled box represents a strong user whose received signal power is much larger than those of the other two users. Furthermore, even with careful power control, power-imbalance can still occur in certain applications. For instance, in multi-rate (or variable rate) DS-CDMA systems, received signal powers are deliberately disparate and proportional to the bit rate and quality of service desired by each user [19, 20].

As mentioned earlier in section 1.1.1, signal transmissions in DS-CDMA are, in general, not orthogonal. Consequently, the signal of each user represents a source of interference to every other user in the system. In addition, system capacity depends heavily upon on the maximum tolerable level of MAI each user can withstand. Power-imbalance, however, raises the level of MAI to unacceptable levels for many of the users. Thus, it severely degrades the performance of receivers and, ultimately, reduces system capacity. This weakness of DS-CDMA, due to the non-orthogonality of DS-CDMA signals, is referred to as the *power-imbalance problem.*[1] In contrast, in systems using orthogonal multiple-access schemes, power-imbalance has no such effect as long as orthogonality among users' signals is maintained. Methods of resolving this critical problem associated with DS-CDMA systems are considered in section 1.2.3.

1.2.2 DS-CDMA Applications

Applications of DS-CDMA are briefly surveyed to illustrate potential areas where the results of this thesis may be of value. Examples of DS-CDMA systems either in service or in the process of development are mentioned as well.

<u>Second generation cellular communication systems</u>

To support the continued growth of cellular subscribers, DS-CDMA has been applied to mobile cellular communications for voice service as a second generation system to AMPS [3]. This system, commonly referred to as IS-95, has recently begun service in many parts of the world and North America. Its capacity is theoretically ten to twenty times that of AMPS [15, 17]. However, the capacity is critically dependent upon tight power control and other factors [21, 22]. In comparison, GSM [23, p. 52] and the North American TDMA system (IS-54) can roughly support, respectively, three and three (or six) times that of AMPS [23, p. 52]. The larger potential capacity of IS-95 is the primary reason for the great interest in DS-CDMA systems.

[1] With respect to terminology, it is acknowledged that the power-imbalance problem is widely referred to as the *near-far problem*. However, the term power-imbalance is introduced to characterize precisely the source of the problem which, as exemplified by multi-rate DS-CDMA systems, is the non-uniform levels of received signal powers which occurs even under ideal power control.

Fixed wireless systems

DS-CDMA has also been applied to fixed wireless systems as a substitute to fixed wireline local loop access [24, 25, 26]. Compared to mobile cellular systems, fixed wireless systems enjoy a number of advantages [24]. The channels remain relatively static since the users are immobile. The antennas of the fixed users can be perched in high locations to improve the quality of signal reception. Moreover, directional antennas can be installed at the transmitter terminals and receiver stations to improve channel quality and increase frequency re-use. Because of these advantages, the capacity of fixed versions of their mobile counterparts can be increased significantly. For example, under the conditions specified in [24, Table 1], a fixed wireless system based on IS-95 can provide roughly 2.5 times the capacity compared to that of a fixed system based on IS-54 (now known as IS-136) and roughly 5.4 times that of a GSM based system.[2]

Third generation of cellular communication services

Many telecommunication manufacturers are presently engaged in the development of third generation cellular communication systems based on DS-CDMA [27, pp. 422-431]. Compared to the second generation cellular systems, future systems promise greater user capacity, improved quality of speech and the option of data service for wireless multimedia applications. Another distinguishing feature stems from the amount of bandwidth under consideration for spreading. In comparison to the 1.25 MHz used in IS-95, future DS-CDMA cellular systems may utilize bandwidths ranging from 5 to 20 MHz.

A number of competing systems are currently being tested and developed [27, pp. 418-431]. These include the Code-Division Testbed (CODIT) project [28], the coherent multicode DS-CDMA system [29, 30] and the wideband CDMA system standardized as IS-665 for the U.S. PCS frequency bands [31].

Satellite communication systems

DS-CDMA has been applied as a hybrid with frequency hopping to a mobile satellite messaging system known commercially as OmniTRACS [32]. It is also being considered for future mobile satellite communication systems which would enable wireless communication from potentially any location on earth by creating a network of low earth orbit (LEO) satellites [33, 3]. One particular candidate, based on DS-CDMA

[2]Note that differences between the fixed and mobile systems exist [24]. For example, in the fixed version of IS-136, the frequency re-use factor has been lowered from 7 to 4 and its required signal-to-noise ratio (SNR) specification has been lowered from 18 to 14 dB. In addition, in the fixed version of IS-95 system, its required SNR specification has been reduced from 7 to 6 dB.

and known as Globalstar, envisages 48 satellites circling the earth at an altitude of 1400 km [34, 3]. There are several benefits of using DS-CDMA in satellite communications. It offers minimum coordination among active users, the flexibility to service different applications (such as voice, data and mixed traffic), the adaptability for different network configurations, the flexibility to handle variable traffic patterns (providing the option of graceful performance degradation in non-nominal conditions) and the adaptability for different network configurations. Further details can be found in [35].

The potential disadvantage of DS-CDMA in satellite communication systems is its poor spectral efficiency (and, hence, capacity) relative to that of FDMA as pointed out in [14]. However, it has been shown that the conclusion of [14] can be reversed when additional system features are taken into account [32]. These features include the reduction of MAI due to the voice activity factor in voice services and the frequency re-use factor of 1 of DS-CDMA when satellites with multi-beam antennas are used. Multi-beam antennas permit frequency re-use to improve spectral efficiency as in cellular communication systems by separating a satellite coverage area into beamwidths of, for instance, 3°.

1.2.3 Methods for Resolving the Power-Imbalance Problem and Increasing Capacity

As discussed in section 1.2.1, the main obstacle in the design of DS-CDMA systems and in the realization of their full potential in terms of capacity was identified to be the power-imbalance problem. This problem can be countered by three distinct methods which can be used in tandem. One method implements power control to maintain uniform received signal powers among all the users [1, 21]. This method is used in IS-95. However, power control alone may not be able to completely alleviate the power-imbalance problem. For example, in mobile applications where signal powers may fluctuate rapidly, the tracking ability of the power control algorithm is not ideal [21, 22]. Furthermore, in the mixed-rate DS-CDMA systems mentioned earlier, power control simply maintains the different power levels of the users [19, 20] and cannot resolve the power-imbalance problem.

A second method implements spatial filtering with smart antennas to separate the signals of users by their direction of arrival [36]. In this method, by adjusting the beam pattern of the antenna, the signal of a strong user arriving from one particular direction can be attenuated while that of a desired user arriving from another angle can be amplified. The third method considers improving the design of DS-CDMA receivers. Specifically, it examines the design of that portion of the receiver in Fig. 1.3 between the channel decoder and the carrier demodulation stage. The second and third methods are both the subject of current research and development. Moreover, they can improve capacity even in the absence of power-imbalance. This thesis focuses on the third method — the study of improved receiver design — to counter the power-imbalance problem and, ultimately, to improve system capacity whether or not power-imbalance exists.

1.3 Thesis Statement and Contributions

This section presents the thesis statement and contributions of this work. The thesis statement will be expressed mathematically in more precise terms in section 2.3. Part of this work has been previously published in [37, 38].

1.3.1 The Thesis Statement

As explained in the previous section, DS-CDMA possesses a number of advantages over FDMA and TDMA. Its weakness, however, was identified to be the power-imbalance problem which degrades communication performance and user capacity. In an effort to counter the power-imbalance problem and achieve the broader goal of improving user capacity in DS-CDMA, a large number of receivers have been developed over the past decade. These are reviewed in section 2.2. Those receivers which can enhance capacity considerably have two drawbacks. Most have prohibitively large computational complexity per bit symbol detected. And those with low-complexity, place an impractical constraint on the method of direct-sequence spreading. That is, they require short sequence spreading whereby the spreading sequence for each consecutive bit remains fixed for each user. Consequently, they are incompatible with systems such as IS-95 [1] and with nearly all those proposed for the third generation of cellular systems [27, 29, 31] where this constraint is removed [39]. The effect of removing this constraint in the design of DS-CDMA receivers shall be explained in more detail in section 2.2.5.

> Therefore, the primary goal of the thesis is to develop, without the constraint of short sequence spreading, receivers with reasonably low complexity which can enhance DS-CDMA system capacity in either the presence or absence of power-imbalance conditions.

1.3.2 Original Contributions

The contributions of the thesis are stated. First, the thesis derives a receiver, referred to as the chip-delay locked MF (CLMF). The CLMF represents the main contribution of the thesis. It is an LTI filter which maximizes SNR for bit symbol detection, requiring no knowledge of interferer spreading sequences, but only knowledge of interferer chip delays (bit delays modulo one chip period) and signal powers. Its structure is shown to assume a form similar to that of the conventional MF (CMF); the baseband chip filter of the receiver in Fig. 1.3 is replaced by a new chip filter which maximizes SNR for chip symbol detection. Moreover, with respect to implementation, its computational complexity per bit symbol is reasonably low. The computation of its filter response is required only when an interferer parameter changes. The complexity of computation grows linearly with the number of interferers. In addition, since the CLMF can be implemented with or without the constraint of short sequence spreading, it has the desirable feature of being compatible with those systems, such as IS-95, based on long sequence spreading.

Second, the thesis investigates the performance of the CLMF in terms of SNR, near-far resistance, bit error rate (BER), probability of outage and capacity over a multiple-access channel corrupted with AWGN. Improvements in performance delivered by the CLMF, with respect to the CMF and another known as the noise-whitening MF (NWMF), are demonstrated by numerical examples whether or not power-imbalance exists. Third, the thesis provides directions to the design of adaptive versions of the CLMF. Adaptive versions avoid the need for estimates of any interferer signal parameters. And fourth, the thesis presents a unifying framework of SNR maximizing LTI filter receivers for DS-CDMA over several models of signal parameters and the two types of spreading methods. Based on this framework, it is possible to synthesize, not only the CLMF, but a number of other one-shot linear receivers developed previously. In addition, it is demonstrated that, in the limit when AWGN disappears, the NWMF and CLMF reduce to decorrelator-type structures independent of signal power parameters.

1.4 Organization of Thesis

The organization of the thesis is as follows. Chapter 2 describes the DS-CDMA system model, reviews DS-CDMA receivers and formulates the objectives and approach of the thesis. Chapter 3 presents the synthesis of the various MFs for DS-CDMA when the observation interval of the received signal is finite. Chapter 4 repeats the synthesis when the observation interval of the received signal is extended to an infinite interval. Chapter 5 analyzes the performance of the MFs in terms of SNR, near-far resistance, bit error rate (BER) and the probability of outage. Chapter 6 considers several adaptive implementations of the CLMF. And finally, Chapter 7 summarizes the thesis by presenting conclusions and directions for future research.

Chapter 2

Design of DS-CDMA Receivers

This chapter discusses the design of receivers in DS-CDMA. Section 2.1 describes a general DS-CDMA system model. Section 2.2 reviews the state of the art in DS-CDMA receivers. Section 2.3 formulates the problem to be tackled and the approach taken for its resolution. It represents the *raison d'être* of the thesis. Finally, section 2.4 presents a unifying framework of enhanced single-user receivers for DS-CDMA.

2.1 System Model

An overview of the DS-CDMA system model under consideration is shown in Fig. 2.1. The complex baseband representation of bandpass signals is used where $\tilde{}$ denotes the complex envelope of a bandpass signal whose carrier frequency $\frac{\omega_c}{2\pi}$ is much larger than its bandwidth. A total of $K+1$ users transmit asynchronously to a common receiver over an additive white Gaussian noise (AWGN) channel. An arbitrary user is designated as the desired user and indexed as user 0. The remaining K users represent the interferers whose signals form the multiple-access interference (MAI). The following sections cover, in sequence, the modelling of the transmitters, signal parameters, and received signal. The design of the receiver labelled as Rx 0 in Fig. 2.1 is the focus of the thesis. Its description shall be provided in section 2.3.3 after the review of DS-CDMA receivers.

2.1.1 Transmitter Model

The transmitter block of the kth user, Tx k, in Fig. 2.1 is expanded in Fig. 2.2. It represents the mathematical model of the transmitter presented earlier in Fig. 1.3. The channel encoder, however, has been excluded for clarity. The function of the

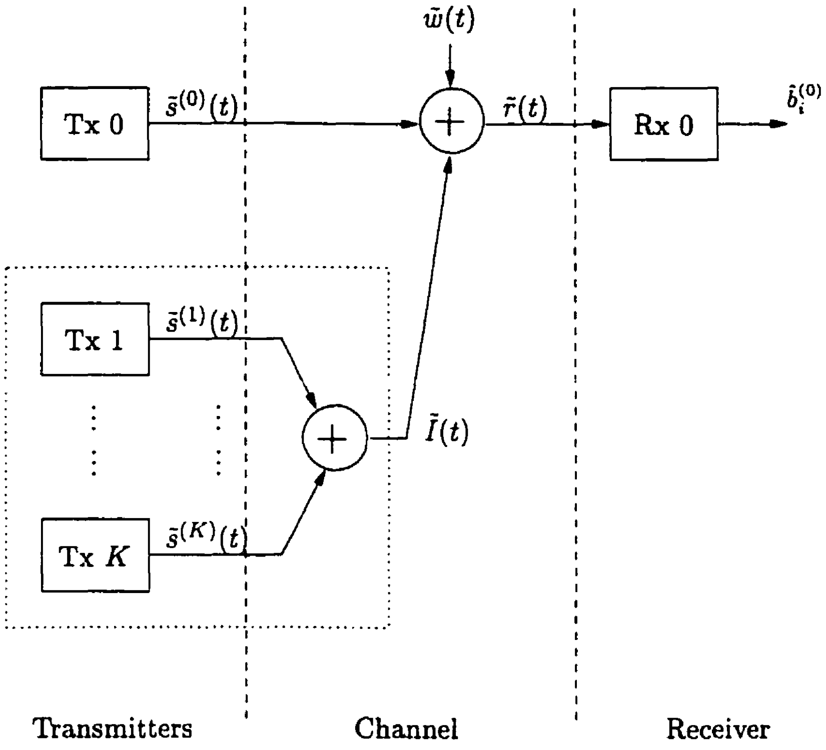

Fig. 2.1 System Model.

transmitter is to transmit the kth user's bit symbols $b_i^{(k)} \in \{\pm 1\}$ indexed by the integer $i \in (-\infty, \infty)$ at the bit rate of $1/T_b$. The bit symbols are assumed to be independent and equally probable such that $\mathrm{E}[b_n^{(k)}] = 0$ and

$$\mathrm{E}[b_i^{(k)} b_m^{(k)*}] \;=\; \delta_{im} \tag{2.1}$$

where the kronecker delta is defined as $\delta_{im} = 1$ for $m = i$ and $\delta_{im} = 0$, otherwise.

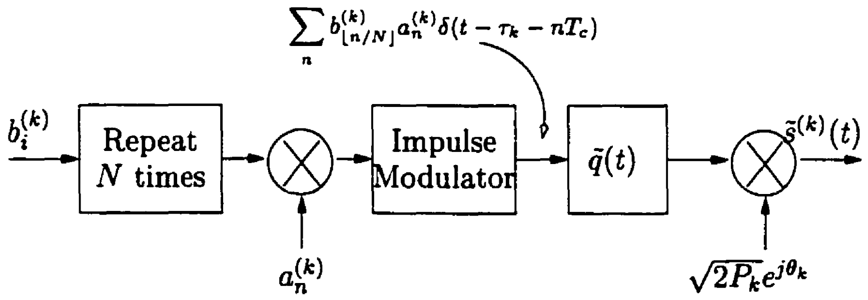

Fig. 2.2 Transmitter block for Tx k.

Direct-sequence spreading stage

Each bit symbol is repeated N times, indexed by n, and output as $b^{(k)}_{\lfloor n/N \rfloor}$, at a higher rate of $1/T_c = N/T_b$ referred to as the chip rate. The term N, representing the ratio of the chip rate to the bit rate, is referred to as the *spreading factor.* Each symbol $b^{(k)}_{\lfloor n/N \rfloor}$ is multiplied at the chip rate by the chip symbols $a^{(k)}_n$, indexed by n, which form the spreading sequence of the kth user. In effect, N samples of one bit symbol are multiplied by N chip symbols of a spreading sequence at the first multiplier element.

The chip symbols $a^{(k)}_n$ can be complex and satisfy $|a^{(k)}_n| = 1$. In particular, $a^{(k)}_n \in \{\pm 1\}$ for direct-sequence binary phase-shift keying (DS-BPSK) and $a^{(k)}_n \in \{\pm 1, \pm j\}$ for direct-sequence quaternary phase-shift keying (DS-QPSK). The term j represents the imaginary number $\sqrt{-1}$. The spreading sequences are assumed to be periodic sequences created from a pseudo-noise (PN) sequence of length N_p such that

$$a^{(k)}_{n+N_p} = a^{(k)}_n. \tag{2.2}$$

This work is not concerned with the design nor selection of spreading sequences which give optimal performance. Rather, the concern here is on receiver design once given a set of spreading sequences. Details on the design and selection of spreading sequences can be found in [7, 2].

As mentioned earlier in section 1.3 and as will be discussed in section 2.2.5, the method of direct-sequence spreading has a serious impact on receiver design. The method is determined by N and N_p. In short sequence spreading, the PN sequence length is constrained to satisfy $N_p = N$ whereas in long sequence spreading, $N_p > N$. Systems using the former and those using the latter are also referred to as, respectively, deterministic-CDMA and random-CDMA systems [39]. This thesis deals primarily with the latter.

Each product of the bit and chip is then passed to an impulse modulator which generates an impulse function $\delta(t)$ every T_c seconds. The impulse function is scaled by the input $b^{(k)}_{\lfloor n/N \rfloor}\, a^{(k)}_n$ and delayed by τ_k. The parameter τ_k represents the bit delay of user k's signal relative to that of user 0 at the receiver. Bit synchronization is assumed for user 0 such that $\tau_0 = 0$. The chip delay is defined as

$$T_k = \tau_k \bmod T_c \tag{2.3}$$

such that $T_k \in [0, T_c)$. The bit delay and chip delay between the signals of user k and the desired user are illustrated in Fig. 2.3 when a single bit symbol is spread by four chips ($N = 4$).

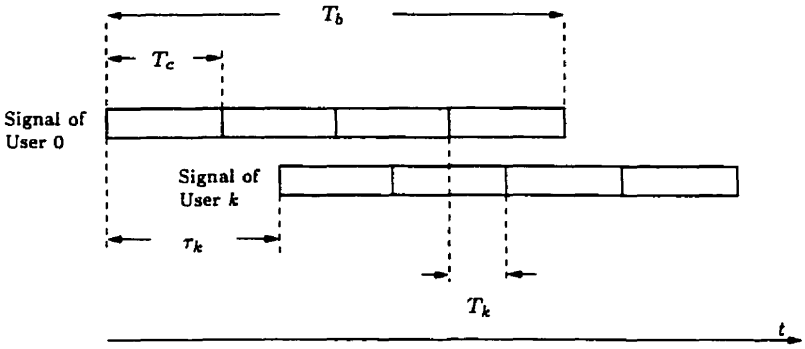

Fig. 2.3 An illustration of the relative bit delay τ_k and chip delay T_k between the signals of user k and the desired user when a bit symbol is spread by four chips ($N = 4$).

Chip filtering stage

Next, the signal is passed through a chip filter with an impulse response of $\tilde{q}(t)$. This is also referred to as the chip waveform. The waveform $\tilde{q}(t)$, which can be either time-limited or band-limited, satisfies the energy constraint: $\int_{-\infty}^{\infty} |\tilde{q}(t)|^2 dt = T_c$. In addition, the chip waveform is characterized by the parameter α which represents the percentage of its bandwidth in excess of the minimum bandwidth $\frac{1}{2T_c}$ required for symbol transmission at the chip rate of $1/T_c$. Hence, the bandwidth of the chip waveform is

$$B = \frac{1+\alpha}{2T_c}. \tag{2.4}$$

It is now possible to describe an important system parameter in DS-CDMA known as the *processing gain*, PG. It provides a rough measure for the amount of interference or jamming that a particular user can sustain. PG can be defined in terms of signal space concepts as the ratio of the dimensionality of the signal space in which a signal can be transmitted to the dimensions required to actually transmit the signal [7][18, p. 343]

$$\begin{aligned} \text{PG} &= 2BT_b \\ &= N(1+\alpha). \end{aligned} \tag{2.5}$$

It is also referred to as the *bandwidth expansion factor* since it is equivalent to the ratio of the chip waveform bandwidth to the minimum bandwidth required for the transmission of bit symbols at a rate of $1/T_b$. For example, given a chip waveform with 100% excess bandwidth, $\alpha = 100\%$, $B = 1/T_c$ and PG $= 2N$. In the special case where the chip waveform has zero-excess bandwidth, PG $= N$ and the processing gain is equivalent to the bit symbol spreading factor.

Transmitted Signal

The chip filter output is next multiplied by $\sqrt{2P_k}e^{j\theta_k}$. The term P_k represents the received power of user k's signal. The term θ_k represents the phase-offset of user k's signal relative to that of user 0 at the receiver. In reality, the bit delays, signal powers and phase-offsets are parameters perceived by the receiver. Although they are determined by the channel and transmitter together, they have been combined and incorporated in the transmitter block for mathematical convenience. Similarly, the received chip waveform can be defined as $\tilde{q}_r(t) = \tilde{q}(t) \star \tilde{h}_c(t)$ where $\star$ and $\tilde{h}_c(t)$ represent, respectively, the convolution operation and the channel impulse response (assumed to be linear and time-invariant). Hereafter, for notational convenience, $\tilde{q}(t)$ shall refer to the received chip waveform.

Carrier-phase synchronization for the desired user is assumed such that $\theta_0 = 0$. Coherent detection can be accomplished by periodically transmitting reference symbols known to the receiver [40, 41] (as in the multicode system [29]) or by continuously transmitting a pilot signal in addition to the information-bearing signal [42, 43] (as in IS-665 [31]). Similarly, chip synchronization is assumed such that $T_0 = 0$. To achieve chip synchronization, a delay-locked loop (DLL) can be implemented as described in [9, pp. 60–66] [44, p. 749, Fig. 13-5-5, and p. 749, Fig. 6-3-5]. Using later results of the thesis, the performance of the DLL can be improved in two ways. First, the chip filter $\tilde{q}^*(t)$ can be replaced by a new chip filter $G^{(C)}(f)$, developed in section 4.4, to reduce the effects of MAI in timing jitter. And second, as shown later in section 5.5.3, unlike the conventional MF, the application of the chip-delay locked MF (CLMF — developed in Chapters 3 and 4) allows the use of pulses with larger excess bandwidth at a much smaller loss in user capacity. Chip synchronization tends to improve with larger excess bandwidth [45, pp. 314–316].

The resulting transmitted signal for the kth user is

$$\tilde{s}^{(k)}(t) \;=\; \sqrt{2P_k}e^{j\theta_k} \sum_{n=-\infty}^{\infty} b^{(k)}_{\lfloor n/N \rfloor} a^{(k)}_n \tilde{q}(t - \tau_k - nT_c) \tag{2.6}$$

where $-\infty < t < \infty$. In short sequence spreading where $N_p = N$, the transmitted signal can be expressed instead as

$$\tilde{s}^{(k)}(t) = \sqrt{2P_k}e^{j\theta_k} \sum_{i=-\infty}^{\infty} b_i^{(k)} \tilde{a}^{(k)}(t - \tau_k - iT_b) \tag{2.7}$$

where the spreading waveform which no longer changes with each bit symbol is

$$\tilde{a}^{(k)}(t) = \sum_{n=0}^{N-1} a_n^{(k)} \tilde{q}(t - nT_c). \tag{2.8}$$

2.1.2 Model of Signal Parameters

The model for the signal parameters introduced in section 2.1.1 is specified next and is also summarized in Table 2.1. The signal parameters consist of spreading sequences,

Table 2.1 Model of signal parameters.

Signal parameter	Model	
spreading sequences $\{a_n^{(k)} \mid k \in [1, K], n \in (-\infty, \infty)\}$	short	long
bit delays $\{\tau_k\}_{k=1}^{K}$	fixed	random
signal powers $\{P_k\}_{k=1}^{K}$	fixed	
phase offsets $\{\theta_k\}_{k=1}^{K}$	fixed	random

bit delays, received signal powers and phase-offsets. The method of spreading can be either long or short sequence spreading. In short sequence spreading, the sequences of the interferers are assumed to be known. In long sequence spreading, the spreading sequences are usually constructed from PN sequences with extremely large N_p. For instance, in IS-95, $N_p = 2^{42} - 1$ [1, p. 6-24]. Moreover, the spreading sequences can be modelled as independently and identically distributed (i.i.d.) random sequences [46]. The kth user's spreading sequence is modelled as a random sequence (or, more precisely, as a discrete WSS random process) with $\mathrm{E}[a_n^{(k)} a_m^{(k)*}] = \delta_{nm}$. The bit delays can be characterized as being either fixed or i.i.d. with τ_k uniformly distributed over $[0, T_b)$. The signal powers of the interferers are assumed to be fixed. The phase-offsets can be characterized as being either fixed or i.i.d. with θ_k uniformly distributed over $[0, 2\pi)$.

2.1.3 Received signal

The received signal consists of the transmitted signal of the desired user, the transmitted signals of the K interfering users and additive white Gaussian noise (AWGN) (modelling background thermal noise) as shown in Fig. 2.1. The received signal can be written as

$$\tilde{r}(t) = \tilde{s}^{(0)}(t) + \tilde{I}(t) + \tilde{w}(t) \tag{2.9}$$

where $\tilde{w}(t)$ is a proper [47], complex, zero-mean AWGN process with a two-sided noise power spectral density of $2N_o$. Proper complex random processes, known also as circularly symmetric complex random processes [18, pp. 311–316], are discussed in more detail in section 3.6. The expression for the MAI is

$$\tilde{I}(t) = \sum_{k=1}^{K} \tilde{s}^{(k)}(t). \tag{2.10}$$

2.2 Review of DS-CDMA Receivers — State of the Art

This section reviews the state of the art in DS-CDMA receivers. It provides the background information necessary to understand the motivation and objectives of the thesis which shall be discussed later in section 2.3.

The function of a receiver is to estimate the transmitted bit symbols of one particular user, a subset of the users or all the users by processing the received signal. The receiver used presently in most spread spectrum and DS-CDMA systems is the the conventional MF (CMF) receiver described in section 2.2.1. Its weakness is its poor performance under power-imbalance conditions. It was this shortcoming which prompted the research and development of other DS-CDMA receivers.

All DS-CDMA receivers can be characterized, in general, by three important specifications: their performance, complexity and requirement of user signal parameters. The first relates to capacity and service quality especially with respect to the power-imbalance problem whereas the second relates to cost and complexity involved with implementation. The third specification is peculiar to DS-CDMA receivers. For bit detection of a particular user, this specification refers to the possible requirement of signal parameters of other users (ie. interferers). The parameters may include some subset of those listed in Table 2.2. Generally, the utilization of such information in receiver design tends to enhance performance while increasing complexity.

As depicted in Fig. 2.4, DS-CDMA receivers can be broadly classified into two

Table 2.2 Signal parameters of interferers.

Signal Parameters	Mathematical representation
spreading sequences	$\{a_n^{(k)} \mid k \in [1, K], n \in (-\infty, \infty)\}$
bit delays	$\{\tau_k\}_{k=1}^{K}$
chip delays	$\{T_k\}_{k=1}^{K}$
signal powers to AWGN PSD level	$\{P_k/N_o\}_{k=1}^{K}$
net MAI power to AWGN PSD level	γ/N_o
phase offsets	$\{\theta_k\}_{k=1}^{K}$

major categories: multi-user and single-user receivers. In the category of multi-user

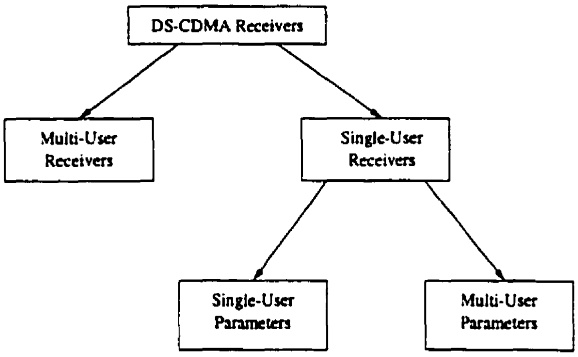

Fig. 2.4 Classification of DS-CDMA receivers.

receivers, bit detection is performed for all users jointly in a centralized fashion. In general, they are much less affected by the power-imbalance problem. In contrast, in the category of single-user receivers, bit detection is performed for a single-user in a de-centralized fashion. The signal of a particular user (the desired user) is designated as the desired signal while those of the remaining users are regarded as MAI. Single-user receivers can be further sub-divided into those requiring single-user parameters and those requiring multi-user parameters. In the former, the signal parameters of only the desired user are required for its bit detection. In the latter, referred to later as enhanced single-user receivers, the signal parameters of other users in addition to the desired user are utilized for bit detection of the desired user.

The next three sections from section 2.2.2 to section 2.2.4 present a review of multi-user receivers, single-user receivers using single-user parameters and enhanced single-user receivers using multi-user parameters, respectively. For clarity in presentation, short sequence spreading is assumed throughout the review since the majority of the receivers were developed under this assumption. The ramifications of removing this assumption is discussed in section 2.2.5 when systems using long sequence spreading are considered. A comprehensive overview of DS-CDMA receivers can be found in [48, 49, 50].

2.2.1 The Conventional MF

The least complex among DS-CDMA receivers is the conventional MF (CMF) receiver [7] used presently in well-established systems such as IS-95. It consists of a MF whose output is sampled every bit interval and input into a threshold device for a hard bit decision. The MF is composed of the chip filter $\tilde{q}^*(T_c - t)$ and a despreading filter (or correlator). For example, with respect to user 0 designated as the desired user, the MF impulse response is set to the time-reversed and conjugated version of its transmitted spreading waveform: $\tilde{a}^{(0)*}(T_b - t)$. It is the optimum receiver in terms of minimizing probability of bit error for a point-to-point single-user communication system when the noise is additive white Gaussian noise (AWGN).

The optimality of the CMF disappears in DS-CDMA systems since noise, which includes MAI as defined in (2.10), is generally neither white nor Gaussian [51]. Furthermore, since MAI consists of signals not orthogonal to that of the desired user, the performance of the CMF receiver degrades either as the number of users grows or as the received signal powers of others, relative to that of the desired user, grows (ie. the power-imbalance problem).

2.2.2 Multi-User Receivers

The development of multi-user receivers was initiated by the poor performance of the CMF in DS-CDMA especially under power-imbalance conditions. The term *multi-user* stems from the fact that the signals of all users are demodulated jointly. Moreover, these receivers have the common feature of requiring, at least, the spreading sequences and bit delays of each user in the system. Depending on the multi-user receiver, signal power and phase-offset parameters may be required as well. Such detectors may be well suited to single-cell applications where parameter estimates for all users are readily available at the base station receiver. On the other hand, in multiple-cell applications, signal parameters of users from neighbouring cells (usually inaccessible) may have to be estimated. In the absence of accurate estimates, the effectiveness of the multi-user receivers may deteriorate to the point where their performance may fall below that of the CMF.

The classification of multi-user receivers is given in Fig. 2.5. They can be subdi-

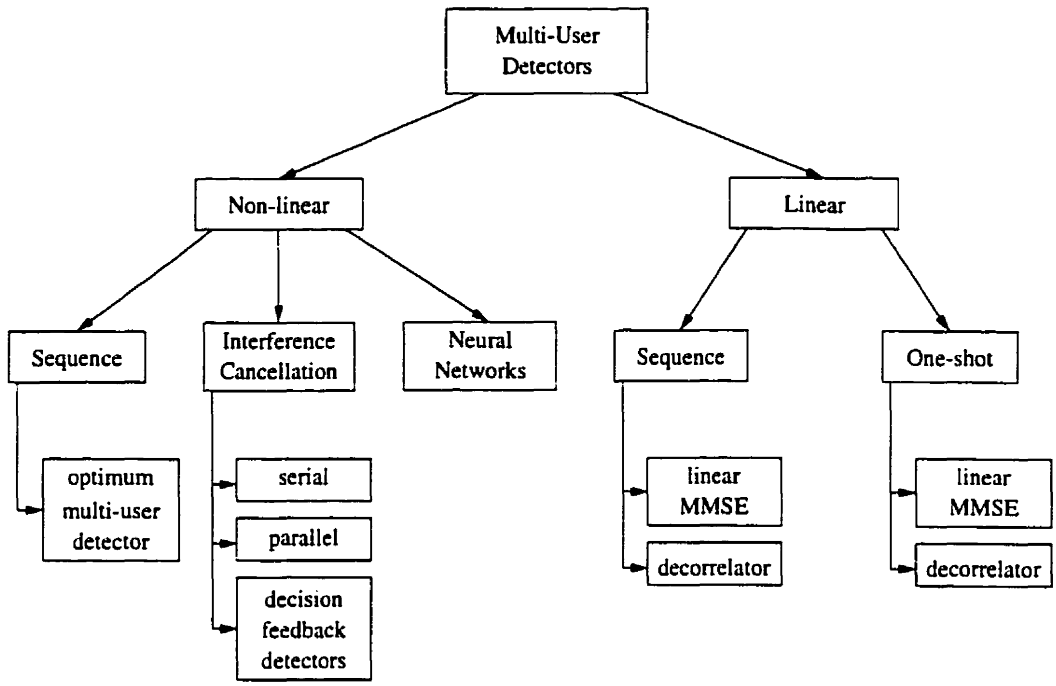

Fig. 2.5 Classification of multi-user receivers.

vided into non-linear and linear receivers. A discussion of the two types follows.

Non-Linear Multi-User Receivers

Non-linear multi-user receivers can be further grouped as receivers based on sequence estimation, interference cancellation or neural networks.

Optimum multi-user detector

The optimum multi-user detector [52] performs joint sequence estimation of all users' bit sequences based on either minimizing error probability or maximizing likelihood. Both forms of the detector deliver minimum BER in regions of low background noise (where the BERs are indistinguishable) while providing optimum near-far resistance [51]. The difficulty with either detector is complexity. The latter form of the detector (of less complexity than the former) requires a computational complexity per bit symbol which increases exponentially with the total number of users [52]. Hence, either form of the optimum detector is impractical unless the number of users is quite small.

Interference Cancellation (IC)

In non-linear receivers based on interference cancellation, feedback of bit estimates (decision feedback) and information on each user's signal parameters are utilized to estimate the MAI and subtract it from the received signal [53]. This operation is performed across all or some subset of the users. Its advantage is its ability to cancel more reliably those signals from strong interferers who constitute the primary source of the power-imbalance problem; signals from weaker interferers do not have to be cancelled. As long as the bit estimates and signal parameter estimates are reliable, the IC receivers can deliver near-optimum performance. Its complexity per bit symbol grows linearly with respect to the number of users whose signals are being cancelled. This, however, is still comparatively high for implementation purposes. A large number of IC receivers have been proposed. They can be grouped as serial (or successive) IC [54, 53], parallel IC [55, 56, 57] and decision-feedback detectors [58]. Further details can be found in [50, 49].

Neural Networks

Multi-user receivers based on neural networks can achieve near-optimum performance [59]. However, they have two major drawbacks. First, their hardware complexity in terms of number of nodes grows exponentially with the number of users. And second, the training period before data transmission tends to be extremely long. This implies that neural networks may not be feasible in applications involving dynamically changing channel conditions where signal parameters change and users enter or depart from the system [48].

Linear Multi-User Receivers

Linear multi-user receivers can be grouped as receivers based on either sequence estimation or one-shot detection. Both types of linear receivers have the flexibility of performing bit symbol or bit sequence demodulation jointly with all users in a centralized fashion or for a single user in a decentralized fashion [60]. Thus, the one-shot detectors have the special property of being implementable and classifiable as either multi-user receivers or the enhanced single-user receivers to be discussed in section 2.2.4.

Linear sequence estimation

In an effort to reduce the computational complexity of the optimum multi-user detector, suboptimum versions which yield excellent performance have been developed based on linear sequence estimation [49]. Sequence estimation in these detectors is based on either a minimum mean squared error (MMSE) formulation [61] or zero-forcing criterion [60] in place of the maximum likelihood criterion. The sequence-type decorrelator, based on the zero-forcing criterion, does not require the signal power parameters. Its advantage appears in systems where signal powers are either changing rapidly or unknown as long as MAI dominates the background AWGN. The sequence-type linear MMSE receiver, based on minimizing MSE, requires estimates of signal power parameters. In MAI-limited environments where the signal powers dwarf the background thermal noise, the linear MMSE reduces to the decorrelator. The problem with either of these receivers is that, like the IC receivers, the computational complexity per bit symbol increases linearly with the total number of users and their performance depends on the accuracy of at least the bit delay estimates.

One-shot linear detectors — one-shot linear MMSE and decorrelator

The two one-shot linear detectors can be interpreted as modifications to the previously discussed sequence estimation-type receivers. Here, the signal observation interval is restricted to the duration of one or several consecutive bit symbols to produce a hard decision on a bit symbol. For clarity, the two detectors are described in the context of symbol detection for each user in a decentralized fashion as an enhanced single user receiver. Both are based on a linear time-invariant (LTI) filter structure.

In the one-shot decorrelator, the filter is designed under the criterion of eliminating MAI entirely (zero-forcing) [51, 60]. This approach to filter design is analogous to that used to eliminate intersymbol interference (ISI) using the zero-forcing criterion. Since it enhances background thermal noise, it is inappropriate in channels dominated by AWGN.

The weakness of the one-shot decorrelator is remedied by taking the presence of the AWGN into account as well. Both AWGN and MAI can be suppressed by minimizing the mean square error (MSE) formed between the output of an LTI filter and a training (or desired) symbol while using the knowledge of signal parameters for all users [62]. This yields the one-shot linear MMSE detector [62]. As shall be discussed again later, this detector which minimizes MSE also maximizes SNR [62, p. 3180]. Moreover, it reveals the structure and performance benchmarks of the adaptive linear receivers to be discussed later in section 2.2.3. In the limit, as MAI power increases relative to the thermal noise, the one-shot linear MMSE approaches the one-shot decorrelator.

Both of the one-shot detectors have a reduced computational complexity per bit symbol (under short sequence spreading). Each time an interferer bit delay changes, a re-computation of its filter response requires the solution of $2K$ linear equations with $2K$ unknowns [51] and the computation of a set of cross-correlation coefficients across the spreading waveforms. This requires, at minimum, $\mathcal{O}\left(\frac{(2K)^3}{3}\right)$ numerical operations [63, p. 154]. The complexity of the one-shot linear MMSE can be reduced further by suboptimum versions such as the N-tap MMSE detector (consisting of an N-tap tapped-delay line (TDL) filter) and others with a lower number of taps [62].

2.2.3 Single-User Receivers: Single-User Parameters

The second category of DS-CDMA receivers is based on single-user detectors using single-user parameters. The term *single-user* stems from the approach of performing detection with respect to one particular user referred to as the desired user. In this approach, the remaining users are interpreted and lumped together as MAI. However, unlike the third category to be discussed in section 2.2.4, this category of receivers does not require the signal parameters of users other than those of the desired user. This makes them particularly attractive for implementation in multiple cell applications. The classification of single-user DS-CDMA receivers using single-user parameters is given in Fig. 2.6. They can be subdivided into either fixed or adaptive receivers.

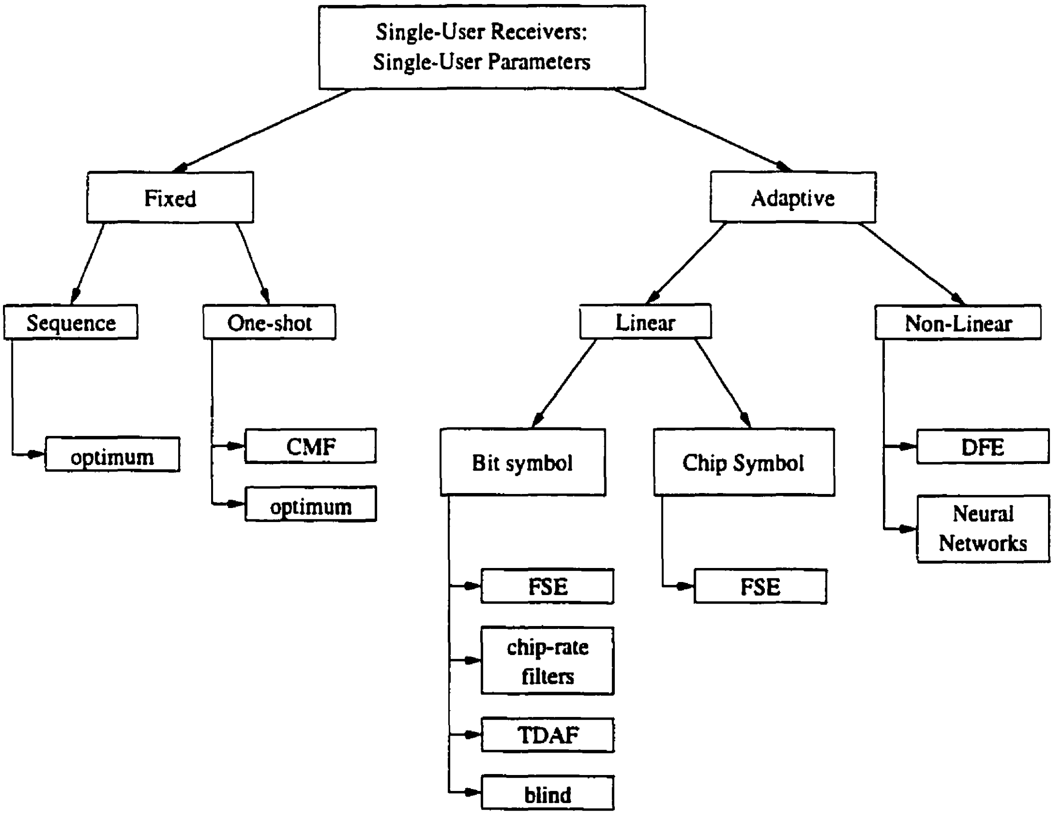

Fig. 2.6 Classification of single-user receivers using single-user parameters.

Fixed single-user receivers

Fixed single-user receivers, referring to non-adaptive realizations, can be grouped as receivers based on either sequence estimation or one-shot detection.

Sequence estimation — the optimum single-user detector

The optimum single-user DS-CDMA detector is based upon maximum-likelihood sequence estimation of the desired user's bit sequence. Like the optimum multi-user detector, however, its computational complexity per bit symbol increases exponentially with the total number of users [64]. Hence, it, too, is impractical unless the number of users is quite small.

One-shot single-user detectors

Instead of detecting the entire bit sequence of the desired user, one-shot detectors make a decision for a single bit independent of previous or future bit decisions. The CMF, described in section 2.2.1, is an example of a one-shot single-user detector.

Optimum one-shot single-user detector

Under the condition of demodulating a single symbol at a time, the optimum one-shot detector delivers minimum probability of bit error based on comparing a likelihood ratio to a threshold. The likelihood ratio contains two terms: the usual statistic obtained at the sampled CMF output and a correction statistic which takes the MAI into account. Like the optimum single-user sequence estimation type, its computational burden is at least the same order of complexity as the optimum multi-user detector and the optimum single-user detector [64].

Adaptive single-user receivers

The development of adaptive single-user receivers is more recent and is surveyed in [65]. They can deliver substantial improvement in performance over the CMF without the knowledge of interferer signal parameters. Adaptive receivers can be organized into two groups: linear or non-linear adaptive receivers.

Linear adaptive receivers

This group of linear adaptive receivers is based on the standard TDL filter known also as the linear transversal filter [66] [18, pp. 486-487, 517-520] [44, pp. 601-620, 636-644]. The filter tap coefficients are adapted to minimize the difference or error between the expected filter output and the sampled filter output. The expected filter output can be either bit symbols or the product of bit and chip symbols. Subsequently, this group can be subdivided into schemes for either bit symbol equalization or chip symbol equalization. Unlike their one-shot multi-user counterparts, the computational complexity of these adaptive schemes is proportional to the number of taps in the TDL filter and is, thus, independent of the number of users $K + 1$ in the system.

Bit symbol adaptive filters
In bit symbol adaptive filters, each sampled filter output represents an estimate of each transmitted bit (or training symbol). Furthermore, the estimates and the discrete-time samples of the error signal (formed between the estimate and filter output) are generated at the bit rate. The response of the TDL filter should converge ideally to that of the one-shot linear MMSE multi-user detector [62] in its enhanced single-user form as discussed earlier. The time duration of the filter impulse response is greater than or equal to T_b. These schemes can be further broken down into structures which differ in terms of tap delay spacing and updating algorithms. The updating algorithms of the first three schemes aim to minimize MSE whereas that of the fourth uses a different criterion instead.

Bit symbol adaptive FSE
A fractionally-spaced equalizer (FSE) is a TDL filter whose delay elements are set to $T_s = T_c/N_s$ where $N_s \geq 1$ is an integer. In bit symbol FSE schemes, the input to the FSE is obtained by sampling either the down-converted received signal directly or the output of the chip filter $\tilde{q}^*(T_c - t)$ [67, 68, 48]. The selection of the sampling rate is determined by the signal bandwidth given in (2.4) and the Nyquist sampling theorem. The sampling rate is set to satisfy $1/T_s \geq 2B = (1 + \alpha)/T_c$ and then set to an integer multiple of the chip rate. Thus, $1/T_s = N_s/T_c$ where $N_s = 1 + \lceil \alpha \rceil$.

Bit symbol adaptive chip-spaced equalizers
In bit symbol adaptive chip-spaced equalizers, the delay elements of the TDL are set to T_c. This is equivalent to constraining $N_s = 1$ in the FSE and having $1/T_s = 1/T_c$ [62, 69]. When the number of taps is N, this scheme represents the adaptive version of the N-tap MMSE detector. Other versions which reduce computational complexity at the expense of further reduction in performance are developed in [62] by further reducing the number of taps.

Bit symbol frequency domain TDAF
The development of the bit symbol frequency domain time-dependent adaptive filter (TDAF) has its roots in Frequency-Shift (FRESH) filtering theory for linear signal estimation in cyclostationary noise [70, 48, 71]. The FRESH filter exploits spectral coherence in the received signal by summing appropriately weighted and frequency-

shifted versions of the received signal [70]. In the one-shot detection of PAM signals, the FRESH filter can be implemented as a modified version of the frequency domain adaptive filter [72] [73, pp. 197–210]. Known as the frequency domain TDAF [74, 75, 76], this realization processes the received signal in the frequency domain. The frequency domain TDAF is closely related to the bit symbol adaptive FSE described previously. With respect to the estimation and filtering of PAM signals, the FRESH filter output, when sampled at the bit symbol rate, reduces mathematically to an FSE [70, p. 566].

There are two potential benefits of implementing the frequency domain TDAF over the adaptive FSE [76, p. 393]. Given a large number of taps, the number of computations in terms of multiplication and add operations can be reduced significantly. This is because convolution in the time domain can be performed with less operations in the frequency domain via the Fast Fourier Transform (FFT) [73]. Furthermore, the rate of convergence can be improved. This is because the received signal is divided into contiguous spectral bands each with their own convergence rate and step size value [76][73, pp. 205–210].

There appears to be no mention of problems associated with the frequency domain TDAF in [74, 75, 76]. However, generally, frequency domain adaptive filter implementations have two weaknesses. First, leakage of signals from one band to other bands can occur and reduce filter performance [73, p. 206]. And second, the updating of tap coefficients incurs a delay during the processing of a block of samples via the FFT. This necessitates small step size values and reduces the convergence rate [72].

Blind Adaptive Receiver

Blind adaptive receivers are investigated in [77, 65]. The term *blind* arises from the fact that no training sequence is required. They consists of two parallel filters whose outputs are summed. One is the CMF for the desired user which is fixed and the other is a TDL filter whose taps can vary. Based on the criterion of minimizing the sampled output energy, the combined response can converge to the one-shot multi-user linear MMSE. Bit decisions are not used in the tap coefficient updating algorithm. The advantage of this scheme surfaces in situations where the decision-directed mode of updating the coefficients proves unreliable. This can occur either when other users go on and off line, or when sudden changes in signal powers occur. A generalization of this blind adaptive approach, in the context of inverse filtering, has been considered for channels with multipath and ISI [78].

Chip symbol adaptive filters — chip symbol adaptive FSE

In chip symbol adaptive filters, each sampled filter output represents an estimate of $b^{(k)}_{\lfloor n/N \rfloor} a^{(k)}_n$ (or a training symbol). Furthermore, the estimates and the discrete-time samples of the error signal (formed between the estimate and filter output) are generated at the chip rate. This idea appears to have been first introduced in [79] as a structure to realize the noise-whitening MF (NWMF) to be discussed in section 2.2.4. A few changes to the bit symbol adaptive FSE occur when applied to chip symbol adaptive filtering. First, in training mode, each training symbol represents a chip instead of a bit. Second, in decision directed mode, each training symbol is an estimate of a transmitted bit re-spread by the spreading sequence: $\hat{b}^{(0)}_{\lfloor n/N \rfloor} a^{(0)}_n$. Although each chip $a^{(0)}_n$ is known *a priori*, bit decisions incur a delay of at least T_b. And third, the number of delay elements in the chip symbol FSE can be considerably reduced in comparison to the bit symbol FSE.

There are two advantages of the chip symbol adaptive filtering over its bit symbol counterpart. It reduces computational complexity since the number of tap delay coefficients is considerably reduced. And most notably, it is the only linear adaptive scheme that remains feasible under long sequence spreading. This issue shall be elaborated on in section 2.2.5. Its disadvantage is its limited gain in performance in comparison to that of bit symbol adaptive receivers [79].

Non-linear adaptive receivers

Non-linear adaptive receivers can be broken down into bit symbol decision feedback equalizers (DFE) and adaptive receivers based on neural networks.

Bit symbol DFE

A DFE consists of two TDL filters: a feed forward filter whose input is the received signal and a feedback filter which is fed with bit symbol decisions [66][44, pp. 621–627, 649–650][80, pp. 500–510]. The feed forward filter output is subtracted by the feedback filter output and fed to a slicer. The application of the DFE in place of the FSE is investigated in [81, 82] and is motivated by its ability to handle ISI and delayed replicas of the desired signal due to multiple propagation paths.

Adaptive single-user neural networks

The application of neural networks to DS-CDMA receiver design is outlined in [48]. It can deliver near-optimal performance [83] like its multi-user neural network receiver counterpart since it can detect signals in non-stationary and non-Gaussian noise [84]. However, it has two shortcomings which prohibit it from practical consideration. With present neural net equalization techniques, there is no guarantee of reaching an optimal solution and its rate of convergence is very slow [48]. It, thus, requires extremely long training sequences [85].

2.2.4 Enhanced Single-User Receivers: Multi-User Parameters

In the previous section, single-user receivers were described under the constraint that signal parameters of only the desired user were utilized. In this section, the constraint is lifted to improve the design and performance of the single-user receivers. The term *enhanced* denotes the inclusion of signal parameters of other users (ie. multi-user parameters). Moreover, these receivers are constrained to be one-shot linear detectors. The enhanced single-user receivers are summarized in Fig. 2.7. The one-shot linear

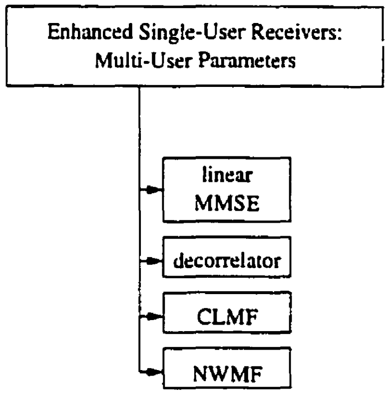

Fig. 2.7 Classification of enhanced single-user receivers using multi-user parameters.

MMSE detector and decorrelator have already been described in section 2.2.2 in the discussion on one-shot linear detectors in the context of multi-user receivers. Both are included in Fig. 2.7 and Fig. 2.5 since, as explained previously, they can be implemented as either multi-user or enhanced single-user receivers. The one-shot detector labelled as chip-delay locked MF (CLMF) in Fig. 2.7 shall be discussed in more detail in section 2.4 and derived in Chapter 3 and Chapter 4. Consequently, the remaining enhanced single-user receiver that needs to be described is the NWMF.

NWMF

When the only known parameter concerning interfering users is the ratio of total MAI power to thermal noise power, whitening of the interference can be applied to produce the noise-whitening MF (NWMF) [86]. It provides improvement in performance over that of the CMF by the addition of a noise-whitening filter either before or after the chip filter. The improvement, however, is much less than that achievable by multi-user receivers. Its advantage is its low complexity per bit symbol. The complexity of computing its filter response is independent of K and the method of spreading. Another method of implementing the NWMF joins the whitening filter and the chip filter to produce a modified despreading chip waveform which changes according to the MAI power and desired user's spreading sequence. This idea has been investigated for the specific case of rectangular pulses in [87]. In addition, to enhance the performance of IC-receivers, the NWMF can replace the CMF in the front end of the IC-receivers to improve the reliability of preliminary bit estimates.

2.2.5 Ramifications of Spreading Method

The previous section reviewed DS-CDMA receivers in the context of DS-CDMA systems based on short sequence spreading. This was because most receivers, until recently, were developed under the assumption of short sequence spreading. Practical systems, however, such as IS-95 [1] and nearly all those proposed for third generation cellular communication systems [27, 29, 31] have been designed based on long sequence spreading. The sole exception is the proposal known as FRAMES FMA2 where long sequence spreading serves, instead, as an option to short sequence spreading [27, p. 425, Table 2]. The aim of this section is to show that the majority of DS-CDMA receivers (designed to counter the power-imbalance problem) are rendered inapplicable in systems based on long sequence spreading due to either excessive complexity or incompatibility. This observation shall serve as the driving force which motivates the thesis and the development of receivers feasible under long sequence spreading. Later, reasons for the selection of long sequence spreading are described.

The assumption of long sequence spreading adversely affects the design of all DS-CDMA receivers except for the IC, NWMF, chip symbol adaptive FSE and CMF. In the case of multi-user detectors, their computational complexity per bit symbol explodes since the cross-correlation coefficients among the spreading waveforms of each pair of users now change with each bit symbol. Before, under short sequence spreading, these coefficients remained fixed until a change occurred in the bit delay of at least one interferer. However, under long sequence spreading, the coefficients must either be re-computed at the bit rate or fetched if stored beforehand. Furthermore, the complexity of the one-shot linear receivers (the least complex among the multi-user receivers under short sequence spreading) explodes, nonetheless, even when the cross-correlation coefficients are available. Previously, a minimum of $\mathcal{O}\left(\frac{(2K)^3}{3}\right)$ operations were required to compute the one-shot linear MMSE or decorrelator when a bit delay parameter changed. Under long sequence spreading, however, the operations must be repeated at the bit rate for each consecutive bit to be detected [55]. In contrast, non-linear IC schemes are unaffected since the MAI is estimated on-line by multiplying the bit decisions with the spreading sequence regardless of the spreading method. Despite this property, as described earlier, their complexity per bit symbol, which increases linearly with K, remains high.

Long sequence spreading also poses an insurmountable problem to single-user bit symbol adaptive filters. These were developed under the assumption of short sequence spreading whereby the desired user's spreading sequence for each consecutive bit remained fixed. This made it possible for the adaptive filter to converge to the one-shot linear MMSE solution. However, under long sequence spreading, the MMSE solution changes with each consecutive bit symbol. Consequently, the bit-symbol adaptive filters are rendered inutile. Therefore, the NWMF and chip symbol adaptive FSE (proposed to realize the NWMF) remain as the only low-complexity alternatives to the CMF feasible under long sequence spreading.

Reasons for Long Sequence Spreading

The reasons for choosing long sequence spreading over short sequence spreading in DS-CDMA are described. The primary reason relates to channel coding which plays a fundamental role in the design of not only DS-CDMA systems [39], but, in general, any reliable digital communication system. In practice, therefore, as shown earlier in Fig. 1.3, bandwidth expansion for bit transmission is performed by channel coding in addition to direct-sequence spreading. By taking into account the coding rate R_c (ratio of the information bit rate to the coded bit rate) of the channel encoder, PG in (2.5) is modified to $\mathrm{PG} = N(1+\alpha)\cdot 1/R_c$ and $N = \mathrm{PG}/[(1+\alpha)\cdot 1/R_c]$. In effect, channel coding reduces N by a factor of $1/R_c$. For example, in the uplink of the IS-95 system based on long sequence spreading, $\mathrm{PG}/(1+\alpha) = 128$, $1/R_c = 32$ and $N = 4$. Each coded bit (or Walsh chip) is spread by a sequence of $N = 4$ chips [1, p. 6-11, Table 6.1.3.1.1-1] taken from consecutive and contiguous segments of a longer PN sequence of length $N_p = 2^{42} - 1$ [1, p. 6-24]. Under short sequence spreading, not many distinct sequences of length $N_p = N = 4$ can be constructed. Through this example, it can be seen that, in systems where a large portion of PG is allocated to channel coding, long sequence spreading would be preferable to short sequence spreading.

If short sequence spreading were desired, nonetheless, a lower limit to R_c would have to be imposed to maintain a sufficiently large N. Such a restriction would, however, come at the loss of potential gain in performance and capacity. This observation comes as a result of the recent work of [88, pp. 27-30] and [89, pp. 50-51] which advocate allocating as much of the PG to channel coding as possible. As shown in [89, pp. 50-51], when all of the PG is consolidated to channel coding by setting $R_c = 1/\text{PG}$ and $N = 1$, channel capacity in an AWGN channel is maximized. Therefore, long sequence spreading appears to be unavoidable in systems geared towards maximizing performance and capacity.

The second reason for avoiding short sequence spreading relates to issues of privacy and security in the communication links. In long sequence spreading, each consecutive bit is spread by a different sequence instead of the same sequence. This adds an extra level of security in the air interface.

2.3 Detailed Thesis Statement

This section provides a precise statement of the thesis in three parts. First, the problem of receiver design in DS-CDMA is formulated and justified in the context of the background information presented thus far in the thesis. Second, the goals of the thesis are stated. And third, the approach taken to achieve the goals is described.

2.3.1 Formulation of Problem

The previous section has established that the CMF, NWMF and chip symbol adaptive FSE (proposed to realize the NWMF) are the only low-complexity receivers compatible with DS-CDMA systems based on long sequence spreading. It was shown that all other receivers suffer from either excessive complexity or incompatibility under long sequence spreading. The problem with the CMF and NWMF, however, is their limited performance under power-imbalance conditions. As shall be shown in Chapter 5, the near-far resistance (a measure quantifying receiver robustness to the power-imbalance problem) of the NWMF, like that of the CMF, is zero. Based on these observations, several questions can be posed. Does there exist a low-complexity receiver compatible with long sequence spreading which delivers performance greater than that of the NWMF? If such a receiver did exist, how much of an increase in performance would it yield? And, what would its complexity be? These are the primary questions which the thesis seeks to answer.

The questions merit consideration because of the need, in DS-CDMA systems, for low-complexity receivers less vulnerable to the power-imbalance problem. Should such receivers compatible with long sequence spreading exist, they could significantly boost the performance and capacity of present systems (such as IS-95) and future DS-CDMA systems implementing long sequence spreading.

2.3.2 Goals

The goals of the thesis shall now be stated with respect to the problems formulated in section 2.3.1. The primary goal of the thesis is to derive a receiver, suited for systems based on long sequence spreading, which offers an improvement in performance over the NWMF. This will lead to the proposed chip-delay locked MF (CLMF). The second goal is to determine the gain in performance associated with the CLMF in comparison to the NWMF. The third goal is to offer directions to the development of adaptive versions of the CLMF amenable to practical implementation. And the final goal is to develop a general framework for deriving one-shot linear receivers including the enhanced single-user detectors.

2.3.3 Approach

The approach taken in achieving the first goal stated in section 2.3.2 shall be described in four stages corresponding to: the selection of the receiver structure, the selection of the optimization criterion, information requirements and the description of the method of synthesis. This essentially follows the heuristic approach outlined in [90, pp. 12-15] and [91, pp. 186-187]. Moreover, this approach is similar to that of [86] but differs in the third stage with respect to the modelling of the interferer bit delays.

Structure

The structure of the receiver is based upon a linear time-invariant (LTI) filter receiver as depicted in Fig. 2.8 in complex envelope form. This is the proposed receiver for

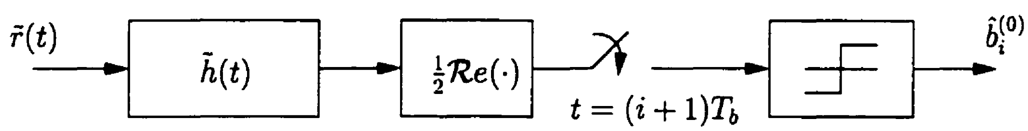

Fig. 2.8 Rx 0 — The LTI filter receiver for user 0.

Rx 0 in Fig. 2.1. It consists of an LTI filter $\tilde{h}(t)$, a sampler and a slicer (hard-decision device) [80, pp. 79-87] [18, pp. 224-229] [44, pp. 238-244] and [86]. The real part of the filter output, scaled by a factor of 1/2, is sampled every T_b seconds and fed to the slicer to produce the bit estimate $\hat{b}_i^{(0)}$. As discussed in section 2.1.1, it is assumed that both carrier-phase and bit-timing recovery has been accomplished.

The LTI filter structure is selected for the following reasons. As observed in the progression from the optimum multi-user detector to the one-shot linear detectors, this structure tends to result in receivers with reduced complexity. Furthermore, once the solution is established, it can guide the development of adaptive versions suitable for implementation. Not only would this reveal the underlying structure of the adaptive filter, but it would also provide the filter response to which the adaptive versions should ideally converge. Thus, the LTI filter receiver structure is selected in the hope of developing implementations which deliver performance beyond that of the NWMF while maintaining low complexity per bit symbol.

Optimization Criterion

In general, the selection of an appropriate optimization criterion is important in two respects. One, it serves as a measure to assess receiver performance. And two, it influences the practicality of the design. Here, the criterion is selected primarily for the purpose of design rather than performance. In fact, in terms of performance, selection of probability of bit error P_e would be ideal. However, the problem with P_e is that it leads to either untractable or computationally expensive solutions such as the optimal one-shot single-user detector as discussed in section 2.2.3. Thus, for the purpose of developing a practical receiver with much less computational requirements, a second order criterion known as signal-to-noise ratio (SNR) [91, 92, 93] is selected. The SNR criterion is defined mathematically later in (2.15) and explained in section 3.1 in more detail. As evident in the NWMF [86], designs based on the LTI filter structure and the SNR criterion tend to result in implementations with low complexity.

The problem with the SNR criterion is that it does not necessarily guarantee an improvement in P_e which is ultimately the criterion of interest from the perspective of performance rather than design. Although the relationship that increasing SNR monotonically lowers P_e makes sense intuitively, it does not hold in all cases. An example of a degenerate case where SNR may be misleading arises in a point-to-point direct-sequence spread spectrum system with narrowband interference. In comparing the P_e performance of two different filters in this situation, a filter providing larger SNR compared to another may not necessarily deliver lower P_e when PG is small (eg. PG $= 7$) [94]. It may in fact deliver higher P_e. On the other hand, as long as PG is moderately large (eg. PG ≥ 63), SNR provides a useful measure of P_e performance

[94]. It is conjectured that in wideband interference, the same result would hold. That is, SNR should provide an adequate measure of P_e performance in DS-CDMA systems as long as PG is moderately large.

SNR vs. MSE

The LTI filter which maximizes SNR is referred to as a matched filter (MF) [91, 92, 93]. There exists another second-order criterion known as mean square error (MSE) [18, p. 467–469] [80, p. 489–491] intimately related to SNR. The error is the difference between the filter output and the expected (or desired) output. As shown in [95, pp. 252-261], the LTI filter which minimizes MSE is identical to the MF (except for a possible scaling factor) in the one-shot linear estimation of PAM signals. This result is obtained under the assumptions of an infinite observation interval and WSS noise. The relationship is re-investigated in Appendix A when both assumptions are removed. In addition, an expression which relates minimum MSE to maximum SNR (for the same filter which minimizes MSE and maximizes SNR) is derived.

Information Requirements

Next, the information required to derive the MF is discussed. With respect to the desired user, it is assumed that its spreading sequence is known to the receiver. With respect to the interferers, knowledge of their spreading sequences is unnecessary. However, it is assumed that each of their chip delays and signal powers are known. It is this assumption which distinguishes this work from [86] where the bit delays were assumed to be random and unknown. Later, the requirement of interferer chip delays and signal powers can be dropped when adaptive implementations are considered in Chapter 6.

Based on the approach to be outlined shortly, it will be possible to synthesize not only the CLMF, but also other enhanced single-user receivers such as the NWMF, one-shot linear MMSE and decorrelator as described in section 2.2.4. This ability to synthesize other enhanced single-user receivers is achieved by altering the level of interferer signal parameters available to the receiver. It is summarized under a general framework considered in section 2.4.

Method of Synthesis

This section reviews, in general terms, the process of designing the SNR maximizing filter component $\tilde{h}(t)$ in the LTI filter receiver in Fig. 2.8. The filter is shown in Fig. 2.9. The design, based on MF theory, is explained in more detail in [91, 92, 93, 96].

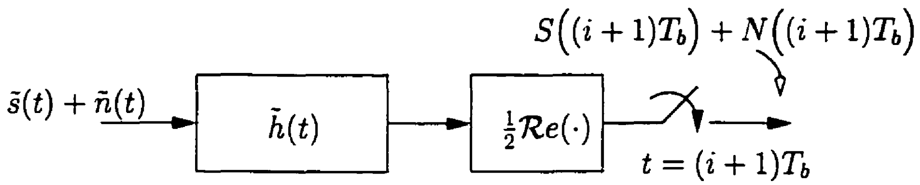

Fig. 2.9 The filter component of the MF receiver.

The received signal of (2.9) can be separated into two parts:

$$\tilde{r}(t) \;=\; \tilde{s}(t) + \tilde{n}(t). \tag{2.11}$$

The signal $\tilde{s}(t)$ represents the desired signal to be detected whereas $\tilde{n}(t)$ represents the noise. The filter is designed to detect the signal associated with the desired user's ith bit $b_i^{(0)}$ where, based on (2.6),

$$\tilde{s}(t) \;=\; \sqrt{2P_0}\, b_i^{(0)} \sum_{n=iN}^{(i+1)N-1} a_n^{(0)} \tilde{q}(t - nT_c). \tag{2.12}$$

The signal to be detected changes with each bit under long sequence spreading. In terms of MF design, this implies that the filter response must change at the bit rate to detect each new bit. Consequently, the MF may have to be re-computed repeatedly at the bit rate as well. However, as will be shown in Chapter 4, when the observation interval is infinite, an important simplification arises which circumvents this difficulty. In contrast, under short sequence spreading, (2.12) reduces to $\tilde{s}(t) = \sqrt{2P_0}\, b_i^{(0)} \tilde{a}^{(0)}(t - iT_b)$ where $\tilde{a}^{(0)}(t)$ is defined by (2.8) for $k = 0$. Since the signal to be detected remains the same for each bit, the MF response remains the same for the detection of each bit symbol of user 0 as long as interferer signal parameters remain fixed. Without loss of generality, the development of the MFs for the remainder of the thesis assumes the detection of the zeroth bit $b_0^{(0)}$ such that (2.12) becomes $\tilde{s}(t) = \sqrt{2P_0}\, b_0^{(0)} \tilde{a}^{(0)}(t)$. To design the MF for the detection of $b_i^{(0)}$, $\tilde{a}^{(0)}(t)$ can be re-defined by replacing $a_n^{(0)}$ with $a_{n+iN}^{(0)}$ in (2.8) for $k = 0$.

The noise, comprised of the remaining signals in the DS-CDMA system, can be written as

$$\tilde{n}(t) \;=\; \tilde{I}(t) + \tilde{w}(t) + \tilde{\zeta}(t) \tag{2.13}$$

where MAI $\tilde{I}(t)$ and background AWGN $\tilde{w}(t)$ have been defined in (2.10) and in section

2.1.3, respectively. The third term, representing intersymbol interference (ISI), can be expressed as

$$\tilde{\zeta}(t) = \sqrt{2P_k}\left\{\sum_{n=-\infty}^{-1} b_{\lfloor n/N\rfloor}^{(0)} a_n^{(0)} \tilde{q}(t-nT_c) + \sum_{n=N}^{\infty} b_{\lfloor n/N\rfloor}^{(0)} a_n^{(0)} \tilde{q}(t-nT_c)\right\}. \quad (2.14)$$

The ISI consists of the desired user's signal $s^{(0)}(t)$ associated with the bits $b_n^{(0)}$ for $n \neq 0$. The first sum in (2.14) represents the precursor ISI from previous bit and chip symbols while the second sum represents the postcursor ISI from future bit and chip symbols. In general, the ISI term $\tilde{\zeta}(t)$ can be ignored when PG >> 1 as is the case for most spread spectrum signals [18, p. 306, 339]. This occurs when either N or α is large. As a rather extreme example, the ISI at a filter output is zero for a chip waveform $\tilde{q}(t)$ (such as the rectangular pulse) that exists only over the interval $t \in [0, T_c)$ even if $N = 1$. Initially, it is assumed that PG is sufficiently large so that the effect of ISI can be safely ignored. This assumption is made to prevent obscuring the development of the MFs which can suppress MAI. The effect of ISI on the MF derivation is investigated in Appendix D.

The received signal is passed through a linear time-invariant (LTI) filter with an impulse response of $\tilde{h}(t)$. The real component of the output, scaled by a factor of 1/2, is then sampled at $t = T_b$. The sampled output can be separated into two parts: the desired component $S(T_b)$ corresponding to the desired signal $\tilde{s}(t)$ and the noise component $N(T_b)$ corresponding to the noise $\tilde{n}(t)$.

In this framework, the objective in MF design is to derive the LTI filter, $\tilde{h}(t)$, which maximizes the sampled output SNR [86, 92].

$$\mathrm{SNR} = \frac{S^2(T_b)}{\mathrm{E}\left[N^2(T_b)\right]} \quad (2.15)$$

given the received signal $\tilde{r}(t)$ defined in (2.11) as input over an observation interval of $t_1 \leq t \leq t_2$. The function $\mathrm{E}[\cdot]$ represents the expectation operator. The filter $\tilde{h}(t)$ which delivers the maximum SNR is referred to as the SNR maximizing LTI filter or MF. As pointed out earlier in the discussion on the optimization criterion, except for a possible scaling factor, the impulse response of the MF is equivalent to the LTI filter which minimizes MSE.

As shown in [38, 97], the MF for the detection of the zeroth bit $b_0^{(0)}$ is the solution to the following complex Fredholm integral equation based on the complex baseband representation of bandpass signals

$$\frac{1}{4}\int_{t_1}^{t_2}\left[R_{\tilde{n}}(t,u)\tilde{h}^*(T_b-u)+\tilde{R}_{\tilde{n}}(t,u)\tilde{h}(T_b-u)\right]du \;=\; \tilde{a}^{(0)}(t),\;\; t_1\le t\le t_2. \quad (2.16)$$

Strictly speaking, the impulse response is $\tilde{h}(u)e^{jw_cT_b}$. However, for clarity, it is assumed that $w_cT_b = 2\pi l$ where l is an integer so that $e^{jw_cT_b} = 1$. The term $R_{\tilde{n}}(t,u)$ represents the autocorrelation function of the noise while $\tilde{R}_{\tilde{n}}(t,u)$ represents the pseudo-autocorrelation or complementary autocorrelation function of the noise [47][18, p. 312]. In general, given a complex random process $\tilde{X}(t)$, the autocorrelation function and pseudo-autocorrelation functions are defined as

$$R_{\tilde{X}}(t,u) \;=\; \mathrm{E}\left[\tilde{X}(t)\tilde{X}^*(u)\right], \quad (2.17)$$

$$\tilde{R}_{\tilde{X}}(t,u) \;=\; \mathrm{E}\left[\tilde{X}(t)\tilde{X}(u)\right], \quad (2.18)$$

respectively. Both the autocorrelation and pseudo-autocorrelation functions are needed to provide a complete second-order characterization of the joint statistics of the in-phase (real) component and quadrature (imaginary) component of the noise [18, pp. 311-313]. When $\tilde{R}_{\tilde{n}}(t,u) = 0$ for all t and u, the noise $\tilde{n}(t)$ is categorized as *proper* or *circularly symmetric* [47][18, pp. 311-316]. In this situation, (2.16) reduces to the usual integral equation given in [96, pp. 481-484 (13-7.15)] for signal detection in proper complex noise

$$\frac{1}{4}\int_{t_1}^{t_2} R_{\tilde{n}}(t,u)\tilde{h}^*(T_b-u)du \;=\; \tilde{a}^{(0)}(t),\;\; t_1\le t\le t_2. \quad (2.19)$$

Otherwise, when the noise is *improper* (or no longer circularly symmetric), (2.16) must be solved instead.

In summary, once $\tilde{a}^{(0)}(t)$ is given, the MF solution $\tilde{h}(t)$ will depend upon the form of the two noise autocorrelation functions: $R_{\tilde{n}}(t,u)$ and $\tilde{R}_{\tilde{n}}(t,u)$. Their forms, which depend on the modelling of the interferer signal parameters, are described in Chapter 3.

2.4 Unifying Framework for Enhanced Single-User DS-CDMA Receivers

This section describes a general framework for the synthesis and organization of enhanced single-user DS-CDMA receivers. As mentioned in section 2.3.3, information on interferer signal parameters plays an important role in designing the LTI filter which maximizes SNR. Although the primary interest of the thesis is in developing the CLMF, by altering the amount of signal parameter information available to the receiver, other forms of the filter (including each of the enhanced single-user detectors described in section 2.2.4 and Fig. 2.7) can be designed.

Section 2.4.1 describes a generalized model of information on interferer signal parameters. Section 2.4.2 then describes the various filter realizations whose form changes according to the level of information available to the receiver. The description shall be conceptual in nature. Rigorous mathematical descriptions are relegated to Chapters 3 and 4.

2.4.1 Generalized Model of Information on Interferer Signal Parameters

A generalized model of information on interferer signal parameters is presented. As listed in Table 2.2, the information on interferer signal parameters may consist of their spreading sequences $\{a_n^{(k)} \mid k \in [1, K], n \in (-\infty, \infty)\ \}$, bit delays $\{\tau_k\}_{k=1}^K$, chip delays $\{T_k\}_{k=1}^K$, signal powers to N_o ratio $\{P_k/N_o\}_{k=1}^K$ or net MAI powers to N_o ratio γ/N_o. The set of phase-offsets $\{\theta_k\}_{k=1}^K$ are assumed to be random and i.i.d. where each θ_k is uniformly distributed over $\theta_k \in [0, 2\pi)$. The effect of fixed phase-offsets is considered later. Moreover, among the four sets of parameters, it is essentially the modelling of the spreading sequences and bit delays which determines the three distinctive models. The three basic models, which are the primary focus of this thesis, are summarized in Table 2.3. These are, in order of increasing information, unlocked, chip-delay

Table 2.3 The three basic models of information on interferer signal parameters. The symbol $\surd$ indicates those parameters which are required.

Model of interferers	Spreading sequences $a_n^{(k)}$	Bit delays $\{\tau_k\}_{k=1}^K$	Chip delays $\{T_k\}_{k=1}^K$
unlocked			
chip-delay locked			$\surd$
bit-delay locked	$\surd$	$\surd$	

locked and bit-delay locked interferers. For example, the model of chip-delay locked interferers refers to the case where interferer chip delays are known whereas their spreading sequences are unknown.

In the first two models, long sequence spreading is assumed. In the third model of bit-delay locked interferers, however, short sequence spreading is assumed as a special case. As pointed out in section 2.2.4, the one-shot linear MMSE and decorrelator were developed under the constraint of short sequence spreading. Thus, to derive the same filters under this common framework, short sequence spreading shall be assumed when interferer spreading sequences are known. If, on the other hand, long sequence spreading were employed, their filter response would have to be re-computed at the bit rate as discussed in section 2.2.5.

The main emphasis of the thesis is on the three basic parameter models just described. However, several variants of the three models are considered as well in Chapter 3, Chapter 4 and Appendix D. The variants can be formed by considering: the effect of information on interferer phase-offsets, the presence of inter-symbol interference (ISI) and the presence of both unlocked and chip-delay locked interferers. The effect of phase-offsets and ISI are examined, respectively, for applications such as fixed wireless local loops (where the phase-offsets of users may change very slowly during bit transmissions) and applications where N may very small. Furthermore, the thesis considers the combination of only unlocked and chip-delay locked interferers to obtain realizations compatible with long sequence spreading.

2.4.2 Enhanced Single-User DS-CDMA Receivers

The various models concerning information on interferer signal parameters have now been established. The purpose of this section is to illustrate how the model determines the form of the SNR maximizing LTI filter and how each of the enhanced single-user receivers in Fig. 2.7 can be derived. Table 2.4 summarizes the parameter requirements for each of the enhanced single-user receivers. As will explained later, the BLMF refers to the one-shot linear MMSE detector while the D-BLMF refers to the one-shot decorrelator. The table includes the limiting form of the NWMF and CLMF referred to as D-NWMF and D-CLMF, respectively, as $N_o \to 0$. The order of receiver description in the following section proceeds from top to bottom from the knowledge of absolutely no interferer parameters to the knowledge of all interferer parameters. The column furthest to the right characterizes the MAI process as being either wide-sense stationary (WSS) or wide-sense cyclostationary (WSCS) with a period of either T_c or T_b.

Table 2.4 Realization of the enhanced single-user receivers according to known signal parameters. The symbol $\surd$ indicates those parameters required by the receiver. The characterization of the MAI is listed as well.

Enhanced single-user receiver	Spreading sequences $a_n^{(k)}$	Bit delays $\{\tau_k\}_{k=1}^K$	Chip delays $\{T_k\}_{k=1}^K$	Signal powers to N_o level $\{P_k/N_o\}_{k=1}^K$	Net MAI power to N_o level γ/N_o	MAI characterization
CMF						white WSS
NWMF					$\surd$	coloured WSS
D-NWMF						coloured WSS
CLMF			$\surd$	$\surd$		WSCS T_c
D-CLMF			$\surd$			WSCS T_c
BLMF	$\surd$	$\surd$		$\surd$		WSCS T_b
D-BLMF	$\surd$	$\surd$				WSCS T_b

Two additional comments regarding the following sections are in order. First, the CMF is listed in Table 2.4 and included in the following descriptions as the starting point of the enhanced single-user receivers. That is, the CMF corresponds to the degenerate situation where no information on interferers is necessary. And second, the sections make liberal references to the results of Chapters 3 and 4 to justify the framework and to provide an understanding of the organization of the two chapters.

No Information on Interferers — CMF

When the power spectral density (PSD) of MAI is flat, MAI can be characterized as a white WSS process. As pointed out in section 4.3.2, this characterization occurs when each interferer bit delay is uniformly distributed over $\tau_k \in [0, T_b)$ and the frequency response of the chip filter is constant over the bandwidth B of interest. In this case, the SNR maximizing LTI filter is the conjugated and time-reversed version of the transmitted spreading waveform. This is the well-known CMF.

Unlocked Interferers — NWMF

This realization takes advantage of the observation that the PSD of MAI is generally not flat for practical chip filter designs. When the bit delays and spreading sequences of the interferers are unknown, the interferers and the MAI are referred to as being *unlocked*. As shown in sections 3.2.1 and 4.3.1, when interferers are unlocked, the

PSD of the MAI is determined by $\tilde{q}(t)$, γ and T_c. As long as the frequency response of the chip filter is not constant over the bandwidth B of interest (and each interferer bit delay is uniformly distributed over $\tau_k \in [0, T_b)$), the MAI can be characterized as a coloured WSS random process. As shown in sections 3.2 and 4.3, the SNR maximizing LTI filter in this case is the noise-whitening MF (NWMF) derived previously in [86].

Unlocked Interferers — D-NWMF

Under MAI-limited conditions where the AWGN PSD level is small (ie. $N_o \to 0$), the NWMF reduces to a decorrelator-type NWMF referred to as the D-NWMF. As shown in section 4.3.2, it consists of an inverse chip filter followed by a despreading filter. It can be formed from the CMF by replacing the CMF chip filter with the inverse chip filter. Similar to the CMF, the D-NWMF has the feature of being completely independent of all interferer signal parameters.

Chip-Delay Locked Interferers — CLMF

When the chip delays of interferers are fixed and known, the interferers and the MAI are referred to as being *chip-delay locked*. As shown in section 3.3.1, the MAI can be modelled as being WSCS [71, 98, 99] with a period of T_c when the interferer spreading sequences are modelled as random sequences. Given the knowledge of each interferer signal power to N_o ratio as well as their chip delays, the SNR maximizing filter assumes a form referred to as the chip-delay locked MF (CLMF). Knowledge of interferer spreading sequences is unnecessary. The CLMF is derived in sections 3.3 and 4.4. Furthermore, as pointed out in section 4.4.1, it reduces to the NWMF when the excess bandwidth of the chip waveform is $\alpha = 0$ (since the WSCS MAI then becomes WSS).

Chip-Delay Locked Interferers — D-CLMF

Under MAI-limited conditions where $N_o \to 0$, the CLMF converges to a filter whose response is independent of interferer signal powers. This yields the decorrelator-type chip-delay locked MF (D-CLMF) derived in section 3.3.6. The D-CLMF is analogous to the application of the zero-forcing criterion for the complete suppression of ISI [18] without regards to the enhancement of the background AWGN. In this case, the MAI is completely suppressed [18].

Bit-Delay Locked Interferers — BLMF

When interferer spreading sequences (under the condition of short sequence spreading) and bit delays are fixed and known, the interferers and the MAI are referred to as being *bit-delay locked.* As shown in section 3.4.1, the bit-delay locked MAI can be modelled as being WSCS with a period of T_b (under the constraint of short sequence spreading). Given the knowledge of the signal power to N_o for each bit-delay locked interferer, as shown in section 3.4, the SNR maximizing filter is the one-shot linear MMSE detector derived previously in [62]. To conform with the framework of this thesis, the one-shot linear MMSE detector is also referred to as the bit-delay locked MF (BLMF).

Bit-Delay Locked Interferers — D-BLMF

Similar to the D-NWMF and D-CLMF, under MAI-limited conditions where $N_o \to 0$, the BLMF converges to a filter whose response is independent of the interferer signal powers. As shown in section 3.4.6, the BLMF converges to the the one-shot decorrelator derived previously in [51, 60]. To conform with the framework of this thesis, the one-shot decorrelator is also referred to as the decorrelator-type bit-delay locked MF (D-BLMF).

Chapter 3

Matched Filters for DS-CDMA: Finite Observation Interval

The aim of this chapter is to derive MFs for DS-CDMA systems when the observation interval of the received signal is finite. The derivation of the MFs when the observation interval is infinite is presented in Chapter 4. Section 3.1 explains the steps involved in the synthesis of MFs for the finite observation case. The following four sections then derive the MF under the various models of information on interferer signal parameters as described in section 2.4.1. Section 3.6 discusses the effect of information on interferer phase-offsets. Section 3.7 presents a signal space interpretation of the MFs.

3.1 Method of Synthesis

This section explains the process in designing the MF for the finite observation interval case. First, the form of the integral equation to be solved is developed. Second, the steps involved in solving the integral equation to obtain the MF impulse response are outlined. And third, a note on the numerical examples contained in this chapter is given.

3.1.1 Development of the Integral Equation

In the finite observation interval case, the received signal is observed over the duration of one bit symbol period. The period selected corresponds to the zeroth symbol of the desired user $b_0^{(0)}$ such that $t \in [0, T_b]$. By setting the limits $t_1 = 0$ and $t_2 = T_b$, the integral equation in (2.16) becomes

$$\frac{1}{4}\int_0^{T_b} R_{\tilde{n}}(t,u)\tilde{h}^*(T_b-u)+\tilde{R}_{\tilde{n}}(t,u)\tilde{h}(T_b-u)du \quad = \quad \tilde{a}^{(0)}(t), \quad 0 \le t \le T_b. \qquad (3.1)$$

The filter impulse response $\tilde{h}(u)$ which maximizes SNR is obtained by solving the integral equation in (3.1). The next step is to determine the expressions for the autocorrelation and pseudo-autocorrelation functions of the noise in (3.1).

Assuming that the thermal noise $\tilde{w}(t)$ and MAI $\tilde{I}(t)$ are independent processes, the autocorrelation function of the noise $\tilde{n}(t)$ from (2.13) can be evaluated and written as

$$R_{\tilde{n}}(t,u) \quad = \quad R_{\tilde{w}}(t,u)+R_{\tilde{I}}(t,u). \qquad (3.2)$$

The autocorrelation function of the background AWGN $\tilde{w}(t)$ is, from section 2.1.3,

$$R_{\tilde{w}}(t,u) \quad = \quad 2N_o\delta(t-u). \qquad (3.3)$$

The autocorrelation function of the MAI $\tilde{I}(t)$, represented by $R_{\tilde{I}}(t,u)$, has yet to be determined. As described in section 2.4.1, its form shall depend on how the interferers are modelled. The noise pseudo-autocorrelation function can be written as

$$\tilde{R}_{\tilde{n}}(t,u) \quad = \quad \tilde{R}_{\tilde{I}}(t,u) \qquad (3.4)$$

since AWGN is assumed to be proper and $\tilde{R}_{\tilde{w}}(t,u)=0$. The substitution of (3.2), (3.3) and (3.4) into (3.1) transforms (3.1) into a Fredholm integral equation of the second kind [100]

$$\tilde{f}^*(t)+\frac{1}{2N_o}\int_0^{T_b} R_{\tilde{I}}(t,u)\tilde{f}^*(u)+\tilde{R}_{\tilde{I}}(t,u)\tilde{f}(u)du \quad = \quad \tilde{a}^{(0)}(t), \quad 0 \le t \le T_b \qquad (3.5)$$

where for notational compactness, the correlating signal

$$\tilde{f}(t) \quad = \quad \frac{N_o}{2}\tilde{h}(T_b-t) \qquad (3.6)$$

has been introduced. Once the correlating signal is determined, the impulse response of the MF can then be obtained from $\tilde{h}(t)=\frac{2}{N_o}\tilde{f}(T_b-t)$.

The next step required to solve for the MF involves determining the expressions for two MAI autocorrelation functions: $R_{\tilde{I}}(t,u)$ and $\tilde{R}_{\tilde{I}}(t,u)$ embedded in (3.5). Their form will depend on the models discussed in section 2.4.1. Once these expressions are determined, the remaining step involves solving the integral equation of (3.5) to obtain the LTI filter $\tilde{f}(t)$ which maximizes SNR. The solution $\tilde{f}(t)$ to the integral equation will depend upon $\tilde{a}^{(0)}(t)$ and the form of the two MAI autocorrelation functions. Depending on the MAI model, this eventually leads to the realization of either the NWMF, CLMF, BLMF or several other variants of these solutions. The variants occur under three additional conditions as described in section 2.4.1. These are the MAI-limited condition where $N_o \to 0$, the condition where phase-offset parameters of the interferers are known and the condition where both unlocked and chip-delay locked interferers are present.

In the single-user case ($K = 0$), $\tilde{I}(t) = 0$ and, hence, $R_{\tilde{I}}(t,u) = \tilde{R}_{\tilde{I}}(t,u) = 0$. In this case, the solution to the integral equation of (3.5) is $\tilde{f}(t) = \tilde{a}^{(0)*}(t)$. Thus, $\tilde{h}(t) = \frac{2}{N_o}\tilde{a}^{(0)*}(T_b - t)$. This is the well-known impulse response of the CMF which maximizes SNR in additive white noise.

3.1.2 On Solving the Fredholm Integral Equation

Various methods of solving the integral equation (3.5) associated with the finite observation interval exist. Two methods are employed: the discretization of the integral equation (via numerical integration) and the method of separable kernels [100, Chapter 2] [101, Chapter 5]. The former is a brute-force method whereby the integration interval is discretized and the integral is approximated by a summation. The accuracy of this method depends upon the coarseness of discretization. The latter, though much more mathematically involved, offers several advantages over the former. It leads to an exact solution, insight into the MF design and analytical expressions for both the SNR and near-far resistance. With regards to terminology, the term, kernel, refers to either of the two autocorrelation functions in the integrand of the integral equation (3.5). In addition, separable kernels are also known as degenerate kernels [102, p. 13] or Pincherle-Goursat kernels [100, p. 55].

3.1.3 Note on Numerical Examples

In all the numerical examples to be presented in this chapter, each transmitter employs direct-sequence binary phase-shift keying (DS-BPSK) and the rectangular chip waveform

$$\tilde{q}(t) = \begin{cases} 1, & 0 \le t < T_c \\ 0, & \text{otherwise.} \end{cases} \tag{3.7}$$

The spreading factor is $N = 8$ and the desired user's spreading sequence is $\mathbf{a}^{(0)} = [+ - + + - - - +]$. The symbols + and − refer to 1 and −1, respectively, while, for the kth user,

$$\mathbf{a}^{(k)} = [a_0^{(k)}, a_1^{(k)}, \ldots, a_{N-1}^{(k)}]. \quad (3.8)$$

3.2 Unlocked Interferers

In this section, the MF is derived for the situation where the interferers are unlocked as explained in section 2.4.2. This has already been solved for the particular case of the rectangular chip pulse in [86]. Nonetheless, the case of unlocked users is re-examined for three reasons. First, it supplements the work of [86] in that a general solution is derived to accommodate any desired chip waveform. Second, this lends insight into the internal structure of the NWMF solution. And third, it provides part of the building blocks necessary when the combination of unlocked and chip-delay locked interferers is considered later in section 3.5.

3.2.1 MAI Autocorrelation Function — NWMF

Since the interferers are unlocked, the bit delays $\{\tau_k\}_{k=1}^{K}$ of the interferers are unknown. The bit delays are modelled as being independently and identically distributed (i.i.d.) where each τ_k is uniformly distributed over $\tau_k \in [0, T_b)$. As shown in Appendix B.1.1, the autocorrelation function for the unlocked MAI can then be expressed as

$$R_{\tilde{I}}^{(U)}(t,u) = 2\gamma R_{\tilde{q}}^{(U)}(t-u) \quad (3.9)$$

where the net power of the unlocked MAI is represented by

$$\gamma = \sum_{k=1}^{K} P_k. \quad (3.10)$$

The autocorrelation function of the chip waveform is

$$R_{\tilde{q}}^{(U)}(\tau) = \frac{1}{T_c}\int_{-\infty}^{\infty} \tilde{q}(y+\tau)\tilde{q}^*(y)dy. \quad (3.11)$$

Since (3.9) is time-invariant, the MAI is WSS. The PSD expression of the MAI is derived in Appendix F.1 and given by (F.1). With respect to the MAI pseudo-autocorrelation function, as shown in Appendix B.1.2, knowledge of interferer phase-offsets does not affect the unlocked case since

$$\tilde{R}_{\tilde{I}}^{(U)}(t,u) \equiv 0. \tag{3.12}$$

3.2.2 Towards a Separable Kernel — NWMF

To solve the integral equation based on the method of separable kernels, the MAI autocorrelation function $R_{\tilde{I}}^{(U)}(t,u)$ in (3.9) must be approximated by a separable kernel. A separable kernel or degenerate kernel possesses the special form: $\sum_l^L A_l(x)B_l^*(y)$ where $L < \infty$ [102, p. 13]. The approximation can be realized by noting that the kernel $R_{\tilde{I}}^{(U)}(t,u)$ is square integrable, positive definite and Hermitian. A sufficient condition for a kernel $R(t,u)$ to be positive definite is that $R(t,u)$ be the Fourier transform of a spectral density [103, p. 726] [104, pp. 376–377] [105, Appendix A]. The kernel $R_{\tilde{I}}^{(U)}(t,u)$ in (3.9) satisfies this condition since its Fourier transform is given by $S_{\tilde{I}}^{(U)}(f)$ in (F.1). A kernel is characterized as being Hermitian (or symmetric in the real case) when $R^*(u,t) = R(t,u)$. Thus, since $R_{\tilde{I}}^{(U)}(t,u)$ is continuous, Hermitian and has only positive eigenvalues, then according to Mercer's theorem [100, 101, 102], the following series

$$\sum_{j=1}^{\infty} \lambda_j \phi_j(t)\phi_j^*(u) \tag{3.13}$$

converges to the kernel of (3.9) absolutely and uniformly. The eigenvalues λ_j and eigenfunctions $\phi_j(t)$ can be obtained by solving the homogeneous Fredholm integral equation

$$\lambda\phi(t) = \int_0^{T_b} R_{\tilde{I}_U}(t,u)\phi(u)du. \tag{3.14}$$

Upon substitution of (3.9), this becomes

$$\lambda'\phi(t) = \int_0^{T_b} R_{\tilde{q}}^{(U)}(t-u)\phi(u)du \tag{3.15}$$

where $\lambda' = \lambda/(2\gamma)$ and the normalized eigenvalues $\lambda_j' = \lambda_j/(2\gamma)$ are independent of γ and depend only the chip waveform. Since a finite series is required for a separable kernel, we can use the approximation

$$R_{\tilde{I}}^{(U)}(t,u) = 2\gamma \sum_{j=1}^{N_U} \lambda_j' \phi_j(t)\phi_j^*(u). \tag{3.16}$$

The issue of how large an N_U to choose is delayed until the next section.

3.2.3 Solution — NWMF

To calculate the MF solution for unlocked interferers via the separable kernel method, (3.16), $R_{\bar{I}}(t,u) = R_{\bar{I}}^{(U)}(t,u)$, (3.12) and $\tilde{R}_{\bar{I}}(t,u) = \tilde{R}_{\bar{I}}^{(U)}(t,u)$ are substituted into the integral equation of (3.5). With some simplifications, this leads to

$$\tilde{f}^*(t) + \frac{\gamma}{N_o}\sum_{j=1}^{N_U} \lambda'_j f_j^{(U)*}\phi_j(t) = \tilde{a}^{(0)}(t), \quad 0 \le t \le T_b \tag{3.17}$$

where

$$f_j^{(U)} = \int_0^{T_b} \phi_j(u)\tilde{f}(u)du. \tag{3.18}$$

As shown in Appendix C.1, the coefficient can be expressed as

$$f_j^{(U)} = \frac{a_j^{(U)}}{1 + \frac{\gamma}{N_o}\lambda'_j} \tag{3.19}$$

where

$$a_j^{(U)} = \int_0^{T_b} \tilde{a}^{(0)*}(t)\phi_j(t)dt. \tag{3.20}$$

Re-arrangement of (3.17) using (3.19) gives the approximated matched filter solution:

$$\hat{f}(t) = \tilde{a}^{(0)*}(t) - \sum_{j=1}^{N_U} \frac{\frac{\gamma}{N_o}\lambda'_j}{1 + \frac{\gamma}{N_o}\lambda'_j} a_j^{(U)}\phi_j^*(t), \quad 0 \le t \le T_b \ . \tag{3.21}$$

This filter which maximizes SNR for unlocked interferers is referred to as the NWMF [86]. It consists of two parts: the CMF $\tilde{a}^{(0)*}(t)$ and a second filter which estimates that part of the MAI correlated with $\tilde{a}^{(0)}(t)$. The latter, referred to as the MAI estimation filter, is a linear combination of the N_U eigenfunctions $\{\phi_j^*(t)\}_{j=1}^{N_U}$. In computing the MAI estimation filter, λ'_j, $a_j^{(U)}$ and $\phi_j^*(t)$ for $j \in [1, N_U]$ can be pre-computed and stored. The problem, however, is that a large bank of these coefficients would have to be stored since the spreading waveform $\tilde{a}^{(0)}(t)$ changes with each bit symbol under long sequence spreading. If this were feasible, the only varying parameter would be γ/N_o and the complexity in computing $\hat{f}(t)$ in (3.21) would be independent of K and N.

The issue of selecting N_U can now be treated. The N_U is chosen so that the solution in (3.21) approximates to a desired degree of accuracy, the ideal solution which sets $N_U \to \infty$. First, the error function is defined as $\epsilon_U(t) = \tilde{f}(t) - \hat{f}(t)$, It describes the difference between the approximated solution $\tilde{f}(t)$ in (3.21) and the ideal solution. This leads to $\epsilon_U(t) = -\sum_{j=N_U+1}^{\infty} \frac{\frac{\gamma}{N_o}\lambda'_j}{1+\frac{\gamma}{N_o}\lambda'_j} a_j^{(U)} \phi_j^*(t)$. The L_2 norm is selected as the error criterion of interest. Using (3.18), the L_2 norm of the normalized error function over $t \in [0, T_b]$ becomes

$$\|\epsilon_U(t)\|_2^2 = \sum_{j=N_U+1}^{\infty} |a_j^{(U)}|^2 \left(1 + \frac{N_o}{\gamma\lambda'_j}\right)^{-2}. \tag{3.22}$$

By applying the Schwarz inequality to (3.20), $|a_j^{(U)}|^2 \leq E_a$ where $E_a = \int_0^{T_b} |\tilde{a}^{(0)}(t)|^2 dt$. Substitution of this into (3.22) yields $\|\epsilon_U(t)\|_2^2 \leq E_a \sum_{j=N_U+1}^{\infty} \left(1 + \frac{N_o}{\gamma\lambda'_j}\right)^{-2}$. Hence, given γ/N_o and the maximum tolerable error, ϵ_U, in the L_2 norm sense, N_U is chosen to satisfy the inequality

$$E_a \sum_{j=N_U+1}^{\infty} \left(1 + \frac{N_o}{\gamma\lambda'_j}\right)^{-2} \leq \epsilon_U. \tag{3.23}$$

Next, the limiting form of the NWMF is examined when either $\gamma \to 0$ or $N_o \to 0$. In the limit, as $\gamma \to 0$, (3.21) reduces to the CMF of $\hat{f}(t) = \tilde{a}^{(0)}(t)$. This should be expected since the MAI then disappears and only AWGN remains. On the other hand, in the MAI limited case when $N_o \to 0$, (3.21) can be simplified using

$$\tilde{a}^{(0)*}(t) = \sum_{j=1}^{\infty} a_j^{(U)} \phi_j^*(t). \tag{3.24}$$

The expression in (3.24) utilizes the property that, since $R_{\tilde{I}}^{(U)}(t, u)$ is positive definite (as explained in section 3.2.2), the eigenfunctions $\{\phi_j^*(t)\}_{j=1}^{\infty}$ form a complete orthonormal set over $t \in [0, T_b]$ [104, pp. 376–377]. Substitution of (3.24) into (3.21) and (3.21) into (3.6) leads to

$$\tilde{h}(T_b - t) = \sum_{j=1}^{\infty} \frac{1}{\frac{N_o}{2} + \frac{\gamma}{2}\lambda'_j} a_j^{(U)} \phi_j^*(t). \tag{3.25}$$

In the limit, as $N_o \to 0$, (3.25) reduces to $\tilde{h}(T_b - t) = \frac{2}{\gamma}\sum_j \frac{1}{\lambda'_j} a_j^{(U)} \phi_j^*(t)$. This solution is referred to as the decorelator-type NWMF (D-NWMF). By removing the scaling factor $2/\gamma$ (which does not affect filter design [92, p. 174]), it can be seen that the impulse response is independent of all interferer signal parameters. Based on signal space concepts, from (3.16), $2\gamma\lambda'_j$ represents the interferer power associated with the MAI projected on $\phi_j(t)$. By expressing the received signal in terms of its projections on $\phi_j(t)$, it can be seen that the D-NWMF tends to emphasize those projections where MAI is weak (small $2\gamma\lambda'_j$) and de-emphasize those projections where MAI is strong (large $2\gamma\lambda'_j$).

3.2.4 Structure —NWMF

The internal structure of the NWMF is illustrated in Fig. 3.1. The top branch is

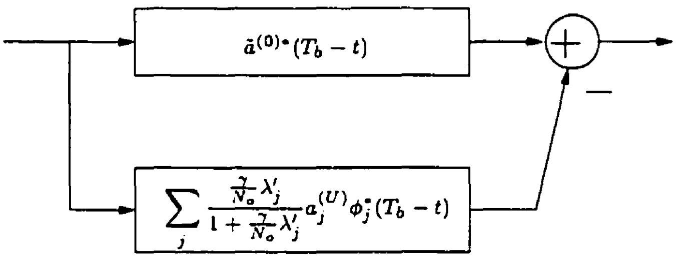

Fig. 3.1 Internal structure of the MF solution $\frac{N_o}{2}\tilde{h}(t)$ when the interferers are unlocked.

the conjugate and time-reversed version of the spreading waveform of the desired user given in (2.8) for $k = 0$. This branch alone corresponds to the CMF for the desired user. The function of the bottom branch is to estimate that part of the unlocked MAI which is correlated with the desired user's spreading waveform. The output of the bottom filter is then subtracted from the CMF output to remove the undesired contributions from the unlocked MAI. The structure has a linear interference cancellation type structure.

3.2.5 Numerical Example — NWMF

Fig. 3.2 shows an example of the MF solution in the presence of a single interferer ($K = 1$) at a power level equal to that of the desired user ($P_1 = P_0$). This is labelled as and is equivalent to the NWMF [86]. Unlike the CMF response, the NWMF response attempts to take into account the presence of MAI. Given an interferer chip delay of T_1 (for example, $T_1 = 0.5T_c$), it is important to note that the interferer signal remains constant (at a value of either ± 1) over each sub-interval $t \in (lT_1, (l+1)T_1)$ for $l \in [-1, 7]$. The correlation over each sub-interval is very small as long as $T_1 \neq 0$.

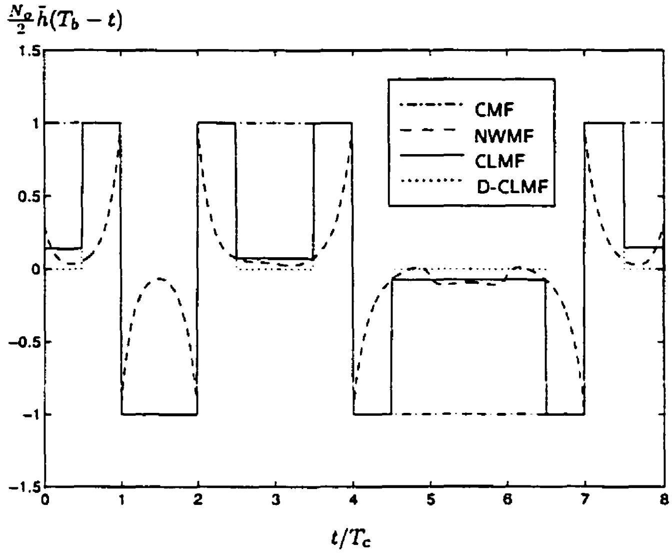

Fig. 3.2 $\frac{N_o}{2}\tilde{h}(T_b - t)$ when $E_b/N_o = 20$ dB, $K = 1$, $P_1 = P_0$ and $T_1 = 0.5T_c$.

Consequently, the NWMF response tends to suppress the interfering signal. On the other hand, the correlation between the NWMF response and the desired signal is reduced as well. Furthermore, the loss of effectiveness of the NWMF with respect to AWGN can be observed from the amount of deviation of its response from the CMF response (which is optimal in AWGN). In addition, as the MAI to thermal noise power diminishes, the solution approaches the unfiltered version of the spreading waveform (ie. the CMF). In effect, the NWMF strikes a balance in the suppression of both MAI and AWGN to maximize SNR without the knowledge of interferer chip delays or other individual signal parameters. To obtain the eigenfunctions and eigenvalues, the homogeneous equation (3.14) was solved via the discretization method. In this plot where $E_b/N_o = 20$ dB and $\epsilon_U = 0.05$ (as defined in (3.23)), a value of $N_U = 100$ was used.

3.3 Chip-Delay Locked Interferers

The MF for chip-delay locked interferers is derived next. This section proceeds in a fashion similar to the development of the NWMF. The difference between the two sections appears in the model of information on interferer signal parameters as described in section 2.4.2. Initially, it is assumed that the individual signal power to N_o ratios are known. Later, section 3.3.6 considers the MF realization under MAI-limiting conditions ($N_o \to 0$) when knowledge of signal powers becomes unnecessary.

3.3.1 MAI Autocorrelation Function — CLMF

The two autocorrelation functions for the chip-delay locked interferers are derived. They are both conditioned on the chip delays and signal powers of the interferers. As shown in Appendix B.2.1, the MAI autocorrelation function can be expressed as

$$R_{\tilde{I}}^{(C)}(t,u) = \sum_{k=1}^{K} R_{\tilde{s}(k)}^{(C)}(t,u) \tag{3.26}$$

where

$$R_{\tilde{s}(k)}^{(C)}(t,u) = 2P_k \sum_{n=-\infty}^{\infty} \tilde{q}(t - T_k - nT_c)\tilde{q}^*(u - T_k - nT_c). \tag{3.27}$$

There are several important observations concerning the autocorrelation function. First, the phases, $\{\theta_k\}_{k=1}^{K}$, disappear from (3.26) regardless of whether they are known or unknown. Second, $R_{\tilde{I}}^{(C)}(t,u)$ is a function of the chip delays T_k, defined in (2.3), and not the bit delays τ_k. Third, the autocorrelation function in (3.26) is periodic with respect to T_c since $R_{\tilde{I}}^{(C)}(t + T_c, u + T_c) = R_{\tilde{I}}^{(C)}(t,u)$. The periodic property of (3.26) indicates that the chip-delay locked MAI is, in fact, wide-sense cyclostationary (WSCS) with a period of T_c [71, 98]. This observation is the critical point of departure from the characterization of the MAI as a coloured WSS process in the unlocked case. And fourth, characteristic of WSCS processes, the instantaneous MAI power $\mathrm{E}[|\tilde{I}(t)|^2] = R_{\tilde{I}}^{(C)}(t,t) = R_{\tilde{I}}^{(C)}(t + T_c, t + T_c)$ is periodic with T_c [106]. An example of $R_{\tilde{I}}^{(C)}(t,u)$ is given in Fig. 3.3 for rectangular chip pulses when $K = 1$, $T_1 = 0.5T_c$ and $P_1 = 1/2$ over $0 \le t, u \le 8T_c$. The example illustrates the periodic nature of $R_{\tilde{I}}^{(C)}(t,u)$. The chip delay T_1 shifts $R_{\tilde{I}}^{(C)}(t,u)$ along the diagonal $u = t$. With respect to the MAI pseudo-autocorrelation function, as shown in Appendix B.2.2, since the phase-offsets θ_k are unknown and modelled as uniformly distributed over $\theta_k \in [0, 2\pi)$, $\tilde{R}_{\tilde{I}}^{(C)}(t,u) \equiv 0$ and the MAI is proper.

3.3.2 Towards a Separable Kernel — CLMF

The chip-delay locked kernel of (3.26) nearly possesses the form of a separable kernel except for the infinite number of terms in (3.27). This obstacle can be overcome by a couple of observations to reduce (3.26) to a series with a finite number of terms. If

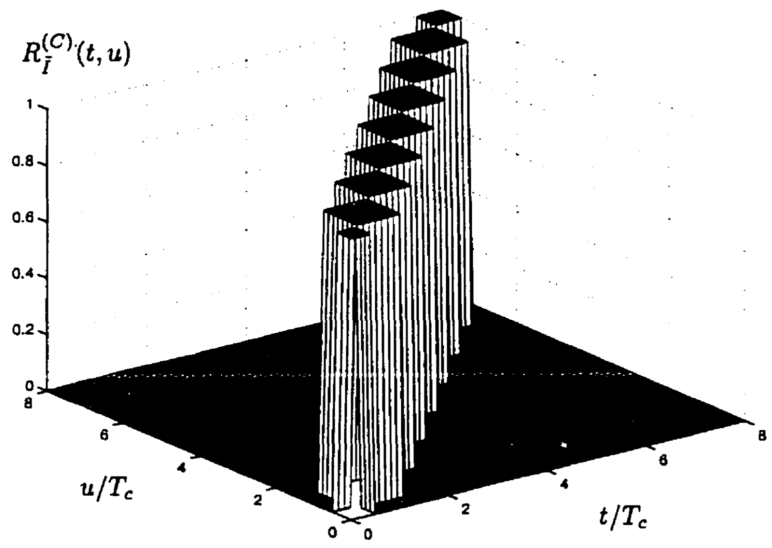

Fig. 3.3 MAI autocorrelation function $R_{\tilde{I}}^{(C)}(t,u)$ for rectangular chip pulses when $K=1$, $T_1 = 0.5T_c$ and $P_1 = 1/2$.

the chip pulse is time-limited (TL) to a duration of $(2M-1)T_c$ such that

$$\tilde{q}(t) \quad = \quad 0, \quad \text{if } t < (-M+1)T_c \text{ or } t \geq MT_c \tag{3.28}$$

for an integer, M, satisfying $1 \leq M < \infty$, then the only terms needed in (3.27) must have indices satisfying $t - T_k - MT_c < nT_c < t - T_k + (M-1)T_c$ and $u - T_k - MT_c < nT_c < u - T_k + (M-1)T_c$ given t, u and T_k. Since the interval of interest in the integral equation is $0 \leq t, u < T_b$ and since the chip delay satisfies $0 \leq T_k < T_c$, therefore, the only required terms satisfy $-M \leq n \leq N + M - 2$. For example, for the rectangular pulse, $M = 1$ and $-1 \leq n \leq N - 1$.

When the chip pulses are strictly bandlimited (BL), $\tilde{q}(t)$ can be readily approximated by a truncated TL version. This can be achieved by selecting a sufficiently large M whereby the truncated TL pulse contains nearly all (eg. 99.99%) of the energy of the original BL pulse. Hence, with some re-arrangement, (3.27) can be rewritten as, for $0 \leq t, u \leq T_b$,

$$R_{\tilde{s}(k)}^{(C)}(t,u) \quad = \quad 2P_k \sum_{n=-M}^{N+M-2} \tilde{q}(t - T_k - nT_c)\tilde{q}^*(u - T_k - nT_c) \tag{3.29}$$

which is now in the form of a separable kernel.

3.3.3 Solution — CLMF

To calculate the MF solution for the chip-delay locked interferers, $R_{\bar{I}}(t,u) = R_{\bar{I}}^{(C)}(t,u)$, $\tilde{R}_{\bar{I}}(t,u) \equiv 0$, (3.26) and (3.29) is substituted into the integral equation of (3.5). This leads to

$$\tilde{f}^*(t) + \sum_{k=1}^{K} \frac{P_k}{N_o} \sum_{n=-M}^{N+M-2} f_{k,n}^{(C)*} \tilde{q}(t - T_k - nT_c) \quad = \quad \tilde{a}^{(0)}(t), \quad 0 \le t \le T_b \tag{3.30}$$

where

$$f_{k,n}^{(C)} \quad = \quad \int_0^{T_b} \tilde{q}(u - T_k - nT_c)\tilde{f}(u)du. \tag{3.31}$$

The calculation of the unknown coefficients, $f_{k,n}^{(C)}$, has been relegated to Appendix C.2. Computation of these coefficients requires $K^2(N+2M-1)(N+2M)$ integrations and the solution of a set of $K(N+2M-1)$ linear equations with $K(N+2M-1)$ unknowns which are the coefficients $f_{k,n}^{(C)}$. The number of operations required to solve the set of equations is on the order of $\mathcal{O}\big(K^3(N+2M-1)^3/3\big)$ [63]. Once the coefficients are computed, the MF remains the same until either the spreading sequence of the desired user changes under long sequence spreading or when the signal parameters of interferers change. Under long sequence spreading, since the coefficients would have to re-computed at the bit rate, this would involve an extremely large number of numerical operations which would pose a significant problem in the context of implementation. As will be shown in Chapter 4, the large computational complexity per bit symbol associated with the CLMF can be significantly reduced.

By re-arranging and conjugating (3.30), the solution to the integral equation becomes

$$\tilde{f}(t) \quad = \quad \tilde{a}^{(0)*}(t) - \sum_{k=1}^{K} \frac{P_k}{N_o} \sum_{n=-M}^{N+M-2} f_{k,n}^{(C)} \tilde{q}^*(t - T_k - nT_c), \quad 0 \le t \le T_b. \tag{3.32}$$

This filter which maximizes SNR when interferers are chip-delay locked shall be referred to as the CLMF. As in the unlocked MAI case, the CLMF in (3.32) consists of two parts: the CMF and a second filter which estimates that part of the MAI correlated with $\tilde{a}^{(0)}(t)$. The MAI estimation filter of the CLMF is a linear combination of the $K(N+2M-1)$ basis functions $\{\tilde{q}^*(t - T_k - nT_c) |\ n \in [-M, N+M-2],\ k \in [1,K]\}$. The basis function indexed by n and k is the conjugated chip filter $\tilde{q}^*(t)$ delayed by $T_k + nT_c$. The same set of basis functions can be used to construct the chip-delay locked MAI $\tilde{I}(t)$ given by (2.10) and (2.6).

3.3.4 Structure — CLMF

The structure of the CLMF is illustrated in Fig. 3.4. As in the NWMF solution,

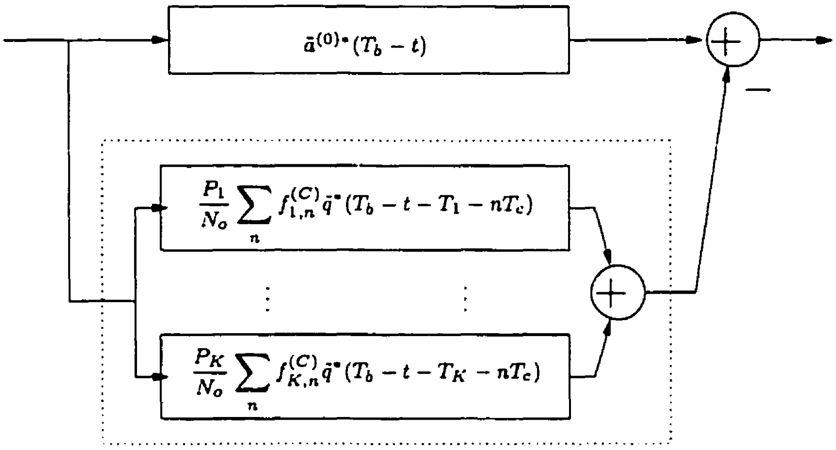

Fig. 3.4 Internal structure of the MF solution $\frac{N_o}{2}\tilde{h}(t)$ when the interferers are chip-delay locked.

the top branch represents the CMF for the desired user. Each of the remaining K branches enclosed inside the dotted box estimates that part of the MAI from a chip-delay locked interferer correlated with the desired user's spreading waveform. The sum of the outputs from the lower branches constitutes an estimate of the MAI embedded in the CMF output. The estimate is then subtracted from the CMF output resulting in a linear interference cancellation structure.

In comparing, the MAI estimation filters of the NWMF and CLMF, the former attempts to remove signals of interferers, which could potentially have any chip delay, correlated with $\tilde{a}^{(0)}(t)$. That is, the former estimates the MAI whose basis functions span the infinite set $\{\tilde{q}^*(t - x - nT_c) | \, x \in [0, T_c)\}$ even though the set is, in fact, finite under chip-delay locked conditions. Consequently, the latter need only estimate and remove MAI contained in a smaller signal space spanned by the finite set of basis functions.

3.3.5 Numerical Example — CLMF

Fig. 3.2 illustrates an example of the chip-delay locked MF (CLMF) solution and the conventional MF (CMF) when $K = 1$, $P_1 = P_0$, $E_b/N_o = 20$ dB and at a chip delay of $T_\mathrm{I} = 0.5T_c$. The solution strikes a balance in suppressing both AWGN and locked MAI. However, unlike the NWMF, it takes advantage of the interferer chip delay information for improved noise suppression. The chip delay parameter allows the receiver to know a-priori the permissible transition instants of the interferer's spreading signal. This is possible even though the interferer's spreading sequence is unknown since the chip rates among all the users are identical. The interferer signal remains constant (at a value of either ± 1) over each sub-interval $t \in (lT_\mathrm{I}, (l+1)T_\mathrm{I})$ for $l \in [-1, 7]$. The correlation of the CLMF response with the interferer signal over each sub-interval is very small. In fact, for the D-CLMF solution to be explained in the following section, the correlation over each sub-interval is zero. Consequently, like the NWMF response, the CLMF response effectively suppresses the interfering signal. In contrast to the NWMF, however, the correlation of the CLMF response with the desired signal is increased. The difference between the responses of the CLMF and NWMF of [86] serves as an early indication of the gain in SNR achievable by the CLMF over the NWMF to be discussed in section 5.2. In addition, as $P_\mathrm{I} \to 0$ leaving only AWGN, the MF approaches the CMF.

3.3.6 Effect of MAI-Limited Conditions — D-CLMF

In this section, the CLMF solution of (3.32) is re-examined when the noise is dominated by MAI as $N_o \to 0$. This results in a decorrelator-type CLMF (D-CLMF) which does not need signal power parameter information. By defining $f_{k,n}^{(DC)} = \frac{P_k}{N_o} f_{k,n}^{(C)}$, (3.32) can be rewritten as

$$\tilde{f}(t) = \tilde{a}^{(0)*}(t) - \sum_{k=1}^{K_L} \sum_{n=-M}^{N+M-2} f_{k,n}^{(DC)} \tilde{q}^*(t - T_k - nT_c) \quad 0 \le t \le T_b. \tag{3.33}$$

Furthermore, from Appendix C.2, as $N_o \to 0$, (C.9) tends to

$$\boldsymbol{C}^{(C)} \boldsymbol{f}^{(DC)^{\mathrm{H}}} = \boldsymbol{a}^{(C)^{\mathrm{H}}} \tag{3.34}$$

where $\boldsymbol{f}^{(DC)^{\mathrm{H}}} = \frac{1}{N_o} \boldsymbol{P}^{(C)} \boldsymbol{f}^{(C)^{\mathrm{H}}}$ and $\boldsymbol{f}^{(C)^{\mathrm{H}}}$ denotes the Hermitian transpose of $\boldsymbol{f}^{(C)}$ (with complex conjugation). The expressions for $\boldsymbol{a}^{(C)^{\mathrm{H}}}$ and $\boldsymbol{C}^{(C)}$ can be found in Appendix C.2. Since the interfering signal powers and N_o disappear in (3.33) and (3.34), the unknown coefficients in (3.33), $f_{k,n}^{(DC)}$, can be obtained by solving (3.34) since $\boldsymbol{f}^{(DC)} = \left[\boldsymbol{f}_1^{(DC)} \cdots \boldsymbol{f}_{K_L}^{(DC)}\right]$ and $\boldsymbol{f}_k^{(DC)} = \left[f_{k,-M}^{(DC)}, \ldots, f_{k,N+M-2}^{(DC)}\right]$ for $k \in [1, K_L]$. An example of the D-CLMF is given in Fig. 3.2 using the parameters given in section 3.3.5. This solution which partially overlaps that for the CLMF is orthogonal to all possible realizations of $\tilde{s}^{(1)}(t)$ given any bit symbols, spreading sequence, or signal power assigned to user 1 as long as $T_1/T_c = 0.5$.

The D-CLMF solution is the desired user's spreading signal with its projection on the space containing all possible constructions of the interferers' signal removed. In contrast to the CLMF, the D-CLMF does not require the interferer signal powers. The D-CLMF requires only the interferer chip delays. Its deficiency is the enhancement of AWGN since it neglects the presence of AWGN.

3.4 Bit-Delay Locked Interferers

The derivation of the MAI autocorrelation function and MF for bit-delay locked interferers which follows is based on the model of information on interferer signal parameters given in section 2.4.2. The resulting MF solutions are equivalent to the one-shot linear MMSE detector [62] and one-shot decorrelator [51, 60]. The difference is the path taken to reach the same solution. The derivation is presented, nonetheless, to emphasize and demonstrate the fact that the inadequacy of the CMF in DS-CDMA is not a shortcoming of MF theory. This section demonstrates that MF theory can yield the same two detectors under the framework given in section 2.4. Furthermore, it is stressed that short sequence spreading is assumed and that knowledge of the interferer bit delays and spreading sequences is required as well. Without the short sequence spreading constraint, as pointed out in section 2.2.5, the complexity associated with re-computing the MF response at the bit rate would be prohibitively high.

3.4.1 MAI Autocorrelation Function — BLMF

The autocorrelation function for the bit-delay locked MAI is conditioned on the knowledge of the spreading sequences, bit delays and signal powers of the interferers. As shown in Appendix B.3.1, it can be expressed as

$$R_{\tilde{I}}^{(B)}(t,u) \quad = \quad \sum_{k=1}^{K} R_{\tilde{s}^{(k)}}^{(B)}(t,u) \tag{3.35}$$

where

$$R_{\tilde{s}^{(k)}}^{(B)}(t,u) \quad = \quad 2P_k \sum_{m=-\infty}^{\infty} \tilde{a}^{(k)}(t-mT_b)\tilde{a}^{(k)*}(u-mT_b). \tag{3.36}$$

The bit-delay locked MAI is a WSCS process [98, 71] with a period of T_b since $R_{\tilde{I}}^{(B)}(t+T_b, u+T_b) = R_{\tilde{I}}^{(B)}(t,u)$. With respect to the MAI pseudo-autocorrelation function, as shown in Appendix B.3.2, since the phase-offsets θ_k are unknown and modelled as uniformly distributed over $\theta_k \in [0, 2\pi)$, $\tilde{R}_{\tilde{I}}^{(B)}(t,u) \equiv 0$.

3.4.2 Towards a Separable Kernel — BLMF

The bit-delay locked kernel of (3.35) nearly possesses the form of a separable kernel except for the infinite number of terms. This obstacle can be overcome in a manner similar to that discussed for the chip-delay locked case in section 3.3.2 by noting that $0 \le \tau_k < T_b$, that $\tilde{a}^{(k)}(t)$ exists only over $-MT_c \le t \le (N+M-1)T_c$ using (2.8) and (3.28) and that the interval of interest in the integral equation is $0 \le t \le T_b$. Under these conditions, the only terms needed in (3.36) satisfy $M_1 \le m \le M_2$ where $M_1 = -1 + \left\lfloor \frac{-(M-1)}{N} \right\rfloor$ and $M_2 = \left\lceil \frac{M-1}{N} \right\rceil$. For example, for the rectangular pulse, $M = 1$, $M_1 = -1$, $M_2 = 0$ and $m \in \{-1, 0\}$. This corresponds to the signal associated with the two bit symbols of an interferer which overlaps that associated with the signal of the desired user's bit symbol $b_0^{(0)}$. Consequently, (3.35) can be expressed in the form of the separable kernel:

$$R_{\tilde{I}}^{(B)}(t,u) = \sum_{k=1}^{K} 2P_k \sum_{m=M_1}^{M_2} \tilde{a}^{(k)}(t-\tau_k-mT_b)\tilde{a}^{(k)*}(u-\tau_k-mT_b) \qquad (3.37)$$

for $0 \le t, u \le T_b$.

3.4.3 Solution — BLMF

To calculate the MF solution for the bit-delay locked interferers, $R_{\tilde{I}}(t,u) = R_{\tilde{I}}^{(B)}(t,u)$, $\tilde{R}_{\tilde{I}}(t,u) \equiv 0$ and (3.37) are substituted into the integral equation of (3.5). This leads to

$$\tilde{f}^*(t) + \sum_{k=1}^{K} \frac{P_k}{N_o} \sum_{m=M_1}^{M_2} f_{k,m}^{(B)*}\tilde{a}^{(k)}(t-\tau_k-mT_b) = \tilde{a}^{(0)}(t), \quad 0 \le t \le T_b \qquad (3.38)$$

where

$$f_{k,m}^{(B)} = \int_0^{T_b} \tilde{a}^{(k)}(u-\tau_k-mT_b)\tilde{f}(u)du. \qquad (3.39)$$

The calculation of the unknown coefficients, $f_{k,m}^{(B)}$, has been relegated to Appendix C.3. Computation of these coefficients requires $K^2M_3(M_3-1)$ integrations where

$M_3 = M_2 - M_1 + 1$ and the solution of a set of KM_3 linear equations with the KM_3 unknowns $f_{k,m}^{(B)}$. The number of operations required to solve the set of equations is on the order of $\mathcal{O}\left(\frac{(KM_3)^3}{3}\right)$ [63]. Once the coefficients are computed, the MF remains the same until there is a change in the signal parameters of interferers only under the condition of short sequence spreading. Otherwise, like the CLMF, they would have to be re-computed at the bit rate.

By re-arranging and conjugating (3.38), the solution to the integral equation becomes

$$\tilde{f}(t) \quad = \quad \tilde{a}^{(0)*}(t) - \sum_{k=1}^{K} \frac{P_k}{N_o} \sum_{m=M_1}^{M_2} f_{k,m}^{(B)} \tilde{a}^{(k)*}(t - \tau_k - mT_b), \quad 0 \leq t \leq T_b. \quad (3.40)$$

This filter which maximizes SNR when interferers are bit-delay locked is the one-shot linear MMSE filter developed in [62]. For brevity, it shall be referred to as the BLMF. As in the previous unlocked and chip-delay locked cases, the BLMF in (3.40) consists of two parts: the CMF and a second filter which estimates that part of the MAI correlated with $\tilde{a}^{(0)}(t)$. When interferers are bit-delay locked, the MAI estimation filter is a linear combination of the KM_3 basis functions $\{\tilde{a}^{(k)*}(t-\tau_k-mT_b)\,|\; n \in [M_1, M_2],\, k \in [1, K]\,\}$. These are the same basis functions which can represent the bit-delay locked MAI $\tilde{I}(t)$ given by (2.10) and (2.7). The basis function indexed by m and k is the conjugated spreading waveform $\tilde{a}^{(k)*}(t)$ associated with the kth interferer delayed by $T_k + nT_c$. For example, when the rectangular pulse is used, $M_3 = 2$ and the number of basis functions is then $2K$. In general, the number of basis functions is much smaller for the BLMF in comparison to that for the CLMF.

3.4.4 Structure — BLMF

The structure of the BLMF is illustrated in Fig. 3.5. The top branch represents the CMF for the desired user. The lower set of filters enclosed in the dotted box is the MAI estimation filter. Each of the K filter enclosed within the box estimates that part of the MAI from a bit-delay locked interferer correlated with the desired user's spreading waveform. The net contribution constitutes an estimate of the MAI correlated with $\tilde{a}^{(0)}(t)$ which is then subtracted from the CMF output.

Next, the MAI estimation filters of the CLMF and BLMF are compared. To maintain clarity, $K = 1$; the observations which follow can be generalized for $K > 1$. Given the interferer chip delay and signal power, the former removes MAI generated by all possible spreading sequences since the CLMF assumes random chips. In reality,

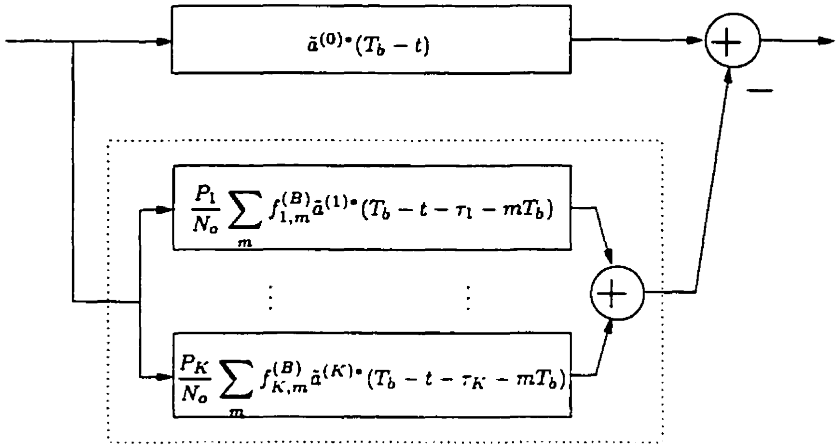

Fig. 3.5 Internal structure of the MF solution $\frac{N_o}{2}\tilde{h}(t)$ when the interferers are bit-delay locked.

however, only a small subset of spreading sequences are permissible due to bit modulation and the constraint of short sequence spreading. In contrast, since the latter has knowledge of the interferer's spreading sequence and bit delay, only the MAI, formed from the permissible subset of spreading sequences with the basis functions $\{\tilde{a}^{(1)*}(t - \tau_1 - mT_b)\}$, is removed.

The development of the BLMF assumed short sequence spreading. The effect of removing this constraint is examined. Under long sequence spreading, $\tilde{a}^{(k)}(t)$ for $k \in [0, K]$ would have to be re-defined such that $a_{n+iN}^{(k)}$ would replace $a_n^{(k)}$ in (2.8). As described in section 3.4.3, $K^2 M_3(M_3 - 1)$ integrations and an additional $\mathcal{O}\left(\frac{(KM_3)^3}{3}\right)$ operations would be necessary for each bit to be detected. Thus, although the BLMF can be designed for long sequence spreading, its excessive computational complexity severely limits its practical usefulness.

3.4.5 Numerical Example — BLMF

Fig. 3.6 illustrates an example of the BLMF when $K = 1$, $P_1 = P_0$, $E_b/N_o = 5$ dB and $\tau_1 = 0$. The spreading sequence of the interferer is $\mathbf{a}^{(1)} = [- + - - + - ++]$. As with the CLMF, the BLMF strikes a balance in suppressing both the AWGN and bit-delay locked MAI. As $P_1 \to 0$, the BLMF approaches the CMF as can be expected when MAI disappears and the noise is AWGN. As $N_o \to 0$, the MF approaches the decorrelator-type BLMF (D-BLMF) to be discussed in section 3.4.3.

The ability (and, hence, performance) of the BLMF, relative to that of the CLMF,

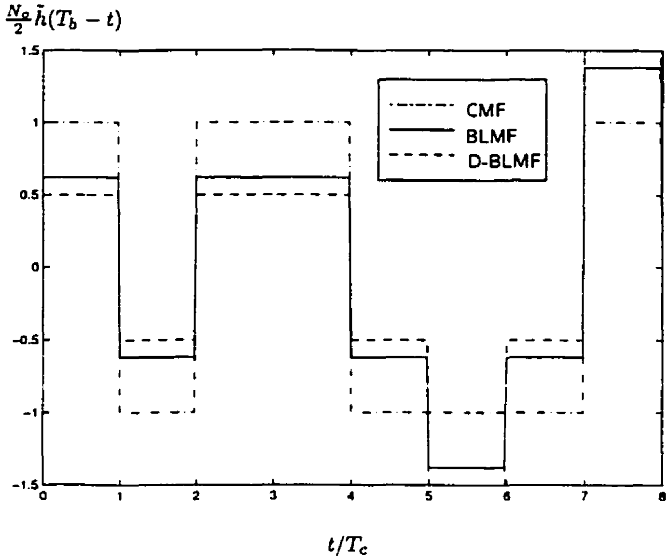

Fig. 3.6 $\frac{N_o}{2}\tilde{h}(T_b - t)$ when $E_b/N_o = 5$ dB, $K = 1$, $P_1 = P_0$ and $\tau_1 = 0$.

in suppressing both MAI and AWGN can be assessed by examining their impulse responses. Since the CMF $\tilde{a}^{(0)*}(T_b - t)$ maximizes SNR in an AWGN dominated environment, how closely the CLMF and BLMF resemble the CMF indicates how well either performs against the AWGN component of the noise. Due to the presence of MAI, however, both responses deviate from that of the CMF. The CLMF response differs more so than that of the BLMF. This is because, as pointed out in section 3.4.4, given the interferer bit delays and spreading sequences, the MAI estimation filter of the BLMF can estimate more accurately the MAI, formed from a restricted set of spreading sequences, correlated with $\tilde{a}^{(0)*}(T_b - t)$. In contrast, with only chip delay information, the MAI estimation filter of the CLMF removes much more from $\tilde{a}^{(0)*}(T_b - t)$ than necessary since it accounts for all potential spreading sequences.

3.4.6 Effect of MAI-Limited Conditions — D-BLMF

In the same spirit of section 3.3.6, the BLMF solution (3.32) is re-examined when the noise is dominated by MAI as $N_o \to 0$. This results in the D-BLMF (or one-shot decorrelator [51, 60]) which does not require interferer signal powers. By defining $f_{k,m}^{(DB)} = \frac{P_k}{N_o} f_{k,m}^{(B)}$, (3.40) can be rewritten as

$$\tilde{f}(t) \quad = \quad \tilde{a}^{(0)*}(t) - \sum_{k=1}^{K} \sum_{m=M_1}^{M_2} f_{k,m}^{(DB)} \tilde{a}^{(k)*}(t - \tau_k - mT_b), \quad 0 \le t \le T_b. \qquad (3.41)$$

Furthermore, from Appendix C, as $N_o \to 0$, (C.16) tends to

$$\boldsymbol{C}^{(B)} \boldsymbol{f}^{(DB)^{\mathrm{H}}} = \boldsymbol{a}^{(B)^{\mathrm{H}}} \tag{3.42}$$

where $\boldsymbol{f}^{(DB)^{\mathrm{H}}} = \frac{1}{N_o} \boldsymbol{P}^{(B)} \boldsymbol{f}^{(B)^{\mathrm{H}}}$. The expressions for $\boldsymbol{a}^{(B)^{\mathrm{H}}}$ and $\boldsymbol{C}^{(B)}$ can be found in Appendix C.3. Since the interfering signal powers and N_o disappear in (3.41) and (3.42), the unknown coefficients in (3.41), $f_{k,m}^{(DB)}$, can be obtained by solving (3.42) since $\boldsymbol{f}^{(DB)} = \left[\boldsymbol{f}_1^{(DB)} \dots \boldsymbol{f}_{K_L}^{(DB)}\right]$ and $\boldsymbol{f}_k^{(DB)} = \left[f_{k,1}^{(DB)}, \dots, f_{k,N_L}^{(DB)}\right]$ for $k \in [1, K_L]$. An example of the D-BLMF impulse response is given in Fig. 3.6 using the parameters given in section 3.4.5. The response is completely orthogonal to the interferer signal, regardless of its bits or signal power, as long as $\tau_1 = 0$. This can be shown through Fig. 3.6 by graphically computing the correlation between the impulse response labelled as D-BLMF and a scaled version of the spreading waveform of the interferer $c_1 \tilde{a}^{(1)}(t)$. Regardless of the magnitude or polarity of the scaling factor c_1, the correlation is zero.

In general, the D-BLMF is the desired user's spreading signal with its projection on the space containing all possible constructions of the interferers' signal removed. In contrast to the BLMF, it does not require interferer signal powers. However, like the BLMF, it requires the spreading sequences and bit-delays of each interferer.

3.5 Combination of Unlocked and Chip-Delay Locked Interferers

This section considers the MF realization corresponding to the model in which a combination of unlocked and chip-delay locked interferers are present. It relies on many of the results developed in sections 3.2 and 3.3.

3.5.1 Solution — CUMF

The K interferers are divided into two classes of users. The first class consists of K_C chip-delay locked interferers as described in section 3.3 indexed from $k \in [1, K_C]$. The second class consists of K_U unlocked interferers as described in section 3.2 indexed from $k \in [K_C + 1, K_C + K_U]$ such that $K_C + K_U = K$. The MAI autocorrelation function then becomes a combination of (3.26), (3.29) and (3.16):

$$R_I^{(CU)}(t,u) = \sum_{k=1}^{K_C} 2P_k \sum_{n=-M}^{N+M-2} \tilde{q}(t - T_k - nT_c)\tilde{q}^*(u - T_k - nT_c) + 2\gamma_{CU} \sum_{j=1}^{N_U} \lambda'_j \phi_j(t) \phi_j^*(u) \tag{3.43}$$

where $0 \leq t, u \leq T_b$ and $\gamma_{CU} = \sum_{k=K_C+1}^{K_C+K_U} P_k$. Using $R_{\tilde{I}}(t,u) = R_{\tilde{I}}^{(CU)}(t,u)$, (3.43) and $\tilde{R}_{\tilde{I}}(t,u) \equiv 0$, the integral equation of (3.5) can be written as

$$\tilde{f}^*(t) + \sum_{k=1}^{K_C} \frac{P_k}{N_o} \sum_{n=-M}^{N+M-2} f_{k,n}^{(C)*} \tilde{q}(t - T_k - nT_c) + \frac{\gamma_{CU}}{N_o} \sum_{q=1}^{N_U} \lambda_q' f_q^{(U)*} \phi_q(t) = \tilde{a}^{(0)}(t) \quad (3.44)$$

where $0 \leq t \leq T_b$. The calculation of the unknown coefficients: $f_{k,n}^{(C)}$ and $f_q^{(U)}$ can be found in Appendix C.4. Thus, the correlating signal solution becomes

$$\tilde{f}(t) = \tilde{a}^{(0)*}(t) - \sum_{k=1}^{K_C} \frac{P_k}{N_o} \sum_{n=-M}^{N+M-2} f_{k,n}^{(C)} \tilde{q}^*(t - T_k - nT_c) - \frac{\gamma_{CU}}{N_o} \sum_{q=1}^{N_U} \lambda_q' f_q^{(U)} \phi_q^*(t) \quad (3.45)$$

where $0 \leq t \leq T_b$. This shall be referred to as the chip-delay locked and unlocked MF solution (CUMF). The eigenvalues λ_q' are real since the kernels are Hermitian [102]. The MF for both unlocked and chip-delay locked interferers contains three parts: the CMF and two filters which when combined estimate the MAI. The first MAI estimation filter is a linear combination of the $K_C(N + 2M - 1)$ basis functions $\{\tilde{q}^*(t - T_k - nT_c) |\ n \in [-M, N + M - 2],\ k \in [1, K_C]\ \}$. The second MAI estimation filter is a linear combination of the N_U basis functions $\{\phi_j^*(t)\}_{j=1}^{N_U}$.

3.5.2 Structure — CUMF

The internal structure of the MF is shown in Fig. 3.7. The top branch is the CMF for the desired user. The middle group of filters estimate the contributions from the locked MAI while the bottom branch estimates those from the unlocked MAI. These contributions are then subtracted from the CMF output giving the filter a linear interference cancellation type of structure. Knowledge concerning the data decisions, bit delays and spreading sequences of other users is unnecessary.

3.5.3 Numerical Example — CUMF

Fig. 3.8 shows an example of the CUMF when both a locked and unlocked interferer exist with $P_1 = P_2 = P_0$. The NWMF curve represents the NWMF solution for $K_U = 2$, $K_C = 0$. The CUMF solution strikes a balance in trying to suppress the thermal noise, the unlocked and chip-delay locked interferers. As the number of unlocked users increases such that their net power dwarfs that of the locked users, the CUMF approaches the NWMF. However, when the power of the locked user exceeds that of the unlocked users, the CUMF approaches the CLMF.

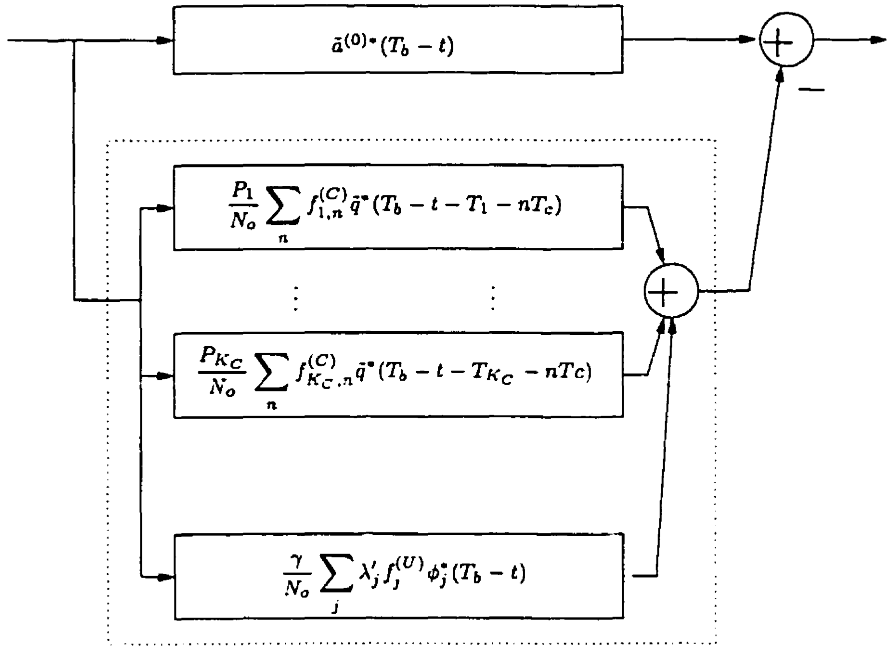

Fig. 3.7 Internal structure of the MF solution $\frac{N_o}{2}\tilde{h}(t)$ with K_C chip-delay locked and K_U unlocked interferers.

3.6 Effect of Phase-Offset Information

This section explains how MF design is affected when the interferer phase-offsets are known to the receiver. As shown in Appendix B.1.2, knowledge of phase-offsets does not affect the NWMF. This section, therefore, examines the effect of phase-offsets on the derivation of the CLMF and BLMF only.

3.6.1 CLMF with Phase-Offset Information

For the CLMF, knowledge of phase-offsets $\{\theta_k\}_{k=1}^{K}$ does not affect the MAI autocorrelation function. As shown in Appendix B.2.2, it does, however, affect the MAI pseudo-autocorrelation function. The function is no longer zero and can be written as

$$\tilde{R}_{\tilde{I}}^{(C)}(t,u) = \sum_{k=1}^{K} 2P_k e^{j2\theta_k} \sum_{n=-M}^{N+M-2} \tilde{q}(t - T_k - nT_c)\tilde{q}(u - T_k - nT_c) \tag{3.46}$$

where the phase-offsets are now imbedded inside (3.46). Substitution of (3.46), (3.26), (3.29), $R_{\tilde{I}}(t,u) = R_{\tilde{I}}^{(C)}(t,u)$ and $\tilde{R}_{\tilde{I}}(t,u) = \tilde{R}_{\tilde{I}}^{(C)}(t,u)$ into (3.5) yields with some

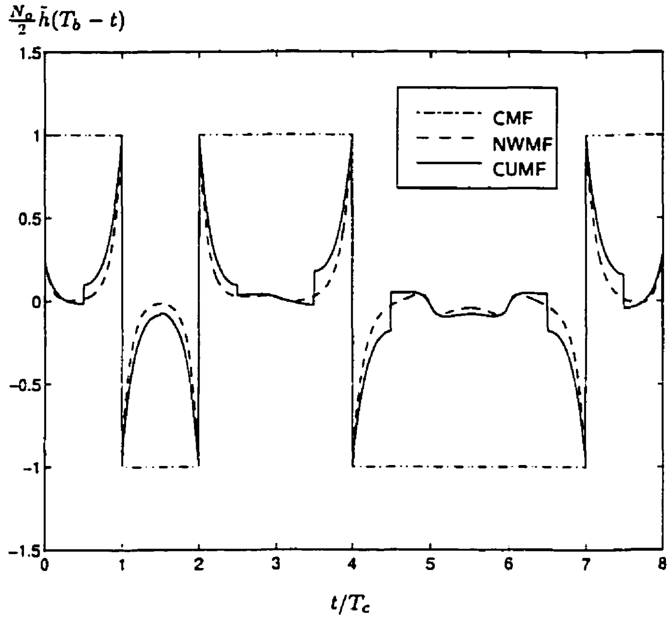

Fig. 3.8 $\frac{N_o}{2}\tilde{h}(T_b - t)$ when $E_b/N_o = 20$ dB, $K_C = 1$, $K_U = 1$ $P_1 = P_2 = P_0$ and $T_1 = 0.5T_c$.

simplifications

$$\tilde{f}(t) = \tilde{a}^{(0)*}(t) - \sum_{k=1}^{K} \frac{2P_k}{N_o} e^{-j\theta_k} \sum_{n=-M}^{N+M-2} |f_{k,m}^{(C)}| \cos\left\{ \arctan\left[\frac{\mathcal{I}m(f_{k,m}^{(C)})}{\mathcal{R}e(f_{k,m}^{(C)})}\right] + \theta_k \right\}$$
$$\cdot \tilde{q}^*(t - T_k - nT_c) \tag{3.47}$$

where $0 \le t \le T_b$ and $f_{k,m}^{(C)}$ has been defined in (3.31). The $K(N + 2M - 1)$ basis functions $\{\tilde{q}^*(t - T_k - nT_c)|\ n \in [-M, N + M - 2],\ k \in [1, K]\ \}$ are the same as those used when the phase-offsets were assumed to be unknown. Knowledge of the phase-offsets enables the filter to estimate the amplitude of an interferer's signal in both its in-phase and quadrature components.

3.6.2 BLMF with Phase-Offset Information

For the BLMF, knowledge of phase-offsets $\{\theta_k\}_{k=1}^{K}$ does not affect the MAI autocorrelation function. As shown in Appendix B.3.2, it does, however, affect the MAI pseudo-autocorrelation function which becomes

$$R_{\tilde{I}}^{(B)}(t, u) = \sum_{k=1}^{K} 2P_k e^{j2\theta_k} \sum_{m=M_1}^{M_2} \tilde{a}^{(k)}(t - \tau_k - mT_b)\tilde{a}^{(k)}(u - \tau_k - mT_b) \tag{3.48}$$

where the same procedure outlined in section 3.4.2 has been used to form a separable kernel. Substitution of (3.48), (3.35), (3.37), $R_{\tilde{I}}(t,u) = R_{\tilde{I}}^{(B)}(t,u)$ and $\tilde{R}_{\tilde{I}}(t,u) = \tilde{R}_{\tilde{I}}^{(B)}(t,u)$ into (3.1) yields with some simplifications

$$\begin{aligned}\tilde{f}(t) &= \tilde{a}^{(0)*}(t) - \sum_{k=1}^{K} \frac{2P_k}{N_o} e^{-j\theta_k} \sum_{m=M_1}^{M_2} |f_{k,m}^{(B)}| \cos\left\{\arctan\left[\frac{\mathcal{I}m(f_{k,m}^{(B)})}{\mathcal{R}e(f_{k,m}^{(B)})}\right] + \theta_k\right\} \\ &\cdot \tilde{a}^{(k)*}(t - \tau_k - mT_b) \qquad (3.49)\end{aligned}$$

where $0 \le t \le T_b$ and $f_{k,m}^{(B)}$ has been defined in (3.39). The KM_3 basis functions $\{\tilde{a}^{(k)*}(t - \tau_k - mT_b)|\ n \in [M_1, M_2],\ k \in [1, K]\ \}$ are the same as those used when phase-offsets were assumed to be unknown. The basic difference between (3.40) and and (3.49) is the presence of the phase-offsets.

In either the chip-delay or bit-delay locked case, knowledge of the phase-offsets introduces a non-zero MAI pseudo-autocorrelation function and requires solving the integral equation (3.5). The resulting impulse responses are, in general, complex even in DS-BPSK when $\tilde{a}^{(0)}(t)$ is real because of the presence of the phase-offset information. Ignoring the pseudo-autocorrelation function by incorrectly assuming that the MAI is proper does not yield the SNR-maximizing filter. On the other hand, a filter derived without the phase-offsets is robust in applications where the phase-offsets change quickly. The effect of phase-offsets upon the CLMF and BLMF has been further investigated in [97] and [38], respectively.

3.7 Signal Space Interpretation

This section presents a signal space interpretation of the MF realizations. Its aim is to provide additional insight into their structure and performance.

As given in (2.9), the received signal consists of: the desired signal $\sqrt{2P_0} b_0^{(0)} \tilde{a}^{(0)}(t)$, MAI $\tilde{I}(t)$ and AWGN $\tilde{w}(t)$. Given a suitable set of orthonormal basis functions spanning the subspace of the MAI, $\mathcal{S}_I$, $\tilde{I}(t)$ from (2.10) and (2.6) can be represented as the column vector $\vec{I}$. An example of $\mathcal{S}_I$ and $\vec{I}$ is given in Fig. 3.9. For unlocked interferers, $\mathcal{S}_I$ is denoted as $\mathcal{S}_I^{(U)}$ and spanned by $\{\phi_j(t)\}_{j=1}^{\infty}$ from section 3.2.2. This set forms a complete orthonormal set over $L_2[0, T_b]$ since $\tilde{R}_{\tilde{I}}^{(U)}(t,u)$ is the Fourier transform of a power spectral density [103, p. 726] [104, pp. 376–377] [105, Appendix A] given by $S_{\tilde{I}}^{(U)}(f)$ in (F.1) where $\tilde{q}(t)$ is assumed to have a Fourier transform $Q(f)$. For chip-delay locked interferers, $\mathcal{S}_I$ is denoted as $\mathcal{S}_I^{(C)}$ and spanned by the set of linearly independent waveforms $\{\tilde{q}(t - T_k - nT_c)|\ k \in [1, K], n \in [-M, N + M - 2]\}$.

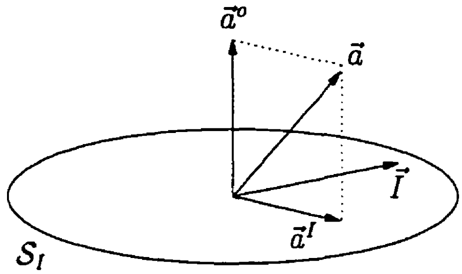

Fig. 3.9 Signal space representation of the desired signal and MAI.

Linear independence is assured as long as $T_k \neq T_i$ where $i \in [1, K]$ and $i \neq k$. If two or more interferers are chip synchronous amongst themselves, the redundant chip waveforms with identical chip delays can be removed. For bit-delay locked interferers, $\mathcal{S}_I$ is denoted as $\mathcal{S}_I^{(B)}$ and spanned by $\{\tilde{a}^{(k)}(t - \tau_k - mT_b) |\ k \in [1, K],\ n \in [M_1, M_2]\ \}$ where M_1 and M_2 are defined in section 3.4.2. These subspaces satisfy $\mathcal{S}_I^{(B)} \subseteq \mathcal{S}_I^{(C)} \subseteq \mathcal{S}_I^{(U)}$.

Proof

The relation $\mathcal{S}_I^{(C)} \subseteq \mathcal{S}_I^{(U)}$ follows since $\mathcal{S}_I^{(U)}$ is the $L_2[0, T_b]$ space. $\mathcal{S}_I^{(C)} \equiv \mathcal{S}_I^{(U)}$ when the excess bandwidth $\alpha = 0$. This is shown by expressing $\tilde{q}(t - T_k - nT_c)$ in terms of its inverse Fourier transform and substituting it into $R_I^{(C)}(t, u)$ in (3.26): $R_I^{(C)}(t, u) = \sum_{k=1}^{K} \frac{2P_k}{T_c} \sum_{n=-\infty}^{\infty} \int_{-\infty}^{\infty} Q(f) Q^*(f - \frac{n}{T_c}) e^{j2\pi f(t-u)} e^{j2\pi n(u-T_k)/T_c} df$. When $\alpha = 0$, $Q(f)Q^*(f - \frac{n}{T_c}) = 0$ for $n \neq 0$ and $R_I^{(C)}(t, u)$ reduces to $R_I^{(U)}(t, u)$ in (3.9).

The relation $\mathcal{S}_I^{(B)} \subseteq \mathcal{S}_I^{(C)}$ follows since only certain linear combinations of the delayed chip waveforms in $\mathcal{S}_I^{(C)}$ are permissible in $\mathcal{S}_I^{(B)}$ (when the spreading sequences are known). $\mathcal{S}_I^{(B)} \equiv \mathcal{S}_I^{(C)}$ when $N = 1$ when $T_b = T_c$, $T_k = \tau_k$ and $\tilde{a}^{(k)}(t - \tau_k - mT_b) = \tilde{q}(t - T_k - mT_c)$.

The desired user's spreading waveform $\tilde{a}^{(0)}(t)$ can be represented as $\vec{a} = \vec{a}^o + \vec{a}^I$ where $\vec{a}^I$ is the projection of $\vec{a}$ on $\mathcal{S}_I$ and $\vec{a}^o$ is the orthogonal component of $\vec{a}$ with respect to $\mathcal{S}_I$. The vector $\vec{a}^o = \vec{0}$ the zero vector in: the unlocked case since $\vec{a}$ lies entirely in $\mathcal{S}_I^{(U)}$; the chip-delay locked case when at least one interferer is chip synchronous with the desired user or when $\alpha = 0$; the bit-delay locked case when interferers are chip synchronous and when $\tilde{a}^{(0)}(t)$ is a linear combination of the spreading waveforms of the interferers. The received signal can be represented as $\vec{r} = \sqrt{2P_0} b_0^{(0)} \vec{a} + \vec{I} + \vec{w}$ where $\vec{w}$ is the vector representation of the AWGN. Its elements, each with zero-mean, satisfy $\mathrm{E}[w_i w_j^*] = 2N_o \delta_{ij}$. An example of the signal space representation of the received signal and its components are depicted in Fig. 3.10.

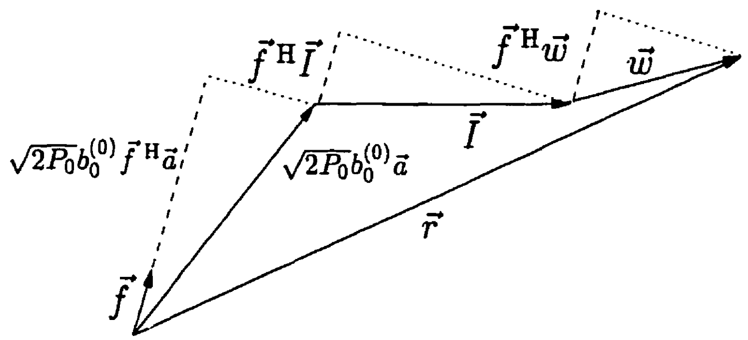

Fig. 3.10 Signal space representation of the received signal $\vec{r}$, its components ($\sqrt{2P_0}b_0^{(0)}\vec{a}$, $\vec{I}$ and $\vec{w}$) and the correlating signal $\vec{f}$.

The LTI filter $\tilde{h}(t)$ is represented by its corresponding correlating signal $\tilde{f}_c(t) = \tilde{h}^*(T_b - t)$ which is represented by the correlating vector $\vec{f}$. The correlating operation can be interpreted as taking the projection of $\vec{r}$ on to $\vec{f}$ if $\vec{f}$ were of unit magnitude. The magnitude of the projection can be broken down into three components: $\sqrt{2P_0}b_0^{(0)}\vec{f}^{\mathrm{H}}\vec{a}$ for the desired user's signal, $\vec{f}^{\mathrm{H}}\vec{I}$ for the MAI and $\vec{f}^{\mathrm{H}}\vec{w}$ for the AWGN. where $\vec{f}^{\mathrm{H}}$ is the Hermitian transpose of $\vec{f}$ (with complex conjugation). Thus, the direction of $\vec{f}$ determines the relative magnitudes of the three components of $\vec{r}$. In fact, when $\vec{a}^o \neq \vec{0}$, by orienting $\vec{f}$ in the same direction as $\vec{a}^o$, the MAI can be completely tuned out. This yields the decorrelator type D-CLMF and D-BLMF solutions.

Using Fig. 3.10 and Fig. 2.9, the SNR in (2.15) can be expressed as SNR $= P_0\left|\mathcal{R}e(\vec{f}^{\mathrm{H}}\vec{a})\right|^2 / \left\{\frac{1}{4}\mathrm{E}\left[|\mathcal{R}e(\vec{f}^{\mathrm{H}}\vec{I} + \vec{f}^{\mathrm{H}}\vec{w})|^2\right]\right\}$. The expression can be re-arranged as

$$\mathrm{SNR} = \frac{P_0\left|\mathcal{R}e(\vec{f}^{\mathrm{H}}\vec{a})\right|^2}{\frac{1}{4}\mathcal{R}e\left\{\vec{f}^{\mathrm{H}}\mathrm{E}\left[\vec{I}\vec{I}^{\mathrm{T}}\right]\vec{f}^* + \vec{f}^{\mathrm{H}}\mathrm{E}\left[\vec{I}\vec{I}^{\mathrm{H}}\right]\vec{f}\right\} + \frac{N_o}{2}\vec{f}^{\mathrm{H}}\vec{f}} \tag{3.50}$$

where $\mathrm{E}\left[\vec{I}\vec{I}^{\mathrm{T}}\right]$ and $\mathrm{E}\left[\vec{I}\vec{I}^{\mathrm{H}}\right]$ are the signal space representations of the MAI pseudo-autocorrelation and MAI autocorrelation functions, respectively, where $\vec{f}^{\mathrm{T}}$ is the transpose of $\vec{f}$ (without the complex conjugation). The SNR value can be adjusted by changing the direction of $\vec{f}$. The direction determines the projection of each received signal component on $\vec{f}$. The vector $\vec{f}$ which maximizes (3.50) is the MF. To solve for the MF, (3.50) can be written as

$$\mathrm{SNR} = \frac{P_0\left(\vec{f}_r^{\,\mathrm{T}}\vec{a}_r\right)^2}{\vec{f}_r^{\,\mathrm{T}}\mathbf{R}_r\vec{f}_r} \tag{3.51}$$

where $\vec{f}_r^{\,\mathrm{T}} = [\mathcal{R}e(\vec{f}^{\,\mathrm{T}}) \mid \mathcal{I}m(\vec{f}^{\,\mathrm{T}})]$, $\vec{a}_r^{\,\mathrm{T}} = [\mathcal{R}e(\vec{a}^{\,\mathrm{T}}) \mid \mathcal{I}m(\vec{a}^{\,\mathrm{T}})]$ and

$$\mathbf{R}_r = \frac{N_o}{2}\mathbf{I} + \frac{1}{2}\begin{bmatrix} \mathrm{E}[\mathcal{R}e(\vec{I})\mathcal{R}e(\vec{I}^{\,\mathrm{T}})] & \mathrm{E}[\mathcal{R}e(\vec{I})\mathcal{I}m(\vec{I}^{\,\mathrm{T}})] \\ \mathrm{E}[\mathcal{I}m(\vec{I})\mathcal{R}e(\vec{I}^{\,\mathrm{T}})] & \mathrm{E}[\mathcal{I}m(\vec{I})\mathcal{I}m(\vec{I}^{\,\mathrm{T}})] \end{bmatrix}. \tag{3.52}$$

As described in [107, pp. 227–229], the MF is $\vec{f}_{\mathrm{r,opt}} = \mathbf{R}_r^{-1}\vec{a}_r$ while the maximum SNR it delivers is $\mathrm{SNR_{opt}} = P_0\,\vec{f}_{\mathrm{r,opt}}^{\,\mathrm{T}}\vec{a}_r$. When the MAI is proper under uniformly distributed phase-offsets $\theta_k \in [0, 2\pi)$, $\mathrm{E}\left[\vec{I}\vec{I}^{\,\mathrm{T}}\right]$ disappears and (3.50) reduces to $\mathrm{SNR} = P_0\,|\mathcal{R}e(\vec{f}^{\,\mathrm{H}}\vec{a})|^2/[\frac{1}{4}\vec{f}^{\,\mathrm{H}}\mathrm{E}(\vec{I}\vec{I}^{\,\mathrm{H}})\vec{f} + \frac{N_o}{2}\vec{f}^{\,\mathrm{H}}\vec{f}]$. In this case, the MF is

$$\vec{f}_{\mathrm{opt}} = \left[\frac{1}{4}\mathrm{E}(\vec{I}\vec{I}^{\,\mathrm{H}}) + \frac{N_o}{2}\mathbf{I}\right]^{-1}\vec{a} \tag{3.53}$$

and $\mathrm{SNR_{opt}} = P_0\,\vec{f}_{\mathrm{opt}}^{\,\mathrm{H}}\vec{a}$. On the other hand, when the MAI is improper where each θ_k is known, the MF solution is given by $\vec{f}_{\mathrm{r,opt}}$ instead. In the absence of MAI, the MF reduces to the CMF where $\vec{f}_{\mathrm{opt}} = \frac{2}{N_o}\vec{a}$ and $\mathrm{SNR_{opt}} = P_0 \cdot \frac{2}{N_o}\vec{a}^{\,\mathrm{H}}\vec{a} = 2E_b/N_o$.

The near-far resistance η_0 of the MF, as shown later in section 5.3.1, is $\eta_0 = \frac{1}{T_b}||\vec{a}^o||^2$ (similar to that given in [62] for the BLMF) where $||\vec{a}^o||^2 = \vec{a}^{o\mathrm{H}}\vec{a}^o$. Since the vector $\vec{a}^o$ is independent of $\vec{f}$, $||\vec{a}^o||^2$ indicates the potential near-far resistance available if $\vec{f}$ is properly designed. The vector $\vec{a}^o$ depends on whether the interferers are unlocked, chip-delay locked or bit-delay locked. When $\mathcal{S}_I \equiv \mathcal{S}_I^{(U)}$, $\vec{a}^o = \vec{0}$ and $\eta_0 = 0$. When $\mathcal{S}_I \equiv \mathcal{S}_I^{(C)}$, $\vec{a}^o = \vec{0}$ and $\eta_0 = 0$ when either $\alpha = 0$ or $T_k = 0$ for at least one interferer. When $\mathcal{S}_I \equiv \mathcal{S}_I^{(B)}$, η_0 for the BLMF reduces to η_0 for the CLMF when $N = 1$ since then $T_b = T_c$, $T_k = \tau_k$, $\tilde{a}^{(k)}(t - \tau_k - mT_b) = \tilde{q}(t - T_k - mT_c)$ and, hence, $\mathcal{S}_I^{(B)} \equiv \mathcal{S}_I^{(C)}$.

3.7.1 Equivalence of Signal Space and Integral Equation MF Solutions

In this section, the NWMF, CLMF and BLMF solutions given in (3.21) (3.32) and (3.40), respectively, are shown to be equivalent to the signal space MF solution $\vec{f}_{\mathrm{opt}}$ for the unlocked, chip delay locked and bit delay locked cases, respectively.

NWMF

For the unlocked case, using (3.17) and noting that $\vec{f}(t) = \frac{N_o}{2}\vec{f}_c^*(t)$, the approximation to $\vec{f}(t)$, $\hat{f}(t)$, can be expressed as

$$\frac{N_o}{2}\vec{f}_{N_U} = \vec{a} - \frac{\gamma}{N_o}\sum_{i=1}^{N_U}\lambda_i' f_i^{(U)*}\vec{\phi}_i \tag{3.54}$$

where $\vec{\phi}_i$ is the signal space representation of the eigenfunction $\phi_i(t)$ and where λ_i' and $\phi_i(t)$ are obtained from solving the homogeneous integral equation in (3.15). From (3.18), $f_i^{(U)} = \frac{N_o}{2}\vec{f}_{N_U}^{\mathrm{H}}\vec{\phi}_i$ and (3.54) can be written as

$$\left[\frac{\gamma}{2}\sum_{i=1}^{N_U}\lambda_i'\vec{\phi}_i\vec{\phi}_i^{\mathrm{H}} + \frac{N_o}{2}\mathbf{I}\right]\vec{f}_{N_U} = \vec{a}. \tag{3.55}$$

As shown in Appendix E.1, $\mathrm{E}[\vec{I}\vec{I}^{\mathrm{H}}] = 2\gamma\sum_{i=1}^{N_U}\lambda_i'\vec{\phi}_i\vec{\phi}_i^{\mathrm{H}}$. Note that $\vec{\phi}_i^{\mathrm{H}}\vec{\phi}_i = \delta_{ij}$ and that $\mathrm{E}[\vec{I}\vec{I}^{\mathrm{H}}]$ is Hermitian and positive definite since $\mathcal{S}_I \equiv \mathcal{S}_I^{(U)}$. Via the unitary decomposition [108, pp. 42–43] of $\mathrm{E}[\vec{I}\vec{I}^{\mathrm{H}}]$, $2\gamma\lambda_i'$ and $\vec{\phi}_i$ form, respectively, the eigenvalues and eigenvectors of $\mathrm{E}[\vec{I}\vec{I}^{\mathrm{H}}]$. The substitution of $\mathrm{E}[\vec{I}\vec{I}^{\mathrm{H}}]$ into (3.55) yields an approximation of $\vec{f}_{\mathrm{opt}}$ in (3.53). The accuracy of the approximation can be determined by first defining $\vec{\epsilon} = \vec{f} - \vec{f}_{N_U}$ where $\vec{f} = \lim_{N_U\to\infty}\vec{f}_{N_U}$. Using (3.55) and (3.21), $\|\vec{\epsilon}\|^2 = \vec{a}^{\mathrm{H}}\vec{a}\sum_{i=N_U+1}^{\infty}[1 + \frac{N_o}{\gamma\lambda_i'}]^{-2}$. Thus, for a maximum tolerable error ϵ_U, N_U is selected to satisfy $\|\vec{\epsilon}\|^2 \leq \epsilon_U$ as in (3.23). Next, it is shown that $\lim_{N_U\to\infty}\|\vec{\epsilon}\|^2 = 0$.

<u>Proof</u>
$\sum_{i=N_U+1}^{\infty}\left[1 + \frac{N_o}{\gamma\lambda_i'}\right]^{-2} = \sum_{i=N_U+1}^{\infty}\left(\frac{\gamma\lambda_i'}{\gamma\lambda_i'+N_o}\right)^2 \leq \sum_{i=N_U+1}^{\infty}\left(\frac{\gamma\lambda_i'}{N_o}\right)^2 = \frac{\gamma}{N_o}\sum_{i=N_U+1}^{\infty}\lambda_i'^2$ where $\lambda_i' > 0$ for all i since $R_{\tilde{I}}^{(U)}(t,u)$ is positive-definite [90, p. 179]. Using the relation: $\sum_{i=1}^{\infty}\lambda_i' = \int_0^{T_b} R_{\tilde{I}}^{(U)}(t,t)dt$ [90, p. 181] [93, p. 144] and $R_{\tilde{I}}^{(U)}(t,u)$ in (3.9), $\sum_{i=1}^{\infty}\lambda_i' = 2\gamma T_b$. Since $(\sum_{i=1}^{\infty}\lambda_i')^2 = (2\gamma T_b)^2$, then $\sum_{i=1}^{\infty}\lambda_i'^2 + \sum_{i=1}^{\infty}\sum_{\substack{j\neq i\\ j=1}}^{\infty}\lambda_i'\lambda_j' = (2\gamma T_b)^2$ and

$$\sum_{i=N_U+1}^{\infty}\lambda_i'^2 = (2\gamma T_b)^2 - \sum_{i=1}^{N_U}\lambda_i'^2 - \sum_{i=1}^{\infty}\sum_{\substack{j\neq i\\ j=1}}^{\infty}\lambda_i'\lambda_j'.$$

Thus, $\lim_{N_U\to\infty}\left(\sum_{i=N_U+1}^{\infty}\lambda_i'^2\right) = (2\gamma T_b)^2 - \lim_{N_U\to\infty}\left(\sum_{i=1}^{N_U}\lambda_i'^2\right) - \sum_{i=1}^{\infty}\sum_{\substack{j\neq i\\ j=1}}^{\infty}\lambda_i'\lambda_j' = 0$ and $\lim_{N_U\to\infty}\|\vec{\epsilon}\|^2 = 0$.

CLMF

For the chip-delay locked case, using (3.32), $\vec{f}(t)$ can be expressed as

$$\frac{N_o}{2}\vec{f} = \vec{a} - \sum_{k=1}^{K} \frac{P_k}{N_o} \sum_{n=-M}^{N+M-2} f_{k,n}^{(C)*} \vec{q}_{k,n} \tag{3.56}$$

where $\vec{q}_{k,n}$ is the signal space representation of $\vec{q}(t - T_k - nT_c)$. From (3.31), $f_{k,n}^{(C)} = \frac{N_o}{2}\vec{f}^{\,\mathrm{H}}\vec{q}_{k,n}$ and (3.56) can be written as

$$\left[\sum_{k=1}^{K} \frac{P_k}{2} \sum_{n=-M}^{N+M-2} \vec{q}_{k,n}\vec{q}_{k,n}^{\,\mathrm{H}} + \frac{N_o}{2}\mathbf{I}\right] \vec{f} = \vec{a}. \tag{3.57}$$

As shown in Appendix E.2, $\mathrm{E}[\vec{I}\vec{I}^{\,\mathrm{H}}] = \sum_{k=1}^{K} 2P_k \sum_{n=-M}^{N+M-2} \vec{q}_{k,n}\vec{q}_{k,n}^{\,\mathrm{H}}$. Its substitution into (3.57) yields $\vec{f}_{\mathrm{opt}}$ in (3.53).

BLMF

For the bit-delay locked case, using (3.40), $\vec{f}(t)$ can be expressed as

$$\frac{N_o}{2}\vec{f} = \vec{a} - \sum_{k=1}^{K} \frac{P_k}{N_o} \sum_{m=M_1}^{M_2} f_{k,m}^{(B)*} \vec{a}_{k,m} \tag{3.58}$$

where $\vec{a}_{k,m}$ is the signal space representation of $\vec{a}(t - \tau_k - mT_b)$. From (3.39), $f_{k,m}^{(B)} = \frac{N_o}{2}\vec{f}^{\,\mathrm{H}}\vec{a}_{k,m}$ and (3.58) can be written as

$$\left[\sum_{k=1}^{K} \frac{P_k}{2} \sum_{m=M_1}^{M_2} \vec{a}_{k,m}\vec{a}_{k,m}^{\,\mathrm{H}} + \frac{N_o}{2}\mathbf{I}\right] \vec{f} = \vec{a}. \tag{3.59}$$

As shown in Appendix E.3, $\mathrm{E}[\vec{I}\vec{I}^{\,\mathrm{H}}] = \sum_{k=1}^{K} 2P_k \sum_{m=M_1}^{M_2} \vec{a}_{k,m}\vec{a}_{k,m}^{\,\mathrm{H}}$. Its substitution into (3.59) yields $\vec{f}_{\mathrm{opt}}$ in (3.53).

3.8 Summary

This chapter has derived the three basic MFs: the NWMF, CLMF and BLMF which maximize SNR for bit symbol detection when interferers are unlocked, chip-delay locked and bit-delay locked, respectively. It has also investigated their variants which arise under: MAI-limited conditions, the presence of both unlocked and chip-delay interferers and the knowledge of interferer phase-offsets. It was found that each realization assumed a canonical structure, similar to that of [65, p. 946], consisting of two parallel LTI filters as shown in Fig. 3.11. The top filter represents the CMF for

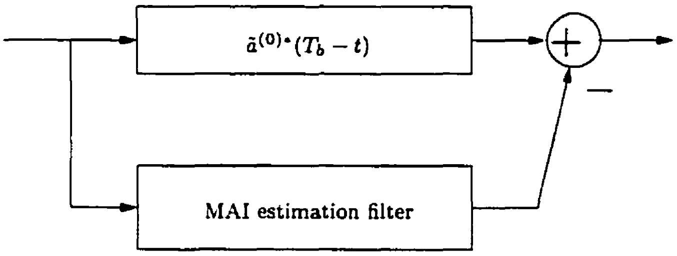

Fig. 3.11 Canonical structure of the MF solution $\frac{N_o}{2}\tilde{h}(t)$.

the desired user. The lower filter estimates noise contributions correlated with the desired user's spreading waveform $\tilde{a}^{(0)}(t)$. The contributions of MAI correlated with $\tilde{a}^{(0)}(t)$ could be more accurately estimated when an increasing amount of information on interferer signal parameters was taken into account in the filter design. When AWGN predominated, the three MF realizations approached the CMF. On the other hand, under MAI-limited conditions ($N_o \to 0$), the three assumed decorrelator-type forms independent of interferer signal powers.

With respect to complexity, it was found that, under the condition of long sequence spreading, the complexity of computing the NWMF at the bit rate was independent of K and N. In contrast, the computational complexity per bit symbol associated with the CLMF and BLMF were very large. The complexity of computing their filter responses, repeatedly at the bit rate, was found to grow with the third power of KN and K, respectively.

Chapter 4

Matched Filters for DS-CDMA: Infinite Observation Interval

This chapter investigates the MFs obtained when the observation interval is extended to infinity [91, 92, 93]. There are two compelling reasons for pursuing the extension to the infinite case. First, it offers an interpretation of MF design in the frequency domain. And second, in comparison to the CLMF developed under the finite observation interval, the extension can lead to significant reductions in computational complexity per bit symbol under long sequence spreading. This shall provide additional insight into the development of adaptive receiver structures, explored later in Chapter 6, which do not require any knowledge of interferer signal parameters.

Section 4.1 describes the method of synthesis for deriving the MFs. Section 4.2 presents the MF solution for the general case when noise is either wide-sense stationary (WSS) or wide-sense cyclostationary (WSCS). The effect of information on interferer phase-offsets is not considered. Their phase-offsets are assumed to be unknown and random. Based on the general solution, sections 4.3 to 4.5 present the MF realizations when interferers are unlocked, chip-delay locked and bit-delay locked, respectively. This yields the NWMF, CLMF and BLMF realizations for the infinite observation interval. Section 4.6 considers the situation when both unlocked and chip-delay locked interferers are present.

4.1 Method of Synthesis

This section explains the process of deriving the MF for the infinite observation interval when interferer phase-offsets are unknown. First, the form of the integral equation to be solved is developed. Second, the steps involved in solving the integral equation to obtain the MF in either WSS or WSCS noise are outlined. And third, one particularly important tool for solving the integral equation known as the Harmonic Series Representation (HSR) of signals is introduced. General treatments of linear filtering in WSCS noise can be found in [109, 70, 74, 82].

4.1.1 Development of the Integral Equation

The form of the integral equation is developed when the duration of the filter impulse response $\tilde{h}(t)$ and, hence, observation interval of the received signal can span $t \in (-\infty, \infty)$. As determined earlier in Chapter 3, when the phase-offset of each interferer is uniformly distributed over $\theta_k \in [0, 2\pi)$, the noise is proper and the pseudo-autocorrelation function disappears. Consequently, the MF response is obtained from the integral equation in (2.19) by letting $t_1 \to -\infty$ and $t_2 \to \infty$ [91, 92, 93] and inserting $R_{\tilde{n}}(t, u)$ from (3.2) and (3.3). This leads to

$$\frac{N_o}{2}\tilde{h}^*(T_b - t) + \frac{1}{4}\int_{-\infty}^{\infty} R_{\tilde{I}}(t, u)\, \tilde{h}^*(T_b - u)\, du \;=\; \tilde{a}^{(0)}(t), \quad -\infty < t < \infty. \quad (4.1)$$

The filter $\tilde{h}(t)$ which maximizes SNR satisfies (4.1).

4.1.2 On Solving the Integral Equation

The method of solving the integral equation (4.1) to obtain the MF solution $\tilde{h}(t)$ is outlined. The description covers the method of solution when the MAI is either WSS or WSCS. In the former, the procedure is fairly straightforward while in the latter, the procedure is much more involved.

When the MAI is WSS, as is the case for unlocked interferers as shown in section 3.2.1, the MAI autocorrelation function satisfies $R_{\tilde{I}}(t, u) = R_{\tilde{I}}(t - u)$ and the integral in (4.1) becomes a convolutional integral. As explained in [92, pp. 175-176] and [91, pp. 199-204], the frequency response of the MF can be obtained readily by taking the Fourier transform of both the left and right hand sides of (4.1) and then conjugating the result. This leads to the MF solution

$$H^{\mathrm{WSS}}(f) \;=\; \frac{Q^*(f)\, \mathcal{A}^{(0)*}(e^{j2\pi f T_c})\, e^{-j2\pi f T_b}}{\frac{N_o}{2} + \frac{1}{4}S_{\tilde{I}}^*(f)} \quad (4.2)$$

using the following relationships. The PSD of the WSS MAI $S_{\tilde{I}}(f)$ is the Fourier transform of $R_{\tilde{I}}(t - u)$. The Fourier transform of $\tilde{a}^{(0)}(t)$ in (2.8) is the product of the Fourier transform $Q(f)$ of the chip waveform $\tilde{q}(t)$ and the discrete-time Fourier transform (DTFT) $\mathcal{A}^{(0)}(e^{j2\pi fT_c}) = \sum_{n=0}^{N-1} a_n^{(0)} e^{-j2\pi nfT_c}$ of the desired user's spreading sequence. When only AWGN is present, $S_{\tilde{I}}(f) = 0$ and (4.2) reduces to the CMF frequency response

$$H^{\mathrm{CMF}}(f) \;=\; \frac{2}{N_o} Q^*(f) \mathcal{A}^{(0)*}(e^{j2\pi fT_c})\, e^{-j2\pi fT_b}. \tag{4.3}$$

This is simply the Fourier transform of the CMF impulse response $\frac{2}{N_o}\tilde{a}^{(0)*}(T_b - t)$. The term $2/N_o$ is a scaling factor which can be removed without affecting the CMF design [92, p. 174].

When, on the other hand, the interferers are chip-delay or bit-delay locked, noise is WSCS with a period of $T \in \{T_c, T_b\}$ as described in sections 3.3.1 and 3.4.1, respectively. The period $T = T_c$ corresponds to the chip-delay locked case while $T = T_b$ corresponds to the bit-delay locked case. In either case, the MAI autocorrelation function no longer satisfies $R_{\tilde{I}}(t, u) = R_{\tilde{I}}(t - u)$. Instead, it is periodically time-varying since $R_{\tilde{I}}(t + T, u + T) = R_{\tilde{I}}(t, u)$. This presents an obstacle to solving the integral equation in (4.1) since the integral is no longer in the form of a convolution. However, the obstacle can be removed by introducing the Harmonic Series Representation (HSR) of signals.

4.1.3 Harmonic Series Representation (HSR) of Signals

In HSR, an arbitrary continuous-time signal is represented by a sum of bandlimited signals [98][109, pp. 247-248]. This is accomplished by passing the continuous-time signal through a set of bandpass filters which in the frequency domain form contiguous segments of the all pass filter with a frequency response of 1 over the bandwidth of the signal. The original signal can be reconstructed by summing all the bandpass filter outputs. The relevance of HSR is its attractive property of enabling the decomposition of a WSCS process into a finite set of jointly WSS processes [98]. This permits the periodically time-varying autocorrelation function $R_{\tilde{I}}(t, u)$ associated with the WSCS MAI process to be expressed as a double Fourier series of time-invariant cross-correlation functions. Consequently, the application of HSR to the signal detection problem in WSCS noise transforms the integral in (4.1) to a sum of convolutional integrals. Hence, (4.1) can be solved by the subsequent application of the Fourier transform as in the WSS case.

Next, the HSRs of $R_{\tilde{I}}(t, u)$, $\tilde{a}^{(k)}(t)$ and $\tilde{h}(u)$ in (4.1) are developed. The introduction of HSR is necessary not only to derive the MF solution when MAI is WSCS, but also to understand the resulting MF structures. The equations (20a) to (21b), (31) and (32) in [109, pp. 247–249] provide a handy reference to the HSR of signals.

HSR of the MAI Autocorrelation Function $R_{\tilde{I}}(t,u)$

In order to obtain the HSR of $R_{\tilde{I}}(t,u)$ for WSCS MAI, the HSR of the MAI is first developed. The WSCS process $\tilde{I}(t)$ with a period of T can be expressed, in terms of bandlimited WSS processes $\tilde{I}_n(t)$, as

$$\tilde{I}(t) = \sum_{n=-M_H}^{M_H} \tilde{I}_n(t) e^{j2\pi nt/T}. \tag{4.4}$$

The process $\tilde{I}_n(t)e^{j2\pi nt/T}$ represents the output of the nth ideal one-sided bandpass filter $W_n(f) = 1$ for $f \in [\frac{n}{T} - \frac{1}{2T}, \frac{n}{T} + \frac{1}{2T}]$ and $W_n(f) = 0$, otherwise, when $\tilde{I}(t)$ is the filter input. Its corresponding baseband representation occupying $f \in [-\frac{1}{2T}, \frac{1}{2T}]$ is simply $\tilde{I}_n(t)$ without the frequency shift term $e^{j2\pi nt/T}$. As a result of bandlimiting the WSCS process with a period of T to a width of $1/T$ [98], $\tilde{I}_n(t)$ is WSS. The term M_H in (4.4) is defined as

$$M_H = \left\lceil BT - \frac{1}{2} \right\rceil \tag{4.5}$$

where B, defined in (2.4), is the bandwidth of the process. Consequently, the total number of WSS processes $\tilde{I}_n(t)$ in (4.4) required to represent $\tilde{I}(t)$ completely is $L_H = 2M_H + 1$.

Based on the HSR of the WSCS MAI, it is now possible to decompose $R_{\tilde{I}}(t,u)$ into a sum of frequency-shifted autocorrelation functions which depend on the time difference $t-u$. The decomposition is achieved by substituting (4.4) into the MAI autocorrelation function $R_{\tilde{I}}(t,u) = \mathrm{E}\left[\tilde{I}(t)\tilde{I}^*(u)\right]$. This yields [109, p. 249]

$$R_{\tilde{I}}(t,u) = \sum_{n=-M_H}^{M_H} \sum_{m=-M_H}^{M_H} r_{nm}^{(\tilde{I})}(t-u) e^{j2\pi nt/T} e^{-j2\pi mu/T} \tag{4.6}$$

where the cross-correlation function $r_{nm}^{(\tilde{I})}(t-u)$ is defined as

$$r_{nm}^{(\tilde{I})}(t-u) = \mathrm{E}[\tilde{I}_n(t)\tilde{I}_m^*(u)]. \tag{4.7}$$

The $r_{nm}^{(\tilde{I})}(t-u)$ in (4.7) depends upon the time difference $t-u$ since each process $\tilde{I}_n(t)$ is WSS. The Fourier transform of $r_{nm}^{(\tilde{I})}(t-u)$ in (4.7) is referred to as the cross spectral density (CSD) and is defined as [98][71, p. 49]

$$R_{nm}^{(\tilde{I})}(f) = \mathcal{F}\left\{r_{nm}^{(\tilde{I})}(\tau)\right\}, \quad |f| \leq \frac{1}{2T}, \tag{4.8}$$

where $\mathcal{F}\{\cdot\}$ denotes the Fourier transform operator. Its actual expression depends on the modelling of the MAI and is presented later in sections 4.3, 4.4 and 4.5.

The HSR can also be used to represent WSS processes and its associated autocorrelation function. This will prove useful in obtaining a general MF solution when MAI is either WSS or WSCS and when MAI includes both unlocked and chip-delay locked interferers. When MAI is WSS, a number of simplifications arise. This is to be expected since HSR is unnecessary in the first place for MAI which is WSS. The correlation between non-overlapping spectral bands disappears and the CSD $R_{nm}^{(\tilde{I})}(f) = 0$ for $m \neq n$ [109]. The $R_{\tilde{I}}(t,u)$ in (4.6) then reduces to the single Fourier series $R_{\tilde{I}}(t-u) = \sum_{n=-M_H}^{M_H} r_{nn}^{(\tilde{I})}(t-u)e^{j2\pi n(t-u)}$. This is the HSR of the autocorrelation function for WSS MAI. The application of the Fourier transform and use of (4.8) returns the PSD for MAI in terms of its HSR: $S_{\tilde{I}}(f) = \sum_{n=-M_H}^{M_H} R_{nn}^{(\tilde{I})}(f - \frac{n}{T})$ where

$$R_{nn}^{(\tilde{I})}(f) = V(f)S_{\tilde{I}}\left(f + \frac{n}{T}\right) \tag{4.9}$$

and where $V(f)$ represents the ideal low pass filter of bandwidth $\frac{1}{2T}$ defined as $V(f) = 1$, if $|f| \leq \frac{1}{2T}$ and $V(f) = 0$, otherwise.

HSR of $\tilde{a}^{(k)}(t)$

Next, the HSR of the kth user's spreading waveform $\tilde{a}^{(k)}(t)$ defined in (2.8) is developed. Based on the HSR of signals described in [109, pp. 247–249], the HSR of the spreading waveform of the kth user is

$$\tilde{a}^{(k)}(t) = \sum_{n=-M_H}^{M_H} \tilde{a}_n^{(k)}(t)\, e^{j2\pi nt/T} \tag{4.10}$$

where the signal $\tilde{a}_n^{(k)}(t)$ represents that part of $\tilde{a}^{(k)}(t)$ bandlimited to $f \in [\frac{n}{T} - \frac{1}{2T}, \frac{n}{T} + \frac{1}{2T}]$ and frequency shifted by n/T to the baseband region of $f \in [-\frac{1}{2T}, \frac{1}{2T}]$. The Fourier transform of $\tilde{a}_n^{(k)}(t)$ is

$$A_n^{(k)}(f) = V(f)A^{(k)}\left(f + \frac{n}{T}\right) \tag{4.11}$$

where $A^{(k)}(f)$, representing the Fourier transform of $\tilde{a}^{(k)}(t)$, can be written as

$$A^{(k)}(f) \quad = \quad Q(f)\,\mathcal{A}^{(k)}(e^{j2\pi fT_c}). \tag{4.12}$$

The Z-transform of the kth user's spreading sequence $a_l^{(k)}$ for $l \in [0, N-1]$ is defined as

$$\mathcal{A}^{(k)}(z) \quad = \quad \sum_{l=0}^{N-1} a_l^{(k)} z^{-l}. \tag{4.13}$$

By substituting (4.12) into (4.11), the Fourier transform of $\tilde{a}^{(k)}(t)$ can be expressed in terms of the HSR of the chip waveform and the discrete-time Fourier transform (DTFT) of the kth user's spreading sequence (obtained by evaluating (4.13) at $z = e^{j2\pi fT_c}$):

$$A_n^{(k)}(f) \quad = \quad Q_n(f)\,\mathcal{A}^{(k)}(e^{j2\pi(f+\frac{n}{T})T_c}). \tag{4.14}$$

The nth HSR component of $Q(f)$ is given by

$$Q_n(f) \quad = \quad V(f)Q\left(f+\frac{n}{T}\right). \tag{4.15}$$

When $T = T_c$ and $k = 0$ for the chip-delay locked case, (4.14) simplifies to $A_n^{(0)}(f) = Q_n(f)\,\mathcal{A}^{(0)}(e^{j2\pi fT_c})$. As will be shown later, this property significantly simplifies the CLMF structure.

HSR of the MF $\tilde{h}(t)$

In a similar fashion, the HSR of the filter response can be expressed as $\tilde{h}(u) = \sum_{l=-M_H}^{M_H} \tilde{h}_l(u)\; e^{j2\pi lu/T}$. Its time-reversed and conjugated version in (4.1) becomes

$$\tilde{h}^*(T_b - u) \quad = \quad \sum_{l=-M_H}^{M_H} \tilde{h}_l^*(T_b - u)e^{j2\pi lu/T} \tag{4.16}$$

noting that T_b is an integer multiple of $T \in \{T_c, T_b\}$. The Fourier transform of the lth HSR component, $\tilde{h}_l(u)$, is

$$H_l(f) \quad = \quad V(f)H\left(f+\frac{l}{T}\right). \tag{4.17}$$

The frequency response of the MF $H(f)$ can then be expressed as the sum of contiguous segments

$$H(f) = \sum_{l=-M_H}^{M_H} H_l\left(f - \frac{l}{T}\right). \tag{4.18}$$

The goal is to now derive the expression for each of the L_H HSR components $H_l(f)$ which in turn define $H(f)$.

4.2 General MF when MAI is Proper WSS or WSCS

Based on the HSR of signals and the MAI autocorrelation function developed in the previous section, this section derives the general MF solution when MAI is proper WSS or proper WSCS. This is followed by a descriptive analysis of the structure of the resulting MF.

4.2.1 Development of the General MF Solution

To solve the integral equation in (4.1), the HSR expressions in (4.6), (4.10) and (4.16) are substituted into (4.1). The subsequent application of the Fourier transform to both sides of the integral equation yields a system of L_H equations with the L_H unknowns $H_m(f)$ which, when conjugated, becomes

$$\frac{N_o}{2}H_n(f) + \frac{1}{4}\sum_{m=-M_H}^{M_H} R_{n,m}^{(\bar{I})*}(f)\, H_m(f) = \mathcal{A}^{(0)*}(e^{j2\pi(f+\frac{n}{T})T_c})\, Q_n^*(f)e^{-j2\pi fT_b}, \tag{4.19}$$

where $|f| \leq \frac{1}{2T}$ and $n \in [-M_H, M_H]$. The $R_{n,m}^{(\bar{I})}(f)$, $\mathcal{A}^{(0)}(z)$, $Q_n(f)$ and $H_n(f)$, are given in (4.8), (4.13) for $k=0$, (4.15) and (4.17), respectively. The L_H equations in (4.19) over $n \in [-M_H, M_H]$ can be expressed as

$$\mathbf{R}(f)\mathbf{H}(f) = \mathbf{Q}(f)\boldsymbol{\mathcal{A}}^{(0)}(e^{j2\pi fT_c})\, e^{-j2\pi fT_b}. \tag{4.20}$$

The matrices and vectors in (4.20) whose elements are functions of $f \leq \frac{1}{2T}$ are defined as follows. The noise CSD matrix $\mathbf{R}(f)$ is defined as

$$\mathbf{R}(f) = \frac{N_o}{2}\mathbf{I}_{L_H} + \frac{1}{4}\mathbf{R}^{(\bar{I})}(f) \tag{4.21}$$

where the MAI CSD matrix is

$$\mathbf{R}^{(\bar{I})}(f) = \begin{bmatrix} R^{(\bar{I})*}_{-M_H,-M_H}(f) & \cdots & R^{(\bar{I})*}_{-M_H,M_H}(f) \\ \vdots & \ddots & \vdots \\ R^{(\bar{I})*}_{M_H,-M_H}(f) & \cdots & R^{(\bar{I})*}_{M_H,M_H}(f) \end{bmatrix}. \tag{4.22}$$

The CSD elements in (4.22) without the conjugation are specified in (4.8). The matrix $\mathbf{R}^{(\bar{I})}(f)$ is Hermitian, since from (4.7), $R^{(\bar{I})*}_{n,m}(f) = R^{(\bar{I})}_{m,n}(f)$. This, in turn, implies that $\mathbf{R}(f)$ in (4.21) is Hermitian. The precise form of $\mathbf{R}^{(\bar{I})}(f)$ shall be specified in the following sections where the interferers may be either unlocked, chip-delay locked or bit-delay locked. The column vector $\mathbf{H}(f)$ specifying the HSR of the MF is the unknown and is defined as

$$\mathbf{H}(f) = \begin{bmatrix} H_{-M_H}(f) \\ \vdots \\ H_{M_H}(f) \end{bmatrix}. \tag{4.23}$$

Its elements are specified in (4.17). The vector $\boldsymbol{\mathcal{A}}^{(0)}(e^{j2\pi fT_c})$ is obtained from $\boldsymbol{\mathcal{A}}^{(k)}(e^{j2\pi fT_c})$ by setting $k=0$ where $\boldsymbol{\mathcal{A}}^{(k)}(e^{j2\pi fT_c})$ is defined as

$$\boldsymbol{\mathcal{A}}^{(k)}(e^{j2\pi fT_c}) = \begin{bmatrix} \mathcal{A}^{(k)*}(e^{j2\pi(f-\frac{M_H}{T})T_c}) \\ \vdots \\ \mathcal{A}^{(k)*}(e^{j2\pi(f+\frac{M_H}{T})T_c}) \end{bmatrix}. \tag{4.24}$$

Its elements without the conjugation are specified in (4.13) for $k=0$. The diagonal matrix $\mathbf{Q}(f)$ specifying the HSR of the chip waveform is defined as

$$\mathbf{Q}(f) = \begin{bmatrix} Q^*_{-M_H}(f) & \cdots & 0 \\ \vdots & \ddots & \vdots \\ 0 & \cdots & Q^*_{M_H}(f) \end{bmatrix}. \tag{4.25}$$

Its elements without the conjugation are specified in (4.15). By re-arranging (4.20), $\mathbf{H}(f)$ is obtained by solving

$$\mathbf{H}(f) = \mathbf{R}^{-1}(f)\mathbf{Q}(f)\boldsymbol{\mathcal{A}}^{(0)}(e^{j2\pi fT_c})\,e^{-j2\pi fT_b}. \tag{4.26}$$

Substitution of the elements of $\mathbf{H}(f)$ from (4.23) into (4.18) yields the frequency response of the MF. The MF solution expressed by (4.26) assumes a form quite similar to its scalar counterpart in WSS noise given in (4.2). The matrices $\mathbf{R}^{-1}(f)$, $\mathbf{Q}(f)$ and vector $\boldsymbol{\mathcal{A}}^{(0)}(e^{j2\pi fT_c})$ correspond to the inverted noise PSD $[2N_o + S_{\tilde{I}}(f)]^{-1}$, the chip filter $Q(f)$ and the DTFT $\mathcal{A}^{(0)}(e^{j2\pi fT_c})$, respectively.

4.2.2 Structure of the General MF Solution

The structure of the MF solution $H(f)$ is illustrated in Fig. 4.1. It consists of L_H

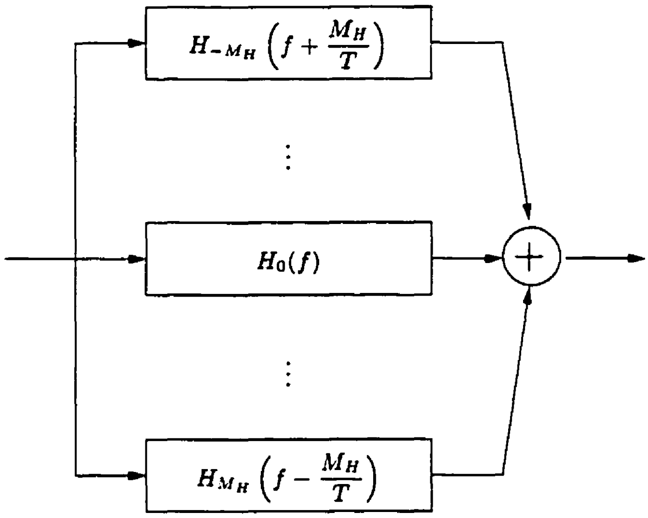

Fig. 4.1 The MF $H(f)$ consists of a set of L_H bandpass filters. The nth bandpass filter $H_n(f - \frac{n}{T})$ where $n \in [-M_H, M_H]$ filters only that part of the received signal bandlimited to $f \in \left[\frac{n}{T} - \frac{1}{2T}, \frac{n}{T} + \frac{1}{2T}\right]$.

bandpass filters which form contiguous segments of $H(f)$ in the frequency domain. The nth filter $H_n(f - \frac{n}{T})$ where $n \in [-M_H, M_H]$ is a one-sided bandpass filter with a center frequency of n/T and a width of $1/T$. The top and bottom bandpass filters $H_{-M_H}(f + \frac{M_H}{T})$ and $H_{M_H}(f - \frac{M_H}{T})$ may have widths of less than $1/T$ when $BT - \frac{1}{2}$ is not an integer. All the bandpass filter outputs are summed to generate the MF output.

The structure of the nth bandpass filter $H_n(f - \frac{n}{T})$ with its frequency shift term n/T removed is given in Fig. 4.2. That is, the structure of $H_n(f - \frac{n}{T})$ is obtained by replacing f by $f - \frac{n}{T}$ in Fig. 4.2. It consists of L_H filter branches. Each filter branch in the nth bandpass filter is bandlimited to a common band of $f \in [\frac{n}{T} - \frac{1}{2T}, \frac{n}{T} + \frac{1}{2T}]$. With respect to the nth bandpass filter, the filter branch outputs are then summed and delayed by a duration of T_b. In total, the MF solution $H(f)$ consists of L_H^2 filter branches.

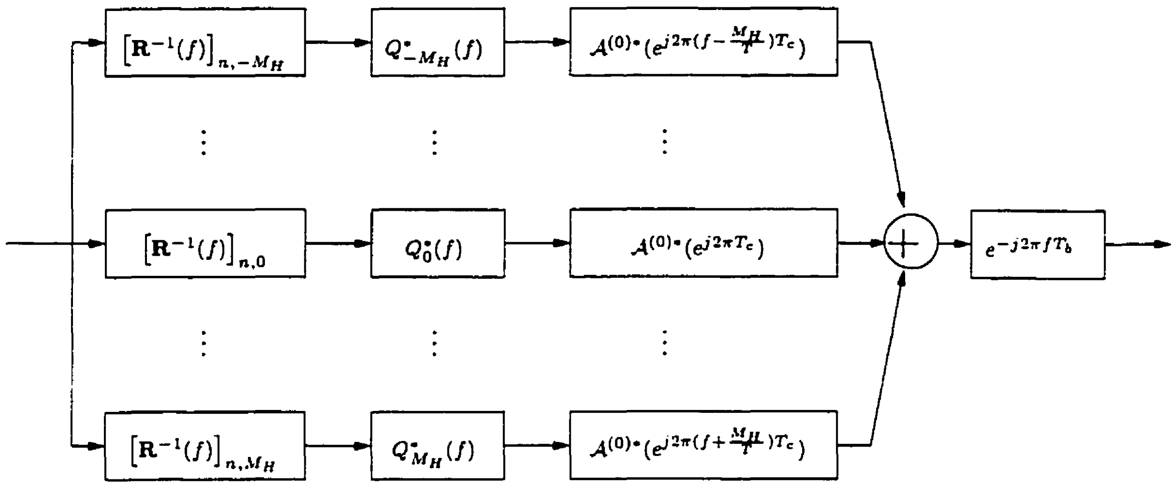

Fig. 4.2 The nth component of the bandpass filter $H_n(f)$ consists of a set of L_H branch filters which overlap in the frequency domain and a delay element of T_b.

The mth filter branch where $m \in [-M_H, M_H]$ in the nth bandpass filter $H_n(f)$ can be broken down into three filter stages. The three filters clearly separate the influence of the noise CSD, the desired user's spreading sequence and the chip waveform in the filter design. The first filter $[\mathbf{R}^{-1}(f)]_{nm}$ represents the n,mth element in the inverse of (4.21), $\mathbf{R}^{-1}(f)$. It depends solely upon the CSD of the WSCS noise. Moreover, it is the only filter among the three filters which has yet to be determined. Its form depends upon the MAI modelling and is developed in the following sections. The second filter $Q^*_m(f)$, defined in (4.15), depends solely on the chip waveform. The third filter $\mathcal{A}^{(0)*}(e^{j2\pi(f+\frac{m}{T})T_c})$, defined in (4.13), depends solely on the desired user's spreading sequence. Thus, the effect of the noise CSD, chip waveform and desired user's spreading sequence has been decoupled and isolated into three separate filters.

When the noise is WSS, the MF structure simplifies considerably since the CSD matrix $\mathbf{R}(f)$ reduces to a diagonal matrix as discussed in section 4.1.3. This is to be expected since the HSR of signals is unnecessary in WSS noise. In this case, $\mathbf{R}^{-1}(f)$ is a diagonal matrix and $[\mathbf{R}^{-1}(f)]_{nm} = 0$ if $m \neq n$. As a result, each of the bandpass filters reduces to a single branch filter since only the $m = n$th branch remains. The nth bandpass filter has a frequency response of $H_n(f) = Q^*_n(f)\mathcal{A}^{(0)*}(e^{j2\pi(f+\frac{n}{T})T_c})\, e^{-j2\pi fT_b} / \left[\frac{N_o}{2} + \frac{1}{4}R^{(\bar{I})*}_{n,n}(f)\right]$. Its substitution into $H(f)$ in (4.18) using (4.9), and (4.15) reduces $H(f)$ to $H^{\mathrm{WSS}}(f)$ in (4.2).

Further simplifications arise when no MAI is present and only the AWGN with a PSD of $2N_o$ remains. In this case, (4.21) reduces to $\mathbf{R}(f) = \frac{N_o}{2}\mathbf{I}_{L_H}$ and (4.26) becomes $\mathbf{H}(f) = \frac{2}{N_o}\mathbf{Q}(f)\boldsymbol{\mathcal{A}}^{(0)*}(e^{j2\pi fT_c})\, e^{-j2\pi fT_b}$. Consequently, $H_n(f) = \frac{2}{N_o}Q_n^*(f)$ $\mathcal{A}^{(0)*}(e^{j2\pi(f+\frac{n}{T})T_c})\ e^{-j2\pi fT_b}$ which, when substituted into (4.18) using (4.15), returns the CMF frequency response $H(f) = H^{\mathrm{CMF}}(f)$ in (4.3). In this case, $\mathbf{H}(f)$ represents the HSR of the CMF frequency response.

4.3 Unlocked Interferers

The MF solution for the infinite observation interval when the interferers are unlocked has already been developed in [86]. Nonetheless, the solution is re-investigated in terms of the HSR of signals to provide part of building blocks, needed later in section 4.6, for the combination of unlocked and chip-delay locked interferers. Furthermore, the limiting form of the NWMF as $N_o \to 0$ is examined as well; this was not investigated in [86, 79]. The development of the MAI and noise CSD matrices are presented first and then followed by the derivation and structure of the NWMF.

4.3.1 MAI and Noise Cross Spectral Density (CSD) Matrices — NWMF

The CSD for unlocked MAI can be obtained readily since the MAI is WSS as discussed in section 2.4.2. As shown in Appendix F.1, the PSD of unlocked MAI can be expressed as

$$S_I^{(U)}(f) = \frac{2\gamma}{T_c}|Q(f)|^2. \tag{4.27}$$

Substituting this into (4.9) returns the CSD for unlocked MAI

$$R_{nm}^{(U)}(f) = \begin{cases} \frac{2\gamma}{T_c}|Q_n(f)|^2, & \text{if } m = n \\ 0, & \text{otherwise.} \end{cases} \tag{4.28}$$

The corresponding CSD matrix for unlocked MAI is the diagonal matrix

$$\mathbf{R}^{(U)}(f) = \frac{2\gamma}{T_c}\mathbf{Q}(f)\mathbf{Q}^{\mathrm{H}}(f). \tag{4.29}$$

The noise CSD matrix $\mathbf{R}(f)$ is obtained by substituting $\mathbf{R}^{(\bar{I})}(f) = \mathbf{R}^{(U)}(f)$ and (4.29) into (4.21)

$$\mathbf{R}(f) = \frac{N_o}{2}\mathbf{I}_{2M_H+1} + \frac{\gamma}{2T_c}\mathbf{Q}(f)\mathbf{Q}^{\mathrm{H}}(f). \tag{4.30}$$

Since (4.30) is a diagonal matrix,

$$[\mathbf{R}^{-1}(f)]_{nm} = \frac{\delta_{nm}}{\frac{N_o}{2} + \frac{\gamma}{2T_c}|Q_n(f)|^2}. \quad (4.31)$$

4.3.2 NWMF Solution

The MF solution for unlocked interferers can be obtained by substituting (4.30) into (4.26).

$$\mathbf{H}^{(U)}(f) = \left[\frac{N_o}{2}\mathbf{I}_{2M_H+1} + \frac{\gamma}{2T_c}\mathbf{Q}(f)\mathbf{Q}^{\mathrm{H}}(f)\right]^{-1} \mathbf{Q}(f)\boldsymbol{\mathcal{A}}^{(0)}(e^{j2\pi fT_c})\, e^{-j2\pi fT_b}. \quad (4.32)$$

This expression can be simplified considerably, as discussed in 4.1.3, since the noise is WSS and the noise CSD matrix to be inverted is diagonal. The frequency response of the nth bandpass filter in Fig. 4.1 becomes $H_n(f) = Q_n^*(f)\mathcal{A}_n^{(0)*}(e^{j2\pi fT_c})/[\frac{N_o}{2} + \frac{1}{4}R_{n,n}^{(U)*}(f)]$ for $f \in [-\frac{1}{2T}, \frac{1}{2T}]$. As discussed in 4.2.2, only the $m = n$th branch remains in Fig. 4.2. For the purpose of verification and completeness, the substitution of $H_n(f)$ into (4.18) using (4.11), (4.15) and (4.31) yields the NWMF frequency response

$$H^{(U)}(f) = \frac{1}{\frac{N_o}{2} + \frac{\gamma}{2T_c}|Q(f)|^2} \cdot Q^*(f)\, \mathcal{A}^{(0)*}(e^{j2\pi fT_c})\, e^{-j2\pi fT_b}. \quad (4.33)$$

The term $1/\left(\frac{N_o}{2} + \frac{\gamma}{2T_c}|Q(f)|^2\right)$ representing the inverse of the noise PSD, is a noise-whitening filter which replaces the constant $\frac{N_o}{2}$ in the CMF response $H^{\mathrm{CMF}}(f)$ given in (4.3).

The NWMF in (4.33) has a straightforward interpretation in the frequency domain. The noise-whitening filter amplifies the spectral components of the received signal where the noise PSD is small while it attenuates those spectral components where the noise PSD is large. The NWMF strikes a balance in suppressing both MAI and AWGN. When AWGN predominates under the condition $\gamma \to 0$, $H^{(U)}(f)$ reduces to $H^{\mathrm{CMF}}(f)$. On the other hand, in an MAI-limited environment where $N_o \to 0$, (4.33) reduces to

$$H^{(U)}(f) = \frac{2T_c}{\gamma} \cdot \frac{1}{Q(f)}\, \mathcal{A}^{(0)*}(e^{j2\pi fT_c})\, e^{-j2\pi fT_b}, \quad (4.34)$$

over $f \in [-B, B]$. This is referred to as the decorrelator-type NWMF (D-NWMF) encountered earlier in section 3.2.3. It consists of the inverse chip filter $1/Q(f)$ and despreading filter $\mathcal{A}^{(0)*}(e^{j2\pi fT_c})\, e^{-j2\pi fT_b}$. The former is the same inverse filter developed for signal detection in stationary clutter for radar applications [110, pp. 170-177] [111]. Moreover, the D-NWMF can be formed from the CMF by replacing the CMF chip filter $\frac{2}{N_o}Q^*(f)$ with $1/Q(f)$. The inverse filter $1/Q(f)$ for $B \to \infty$ has the special property of generating the impulse function $\delta(t)$ given an input $\tilde{q}(t)$. [110, p. 171]. This would imply that, if such an inverse filter existed, it would, in theory, enable perfect detection in the absence of AWGN as long as the interferers were asynchronous.

The MF solution in (4.33) is equivalent to the noise-whitening MF response developed previously in [86]. In fact, the solution can be obtained directly without the HSR of signals by substituting $S_{\tilde{I}}(f) = S_{\tilde{I}}^{(U)}(f)$ and (4.27) into (4.2). In addition, when $Q(f)$ is constant over its entire bandwidth B, the PSD of the MAI is then flat and and the NWMF, apart from a scaling factor, reduces to the CMF (over $f \in [-B, B]$) For example, given the ideal Nyquist filter with $\alpha = 0$ ($Q(f) = T_c$ for $|f| \leq \frac{1}{2T_c}$ and $Q(f) = 0$, otherwise) as the chip filter, the frequency response of the noise-whitening filter becomes the constant $1/\left(\frac{N_o}{2} + \frac{\gamma T_c}{2}\right)$.

4.3.3 NWMF Structure

The NWMF receiver structure illustrated in Fig. 4.3 consists of three parts. The first

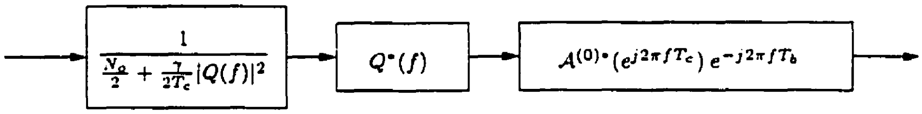

Fig. 4.3 The NWMF $H(f)$ consists of a noise-whitening filter, the conjugate of the chip filter $Q^*(f)$ and a despreading filter.

filter whitens the noise. The second filter is the chip filter $Q^*(f)$. The third filter is the despreading filter with a frequency response of $\mathcal{A}^{(0)*}(e^{j2\pi f T_c})\, e^{-j2\pi f T_b}$ which combines the conjugate of the DTFT of the desired user's spreading sequence and delay of T_b. Its corresponding impulse response can be expressed as $\sum_{n=0}^{N-1} a_n^{(0)*}\, \delta(t - (N-n)T_c)$ from (4.13). The despreading filter is given in its TDL form in Fig. 4.4 and in its correlator form in Fig. 4.5. As can be seen in Fig. 4.3, when no interferers are present, $\gamma = 0$ and the structure of the NWMF reduces to that of the CMF.

4.4 Chip-Delay Locked Interferers

This section considers the MF solution corresponding to the CLMF for the infinite observation interval when the interferers are chip-delay locked. Since the MAI is

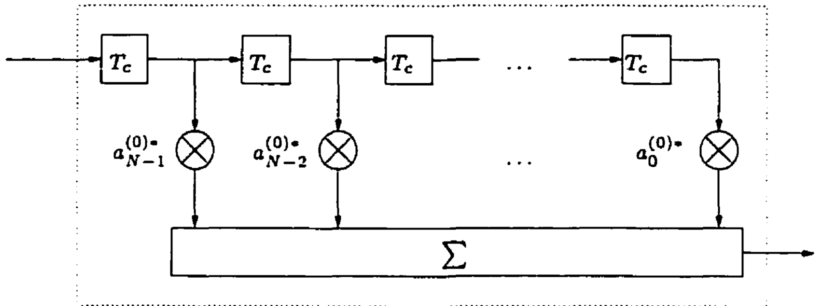

Fig. 4.4 The TDL form of the despreading filter $\mathcal{A}^{(0)*}(e^{j2\pi fT_c})\,e^{-j2\pi fT_b}$ possesses N delay elements (each of duration T_c) and N tap coefficients corresponding to the desired user's spreading sequence.

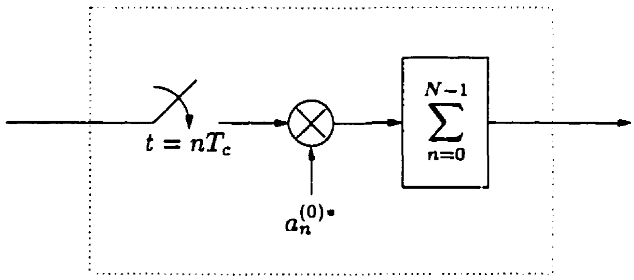

Fig. 4.5 The correlator form of the despreading filter $\mathcal{A}^{(0)*}(e^{j2\pi fT_c})\,e^{-j2\pi fT_c}$ consists of three parts. The input is first sampled at a rate of $1/T_c$. The samples are then multiplied with the desired user's spreading sequence $a_n^{(0)*}$. The N products are summed and output at $t = iT_b$.

WSCS with a period of T_c, T is set to T_c in all the HSR expressions specified in sections 4.1 and 4.2. This shall simplify the general MF structure considerably. In section 4.4.1, the MAI and noise CSD matrices for chip-delay locked interferers are developed. In section 4.4.2, the frequency response of the CLMF is derived. And in section 4.5.3, the structure of the CLMF is described.

4.4.1 MAI and Noise CSD Matrices — CLMF

As shown in Appendix F.2.1, the CSD function of the chip-delay locked MAI can be written as

$$R_{nm}^{(C)}(f) = \frac{1}{T_c} Q_n(f) Q_m^*(f) \sum_{k=1}^{K} 2P_k e^{-j2\pi(n-m)T_k/T_c} \tag{4.35}$$

for $n, m \in [-M_H, M_H]$. The CSD matrix for chip-delay locked MAI can be expressed as the L_H by L_H matrix

$$\mathbf{R}^{(C)}(f) = \frac{1}{T_c}\mathbf{Q}(f)\left[\sum_{k=1}^{K}\mathbf{P}_k^{(C)}\mathbf{P}_k^{(C)^{\mathrm{H}}}\right]\mathbf{Q}^{\mathrm{H}}(f) \tag{4.36}$$

where $\left[\mathbf{R}^{(C)}(f)\right]_{nm} = R_{nm}^{(C)*}(f)$. The power vector for the kth interferer is

$$\mathbf{P}_k^{(C)} = \sqrt{2P_k}\begin{bmatrix} e^{j2\pi(-M_H)T_k/T_c} \\ \vdots \\ e^{j2\pi M_H T_k/T_c} \end{bmatrix} \tag{4.37}$$

where $\left[\mathbf{P}_k^{(C)}\right]_{n,1} = \sqrt{2P_k}\, e^{j2\pi n T_k/T_c}$. The power vector is independent of f and dependent only on the interferer chip-delays and signal powers.

The noise CSD matrix $\mathbf{R}(f)$ is obtained by substituting $\mathbf{R}^{(\bar{I})}(f) = \mathbf{R}^{(C)}(f)$ and (4.36) into (4.21). This leads to

$$\mathbf{R}(f) = \frac{N_o}{2}\mathbf{I}_{2M_H+1} + \frac{1}{4T_c}\mathbf{Q}(f)\left(\sum_{k=1}^{K}\mathbf{P}_k^{(C)}\mathbf{P}_k^{(C)^{\mathrm{H}}}\right)\mathbf{Q}^{\mathrm{H}}(f). \tag{4.38}$$

For the CLMF, since $T = T_c$, M_H in (4.5) simplifies to

$$M_H = \left\lceil \frac{\alpha}{2} \right\rceil \tag{4.39}$$

and is solely dependent upon the excess bandwidth α and independent of N. For example, when $0 < \alpha \leq 200\%$, $M_H = 1$, $L_H = 3$ and only three bandpass filters $H_n(f - \frac{n}{T_c})$, $n \in [-1, 1]$ are required. When $\alpha = 0$, the MAI CSD matrix reduces to a scalar function of f where $n = m = 0$ since $M_H = 0$ and $L_H = 1$. Since this implies that the chip waveform $Q(f)$ is limited to the minimum bandwidth of $\frac{1}{2T_c}$, the WSCS process reduces to a WSS process due to the bandlimitedness property of WSCS processes [98] mentioned earlier. Subsequently, (4.36) reduces to (4.29) since $n = m = 0$ and the CLMF reduces to the NWMF. Moreover, when $Q(f)$ is the ideal Nyquist filter with $B = \frac{1}{2T_c}$, like the NWMF, the CLMF reduces to the CMF. On the other hand, when $\alpha > 0$, the CLMF reduces neither to the NWMF nor CMF since $M_H \geq 1$ and $\mathbf{R}^{(C)}(f)$ in (4.36) is not a diagonal matrix in contrast to $\mathbf{R}^{(U)}(f)$ in (4.29).

4.4.2 CLMF Solution

Compared to the general MF solution, the MF for chip-delay locked interferers is considerably less complex because of the condition $T = T_c$. This is because $\boldsymbol{\mathcal{A}}^{(0)}(e^{j2\pi fT_c})$ in (4.24) for $k = 0$ reduces to

$$\boldsymbol{\mathcal{A}}^{(0)}(e^{j2\pi fT_c}) \;=\; \mathcal{A}^{(0)*}(e^{j2\pi fT_c})\mathbf{u} \tag{4.40}$$

where the unit column vector $\mathbf{u}$ is defined as $[\mathbf{u}]_{n,1} = 1$ for $n \in [-M_H, M_H]$. It is precisely this result which greatly simplifies the CLMF structure. Substitution of (4.40) into (4.26) yields the CLMF response

$$\mathbf{H}^{(C)}(f) \;=\; \mathbf{G}^{(C)}(f)\mathcal{A}^{(0)*}(e^{j2\pi fT_c})\,e^{-j2\pi fT_b} \tag{4.41}$$

where the modified chip filter vector for the CLMF is

$$\mathbf{G}^{(C)}(f) \;=\; \mathbf{R}^{-1}(f)\mathbf{Q}(f)\,\mathbf{u} \tag{4.42}$$

and the inverse of the noise CSD matrix is given in (4.38). By defining $\mathbf{G}^{(C)}(f)$ in (4.42) as

$$\mathbf{G}^{(C)}(f) \;=\; \begin{bmatrix} G^{(C)}_{-M_H}(f) \\ \vdots \\ G^{(C)}_{M_H}(f) \end{bmatrix}, \tag{4.43}$$

the nth element can be expressed as $G_n^{(C)}(f) = \sum_{m=-M_H}^{M_H} [\mathbf{R}^{-1}(f)]_{nm}\, Q_m^*(f)$. To obtain a closed form expression of $G_n^{(C)}(f)$, $\mathbf{R}^{-1}(f)$ must be evaluated using (4.38). As pointed out in section 4.4.1, when $M_H \geq 1$ in the chip-delay locked case, $\mathbf{R}(f)$ in (4.38) is not a diagonal matrix. For large M_H, this can considerably complicate the process of obtaining a manageable closed form expression of its inverse $\mathbf{R}^{-1}(f)$ in (4.38). However, for bandwidth efficient pulses where $0 < \alpha \leq 200\%$, $M_H = 1$ and $\mathbf{R}(f)$ is a 3 by 3 matrix of functions which can be inverted without too much difficulty.

The CLMF frequency response $H^{(C)}(f)$ is described next. From (4.41), $H_n^{(C)}(f) = G_n^{(C)}(f)\mathcal{A}^{(0)*}(e^{j2\pi fT_c})e^{-j2\pi fT_b}$ for $n \in [-M_H, M_H]$. Substituting this into (4.18), yields

$$H^{(C)}(f) \;=\; G^{(C)}(f)\mathcal{A}^{(0)*}(e^{j2\pi fT_c})e^{-j2\pi fT_b} \tag{4.44}$$

where $G^{(C)}(f) = \sum_{n=-M_H}^{M_H} G_n^{(C)}(f - \frac{n}{T_c})$ represents the frequency response of the modified chip filter. By comparing $H^{(C)}(f)$ in (4.44) with that of $H^{\text{CMF}}(f)$ in (4.3), it can seen that the CLMF is formed from the CMF by replacing $\frac{2}{N_o}Q^*(f)$ in the CMF with the modified chip filter $G^{(C)}(f)$.

The complexity involved with the computation of a sampled version of the impulse response $g^{(C)}(t)$ of $G^{(C)}(f)$ is described. As shown in Appendix G.1, $g^{(C)}(t)$ exists over $t \in [(-3M+2)T_c, (3M-1)T_c]$ and has a duration of $T_g = 3(2M-1)$ which is three times longer than that of $\tilde{q}(t)$ where M is defined in (3.28). Since $G^{(C)}(f)$ exists over $f \in [-B, B]$, the sampled version of $g^{(C)}(t)$ requires at least $N_g = \lceil 2BT_g \rceil$ samples. As shown in Appendix G, to compute the sampled $g^{(C)}(t)$, approximately $KL_H + N_g\left(\frac{L_H^3}{3} + 2L_H^2 - \frac{L_H}{3}\right) + \frac{N_g}{2}\log_2 N_g$ multiplications and $KL_H + N_g\left(L_H + \frac{L_H(L_H-1)(2L_H+5)}{6}\right) + N_g\log_2 N_g$ additions are required. For bandwidth efficient pulses satisfying $0 \le \alpha \le 200\%$, $L_H = 3$ and the number of numerical computations is then $6K + N_g(58 + 1.5\log_2 N_g)$ growing linearly with K. For example, as shown in Appendix G, when the chip pulse is the square root raised cosine pulse (Sqrt-RC) defined in (H.1) with $\alpha = 100\%$, a total of $3K + 1488$ multiplications and $3K + 608$ additions would be required.

4.4.3 CLMF Structure

The structure of the CLMF is illustrated in Fig. 4.6. It consists of the modified chip

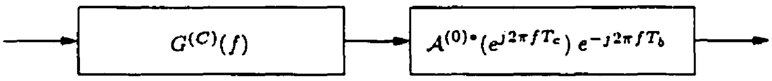

Fig. 4.6 The CLMF $H(f)$ consists of the modified chip filter $G^{(C)}(f)$ and a despreading filter.

filter $G^{(C)}(f)$ and the despreading filter $\mathcal{A}^{(0)*}(e^{j2\pi fT_c})\, e^{-j2\pi fT_c}$. The latter is given in Fig. 4.4 in its TDL form and in its correlator form in Fig. 4.5. As shown in Fig. 4.7, the former consists of L_H bandpass filters $G_n^{(C)}(f - \frac{n}{T_c})$ for $n \in [-M_H, M_H]$. The nth bandpass filter $G_n^{(C)}(f - \frac{n}{T_c})$ has a center frequency of n/T_c and a width of $1/T_c$. It forms contiguous segments of $G^{(C)}(f)$ in the frequency domain. The structure of the nth bandpass filter $G_n^{(C)}(f - \frac{n}{T_c})$ with its frequency shift term n/T_c removed is given in Fig. 4.8. The bandpass filter consists of L_H filter branches whose outputs are summed. Each filter branch is bandlimited to a common band of $f \in [\frac{n}{T_c} - \frac{1}{2T_c}, \frac{n}{T_c} + \frac{1}{2T_c}]$ and, therefore, overlap.

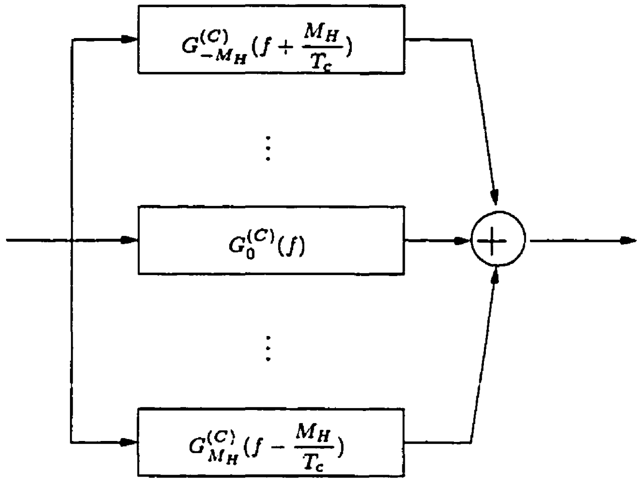

Fig. 4.7 The modified chip filter $G^{(C)}(f)$ for the CLMF consists of a set of L_H bandpass filters. The nth bandpass filter $G^{(C)}_n(f - \frac{n}{T_c})$ where $n \in [-M_H, M_H]$ filters only that part of the received signal bandlimited to $f \in \left[\frac{n}{T_c} - \frac{1}{2T_c}, \frac{n}{T_c} + \frac{1}{2T_c}\right]$.

The mth filter branch where $m \in [-M_H, M_H]$ in the nth bandpass filter $H_n(f)$ can be broken down into two filter stages. The first filter $[\mathbf{R}^{-1}(f)]_{nm}$ represents the n,mth element in the inverse of $\mathbf{R}(f)$ given by (4.38). It depends solely upon the CSD of the MAI and the PSD level of the AWGN. The second filter $Q^*_m(f)$ is the conjugated mth HSR component of $Q(f)$ defined in (4.15).

The consolidation of the L_H DTFT filters in the branch filters in Fig. 4.2 of each bandpass filter to the single DTFT $\mathcal{A}^{(0)*}(e^{j2\pi fT_c})$ in Fig. 4.6 is a consequence of the property that $\mathcal{A}^{(0)*}(e^{j2\pi(f+\frac{n}{T})T_c})$ from (4.13) is independent of n when $T = T_c$ This result has a significant impact on the design of the CLMF. The CLMF structure has been separated into two filters: the modified chip filter $G^{(C)}(f)$ and the despreading filter. That is, the CLMF can be implemented by replacing the chip filter $\frac{2}{N_o}Q^*(f)$ in the CMF in (4.3) by the modified chip filter $G^{(C)}(f)$ in (4.3). Thus, the filtering problem of designing a filter which maximizes SNR for bit symbol detection under chip-delay locked interferers has been reduced to the problem of designing the modified chip filter $G^{(C)}(f)$. The spreading sequence which changes for consecutive bits under long sequence spreading only affects the despreading filter. The $G^{(C)}(f)$ need only be computed when interferer chip delays and signal powers change.

As can be surmised, the modified chip filter $G^{(C)}(f)$ is the same filter which maximizes SNR for chip symbol detection. This result can be obtained by re-posing the

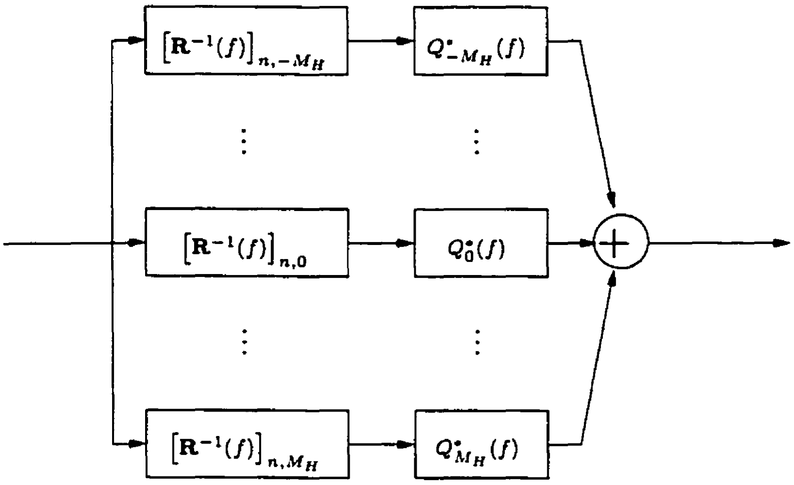

Fig. 4.8 The nth bandpass filter $G_n^{(C)}(f)$ for the CLMF consists of a set of L_H filter branches which overlap in the frequency domain.

filtering problem in terms of chip symbol detection. The integral equation assumes the form of (4.1) where $\tilde{a}^{(0)}(t)$ and $\tilde{h}^*(T_b - t)$ are replaced, respectively, by $\tilde{q}(t)$ and $\tilde{g}^{(C)}(T_c - t)$. This leads to

$$\frac{N_o}{2}\tilde{g}^{(C)*}(T_c - t) + \frac{1}{4}\int_{-\infty}^{\infty} R_{\tilde{I}}(t,u)\,\tilde{g}^{(C)*}(T_c - u)\,du \;=\; \tilde{q}(t), \quad -\infty < t < \infty. \quad (4.45)$$

The solution follows readily from $H^{(C)}(f)$ in (4.44) by setting $N = 1$ and $a_0^{(0)} = 1$ to establish the equalities $\tilde{a}^{(0)}(t) = \tilde{q}(t)$, $T_b = T_c$ and $\mathcal{A}^{(0)*}(e^{j2\pi fT_c}) = 1$. Consequently, (4.44) reduces to $H^{(C)}(f) = G^{(C)}(f)e^{-j2\pi fT_c}$. Therefore, the filter which maximizes SNR for chip symbol detection is the modified chip filter $G^{(C)}(f)$ with the delay term of $e^{-j2\pi fT_c}$. This relationship greatly simplifies the implementation of the CLMF and forms the foundation to the development of adaptive filters to be treated later in Chapter 6.

4.5 Bit-Delay Locked Interferers

This section considers the MF solution corresponding to the BLMF for the infinite observation interval when the interferers are bit-delay locked and short sequence spreading is utilized. The general structure of the BLMF has been previously investigated in [68]. In this section, however, two additional results augmenting the work of [68] are developed. One, an expression of the frequency response of the BLMF is obtained. And two, the underlying structure within in each bandpass filter given in [68] is described.

This section is divided into three parts. In section 4.5.1, the MAI and noise CSD matrices are developed. In section 4.5.2, the frequency response of the BLMF is derived. And in section 4.5.3, its structure is described. Since the MAI is WSCS with a period of T_b, T is set to T_b in all the HSR expressions specified in sections 4.1 and 4.2.

4.5.1 MAI and Noise CSD Matrices — BLMF

As shown in Appendix F.2.2, the CSD for bit-delay locked MAI can be written as

$$R_{nm}^{(B)}(f) = \frac{1}{T_b} Q_n(f) Q_m^*(f) \sum_{k=1}^{K} \mathcal{A}^{(k)}(e^{j2\pi(f+\frac{n}{T_b})T_c}) \mathcal{A}^{(k)^*}(e^{j2\pi(f+\frac{m}{T_b})T_c})\, 2P_k e^{-j2\pi(n-m)\tau_k/T_b} \tag{4.46}$$

for $n, m \in [-M_H, M_H]$. The CSD matrix for bit-delay locked MAI can be expressed as the L_H by L_H matrix

$$\mathbf{R}^{(B)}(f) = \frac{1}{T_b}\mathbf{Q}(f)\left[\sum_{k=1}^{K} \mathbf{P}_k^{(B)} \boldsymbol{\mathcal{A}}^{(k)}(e^{j2\pi f T_c}) \boldsymbol{\mathcal{A}}^{(k)^{\mathrm{H}}}(e^{j2\pi f T_c})\, \mathbf{P}_k^{(B)^{\mathrm{H}}}\right] \mathbf{Q}^{\mathrm{H}}(f) \tag{4.47}$$

where $\left[\mathbf{R}^{(B)}(f)\right]_{nm} = R_{nm}^{(B)*}(f)$. The power matrix for the kth interferer in the bit-delay locked case is the diagonal matrix

$$\mathbf{P}_k^{(B)} = \sqrt{2P_k}\begin{bmatrix} e^{j2\pi(-M_H)\tau_k/T_b} & \dots & 0 \\ \vdots & \ddots & \vdots \\ 0 & \dots & e^{j2\pi M_H \tau_k/T_b} \end{bmatrix}. \tag{4.48}$$

where $\left[\mathbf{P}_k^{(B)}\right]_{n,m} = \delta_{nm}\sqrt{2P_k}\, e^{j2\pi n \tau_k/T_b}$. The noise CSD matrix $\mathbf{R}(f)$ is obtained by substituting $\mathbf{R}^{(\bar{I})}(f) = \mathbf{R}^{(B)}(f)$ and (4.47) into (4.21). This leads to

$$\mathbf{R}(f) = \frac{N_o}{2}\mathbf{I}_{2M_H+1} + \frac{1}{4T_b}\mathbf{Q}(f)\left[\sum_{k=1}^{K} \mathbf{P}_k^{(B)} \boldsymbol{\mathcal{A}}^{(k)}(e^{j2\pi f T_c}) \boldsymbol{\mathcal{A}}^{(k)^{\mathrm{H}}}(e^{j2\pi f T_c}) \mathbf{P}_k^{(B)^{\mathrm{H}}}\right] \mathbf{Q}^{\mathrm{H}}(f). \tag{4.49}$$

For the BLMF, since $T = T_b$, the M_H in (4.5) simplifies to

$$M_H = \left\lceil \frac{(1+\alpha)N}{2} - \frac{1}{2} \right\rceil \tag{4.50}$$

and is dependent on both N and α. This result is unlike that encountered in the chip-delay locked case where M_H was independent of N and the MAI became WSS when $\alpha = 0$ and $M_H = 0$. In the bit-delay locked case, the MAI remains WSCS even when $\alpha = 0$ since $M_H > 0$ as long as $N > 1$. This property of the bit-delay locked MAI can be attributed to the assumption of short sequence spreading which leads to the WSCS period of $T = T_b$ where the width $1/T_b$ can be much smaller than the bandwidth of interest B. Furthermore, as shown by (4.50), since M_H is proportional to N it can be very large even when $\alpha = 0$. This serves as a preliminary indication of the high order of complexity that can be expected for the BLMF solution in the infinite observation interval for moderate values of N. For example, when $\alpha = 0$ and N is even in (4.50), $M_H = \frac{N}{2}$ and $\mathbf{R}(f)$ in (4.49) becomes an $N+1$ by $N+1$ matrix of CSD functions. For even modest values of N, the task of inverting $\mathbf{R}(f)$ in (4.49), to obtain a closed form expression, would be very tedious.

4.5.2 BLMF Solution

When the interferers were either unlocked or chip-delay locked, many simplifications in the general MF structure in Fig. 4.1 resulted. In the case of bit-delay locked interferers, no such simplifications arises. Consequently, its solution is given by (4.18), (4.23) and (4.26) where the noise CSD matrix is given by (4.49).

4.5.3 BLMF Structure

The structure of the BLMF assumes the general MF structure given in Fig. 4.1 and Fig. 4.2 since no simplifications such as those encountered for the NWMF and CLMF arise. Thus, the BLMF is composed of L_H bandpass filters as was already shown in [68]. However, the derivation of the general MF structure reveals further information regarding the underlying structure within each of the bandpass filters as illustrated in Fig. 4.2. The BLMF can be separated into three parallel sets of filters: $\mathbf{R}^{-1}(f)$, $\mathbf{Q}(f)$ and $\boldsymbol{\mathcal{A}}^{(0)}(e^{j2\pi f T_c})$. The filters of each set depend on either the noise (consisting of the MAI and AWGN), the chip filter $Q(f)$ or the desired user's spreading sequence $\mathbf{a}^{(0)}$. Since $Q(f)$ and $\mathbf{a}^{(0)}$ are fixed, their corresponding sets of filters $\mathbf{Q}(f)$ and $\boldsymbol{\mathcal{A}}^{(0)}(e^{j2\pi f T_c})$ remain fixed as well. Only the filters represented by $\mathbf{R}^{-1}(f)$ change according to changes in the signal parameters of the MAI and the PSD level of AWGN. That is, in every branch filter in Fig. 4.2, $Q_m^*(f)$ and $\mathcal{A}^{(0)*}(e^{j2\pi(f+\frac{m}{T_b})T_c})$ where $m \in [-M_H, M_H]$ remain fixed. Only $[\mathbf{R}^{-1}(f)]_{nm}$ changes according to changes in the signal parameters of the interferers. Therefore, as observed in the CLMF and NWMF, the structure of the BLMF has decoupled the effects of MAI from that of the chip filter and spreading sequence of the desired user. However, in this case, the decoupling occurs only in the HSR components of the filter.

The number of filter components in the BLMF can be quite large even for modest values of N. Continuing with the example discussed in section 4.5.1, when $\alpha = 0$ and N is even in (4.50), the BLMF is composed of $N+1$ bandpass filters each with a set of $N+1$ branch filters. Since each branch, in turn, consists of 3 filters, the BLMF would contain $3(N+1)^2$ filter components in total. In general, the number of filter components grows with the square of N.

4.6 Both Unlocked and Chip-Delay Locked Interferers

The MF is investigated when both unlocked and chip-delay locked interferers are present. The derivation of the MF uses many of the results obtained in sections 4.3 and 4.4. As in section 3.5, there are K_U unlocked interferers and K_C chip-delay locked interferers. The CSD matrix can be expressed as $\mathbf{R}^{(CU)}(f) = \mathbf{R}^{(U)}(f) + \mathbf{R}^{(C)}(f)$ assuming that the signals of the interferers are independent and zero-mean. The CSD matrix $\mathbf{R}^{(U)}(f)$ for the unlocked part of the MAI is given by (4.29) where γ is replaced by $\gamma_{CU} = \sum_{k=K_C+1}^{K_C+K_U} P_k$. The CSD matrix $\mathbf{R}^{(C)}(f)$ for the chip-delay locked part of the MAI is given by (4.36) where K is replaced by K_C. Using these modifications, the CSD matrix for the MAI becomes

$$\mathbf{R}^{(CU)}(f) = \frac{\gamma_{CU}}{2T_c}\mathbf{Q}(f)\mathbf{Q}^*(f) + \frac{1}{T_c}\mathbf{Q}(f)\left[\sum_{k=1}^{K_C}\mathbf{P}_k^{(C)}\mathbf{P}_k^{(C)*}\right]\mathbf{Q}^*(f). \quad (4.51)$$

Thus, the noise CSD matrix is

$$\mathbf{R}(f) = \frac{N_o}{2}\mathbf{I}_{2M_H+1} + \frac{1}{4}\mathbf{R}^{(CU)}(f). \quad (4.52)$$

It can be seen now how the CSD noise matrix $\mathbf{R}(f)$ in (4.52) varies from (4.38) when all the interferers are chip delay locked ($K_U = 0$) to (4.30) when all the interferers are unlocked ($K_C = 0$). The MF solution $H^{(CU)}(f)$ is obtained by substituting (4.52) into (4.26).

The structure of $H^{(CU)}(f)$ assumes the same structure as that of the CLMF given in Figs. 4.6, 4.7 and 4.8. Differences arise only in the filters $[\mathbf{R}^{-1}(f)]_{nm}$, in Fig. 4.8, obtained from inverting $\mathbf{R}(f)$ in (4.52). When all the interferers become unlocked, $\mathbf{R}(f)$ becomes a diagonal matrix and only the $m = n$th branch filter remains in Fig. 4.8. This returns the NWMF given in Fig. 4.3.

4.7 Summary

This chapter has derived the NWMF, CLMF and BLMF for the infinite observation interval. The general structure of the MFs was shown to consist of a set of L_H bandpass filters (Fig. 4.1) each with a set of L_H branch filters (Fig. 4.2). Regardless of the MAI model, the structure was composed of individual filters each affected only by either interferer signal parameters, the chip filter or spreading sequence of the desired user.

For the CLMF and NWMF, the general structure in Fig. 4.1 simplified considerably. The NWMF basically consisted of the CMF with a noise-whitening filter inserted at the front end of the CMF. Moreover, in the limit as $N_o \to 0$, the NWMF approached the D-NWMF composed of an inverse chip filter followed by a despreading filter. The CLMF assumed a slightly different form. It consisted of two filters: an SNR maximizing filter for chip symbol detection and the despreading filter. That is, it had the same form as the CMF except that the former replaced the CMF chip filter. Its computational complexity per bit symbol was shown to be reasonably low. The number of numerical operations required to compute a sampled version of its impulse response was analyzed and found to grow linearly with K. Moreover, in sharp contrast to the CLMF derived in section 3.3 over the finite observation interval, the impulse response of the SNR maximizing chip filter needs re-computation only when an interferer chip delay or signal power changes. For the BLMF, those simplifications encountered for the CLMF did not arise. Since the BLMF response had to be re-computed at the bit rate, its computational complexity per bit symbol remained extremely high.

Chapter 5

Performance Analysis

This chapter investigates the performance of the CLMF derived in Chapter 3 and compares its performance with that of the NWMF and CMF. The performances are analyzed in terms of SNR, near-far resistance, bit error rate (BER) and probability of outage over the multiple-access channel with background AWGN as described in section 2.1. The analysis is restricted to realizations derived under the finite observation interval of $t \in [0, T_b]$. In addition, the analysis of the BLMF performance is not presented for two reasons. Its performance has been previously investigated in [62, 69]. And more importantly, it is rendered impractical because of its large complexity under the condition of long sequence spreading.

Section 5.1 introduces the system parameters used for the numerical examples presented in this chapter. The next three sections investigate filter performance for specific realizations of the signal parameters. Section 5.2 examines the performance of the CLMF in terms of SNR. Its aim is to provide an understanding of how the CLMF performs with respect to chip delays, signal powers and chip waveforms. It also considers the effect of information on interferer phase-offsets and the presence of a combination of chip-delay locked and unlocked interferers. Section 5.3 derives and analyzes the near-far resistance of the NWMF and CLMF. Section 5.4 presents the BER performance of the CLMF for the special case of short sequence spreading and rectangular chip waveforms. The remaining section of 5.5 investigates the performance of the filters under more general conditions based on the probability of outage. Its aim is to illustrate and quantify the gains achievable by the CLMF over the CMF and NWMF in terms of probability of outage as well as user capacity.

5.1 Note on Numerical Examples on Performance

This section presents system parameters used to compute the numerical examples given in this chapter. DS-BPSK modulation is assumed whereby the chip waveforms are real and the chips of the spreading sequences are bipolar such that $a_n^{(k)} \in \{\pm 1\}$. The remainder of this section specifies the chip waveforms, spreading sequences and modelling of the signal parameters.

5.1.1 Chip Waveforms

A total of four chip waveforms for $\tilde{q}(t)$ are considered: the rectangular pulse, the square-root raised cosine (sqrt-RC) 100% pulse with an excess bandwidth of $\alpha = 100\%$, the Sqrt-RC pulse 60% with $\alpha = 60\%$ and the IS-95 pulse. The last three are examples of bandwidth efficient pulses. The rectangular pulse was defined earlier in (3.7). As shown in Appendix H.1, it has an excess bandwidth of $\alpha = 64 \times 100\%$ since $B = 32.5 \cdot \frac{1}{T_c}$ based on a -40 dB rule. The sqrt-RC pulse is parameterized by $\alpha \in [0, 100\%]$ and defined in [18, (6.104), (6.105) p. 228]. Its expression in the time domain is reproduced in Appendix H.2 for reference. Since the sqrt-RC pulse is strictly bandlimited (BL) and extends over $t \in (-\infty, \infty)$, it is truncated under the constraint that 99.99% of the energy of the BL pulse is contained in its truncated version. When $\alpha = 60\%$, $M = 4$ and when $\alpha = 100\%$, $M = 3$ where M is defined in (3.28). The IS-95 pulse refers to the chip waveform defined in the IS-95 standard [1, Section 6.1.3.1.10 on pp. 6-28 to 6-30]. It is important to stress the fact that the IS-95 pulse has a non-zero excess bandwidth. Otherwise, the CLMF would reduce to the NWMF and yield no improvement over the NWMF. As shown in Appendix H.3, the IS-95 pulse has an excess bandwidth of 20.44% based on a -40 dB rule. For the IS-95 pulse, $M = 7$.

5.1.2 Spreading Sequences

With respect to only sections 5.2 to 5.4, a specific spreading sequence is selected. This is done to provide an understanding of the performance of the CLMF, NWMF and CMF with respect to the signal parameters to be discussed in section 5.1.3 for a particular spreading sequence. In these three sections, the desired user is assigned a *Gold sequence* of length $N_p = 31$ given in Table 5.1 for $k = 0$. The spreading sequences of interferers are assumed to be random as discussed in the description of chip-delay locked interferers in section 2.4.2. The remaining sequences in Table 5.1

Table 5.1 Balanced *Gold sequences* of length $N = 31$ constructed from two maximal sequences with the generating polynomials $\mathcal{H} = 45$ and $\mathcal{H} = 75$ based on initial shift register bit loadings of [10011] and [11000], respectively [2]. The symbol + represents 1 while − represents −1.

k	spreading sequence, $\boldsymbol{a}^{(k)}$
0	− + + + − + + + − − + − − + − + − + − − + − + + − − − + − + −
1	+ + + − − − + − + − + − − − + − − + + + + + − − + + − − − + −
2	− − + − + + + + − + − + − + + − − − + + − + + − − − − − − + +
3	+ − + + − + − − + − + + + + + − + − + − − − + + + − − − − − −
4	+ − − − − − + + − + + − + + + + + − − − + − − − + − − − + + +
5	− − + + − − + + + − − − + − − + − + + + − − + − + − + − + − +
6	+ + + + − − − − − − − + − − + − + − − + + − + − − − + + + + +
7	+ + − − − + + + + + − − − − + + + − + + − − − + − − + + − − −

shall be used only under certain circumstances when the performance of the BLMF is considered. In those cases only, the sequences are assigned to interferers as they are needed.

In section 5.5 where probability of outage is examined, the constraint on the spreading sequence is removed. Random spreading sequences shall be used to represent the very long PN sequences employed under long sequence spreading conditions. In this case, the sequences are generated randomly where the chips $a_n^{(0)}$ indexed by n are i.i.d. with $\text{Prob}[a_n^{(0)} = 1] = \text{Prob}[a_n^{(0)} = -1] = \frac{1}{2}$.

5.1.3 Modelling of Signal Parameters

The signal parameters consist of E_b/N_o of the desired user, the interferer chip delays and signal powers. In sections 5.2 to 5.4, specific distributions of the parameters shall be considered. In many of the numerical examples, $E_b/N_o = 20$ dB. This was selected for two reasons. It is a value which represents systems under MAI-limited conditions and it reflects a reasonable received signal bit energy level for a subscriber in the uplink of the IS-95 system (in the absence of noise) [15]. The value is obtained from [15] by using the relation $E_b/N_o = -1 + 10\log_{10}(128) \approx 20$ dB. For notational clarity, two vectors are introduced. The chip delay vector is defined as $\mathbf{T} = [T_1, \ldots, T_K]$. The ratio of the power of the kth interferer to that of the desired user is defined as

$$\beta_k = \frac{P_k}{P_0}. \tag{5.1}$$

The associated vector of signal power ratios is defined as $\boldsymbol{\beta} = [\beta_1, \ldots, \beta_K]$. The phase-offsets are assumed to be i.i.d. where each phase-offset is assumed to be uniformly distributed over $\theta_k \in [0, 2\pi)$ unless otherwise stated.

5.2 Signal-to-Noise Ratio (SNR)

This section examines the SNR performance of the CLMF with respect to the NWMF and CMF. First, SNR expressions for the various MF realizations are derived. Second, numerical examples are presented to provide an understanding of the CLMF performance characteristics. In the discussion of numerical examples, the expression SNR(MF type) is introduced for brevity. It represents the SNR performance of the filter type specified in the argument. The filter type may be either the CMF, NWMF, CLMF or CUMF.

5.2.1 SNR Expressions

The SNR expression of (2.15) for an arbitrary filter $\tilde{h}(t)$ can be written as

$$\mathrm{SNR} = \frac{\frac{P_0}{2}\left\{\int_0^{T_b} \mathcal{R}e\left[\tilde{h}(T_b-u)\tilde{a}^{(0)}(u)\right]du\right\}^2}{\mathcal{R}e\left\{\frac{1}{2}\int_0^{T_b}\tilde{h}(T_b-t)\frac{1}{4}\int_0^{T_b}\left[R_{\tilde{n}}(t,u)\tilde{h}^*(T_b-u)+\tilde{R}_{\tilde{n}}(t,u)\tilde{h}(T_b-u)\right]du\,dt\right\}}. \tag{5.2}$$

Given $\tilde{h}(t)$, the SNR expression is evaluated by using: the desired user's spreading waveform $\tilde{a}^{(0)}(t)$ defined in (2.8) for $k = 0$, the noise autocorrelation function $R_{\tilde{n}}(t,u)$ defined in (3.2) and the noise pseudo-autocorrelation function $\tilde{R}_{\tilde{n}}(t,u)$ defined in (3.4). The form of $R_{\tilde{n}}(t,u)$ and $\tilde{R}_{\tilde{n}}(t,u)$ depends, respectively, upon the form of $R_{\tilde{I}}(t,u)$ and $\tilde{R}_{\tilde{I}}(t,u)$ which, in turn, depends upon how the interferers are modelled. The expressions of the two MAI autocorrelation functions for unlocked, chip-delay locked and bit-delay interferers are given in sections 3.2.1, 3.3.1 and 3.4.1, respectively. With respect to the variants of these three models, the autocorrelation functions for a combination of unlocked and chip-delay locked interferers and for interferers whose phase-offsets are known are given in sections 3.6.1 and 3.6.2, respectively. Furthermore, when taking into account the effect of ISI, $R_{\tilde{n}}(t,u)$ and $\tilde{R}_{\tilde{n}}(t,u)$ assume the form given in (D.1) and (D.2), respectively. The ISI autocorrelation and pseudo-autocorrelation functions: $R_{\tilde{\zeta}}(t,u)$ and $\tilde{R}_{\tilde{\zeta}}(t,u)$ are given in (D.4) and (D.5), respectively, for unlocked interferers. The $R_{\tilde{\zeta}}(t,u)$ and $\tilde{R}_{\tilde{\zeta}}(t,u)$ of the chip-delay locked case are the same as those for the unlocked interferers. For bit-delay locked interferers, $R_{\tilde{\zeta}}(t,u)$ and $\tilde{R}_{\tilde{\zeta}}(t,u)$ are given by (D.10) and (D.11), respectively.

The SNR expression in (5.2) is implicitly a function of: the spreading factor N, E_b/N_o, the chip waveform $\tilde{q}(t)$, the filter impulse response $\tilde{h}(t)$, the number of interferers K, the ratio of signal powers of interferers to that of the desired user $\boldsymbol{\beta}$, the interferers' chip delays $\mathbf{T}$, and the spreading sequence of the desired user $\mathbf{a}^{(0)}$ defined in (3.8). The implicit dependence is summarized by

$$\mathrm{SNR}\left(N, E_b/N_o, \tilde{q}(t), \tilde{h}(t), K, \boldsymbol{\beta}, \mathbf{T}, \mathbf{a}^{(0)}\right). \tag{5.3}$$

For a given spreading waveform and a pair of noise autocorrelation functions, the SNR expression in (5.2) is maximized when $\tilde{h}(t)$ is the MF which satisfies the integral equation (3.1). In this case, by substituting (3.1) and (3.6) into (5.2), (5.2) reduces to

$$\mathrm{SNR}_{\mathrm{opt}} = \frac{2P_0}{N_o}\int_0^{T_b} \mathcal{R}e\left[\tilde{f}(u)\tilde{a}^{(0)}(u)\right] du. \tag{5.4}$$

For example, in AWGN where the CMF maximizes SNR, $\tilde{f}(t) = \tilde{a}^{(0)*}(t)$ and $\mathrm{SNR}_{\mathrm{opt}} = 2E_b/N_o$. It is important to stress that (5.4) applies only to the SNR maximizing filter $\tilde{h}(t)$ which satisfies the integral equation in (3.1). For any other filter, (5.2) must be used to evaluate SNR instead. The $\mathrm{SNR}_{\mathrm{opt}}$ expression in (5.4) can be simplified by using the matrices defined in Appendix C. This is accomplished by substituting into (5.4) the impulse response of either the NWMF in (3.21) when the interferers are unlocked, CLMF in (3.32) when the interferers are chip-delay locked, BLMF in (3.40) when the interferers are bit-delay locked or CUMF in (3.45) when both chip-delay locked and unlocked interferers are present. This leads to the general expression

$$\mathrm{SNR}_{\mathrm{opt}} = \frac{2E_b}{N_o}\cdot\frac{1}{T_b}\left[E_a - \boldsymbol{a}\left(N_o\boldsymbol{P}^{-1} + \boldsymbol{C}\right)^{-1}\boldsymbol{a}^{\mathrm{H}}\right] \tag{5.5}$$

where

$$E_a = \int_0^{T_b} |\tilde{a}^{(0)}(t)|^2 dt. \tag{5.6}$$

When $M = 1$, $E_a = T_b$ and (5.5) reduces to $\mathrm{SNR}_{\mathrm{opt}} = \frac{2E_b}{N_o}\left[1 - \frac{1}{T_b}\boldsymbol{a}\left(N_o\boldsymbol{P}^{-1} + \boldsymbol{C}\right)^{-1}\boldsymbol{a}^{\mathrm{H}}\right]$. The form of the vector $\boldsymbol{a}$, the covariance matrix $\boldsymbol{C}$ and power matrix $\boldsymbol{P}$ can each take on one of four possibilities depending upon the modelling of the MAI. The mappings are summarized in Table 5.2.

Table 5.2 Mapping of vectors and matrices for the $\mathrm{SNR}_{\mathrm{opt}}$ in (5.4) for the various MAI models and MF realizations with cross-referencing to their corresponding equations.

MAI Model	MF Realization	$\boldsymbol{a}$	$\boldsymbol{C}$	$\boldsymbol{P}$
Unlocked	NWMF	$\boldsymbol{a}^{(U)}$ in (C.3)	$\boldsymbol{I}_{N_U}$	$\gamma\boldsymbol{\Lambda}$ in (3.10) & (C.2)
Chip-delay locked	CLMF	$\boldsymbol{a}^{(C)}$ in (C.10)	$\boldsymbol{C}^{(C)}$ in (C.11)	$\boldsymbol{P}^{(C)}$ in (C.12)
Bit-delay locked	BLMF	$\boldsymbol{a}^{(B)}$ in (C.17)	$\boldsymbol{C}^{(B)}$ in (C.18)	$\boldsymbol{P}^{(B)}$ in (C.19)
Both chip-delay locked & unlocked	CUMF	$\boldsymbol{a}^{(CU)}$ in (C.29)	$\boldsymbol{C}^{(CU)}$ in (C.30)	$\boldsymbol{P}^{(CU)}$ in (C.31)

5.2.2 Numerical Examples — SNR

The SNR performance is investigated for the CLMF in comparison to the NWMF and CMF when the chip-delays of interferers are known. Four sets of numerical examples are presented. The examples illustrate SNR performance with respect to chip delays, E_b/N_o, received signal powers through $\boldsymbol{\beta}$ and phase-offsets.

SNR vs. Chip Delay

SNR is examined with respect to the chip delay of a single chip-delay locked interferer under two situations. In the first situation, $K = 1$ where the only interferer present is chip-delay locked. This is represented by the curves associated with case a) in Fig. 5.1 where SNR vs. T_1/T_c is plotted for the CLMF, NWMF and CMF when $E_b/N_o = 20$ dB and $\beta_1 = 1$ under equal power conditions. The SNR of all three filters reach their maximum at $T_1 = 0.5T_c$ and their minimum at $T_1 = 0$. Moreover, the SNR curves are symmetrical about $T_1 = 0.5T_c$. The curves illustrate that the CLMF performs no better than the CMF as the interferer becomes closer to being chip synchronized. On the other hand, as T_1 moves toward $0.5T_c$, the gain provided by the CLMF over both the NWMF and CMF increases. At $T_1 = 0.5T_c$, SNR(CLMF) = 21.7 dB, SNR(NWMF) = 21.1 dB and SNR(CMF) = 19.8 dB. Thus, at $T_1 = 0.5T_c$, the NWMF delivers a 1.3 dB improvement over the CMF while the CLMF provides an additional 0.6 dB improvement over the NWMF. The SNR gain of the CLMF over the NWMF can be as large as 1 dB. At $T_1 = 0.1T_c$, SNR(CLMF) = 19.2 dB, SNR(NWMF) = 18.2 dB and SNR(CMF) = 17.6 dB. Thus, at $T_1 = 0.1T_c$, the NWMF delivers a 0.6 dB improvement over the CMF while the CLMF provides an additional

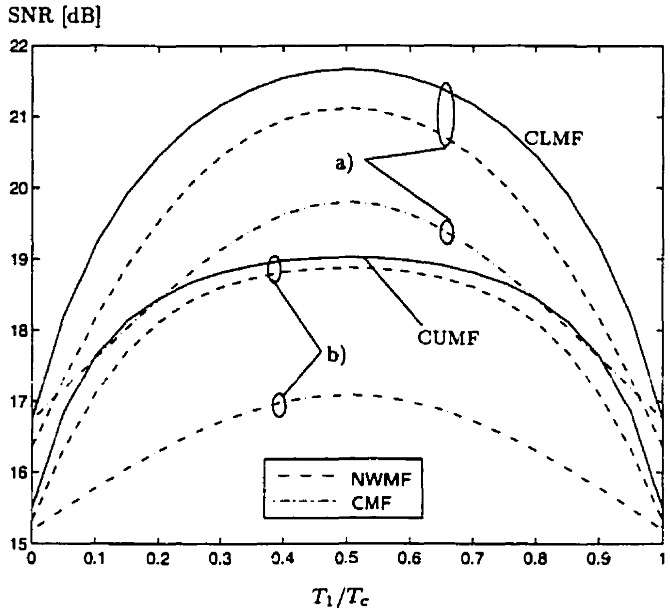

Fig. 5.1 SNR vs. T_l/T_c for the rectangular pulse and uniform signal powers when $N = 31$ and $E_b/N_o = 20$ dB. In case a), $K = 1$ where user 1 is chip-delay locked. In case b), $K_C = 1$ and $K_U = 1$. User 1 is chip-delay locked and user 2 is unlocked.

1 dB improvement over the NWMF.

In the second situation, an unlocked interferer is introduced such that $K_C = 1$ and $K_U = 1$. This is represented by the curves associated with case b) in Fig. 5.1 where SNR vs. T_l/T_c is plotted for the CUMF, NWMF and CMF. Again, the SNR of all three filters reach their maximum at $T_l = 0.5T_c$ and their minimum at $T_l = 0$. At $T_l = 0.5T_c$, SNR(CUMF) = 19.0 dB, SNR(NWMF) = 18.9 dB and SNR(CMF) = 17.1 dB. Thus, at $T_l = 0.5T_c$, the NWMF delivers a 1.8 dB improvement over the CMF while the CUMF provides only an additional 0.1 dB gain over the NWMF. The SNR gain of the CUMF over the NWMF can be as large as 0.5 dB. At $T_l = 0.1T_c$, SNR(CUMF) = 17.6 dB, SNR(NWMF) = 17.1 dB and SNR(CMF) = 15.8 dB. Thus, at $T_l = 0.1T_c$, the NWMF delivers a 1.3 dB improvement over the CMF while the CLMF provides an additional 0.5 dB improvement over the NWMF. The presence of the unlocked interferer reduces the effectiveness of the CUMF compared to the NWMF. Later, the effectiveness of the CUMF will be shown under power-imbalance conditions.

SNR vs. E_b/N_o

Next, the performance of SNR vs. E_b/N_o is considered. Fig. 5.2 presents a plot of SNR vs. E_b/N_o for the CMF, NWMF and CLMF under two contrasting conditions when there are seven locked interferers. Case a) illustrates the condition when the

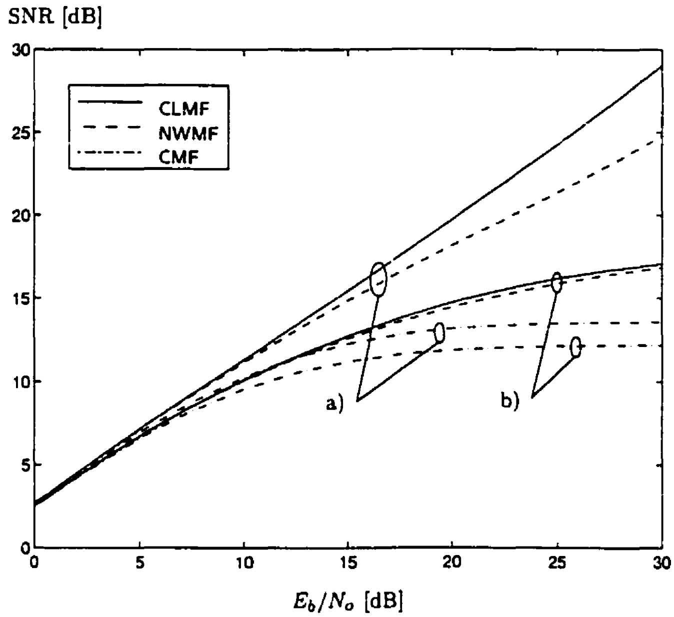

Fig. 5.2 SNR vs. E_b/N_o for the rectangular pulse and uniform signal powers when $N = 31$ and $K = 7$. In case a) $\mathbf{T}\ /T_c = [0.3, 0.35, 0.4, 0.5, 0.55, 0.6, 0.7]$. In case b), $\mathbf{T}\ /T_c = [0, 0.3, 0.4, 0.5, 0.6, 0.7, 0.9]$.

chip delays of the interferers are distributed between $0.3T_c$ to $0.7T_c$. It can be seen that differences in performance among the three filters are minimal when $E_b/N_o < 5$ dB. In fact, they converge as $E_b/N_o \to 0$. This can be expected since the NWMF and CLMF reduce to the CMF when AWGN predominates as the signal powers of the interferers go to zero. SNR gains greater than 1.0 dB for the NWMF and CLMF over the CMF begin to appear and increase for $E_b/N_o \geq 10$ dB. For example, at $E_b/N_o = 20$ dB, SNR(CLMF) = 19.7 dB, SNR(NWMF) = 18.1 dB and SNR(CMF) = 13.2 dB. Thus, at $E_b/N_o = 20$ dB, the SNR gain of the NWMF over the CMF is nearly 5 dB while that supplied by the CLMF provides an additional 1.6 dB above the NWMF.

Case b) illustrates the condition when chip delays are spaced evenly with one interferer chip synchronized to the desired user. Again, differences in performance among the three filters are minimal when $E_b/N_o < 5$ dB. SNR gains greater than 1 dB for the CLMF and NWMF over the CMF only begin to appear for $E_b/N_o \geq 13$ dB. The gain offered by the CLMF over the NWMF is hardly noticeable. For example, at $E_b/N_o = 20$ dB, SNR(CLMF) = 14.7 dB, SNR(NWMF) = 14.4 dB and SNR(CMF) = 11.9 dB. Thus, at $E_b/N_o = 20$ dB, the SNR gain supplied by the NWMF over the CMF is 2.5 dB while that supplied by the CLMF provides only an additional 0.3 dB above the NWMF. In both a) and b), as E_b/N_o increases, the SNR of the CMF tends to level off while that of the two other curves tends to increase. However, compared to a), the SNR performance across the three filters are markedly reduced in b). In general, at large E_b/N_o, (5.5) can be approximated as $\mathrm{SNR}_{\mathrm{opt}} \approx \frac{2E_b}{N_o} \cdot \frac{1}{T_b} \left[E_a - \boldsymbol{a}^{(C)} \boldsymbol{C}^{(C)^{-1}} \boldsymbol{a}^{(C)^{\mathrm{H}}}\right]$ such that $\mathrm{SNR}_{\mathrm{opt}}$ increases linearly with E_b/N_o as long as $E_a > \boldsymbol{a}^{(C)} \boldsymbol{C}^{(C)-1} \boldsymbol{a}^{(C)^{\mathrm{H}}}$.

In summary, E_b/N_o plays an important role in determining the effectiveness of the NWMF and CLMF over the CMF. At low $E_b/N_o < 5$ dB, the SNR performance of the three MFs converge. When $E_b/N_o > 14$ dB, the SNR performance of the CLMF and NWMF provides more than a 1 dB improvement over the CMF. This improvement increases as E_b/N_o increases beyond 14 dB. In comparison to the NWMF, the CLMF offers SNR gains when the interferers have chip delays clustered about $0.5T_c$. The gain diminishes when chip delays are distributed over $T_k \in [0, T_c)$ especially when a chip-synchronous interferer is present.

SNR vs. Interferer Signal Power

Next, the effect of power-imbalance conditions on SNR performance of the filters is examined when $K = 5$. In the example to be considered, there exists one user $k = 1$ at $T_1 = 0.5T_c$ whose received signal power level is much larger than other users in the system. SNR vs. β_1 is shown in Fig. 5.3 when $E_b/N_o = 20$ dB, $K = 5$, $\boldsymbol{\beta} = [\beta_1, 1, 1, 1, 1]$, and the chip-delays of the interferers are $\mathbf{T}/T_c = [0.3, 0.4, 0.5, 0.6, 0.7]$. Two scenarios are presented. In case a), all the interferers are chip-delay locked. As β_1 increases, the SNR of the CMF deteriorates severely while those of the NWMF and CLMF remain significantly higher. For example, at $\beta_1 = 10$ dB, SNR(CLMF) = 19.4 dB, SNR(NWMF) = 17.0 dB and SNR(CMF) = 9.9 dB. Thus, at $\beta_1 = 10$ dB, the SNR gain of the NWMF over the CMF is 7.1 dB while that supplied by the CLMF provides an additional 2.4 dB above the NWMF. As β_1 increases beyond 10 dB, the NWMF performance degrades progressively whereas the SNR of the CLMF slowly tends towards 19.3 dB at $\beta_1 = 30$ dB and is hardly affected by the strong interferer.

In case b), $K_C = 1$ and $K_U = 4$ where only user 1 is chip-delay locked at $T_1/T_c =$

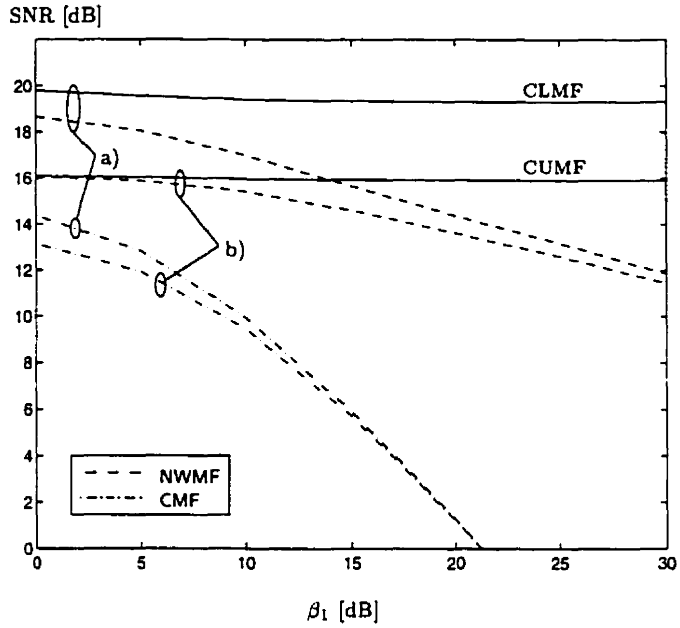

Fig. 5.3 SNR vs. β_1 [dB] for the rectangular pulse when $K = 5$, $\boldsymbol{\beta} = [\beta_1, 1, 1, 1, 1]$, $\mathbf{T}/T_c = [0.3, 0.4, 0.5, 0.6, 0.7]$, $N = 31$ and $E_b/N_o = 20$ dB. In case a), all interferers are chip-delay locked. In case b), $K_C = 1$ and $K_U = 4$. Only user 1 is chip-delay locked at $T_1/T_c = 0.3$ while the remaining 4 users are unlocked.

0.3. This is an example of SNR performance when a combination of unlocked and chip-delay locked interferers are present. Having the strong interferer chip-delay locked permits the SNR performance of the CUMF to remain at roughly 16 dB over $\beta_1 \in [1, 10^3]$. The SNRs of the NWMF and CMF degrade as β_1 increases. For example, at $\beta_1 = 10$ dB, SNR(CLMF) = 16.0 dB, SNR(NWMF) = 15.4 dB and SNR(CMF) = 9.5 dB. Thus, at $\beta_1 = 10$ dB, the SNR gain of the NWMF over the CMF is 5.9 dB while that supplied by the CLMF provides an additional 0.6 dB above the NWMF.

Both cases clearly illustrate the substantial SNR gains achievable by the CLMF, CUMF and NWMF, compared to the CMF, when a strong interferer is present. Additional SNR gains can be obtained by the CLMF and CUMF in comparison to the NWMF. The SNR of the CMF and NWMF continues to deteriorate as the interferer power increases. On the contrary, the CLMF and CUMF maintains a higher, relatively constant SNR regardless of the locked interferer's strength when $T_1 = 0.3T_c$. The same phenomenon is observed for smaller T_1 to a lesser extent as long as $T_1 \neq 0$. In the limit, as $T_1 \to 0$, the SNR performance of the CLMF, CUMF and NWMF converge to that of the CMF.

SNR vs. Phase-Offset

In all the results presented before and after this section, phase-offsets of interferers have been assumed to be unknown and uniformly distributed over $T_k \in [0, T_c)$. In this section, the effect of phase-offset information on the performance of the CLMF is examined briefly.

In Fig. 5.1, the performance of SNR vs. θ_1 is presented for the SNR maximizing filter denoted as phase-CLMF, the CLMF, NWMF and CMF when $K = 1$, $T_1 = 0.5T_c$, $\beta_1 = 1$ and $E_b/N_o = 20$ dB. In the plot, θ_1 ranges from 0 to $\pi/2$ to π when the

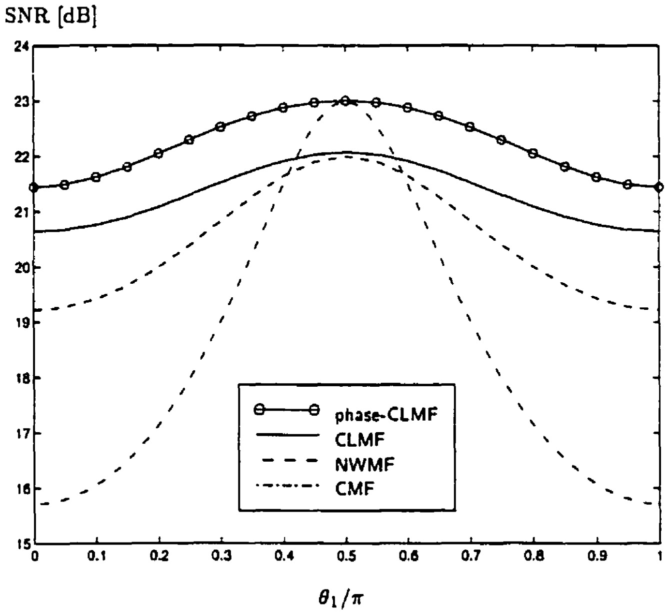

Fig. 5.4 SNR vs. θ_1/π for the rectangular pulse when $K = 1$, $N = 31$, $T_1 = 0.5T_c$, $\beta_1 = 1$ and $E_b/N_o = 20$ dB.

interferer is, respectively, in-phase, in quadrature or 180° out-of phase with the signal of the desired user. The phase-CLMF maximizes SNR across all phase values. As can be expected, the CMF maximizes SNR like the phase-CLMF at $\theta_1 = \pi/2$ when the DS-BPSK interferer is orthogonal to the desired user's signal. However, the SNR of the CMF suffers considerably as θ_1 approaches 0 or π. In contrast, the SNR of the CLMF ranges from 0.8 to 1.0 dB below that of the phase-CLMF. The SNR of the NWMF ranges from 1 to 2.2 dB below that of the phase-CLMF. For example, at $\theta_1 = 0$, SNR(phase-CLMF) = 21.4 dB, SNR(CLMF) = 20.6 dB, SNR(NWMF) = 19.2 dB and SNR(CMF) = 15.7 dB. These are the minimum SNR for each filter type. In this case, the improvement in SNR over the CMF offered by the NWMF, CLMF and phase-CLMF is, respectively, 3.5, 4.9, and 5.7 dB. Thus, in applications where phase remains relatively constant, gains in SNR obtained from chip delay information can be supplemented by taking phase information into account in the design of the MF.

5.3 Near-Far Resistance

Near-far resistance is a measure quantifying the robustness of a receiver against the power-imbalance problem [60, 51]. In this section, the near-far resistances of the CLMF and NWMF are investigated. Its expression for the BLMF has already been derived in [62]. The near-far resistance of the MFs is investigated in two parts. In the first part, the near-far resistance expression is generalized for arbitrary LTI filters and for spreading waveforms $\tilde{a}^{(k)}(t)$ not necessarily constrained to exist only over $t \in [0, T_b)$. Expressions for the CLMF and NWMF are then derived. In the second part, several simple numerical examples are presented to illustrate the near-far resistance over various chip pulses.

5.3.1 Near-Far Resistance Expressions

The near-far resistance expression in [60, 51, 112] is generalized for an arbitrary LTI filter $\tilde{h}(t)$ and for spreading waveforms $\tilde{a}^{(k)}(t)$, as defined in (2.8) and (3.28), which exists over $t \in [-(M-1)T_c, T_b + MT_c]$. Using [112, (10)], given τ_k and P_k, the probability of error in the bit estimate $\hat{b}_0^{(0)}$ is

$$P_{e,0}(\sigma) = \mathrm{E}\left[Q\left(\left\{\sqrt{P_0}D + \sum_{k=1}^{K}\sqrt{P_k}\sum_{m=M_1}^{M_2} b_m^{(k)}\rho_{k,m}(\tau_k)\right\} \Big/ \left(\sigma\sqrt{E_h}\right)\right)\right] \tag{5.7}$$

where $\sigma^2 = N_o/2$ and $\mathrm{Prob}[b_m^{(k)} = 1] = \mathrm{Prob}[b_m^{(k)} = -1] = 1/2$. The energy of the filter impulse response is

$$E_h = \int_0^{T_b} \left|\tilde{h}(T_b - t)\right|^2 dt. \tag{5.8}$$

The desired component of the filter output is

$$D = \mathcal{R}e\left[\int_0^{T_b} \tilde{a}^{(0)}(t)\tilde{h}(T_b - t)dt\right]. \tag{5.9}$$

The partial correlation function between the impulse response and shifted spreading signal associated with the kth interferer's mth bit is

$$\rho_{k,m}(\tau_k) = \mathcal{R}e\left[\int_0^{T_b} \tilde{a}^{(k)}(t-\tau_k-mT_b)\tilde{h}(T_b-t)dt\right]. \quad (5.10)$$

As explained in [112, p. 891], in the low AWGN region where σ is small, the right hand side of (5.7) is dominated by the summand with the smallest argument:

$$z_0(\sigma) = \frac{\sqrt{P_0}D - \sum_{k=1}^{K}\sqrt{P_k}\sum_{m=M_1}^{M_2}|\rho_{k,m}(\tau_k)|}{\sqrt{E_h}}. \quad (5.11)$$

The slope of the $P_{e,0}(\sigma)$ curve at high SNR, representing the *asymptotic efficiency* of the filter [60, 51, 112], is

$$\eta_0 = \max^2\left\{0, \lim_{\sigma\to 0}\frac{z_0(\sigma)}{\sqrt{P_0 T_b}}\right\}. \quad (5.12)$$

For example, given the CMF $\tilde{f}(t) = \tilde{a}^{(0)*}(t)$ (where $\tilde{h}(t)$ is obtained by using (3.6) and removing the scaling factor $N_o/2$), when $K = 1$ and $M = 1$ (such that $M_1 = -1$, $M_2 = 0$), $E_h = D = T_b$ and (5.12) reduces to $\eta_0 = \max^2\left\{0, 1-\sqrt{\frac{P_1}{P_0}}\cdot\frac{1}{T_b}(|\rho_{k,-1}(\tau_1)|+|\rho_{k,0}(\tau_1)|)\right\}$ as given in [51, p. 172 (11)]. Near-far resistance is defined as the minimum asymptotic efficiency over the relative signal powers of the interferers [51]: $\min_{\{\beta_1,\ldots\beta_K\}}\eta_0$. Its value ranges from the minimum of no near-far resistance of 0 to a maximum level of 1. Since, in general, $\rho_{k,m}(\tau_1) \neq 0$, the near-far resistance of the CMF is 0.

Near-Far Resistance of CLMF

The following derivation takes into account the property that the near-far resistance of the BLMF is equivalent to that of its limiting form D-BLMF (as $N_o \to 0$) [77]. The same property applies to the CLMF whose limiting form is the D-CLMF. When all the interferers are chip-delay locked, the substitution of (3.33) into (5.10) results in $\rho_{k,m}(\tau_k) = 0$ for all m under the constraint $\tau_k \bmod T_c = T_k$. Similar to the D-BLMF, the MAI is completed removed. Substitution of (3.33) (or (3.33) using (3.6) (with the removal of the scaling factor $N_o/2$) into (5.8) and (5.9) reduces the CLMF asymptotic efficiency to

$$\eta_0 = \frac{1}{T_b}\left[E_a - \boldsymbol{a}^{(C)}\boldsymbol{C}^{(C)-1}\boldsymbol{a}^{(C)^H}\right] \quad (5.13)$$

where E_a is defined in (5.6). The $\boldsymbol{a}^{(C)}$ and $\boldsymbol{C}^{(C)}$ are given in (C.10) and (C.11), respectively, in Appendix C.2. When $M = 1$, $E_a = T_b$ and (5.13) reduces to a form similar to that for the BLMF in [62, (30)]: $\eta_0 = 1 - \frac{1}{T_b}\boldsymbol{a}^{(C)}\boldsymbol{C}^{(C)-1}\boldsymbol{a}^{(C)^{\mathrm{H}}}$. Since (5.13) is independent of interferer signal powers, it is equivalent to the near-far resistance. Furthermore, it is independent of the spreading sequences of the interferers in contrast to the BLMF and D-BLMF [51, 62]. It is, however, dependent on the desired user's spreading sequence, chip filter selection and chip delays of the interferers imbedded in $\boldsymbol{a}^{(C)}$ and $\boldsymbol{C}^{(C)}$.

Near-Far Resistance of NWMF

For chip filters of finite bandwidth, the near-far resistance of the NWMF is 0 as shown in Appendix I. A non-zero near-far resistance would only be possible if the inverse chip filter $1/Q(f)$ existed (with infinite bandwidth). In fact, as long as no interferers were chip synchronous ($T_k \neq 0$), it would, in theory, deliver the maximum near-far resistance of 1. This interesting result follows since, in the absence of AWGN, the inverse chip filter would generate a train of delta functions [110, pp. 170-177] when excited by the signals of each user in the system. Sampling at the proper time instants would then lead to perfect chip symbol detection. However, as noted in [113], an inverse filter over $f \in (-\infty, \infty)$ is, in general, physically unrealizable. Therefore, for all practical purposes, the NWMF has a near-far resistance of zero.

Signal Space Interpretation of MF Near-Far Resistance

The MF near-far resistance η_0 has a convenient signal space interpretation. By using the signal space representation of signals described in section 3.7, (5.8), (5.9) and (5.10) can be expressed as, respectively, $E_h = \mathcal{R}e[\vec{f}^{\,\mathrm{H}}\vec{f}]$, $D = \mathcal{R}e[\vec{f}^{\,\mathrm{H}}\vec{a}]$ and $\rho_{k,m}(\tau_k) = \mathcal{R}e[\vec{f}^{\,\mathrm{H}}\vec{a}_{k,m}]$. As discussed in section 3.7, in the limit as $N_o \to 0$, $\vec{f} = \vec{a}^o$, $E_h = \vec{a}^{o\mathrm{H}}\vec{a}^o$ and $D = \vec{a}^{o\mathrm{H}}\vec{a}^o$ since $\vec{a}^{o\mathrm{H}}\vec{a} = \vec{a}^{o\mathrm{H}}[\vec{a}^o + \vec{a}^I] = \vec{a}^{o\mathrm{H}}\vec{a}^o + \vec{a}^{o\mathrm{H}}\vec{a}^I$ and $\vec{a}^{o\mathrm{H}}\vec{a}^I = 0$. On the other hand, $\rho_{k,m}(\tau_k) = \mathcal{R}e[\vec{a}^{o\mathrm{H}}\vec{a}_{k,m}] = 0$ since $\vec{a}_{k,m} \in \mathcal{S}_I$ and $\vec{a}^o$ is orthogonal to all vectors in $\mathcal{S}_I$. Substitution of E_h, D and $\rho_{k,m}(\tau_k)$ into (5.12) yields

$$\eta_0 = \frac{1}{T_b}\vec{a}^{o\mathrm{H}}\vec{a}^o \tag{5.14}$$

similar to that given in [62] for the BLMF.

5.3.2 Numerical Examples — Near-Far Resistance

The following numerical examples illustrate the near-far resistance of the CLMF when $K = 1$ over various chip pulse shapes. As discussed earlier, near-far resistance depends upon the desired user's spreading sequence. This implies that in the case of long sequence spreading, the near-far resistance can change with each bit symbol since the desired user's spreading sequence changes. Here, as in the previous numerical examples, the spreading sequence of the desired user is set to that for user $k = 0$ in Table 5.1. Since the near-far resistances of the CMF and NWMF are both zero, they need not be considered. In theory, however, if the inverse filter for the rectangular chip pulse did exist, the NWMF would have a near-far resistance of 1 as long as $T_1 \neq 0$.

In Fig. 5.5, η_0 vs. T_1/T_c is plotted for the rectangular chip pulse. As the interferer

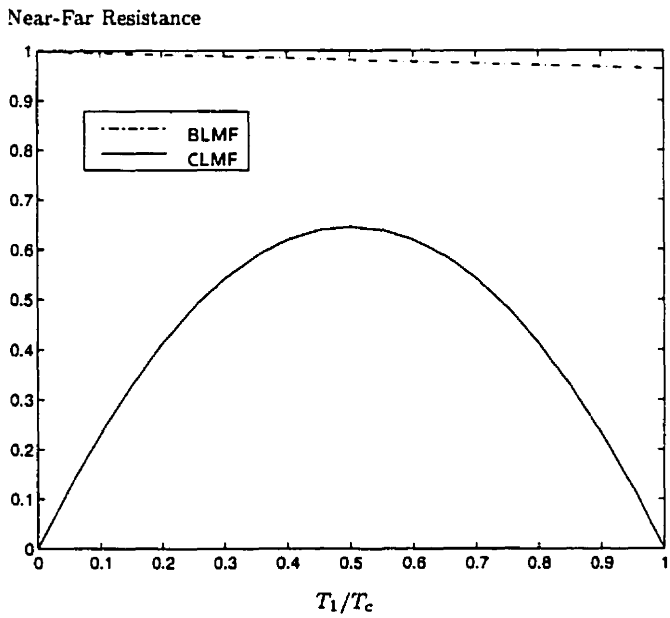

Fig. 5.5 Near-far resistance vs. T_1/T_c for the rectangular chip pulse when $K = 1$ and $N = 31$.

becomes chip synchronous, the near-far resistance goes to zero. When the interferer is furthest from being chip synchronous at $T_1/T_c = 0.5$, a maximum near-far resistance of 0.65 is achieved with respect to the spreading sequence $\mathbf{a}^{(0)}$ defined in section 5.1.2. In general, the near-far resistance of the CLMF will depend on the desired user's spreading sequence, the number of interferers and their chip delay distribution. For comparison, the near-far resistance of the BLMF is plotted where $\tau_1 = T_1$ and $\mathbf{a}^{(1)}$ is defined in section 5.1.2. The near-far resistance of the BLMF is equivalent to that of the D-BLMF (or one-shot decorrelator). As can be expected, knowledge of the interferer's spreading sequence and its bit-delay delivers excellent near-far resistance. Its performance, however, is obtained at the expense of requiring more signal parameters and short sequence spreading.

In Fig. 5.6, η_0 vs. T_1/T_c is plotted for the three bandwidth efficient chip pulses with respect to only the CLMF, As observed with the rectangular pulse shape, for

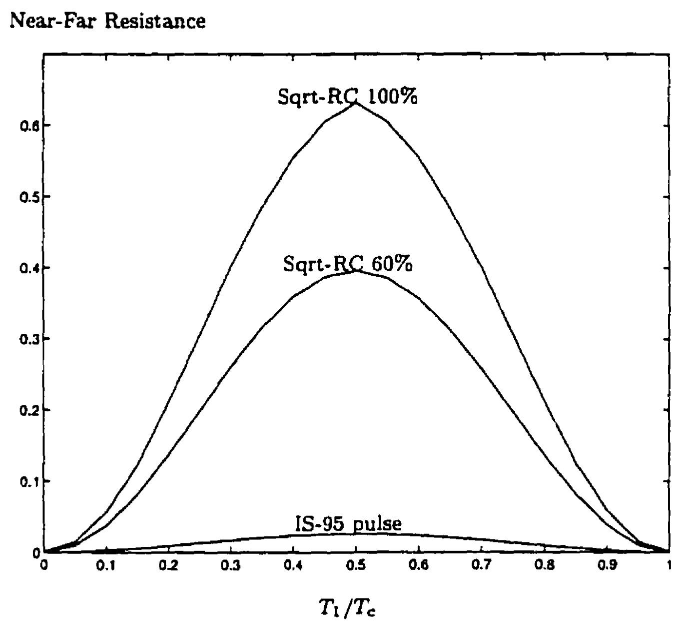

Fig. 5.6 Near-far resistance of the CLMF vs. T_1/T_c for bandwidth efficient chip pulses when $K = 1$ and $N = 31$.

each of the three pulse shapes, η_0 attains its maximum at $T_1 = 0.5T_c$ and its minimum of 0 at $T_1 = 0$. For the sqrt-RC 100%, sqrt-RC 60% and IS-95 pulse, their maximum η_0 are, respectively, 0.63, 0.40, and 0.03. Thus, it is apparent that, as the excess bandwidth of the chip pulse decreases, near-far resistance of the CLMF decreases as well. In the limit as $\alpha \to 0$, since the CLMF reduces to the NWMF, the near-far resistance of the CLMF becomes 0.

5.4 Bit Error Rate (BER)

In this section, the BER ($P_{e,0}$) performances of the CLMF, NWMF and CMF are examined for the special case of short sequence spreading. The user and spreading sequence assignments are listed in Table 5.1. The BER associated with the various filters are calculated by using the characteristic function method of [114] which takes into account the effect of random interferer phase offsets. Modifications to the original expressions in [114] are given in Appendix J.

Several terms are introduced. First, BER(MF type) represents the BER of the MF specified in the argument. Second, the bit-delay vector $\boldsymbol{\tau} = [\tau_1, \tau_2, \ldots, \tau_K]$ holds the interferer bit delays. And third, the chip-delay vector $\mathbf{T} = \boldsymbol{\tau} \bmod T_c$ holds the interferer chip delays.

5.4.1 Numerical Examples — BER

Three sets of numerical examples for BER performance are presented for the rectangular chip pulse. The first two sets consider the situation when the chip delays are distributed from $0.3T_c$ to $0.7T_c$ under varying power-imbalance conditions. The third set considers the situation when the chip delays are distributed over 0 to T_c and when a chip synchronous is present under uniform signal powers.

The BER performance is first examined when $K = 5$ with a bit delay distribution of $\boldsymbol{\tau}/T_c = [6.3, 6.4, 6.5, 6.6, 6.7]$. Fig. 5.7 presents a plot of the BER vs. E_b/N_o for two cases. Case a) illustrates uniform signal power conditions where $\boldsymbol{\beta} = [1, 1, 1, 1, 1]$. To serve as references, BER curves for BPSK, D-BLMF and CMF are plotted as well.

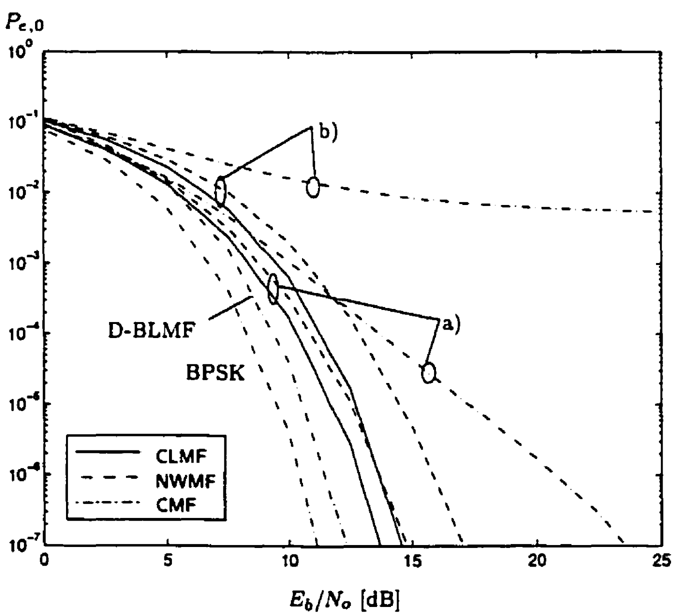

Fig. 5.7 $P_{e,0}$ vs. E_b/N_o when $K = 5$ and all interferers are chip-delay locked at $\boldsymbol{\tau}/T_c = [6.3, 6.4, 6.5, 6.6, 6.7]$. In case a), all signal powers are uniform. In case b), $\boldsymbol{\beta} = [10, 1, 1, 1, 1]$.

The BPSK curve represents the performance of the CMF when $K = 0$ and no MAI is present. It also represents the lower bound in performance of all LTI filters when MAI is or is not present. The D-BLMF curve is provided to illustrate the gain in performance that can be obtained under short sequence spreading when spreading sequence and bit delay information is available. The performance of the NWMF and CLMF falls between that of the CMF and D-BLMF. Over all E_b/N_o, BER(CLMF) $\leq$ BER(NWMF) $\leq$ BER(CMF). At low E_b/N_o, the BERs associated with the three filters hardly differ. This is to be expected since the impulse responses of both the CLMF and NWMF approach that of the CMF as $P_k/N_o \to 0$. Substantial differences in BER begin to appear when $E_b/N_o > 10$ dB. For example, at $E_b/N_o = 12.5$ dB, BER(CLMF) $= 2.7 \times 10^{-6}$. BER(NWMF) $= 1.1 \times 10^{-5}$ and BER(CMF) $= 2.2 \times 10^{-4}$. Thus, at $E_b/N_o = 12.5$ dB, the NWMF delivers a BER improvement of over one order magnitude over the CMF while the CLMF delivers roughly an additional one order of magnitude improvement over the NWMF.

In case b), interferer $k = 1$ has a received signal power 10 times greater than the desired user such that $\beta = [10, 1, 1, 1, 1]$. The BER performance of the CMF suffers considerably and encounters an error floor in that its BER stays above 5×10^{-3} over the range $E_b/N_o \in [0, 25]$ dB. In contrast, the BER of the CLMF and NWMF improves as E_b/N_o increases. For example, at $E_b/N_o = 12.5$ dB, BER(CLMF) $= 1.7 \times 10^{-5}$. BER(NWMF) $= 1.7 \times 10^{-4}$ and BER(CMF) $= 1.1 \times 10^{-2}$. Thus, at $E_b/N_o = 12.5$ dB, the NWMF delivers a BER improvement of roughly two orders of magnitude over the CMF while the CLMF delivers an additional one of order magnitude gain over the NWMF. In comparison to a), the presence of the strong interferer has reduced the BERs of both the CLMF and NWMF by one order of magnitude. For larger interfering powers, further gains between the three filters can be expected as Fig. 5.3 indicates.

Fig. 5.8, illustrates a more severe scenario of power-imbalance where all interferers are 6 dB stronger than the desired user. Again, the BER of the CMF encounters an error floor in that its BER stays above 1.9×10^{-2} over $E_b/N_o \in [0, 25]$ dB. The BERs of the NWMF and CLMF still tend to improve as E_b/N_o increases. At $E_b/N_o = 12.5$ dB, BER(CLMF) $= 2.6 \times 10^{-5}$. BER(NWMF) $= 3.1 \times 10^{-4}$ and BER(CMF) $= 2.6 \times 10^{-2}$. Again, the NWMF delivers a BER improvement of roughly two orders of magnitude over the CMF while the CLMF delivers an additional one order magnitude over the NWMF.

In the third set of numerical examples, the effect of the chip delay distribution on BER is considered for only the CLMF and NWMF. Three chip distributions are

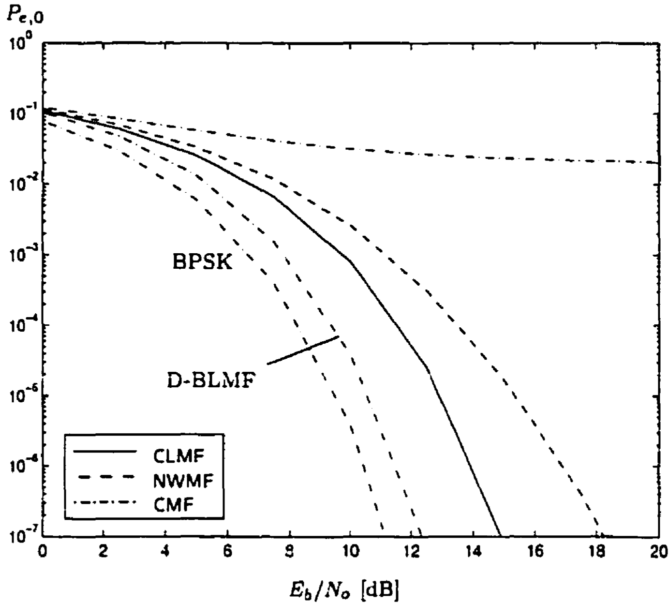

Fig. 5.8 $P_{e,0}$ vs. E_b/N_o when $K = 5$, all interferers are chip-delay locked at $\boldsymbol{\tau}/T_c = [6.3, 6.4, 6.5, 6.6, 6.7]$ and $\boldsymbol{\beta} = [4, 4, 4, 4, 4]$.

considered. The order of the cases progress from chip delays clustered about $0.5T_c$ to the case where the chip delays are spaced evenly across $[0, T_c)$ with one chip-synchronous interferer. Fig. 5.9 presents a plot of BER vs. E_b/N_o for the three cases when $K = 7$ and the received signal powers are uniform. In all cases, the BER of CLMF is always lower or equal to that of the NWMF and the disparity in performance tends to increase as E_b/N_o increases. In case a), the user chip delays are somewhat clustered about $0.5T_c$. For example, at $E_b/N_o = 12.5$ dB, BER(CLMF) $= 2.1 \times 10^{-6}$ and BER(NWMF) $= 1.3 \times 10^{-5}$. The BER of CLMF is roughly one order of magnitude less than that of the NWMF. As the users are spread across the interval $[0, T_c)$, the BER performance of both filters begins to deteriorate and shift to the right. Moreover, the performance gains of the CLMF over the NWMF diminishes as shown in case b). This can be seen at $E_b/N_o = 12.5$ dB where BER(CLMF) $=$ 2.3×10^{-5} and BER(NWMF) $= 4.0 \times 10^{-5}$.

In case c) where user 1 is chip synchronized to the desired user. The BER degrades further for both the CLMF and NWMF while the BER improvement of the CLMF over the NWMF diminishes further. This can be seen again at $E_b/N_o = 12.5$ dB where BER(CLMF) $= 5.2 \times 10^{-5}$ and BER(NWMF) $= 7.6 \times 10^{-5}$.

Hence, under uniform signal power conditions, the presence of chip-synchronous or quasi-chip synchronous users diminishes the gains in BER performance over the

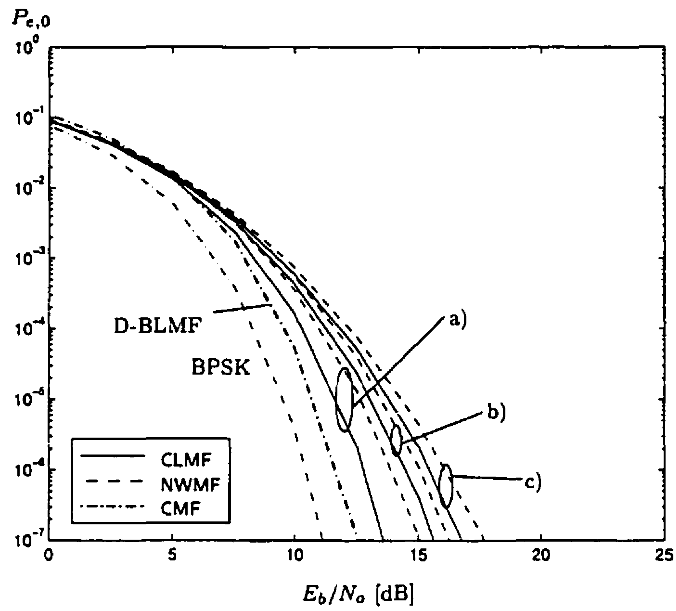

Fig. 5.9 $P_{e,0}$ vs. E_b/N_o when $K = 7$ and all signal powers are uniform. In case a), $\tau\ /T_c = [10.3, 10.35,\ 10.4, 10.5, 10.55,\ 10.6, 10.7]$. In case b), $\tau\ /T_c = [10.1, 10.3,\ 10.4, 10.5, 10.6, 10.7, 10.9]$, In case c), $\tau\ /T_c = [10.0, 10.3, 10.4,\ 10.5, 10.6, 10.7, 10.9]$.

NWMF. When, on the other hand, the interferers are clustered about $0.5T_c$, the improvement in BER performance of the CLMF over the NWMF widens.

5.5 Probability of Outage

In the previous sections, the numerical examples were restricted to a particular spreading sequence of the desired user and particular realizations of signal parameters of the interferers. That is, SNR was computed for specific conditions where each argument in (5.3) was fixed. In this section, performance is investigated under more general conditions since the signal parameters are in fact random variables and can assume a wide range of realizations. Likewise, under long sequence spreading, the spreading sequence associated with each consecutive bit changes as well. In order to assess the performance of the MFs over a wide range of conditions, a measure known as probability of outage P_{out} is introduced. First, the measure is defined and its method of calculation is outlined. This is followed by two sets of numerical examples. The first set illustrates P_{out} according to the four possible chip waveforms when the signal powers of all users are uniform. The second set illustrates P_{out} under power imbalance conditions when the signal powers are no longer uniform for the IS-95 pulse, exclusively. In all numerical examples with bandwidth efficient pulses, ISI is taken into account not only in deriving the NWMF and CLMF but also in computing their SNRs.

5.5.1 Definition of Probability of Outage

The probability of outage is defined as $P_{\text{out}} = \text{Prob}\,(\text{BER} > \text{BER}_{\text{max}})$ where BER_{max} represents the maximum tolerable BER [15]. Under the assumption of an efficient modem, a powerful convolutional code and two-antenna diversity, P_{out} can be approximated as [15]

$$P_{\text{out}} = \text{Prob}\,(\text{SNR} < \text{SNR}_{\text{min}}) \tag{5.15}$$

where SNR_{min} represents the minimum tolerable level of SNR performance. This approximation, used to assess the P_{out} and capacity of the IS-95 system [15], provides a loose interpretation of P_{out} in terms of SNR. For instance, for voice service at $\text{BER}_{\text{max}} = 10^{-3}$ in a cellular system employing convolutional coding with: $R_c = 1/3$, a constraint length of 9 and soft decision decoding, SNR_{min} is typically 7 dB [115, 15].

5.5.2 Method of Calculation

As explained previously, the probability of outage in (5.15) depends upon two quantities: SNR and SNR_{min}. The latter is a constant which is dependent on the type of service to be provided. In each of the numerical examples of P_{out}, voice service is assumed by setting $\text{SNR}_{\text{min}} = 7$ dB. In contrast, the former whose expression is given in (5.2) is a function of a number of parameters as summarized in (5.3). All the arguments in (5.3) except for two are fixed. Specifically, the functions and parameters: $N, E_b/N_o, \tilde{q}(t), \tilde{h}(t), K$ and $\boldsymbol{\beta}$ are fixed while $\mathbf{T}$ and $\mathbf{a}^{(0)}$ are random vectors. Consequently, SNR is a random variable and P_{out} in (5.15) is evaluated over all possible realizations of $\mathbf{T}$ and $\mathbf{a}^{(0)}$. The chip delays in $\mathbf{T}$ are assumed to be i.i.d. where each chip delay T_k in $\mathbf{T}$ is assumed to be uniformly distributed over $T_k \in [0, T_c)$. As noted in section 5.1.2, the spreading sequence of the desired user is randomly generated and changes for each consecutive bit symbol.

There are two ways of evaluating P_{out} in (5.15). The first method requires analytically determining the closed form expression for the probability density function (PDF) of the SNR. The second method instead evaluates the relative frequency of outage events by generating a large number of sampled values of the random variable SNR and counting the number of outage events which occur. This is known as the *Monte Carlo* method. Since a closed form expression for the PDF of the SNR could not be obtained, the first method could not be used and the Monte Carlo method was selected to compute P_{out}.

Monte Carlo Method

In its basic form, the Monte Carlo method generates N_S samples (or outcomes) of the random variable SNR [116, pp. 221–237]. These samples are computed by generating a total of N_S realizations of the parameters which affect SNR. That is, in each sample, a randomly selected realization of $\mathbf{a}^{(0)}$ and $\mathbf{T}$ is used to produce unbiased estimates of SNR. N_a independent realizations of $\mathbf{a}^{(0)}$ and N_T independent realizations of $\mathbf{T}$ are generated to provide $N_S = N_a \times N_T$ samples. Each realization generates an SNR sample indexed by n which is compared to SNR_{min}. An error event occurs when $\text{SNR}_n < \text{SNR}_{\text{min}}$. The probability of outage in (5.15) can then be approximated by

$$P_{\text{out}} \approx \frac{N_{\text{out}}}{N_S} \tag{5.16}$$

where the number of outage events N_{out} is defined as

$$N_{\text{out}} = \sum_{n=1}^{N_S} \mathrm{I}_{\text{ind}}\left(\text{SNR}_n - \text{SNR}_{\text{min}}\right). \tag{5.17}$$

The indicator function $\mathrm{I}_{\text{ind}}(x)$ returns 1 for an outage event and 0 for no outage event. It is defined mathematically as

$$\mathrm{I}_{\text{ind}}(x) = \begin{cases} 1, & \text{if } x < 0 \\ 0, & \text{otherwise.} \end{cases} \tag{5.18}$$

The difficulty with the Monte Carlo method is the computational burden associated with estimating very low values of outage probability. This occurs because of two reasons. One, the sample size N_S needs to be much greater than $1/P_{\text{out}}$. And two, the computational complexity involved in computing each individual SNR sample is quite high. Thus, coupled together, the number of computations required to obtain outage results for $P_{\text{out}} < 10^{-2}$ at even modest values of N can be very large.

Modified Monte Carlo Method

The computational burden of the Monte Carlo method can be reduced significantly by using the *Modified Monte Carlo* method described in [117]. The method modifies the process of sampling the chip delays in the random vector $\mathbf{T}$ using a technique known as importance sampling. The selection of random vector samples is biased towards increasing the probability of an error event which would otherwise occur rarely. With respect to chip delays, error events can be biased to occur more frequently by generating chip delay samples much closer to either 0 or T_c. This takes advantage of the findings in section 5.2 where chip-delay values closer to either 0 (or T_c by symmetry) tended to deliver lower SNR. The resulting biased estimate $P_{\text{out,biased}}$ is then processed to return an unbiased estimate of P_{out}. This method can effectively reduce the required sample size N_S by one to three orders of magnitude. The algorithm for evaluating the probability of outage via the Modified Monte Carlo method is outlined in Appendix K.1.

Interval Estimate of P_{out}

In order to obtain an estimate of P_{out}, the Modified Monte Carlo method of estimating the probability of outage is repeated M_{out} times to generate M_{out} samples of $P_{\text{out,m}}$ indexed by $m \in [1, M_{\text{out}}]$. From these samples, an interval estimate of P_{out} can then be computed. The interval estimate is represented by

$$\text{Prob}\left[P_{\text{out,low}} < P_{\text{out}} < P_{\text{out,upp}}\right] \quad > \quad \gamma_{\text{out}} \tag{5.19}$$

where γ_{out} represents the *confidence coefficient* of the estimate and $[P_{\text{out,low}}, P_{\text{out,upp}}]$ represents the *confidence interval* of P_{out}. The γ_{out} is a parameter whose value is set to a desired degree of confidence. In the numerical examples to follow, it is set to $\gamma_{\text{out}} = 99\%$. The bounds of the confidence interval $P_{\text{out,low}}$ and $P_{\text{out,upp}}$ are then computed based on γ_{out} and the M_{out} samples of $P_{\text{out,m}}$ using the procedure outlined in [116, pp. 244–248] and reproduced in Appendix K.2. Consequently, the probability that P_{out} lies in the interval $[P_{\text{out,low}}, P_{\text{out,upp}}]$ is $\gamma_{\text{out}} = 99\%$. The numerical examples of P_{out} plot both the confidence interval $[P_{\text{out,low}}, P_{\text{out,upp}}]$ and mean of the samples $\overline{P}_{\text{out}}$.

5.5.3 Numerical Examples — Probability of Outage

Numerical examples of probability of outage vs. K are presented in two sets of plots. The first set assumes uniform signal powers while the second set considers the effect of power-imbalance.

Outage under Uniform Signal Powers

The probability of outage is computed for the CMF, NWMF and CLMF when the signal powers of all users are uniform. The examples are investigated according to the selection of one of the four possible chip pulses in the order of decreasing excess bandwidth. It is stressed that most of the P_{out} results for the NWMF are new. Previously, the performance of NWMF vs. K had been investigated for only the rectangular pulse in [86].

Several terms to facilitate the analysis are defined. Associated with each plot and each MF is a *transition region* which is defined arbitrarily as the range of K for which $10^{-6} < P_{\text{out}} < 10^{-1}$. For K to the left of this region, the system operates at $P_{\text{out}} < 10^{-6}$. For K to the right of this region, the system operates at $P_{\text{out}} < 10^{-1}$. Thus, the transition region represents the range of users over which the system moves from low P_{out} to high P_{out}. Systems with wide transition regions tend to move gradually from low to high outage conditions as K increases. On the other hand, systems with narrow transition regions tend to change abruptly between the two extremes. In addition, the expressions P_{out}(MF type) and $\overline{P}_{\text{out}}$(MF type) represent, respectively, the P_{out} and $\overline{P}_{\text{out}}$ of the MF specified in the argument where the MF type may be either the CMF, NWMF or CLMF. And lastly, an estimate of the maximum number of users $K+1$ which the system can support can be obtained by defining an upper bound $P_{\text{out,max}}$ to P_{out}. The user capacity of the system is defined as the maximum value of $K+1$ which is denoted as $K_{\max}+1$ for which the probability of outage satisfies $P_{\text{out}} < P_{\text{out,max}}$. In the ensuing analysis, $P_{\text{out,max}} = 1\%$ is chosen. Thus, user capacity is given by the maximum value of $K_{\max}+1$ which satisfies $P_{\text{out}} < 1\%$,

<u>Probability of Outage for the Rectangular Pulse</u>

The plot of P_{out} vs. K for the rectangular chip pulse is given in Fig. 5.10 where $N = 8$ and $E_b/N_o = 20$ dB. Although N is small, its PG is in fact very large. This is because of the large bandwidth associated with the rectangular pulse. As discussed in section 5.1.1, since $B = 32.5 \cdot \frac{1}{T_c}$, PG $= 65N = 520$ according to (2.5). For $K \leq 3$, outages could not be generated from a sample size exceeding that used to evaluate P_{out} at $K = 4$. This indicates that $P_{\text{out}} << 10^{-5}$ for $K \leq 3$ for all three MFs.

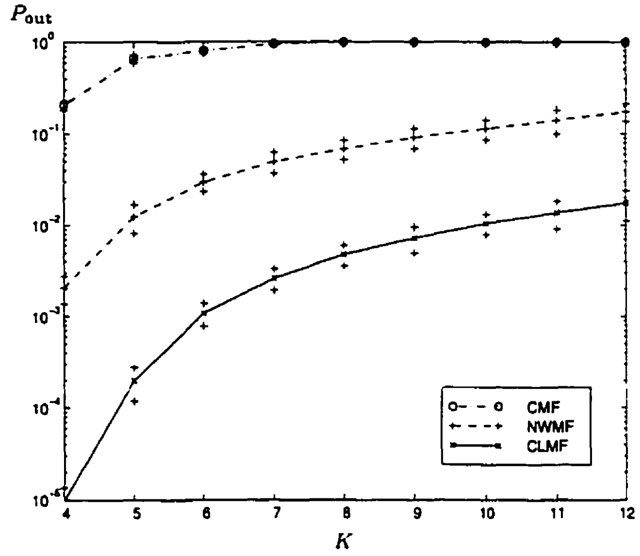

Fig. 5.10 Outage probability vs. K for the rectangular pulse when $N = 8$ and $E_b/N_o = 20$ dB.

The plot is analyzed first with respect to each of the MFs. The transition region for the CMF is nil. Its $\overline{P}_{\text{out}}$ curve shows an abrupt change from $\overline{P}_{\text{out}} << 10^{-5}$ at $K \leq 3$ to $\overline{P}_{\text{out}} = 2.1 \times 10^{-1}$ at $K = 4$. That is, the system moves immediately from a condition of low P_{out} to that of high P_{out} when the system shifts from $K = 3$ to $K = 4$. Moreover, the CMF is essentially ineffective for $K \geq 6$ where $P_{\text{out}} \approx 1$. For the NWMF, the transition region extends from $K \in [4, 8]$. For $K \geq 12$, $P_{\text{out}} > 10^{-1}$. For the CLMF, the transition region is very wide and extends from $K = 4$ to $K > 12$. As K increases over $K \in [4, 12]$, the $\overline{P}_{\text{out}}$ curve gradually degrades from 9.6×10^{-6} to 1.8×10^{-2}.

Next, the curves for the three MFs are compared. As discussed above, the transition region is extended from nil for the CMF to 5 users for the NWMF and more than 9 users for the CLMF. As illustrated in the plot, over the entire range of $K \in [4, 12]$, $P_{\text{out}}(\text{NWMF})$ is roughly one to two orders of magnitude below $P_{\text{out}}(\text{CMF})$ while $P_{\text{out}}(\text{CLMF})$ is an additional one to two orders of magnitude below $P_{\text{out}}(\text{NWMF})$. For example, When $K = 5$, $\overline{P}_{\text{out}}(\text{CMF}) = 6.6 \times 10^{-1}$, $\overline{P}_{\text{out}}(\text{NWMF}) = 1.3 \times 10^{-2}$ and $\overline{P}_{\text{out}}(\text{CLMF}) = 2.0 \times 10^{-4}$. Thus, the CLMF delivers a significant reduction in the probability of outage compared to the CMF and NWMF.

Based on user capacity as defined earlier, the CMF, NWMF and CLMF support, respectively 4, 5 and 10 users. This corresponds to $K_{\max} = 3, 4$ and 9 since user capacity is given by $K_{\max} + 1$. Thus, under these conditions, the CLMF increases capacity by 250% with respect to the CMF and doubles the number of users with respect to the NWMF.

Probability of Outage for the Sqrt-RC Pulse, $\alpha = 100\%$

The plot of P_{out} vs. K for for the sqrt-RC chip pulse, $\alpha = 100\%$, is given in Fig. 5.11 where $N = 19$ and $E_b/N_o = 20$ dB. Since $\alpha = 100\%$, using (2.5), PG = 38. For

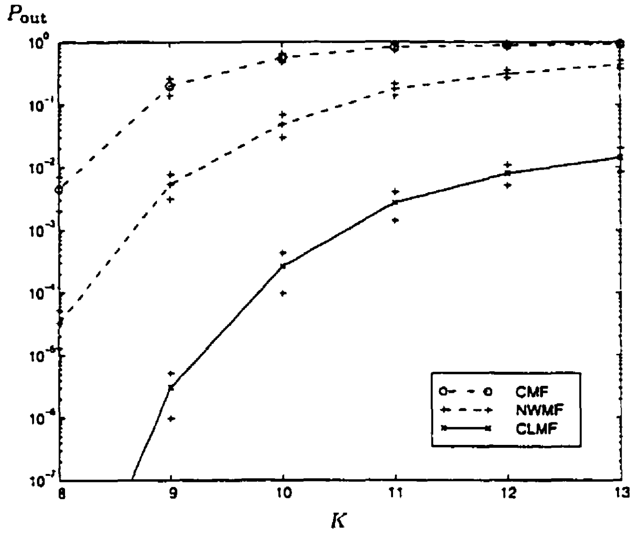

Fig. 5.11 Outage probability vs. K for the $\alpha = 100\%$ square root raised cosine pulse when $N = 19$, (PG = 38) and $E_b/N_o = 20$ dB.

$K \leq 7$, outages could not be generated using a sample size exceeding that used to evaluate P_{out} at $K = 8$. This indicates that $\overline{P}_{out} << 10^{-10}$ when $K \leq 7$ for all three MFs since $\overline{P}_{out}$(CLMF) $= 1.8 \times 10^{-10}$ for $K = 8$.

The plot is analyzed first with respect to each of the MFs. For the CMF, the transition region contains only $K = 8$. The CMF is essentially ineffective for $K \geq 10$ where $P_{out} \approx 1$. Its $\overline{P}_{out}$ curve shows a large jump from $\overline{P}_{out} << 10^{-7}$ at $K = 7$ to $\overline{P}_{out} = 4.5 \times 10^{-3}$ at $K = 8$. For the NWMF, the transition region extends from $K \in [8, 10]$ and $P_{out} > 10^{-1}$ for $K \geq 11$. As K increases over $K \in [8, 10]$, the $\overline{P}_{out}$ curve degrades from 3.3×10^{-5} to 4.9×10^{-2}. For the CLMF, the transition region extends from $K = 9$ to $K > 13$. As K increases over $K \in [9, 13]$, the $\overline{P}_{out}$ curve degrades from 3.1×10^{-6} to 1.4×10^{-2}.

Next, the curves for the three MFs are compared. As discussed above, the transition region is extended from 1 for the CMF to 3 users for the NWMF and more than 4 users for the CLMF. Compared to both the NWMF and CMF, the CLMF delivers consistently lower P_{out} over $K \in [10, 14]$. For example, when $K = 12$, $\overline{P}_{out}(\text{CMF}) = 8.3 \times 10^{-1}$, $\overline{P}_{out}(\text{NWMF}) = 1.8 \times 10^{-1}$ and $\overline{P}_{out}(\text{CLMF}) = 2.7 \times 10^{-3}$. Thus, at $K = 12$, $\overline{P}_{out}(\text{NWMF})$ is roughly one order of magnitude less than $\overline{P}_{out}(\text{CMF})$ while $\overline{P}_{out}(\text{CLMF})$ is nearly two orders of magnitude less than $\overline{P}_{out}(\text{CMF})$.

With respect to user capacity, the CMF, NWMF and CLMF support, respectively 9, 10 and 13 users (corresponding to $K_{max} = 8, 9$ and 12). Thus, under these conditions, the CLMF increases user capacity by 44% with respect to the CMF and by 30% with respect to the NWMF.

Probability of Outage for the Sqrt-RC Pulse, $\alpha = 60\%$

The plot of P_{out} vs. K for for the sqrt-RC chip pulse, $\alpha = 60\%$, is given in Fig. 5.12 where $N = 24$ and $E_b/N_o = 20$ dB. Since $\alpha = 60\%$, using (2.5), PG = 38.4.

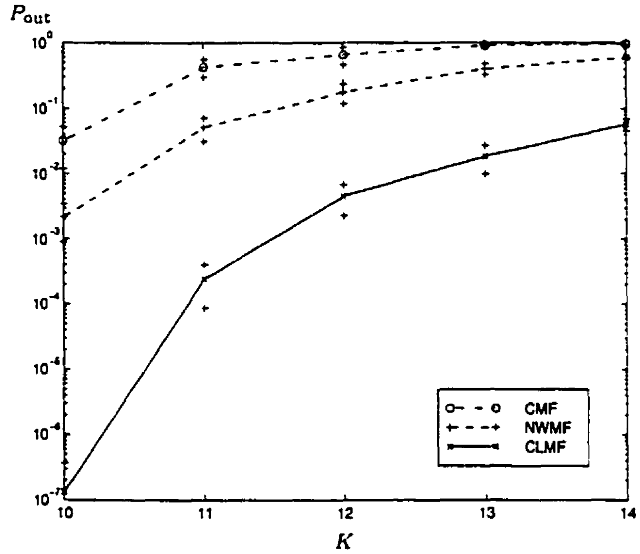

Fig. 5.12 Outage probability vs. K for the $\alpha = 60\%$ square root raised cosine pulse when $N = 24$, (PG = 38.4) and $E_b/N_o = 20$ dB.

For $K \leq 9$, outages could not be generated. This indicates that $\overline{P}_{out} << 10^{-7}$ when $K \leq 7$ for all three MFs.

For the CMF, the transition region contains only $K = 10$. The CMF is essentially ineffective for $K \geq 12$ where $P_{out} \approx 1$. Its $\overline{P}_{out}$ curve shows a large jump from $\overline{P}_{out} << 10^{-7}$ at $K = 9$ to $\overline{P}_{out} = 3.2\times10^{-2}$ at $K = 10$. For the NWMF, the transition region is limited to $K \in [10, 11]$ and $P_{out} > 10^{-1}$ for $K \geq 14$. For the CLMF, the transition region extends from $K \in [10, 14]$. As K increases over $K \in [11, 14]$, the $\overline{P}_{out}$ curve degrades from 2.4×10^{-4} to 5.7×10^{-2}.

The transition region is extended from 1 for the CMF to 2 users for the NWMF and 4 users for the CLMF. Compared to the NWMF and CMF, the CLMF delivers consistently lower P_{out} over $K \in [10, 14]$. For example, when $K = 11$, $\overline{P}_{\text{out}}(\text{CMF}) = 4.3 \times 10^{-1}$, $\overline{P}_{\text{out}}(\text{NWMF}) = 5.2 \times 10^{-2}$ and $\overline{P}_{\text{out}}(\text{CLMF}) = 2.4 \times 10^{-4}$. At $K = 11$, $\overline{P}_{\text{out}}(\text{NWMF})$ is roughly three one order of magnitude less than $\overline{P}_{\text{out}}(\text{CMF})$ and $\overline{P}_{\text{out}}(\text{CLMF})$ is over two orders of magnitude less than $\overline{P}_{\text{out}}(\text{CMF})$. With respect to user capacity, the CMF, NWMF and CLMF support, respectively 10, 11 and 13 users (corresponding to $K = 9, 10$ and 12). Thus, under these conditions, the CLMF increases the number of users by 30% with respect to the CMF and increases the number of users by 18% with respect to the NWMF.

Probability of Outage for the IS-95 Pulse

The plot of P_{out} vs. K for the IS-95 pulse is given in Fig. 5.13 where $N = 32$ and

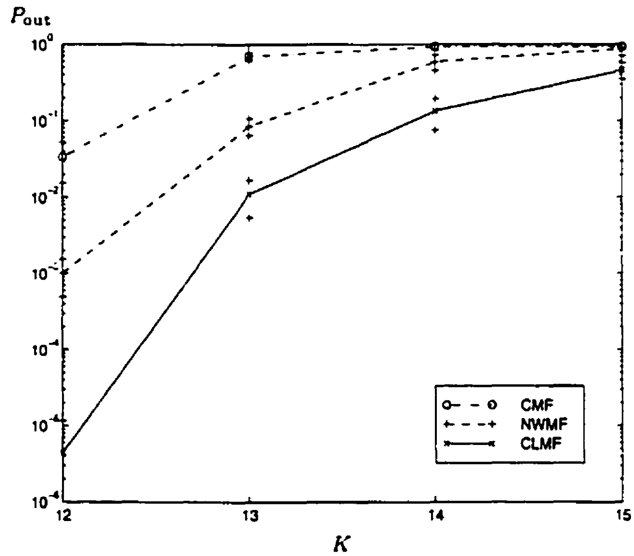

Fig. 5.13 Outage probability vs. K for the IS-95 pulse when $N = 32$, (PG = 38.5) and $E_b/N_o = 20$ dB.

$E_b/N_o = 20$ dB. Since $\alpha = 20.44\%$, using (2.5), PG = 38.5. For $K \leq 11$, outages could not be generated. This indicates that $\overline{P}_{\text{out}} << 10^{-6}$ when $K \leq 11$ for all three MFs. The transition regions for the CMF, NWMF and CLMF overlap and contain, respectively, $K = 12$, $K \in [12, 13]$ and $K \in [12, 13]$. The degradation in P_{out} for all three MFs is very rapid since the transition region is narrow. This can be attributed to the small α. In the limit as $\alpha \to 0$ and the chip pulse approaches the ideal Nyquist pulse of $B = \frac{1}{2T_c}$, the impulse responses of the NWMF and CLMF converge to the

CMF.

Compared to both the NWMF and CMF, the CLMF delivers much lower P_{out} over $K \in [12, 13]$. For example, when $K = 13$, $\overline{P}_{\text{out}}(\text{CMF}) = 7.0 \times 10^{-1}$, $\overline{P}_{\text{out}}(\text{NWMF}) = 8.5 \times 10^{-2}$ and $\overline{P}_{\text{out}}(\text{CLMF}) = 1.1 \times 10^{-2}$. At $K = 13$, $\overline{P}_{\text{out}}(\text{NWMF})$ is roughly one order of magnitude less than $\overline{P}_{\text{out}}(\text{CMF})$ and $\overline{P}_{\text{out}}(\text{CLMF})$ is roughly an additional one order of magnitude less than $\overline{P}_{\text{out}}(\text{CMF})$. With respect to user capacity, the CMF, NWMF and CLMF support, respectively 12, 13 and 14 users (corresponding to $K_{\max} = 11, 12$ and 13). Thus, under these conditions, the CLMF increases the number of users by 17% with respect to the CMF and increases the number of users by 8% with respect to the NWMF.

Comparison of P_{out} at a Common PG and a Varying α

The P_{out} is next compared for the systems based on the three bandwidth efficient pulses: the IS-95 pulse and the two sqrt-RC pulses. As may have been noticed, in the three bandwidth efficient systems considered thus far, PG $\approx$ 38. Actually, the PG of the sqrt-RC 100%, sqrt-RC 60% and IS-95 pulse are 38, 38.4 and 38.5, respectively. Equality among the PGs cannot be achieved since N is constrained to be an integer. The difference among the systems, however, is the spreading factor N which must be increased accordingly as the excess bandwidth of the pulse is decreased to maintain a common PG.

The P_{out} curves in Figs. 5.11 to 5.13 are analyzed for each of the three MFs in order of decreasing excess bandwidth. For the CMF, the transition regions for the sqrt-RC 100% pulse, sqrt-RC 60% pulse and IS-95 pulse with $\alpha = 20.44\%$ are, respectively, $K = 8$, $K = 10$ and $K = 12$. Decreasing α corresponds to shifting the transition region to the right. A similar shift in the transition regions occurs for the P_{out} curves of both the NWMF and CLMF. The P_{out} for the three pulses and three MFs at $K = 12$ is tabulated in Table 5.3. For each MF, as α decreases, P_{out} tends to improve. The

Table 5.3 P_{out} for the three pulses and three MFs at $K = 12$.

Chip Pulse	P_{out}		
	CMF	NWMF	CLMF
Sqrt-RC, $\alpha = 100\%$	8.9×10^{-1}	3.1×10^{-1}	8.0×10^{-3}
Sqrt-RC, $\alpha = 60\%$	6.6×10^{-1}	1.8×10^{-1}	4.6×10^{-3}
IS-95	3.4×10^{-2}	1.0×10^{-3}	4.4×10^{-6}

improvement from sqrt-RC 100% to sqrt-RC 60% is small while that from sqrt-RC 60% to the IS-95 pulse is considerably large. With respect to user capacity, the results are summarized in Table 5.4. The CLMF gives greater user capacity across the three

Table 5.4 User Capacity, $K_{\max} + 1$ for which $P_{\text{out}} < 1\%$.

Chip Pulse	$K_{\max}+1$ CMF	NWMF	CLMF
Sqrt-RC, $\alpha = 100\%$	9	10	13
Sqrt-RC, $\alpha = 60\%$	10	11	13
IS-95	13	13	14

chip pulses. As α increases, $K_{\max+1}$ decreases significantly for the CMF and less so for the NWMF. On the other hand, the CLMF is hardly affected. Even with $\alpha = 100\%$, the CLMF delivers a user capacity very close to the maximum user capacity obtained with very small α. This results indicates that, contrary to the CMF and NWMF, use of the CLMF can permit the design of chip pulses with larger excess bandwidth with only a small decrease in capacity. The possibility of increasing α has two important benefits. In the design of the transmitter chip filter, a larger α reduces its order of complexity. And second, a larger α improves chip synchronization at the receiver [18, pp. 743–746][44, p. 370].

Probability of Outage under Power Imbalance Conditions

The performance of the CMF and CLMF is next investigated under power-imbalance conditions for the IS-95 pulse. All users transmit at a common chip rate of $1/T_c$ over a common bandwidth. The users are divided into two groups: K_1 users in group 1 and K_2 in group 2. The users of the group 1 transmit bits at the rate of $\frac{1}{N_1 T_c}$ with a power level of $\frac{E_b}{N_1 T_c}$ where N_1 represents the spreading factor of users in group 1. The users of group 2 transmit bits at the rate of $\frac{1}{N_2 T_c}$ with a power level of $\frac{E_b}{N_2 T_c}$ where N_2 represents the spreading factor of user in group 2. The ratio of the signal power of a user in group 2 to that of a user in group 1 is $\frac{N_1}{N_2}$. Ideal power control is assumed to maintain the disparate power levels between the two groups of users. Without loss of generality, it is assumed that $N_1 > N_2$. Thus, group 1 represents low-rate users while group 2 represents high-rate users in a dual-rate DS-CDMA system. This is an example of systems which provide mixed rate (or variable rate) data service such as those envisioned in [19, 20]. For example, the low-rate may provide voice service while the high-rate may provide real-time video or data service. In contrast to the IS-95 system where the signal powers of each user are designed to be uniform, in mixed-rate DS-CDMA systems, power-imbalance is deliberate and unavoidable. The aim of the following set of plots is to illustrate the level of improvement the CLMF may potentially offer to systems operating under power-imbalance conditions.

In the numerical examples to follow, $E_b/N_o = 20$ dB as before while $N_1 = 64$ and $N_2 = 8$. Since $\alpha = 20.44\%$, using (2.5), the PG of users in group 1 is $\text{PG}_1 = 77.1$ while the PG of the users in group 2 is $\text{PG}_2 = 9.6$. Consequently, a user in group 2 transmits its bits at a rate 8 times greater than that of a user in group 1 and at a signal power 8 times (or 9 dB) greater than a user in group 1. The examples are presented in order of increasing values of K_2. Only P_{out} for group 1 users is considered since they are the only users adversely affected by the power-imbalance. Users of group 2 do not succumb to this problem. Consequently, the term P_{out} shall refer solely to the probability of outage for users in group 1. Furthermore, $K_{\max,1}$ refers to the maximum K_1 for which $P_{\text{out}} < 1\%$. After the numerical examples are presented, a comparison of the P_{out} over the various K_2 shall be considered.

Probability of Outage for $K_2 = 0$

The plot of P_{out} vs. K_1 for the IS-95 pulse where $K_2 = 0$ is given in Fig. 5.14. Since there are no high rate users, all users have uniform signal powers. This case

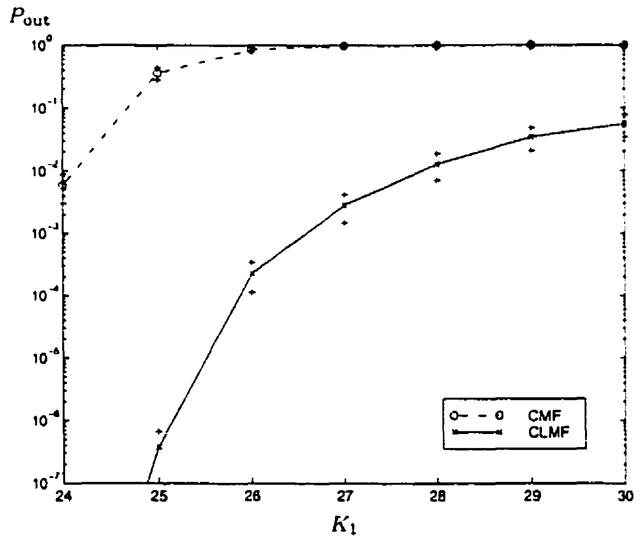

Fig. 5.14 Outage probability of low rate users vs. K_1 for the IS-95 pulse when $K_2 = 0$, $N_1 = 64$, ($\text{PG}_1 = 77.1$), $N_2 = 8$ ($\text{PG}_2 = 9.6$) and $E_b/N_o = 20$ dB.

is provided to serve as a benchmark for the examples to follow where $K_2 > 0$ to illustrate the dramatic loss in low-rate user capacity that results due to the power-imbalance effect. For $K_1 \leq 23$, outages could not be generated. This indicates that

$\overline{P}_{out} << 5 \times 10^{-12}$ when $K_l \leq 23$ for both MFs since $\overline{P}_{out}(\text{CLMF}) = 5 \times 10^{-12}$ when $K_l = 24$. The transition region of the CMF contains $K_l = 10$ while that of the CLMF ranges from $K_l \in [26, 30]$. The increase in PG compared to the $N = 32$ case discussed earlier broadens the transition region for the CLMF.

Compared to the CMF, the CLMF delivers much lower P_{out} over $K_l \in [24, 30]$. For example, when $K_l = 26$, $\overline{P}_{out}(\text{CMF}) = 8.5 \times 10^{-1}$ and $\overline{P}_{out}(\text{CLMF}) = 2.3 \times 10^{-4}$ which is over three orders of magnitude less than that of the CMF. With respect to low-rate user capacity, the CMF and CLMF support, respectively 25 and 28 users (corresponding to $K_{l,\max} = 24$ and $K_{l,\max} = 27$). Thus, under these conditions, the CLMF increases low-rate user capacity by 12% with respect to the CMF.

Probability of Outage for $K_2 = 1$

The plot of P_{out} vs. K_l for the IS-95 pulse where $K_2 = 1$ is given in Fig. 5.15. The

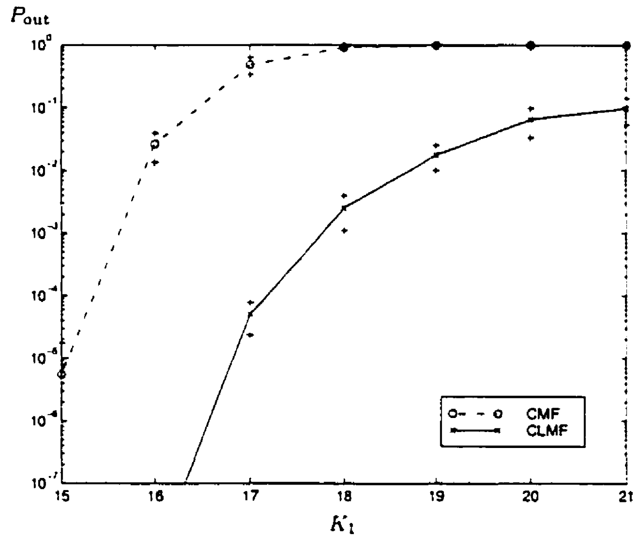

Fig. 5.15 Outage probability of low rate users vs. K_l for the IS-95 pulse when $K_2 = 1$, $N_l = 64$, ($\text{PG}_l = 77.1$), $N_2 = 8$ ($\text{PG}_2 = 9.6$) and $E_b/N_o = 20$ dB.

low-rate users experience the power-imbalance effect since a single user with a signal power 9 dB greater than that of the low rate users is present. For $K_l \leq 14$, outages could not be generated. This indicates that $\overline{P}_{out} << 5.4 \times 10^{-9}$ when $K_l \leq 14$ for both MFs since $\overline{P}_{out}(\text{CLMF}) = 5.4 \times 10^{-9}$ when $K_l = 16$. The transition region of the CMF is $K_l \in [15, 16]$ while that of the CLMF is $K_l \in [17, 20]$.

Compared to the CMF, the CLMF delivers much lower P_{out} over $K_l \in [15, 21]$. For example, when $K_l = 18$, $\overline{P}_{out}(\text{CMF}) = 9.2 \times 10^{-1}$ and $\overline{P}_{out}(\text{CLMF}) = 2.5 \times 10^{-3}$ which is roughly three orders of magnitude less than that of the CMF. With respect to user capacity, the CMF and CLMF support, respectively, 16 and 19 users (corresponding to $K_{1,\max} = 15$ and $K_{1,\max} = 18$). Thus, under the power-imbalance condition where a single strong user is present, the CLMF increases the number of users by 19% with respect to the CMF.

Probability of Outage for $K_2 = 2$

The plot of P_{out} vs. K_1 for the IS-95 pulse where $K_2 = 2$ is given in Fig. 5.16. Two high-rate users each with a signal power 9 dB greater than that of the low-rate

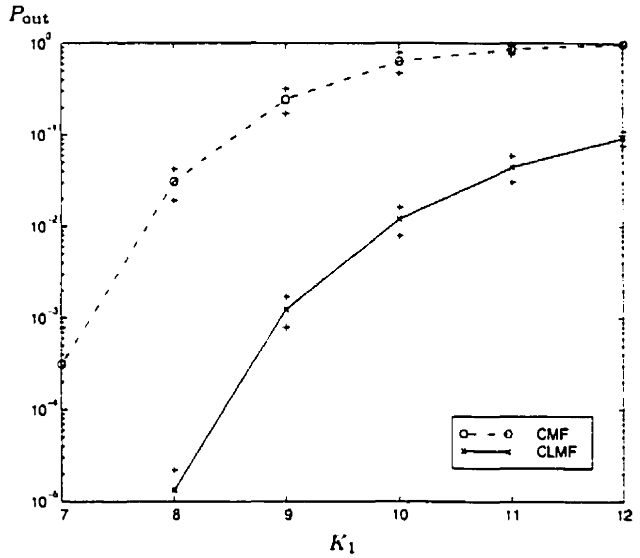

Fig. 5.16 Outage probability of low rate users vs. K_1 for the IS-95 pulse when $K_2 = 2$, $N_1 = 64$, ($\mathrm{PG}_1 = 77.1$), $N_2 = 8$ ($\mathrm{PG}_2 = 9.6$) and $E_b/N_o = 20$ dB.

users are present. For $K_1 \leq 6$, outages could not be generated. This indicates that $\overline{P}_{out} << 1.3 \times 10^{-9}$ when $K_1 \leq 7$. for both MFs since $\overline{P}_{out}(\mathrm{CLMF}) = 1.3 \times 10^{-9}$ when $K_1 = 6$ The transition region of the CMF is $K_1 \in [7,8]$ while that of the CLMF is $K_1 \in [8,12]$.

Compared to the CMF, the CLMF delivers considerably lower P_{out} over $K_1 \in [7,12]$. For example, when $K_1 = 9$, $\overline{P}_{out}(\mathrm{CMF}) = 2.4 \times 10^{-1}$ and $\overline{P}_{out}(\mathrm{CLMF}) = 1.2 \times 10^{-3}$ which is roughly two orders of magnitude less than that of the CMF. With respect to user capacity, the CMF and CLMF support, respectively 8 and 11 users (corresponding to $K_{1,\max} = 7$ and $K_{1,\max} = 10$). Thus, under this power-imbalance condition where two strong users are present, the CLMF increases the number of users by 38% with respect to the CMF.

Probability of Outage for $K_2 = 3$

The plot of P_{out} vs. K_1 for the IS-95 pulse where $K_2 = 3$ is given in Fig. 5.17. Three high-rate users each with a signal power 9 dB greater than that of the low-

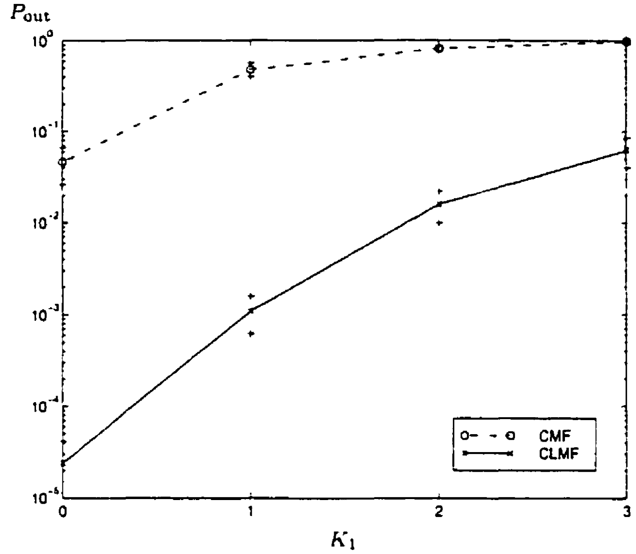

Fig. 5.17 Outage probability of low rate users vs. K_1 for the IS-95 pulse when $K_2 = 3$, $N_1 = 64$, $(\text{PG}_1 = 77.1)$, $N_2 = 8$ $(\text{PG}_2 = 9.6)$ and $E_b/N_o = 20$ dB.

rate users are present. The CMF is essentially rendered ineffective for $K_1 \geq 1$ where $P_{out} \approx 1$. Compared to the CMF, the CLMF delivers considerably lower P_{out} over $K_1 \in [0, 3]$. For example, when $K_1 = 1$, $\overline{P}_{out}(\text{CMF}) = 4.8 \times 10^{-1}$ and $\overline{P}_{out}(\text{CLMF}) = 1.1 \times 10^{-3}$ which is over two orders of magnitude less than that of the CMF. With respect to user capacity, the CMF and CLMF support, respectively 0 and 2 users (corresponding to $K_{1,max} = 0$ and $K_{1,max} = 1$). Since $P_{out} > 1\%$ for the CMF of a low rate user when there are no other low rate users in the system ($K_1 = 0$), the lone low rate user experiences $P_{out} > 1\%$. That is, no low-rate users can be supported by the CMF. Consequently, under this power-imbalance condition where three strong users are present, the CLMF can support up to two low rate users compared to the CMF which cannot support any.

Comparison of P_{out} over the Various K_2

The P_{out} results are compared over $K_2 \in [0, 3]$. The low-rate user capacity $K_{1,max} + 1$ at a given K_2, where $P_{out} < 1\%$ is summarized in Table 5.5. When $K_2 = 4$, $P_{out} > 1\%$ for $K_1 \geq 0$. As can be observed, the low-user capacity decreases rapidly as high rate users are added. Low-rate users cannot be supported once $K_2 \geq 4$. The dramatic drop

Table 5.5 Low-rate user capacity $K_{1,\max}+1$ satisfying $P_{\text{out}} < 1\%$ under power-imbalance conditions for the IS-95 pulse.

K_2	$K_{1,\max}+1$	
	CMF	CLMF
0	25	28
1	16	19
2	7	10
3	0	2
4	0	0

in low-rate user capacity can be understood intuitively by approximating a high-rate user as 8 low-rate users with a common chip delay. The large reduction in capacity is experienced by both the CMF and CLMF. It should be stressed, however, that the CLMF considerably improves P_{out} and low-rate user capacity. For $K_2 \in [0, 3]$, the CLMF consistently allows 2 to 3 more low rate users compared to the CMF.

5.6 Summary

This chapter has investigated the performance of the CLMF, relative to that of the CMF and NWMF, in terms of SNR, near-far resistance, BER and probability of outage, P_{out}. The analysis and numerical results clearly demonstrated the improvement in performance achievable by the CLMF over multiple-access channels corrupted with AWGN. It was found that the gain in SNR and BER performance depended upon the distribution of the interferer chip delays in addition to the relative powers among users' signals and the AWGN. In AWGN dominated conditions, the gain was very small as was to be expected since the CLMF and NWMF then reduced to the CMF. On the other hand, in MAI dominated conditions, the gain increased when interferer chip delays were clustered about a half chip period and as the signal powers of interferers increased relative to that of the desired user. It was also shown that further SNR gains could be obtained with the knowledge of interferer phase-offsets.

In terms of near-far resistance, it was found that the CLMF could achieve non-zero near-far resistance. For the single-interferer case, the near-far resistance of the CLMF ranged from zero with a chip-synchronous interferer to a maximum non-zero value occurring when the interferer chip delay was half the chip period. The maximum value was shown to increase as the excess bandwidth of the chip filter increased. In contrast, the near-far resistance of the NWMF, like that of the CMF, was shown to be zero.

And lastly, the performance of the CLMF, NWMF and CMF was analyzed under more general conditions based on probability of outage P_{out}. Under either uniform or non-uniform received signal power conditions, P_{out} associated with the CLMF was found to be, in general, considerably less than those associated with either the NWMF or CMF. The level of improvement depended upon the excess bandwidth in the chip pulse. The gain in P_{out} increased as the excess bandwidth of the chip pulse increased under uniform signal power conditions. Furthermore, under power-imbalance conditions exemplified by a dual-rate system using the IS-95 pulse (with an excess bandwidth of 20.44%), the CLMF yielded improvements in P_{out} and capacity. In the numerical examples presented for $N = 64$, in comparison to the CMF, the CLMF was able to increase low-rate user capacity by two to three users in the presence of zero to three high-rate (and high-powered) users.

Chapter 6

Implementation

This chapter considers the implementation of a receiver which can realize the CLMF described in Chapter 4. The same receiver can be used to realize the NWMF and CUMF as well. The basic structure of the receiver is illustrated in Fig. 6.1. It is

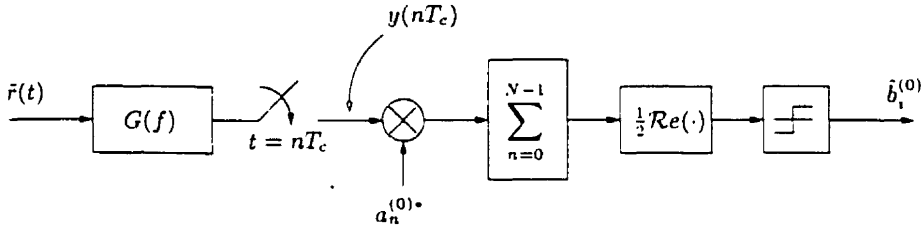

Fig. 6.1 CLMF receiver.

constructed by inserting the CLMF given in Fig. 4.6 into the $\tilde{h}(t)$ block of the LTI filter receiver in Fig. 2.8. The receiver consists of the new chip filter $G(f)$, a chip-rate sampler and a despreading filter in the form of a correlator. Its form is similar to that of the CMF except that the CMF chip filter $Q^*(f)$ is replaced by the SNR maximizing chip filter $G(f)$.

The filter response $G(f)$, which minimizes MSE and maximizes SNR associated with $y(nT_c)$, can take on one of three possible forms depending upon the chip delays of the interferers. When chip delays change very quickly over each consecutive bit and appear to be random, the adaptive filter would ideally converge to the combined response of the noise-whitening filter and chip filter (ie. the first two filters in Fig. 4.3) described in section 4.3.3 and [79]. When the chip delays remain fixed, the filter would ideally converge to $G^{(C)}(f)$ in the CLMF as described in section 4.4.3. When both types of chip delays exist, the filter would tend towards the CUMF discussed in section 4.6.

The question at hand is how to implement the filter $G(f)$. Given knowledge of the signal parameters of chip-delay locked interferers and the net MAI power γ_{CU} of unlocked interferers, $G(f)$ can be solved for directly using the results of Chapter 4. The aim of this chapter, however, is to offer structures with low complexity and hardware requirements which eliminate the need for interferer signal parameters. To this end, adaptive filters are considered to realize $G(f)$. In addition to their ability to adapt to changes in the signal parameters of interferers, they can also handle distortions in the desired user's transmitted waveform caused by the channel.

The theory of linear adaptive filtering is well known [73, 118, 119]. Consequently, the chapter focusses on discussing issues essential to the development of adaptive versions of $G(f)$. The following sections present three adaptive filter structures. Each section describes the structure as well as the design of the training signal(s) and error signal(s) which drive the tap coefficient updating program(s). Section 6.1 presents an adaptive filter based on a single fractionally-spaced equalizer (FSE). This, in fact, is very similar to the chip symbol adaptive FSE proposed in [79] to realize the NWMF. The remaining sections consider adaptive filters which exploit the underlying structure of $G^{(C)}(f)$ as explained in section 4.4.3. Section 6.2 presents a second adaptive structure based on a bank of bandpass filters. Section 6.3 presents a third adaptive structure consisting of two parallel adaptive filters. Although the computational and hardware complexity associated with these two structures increases, they offer substantial advantages depending on the application.

6.1 Structure I — Chip Symbol Adaptive FSE

This section presents the structure of the SNR maximizing chip filter $G(f)$ realized with an adaptive FSE. The structure of the adaptive filter is given in Fig. 6.2. First, the received signal is sampled at the rate of $1/T_s$. The sampling rate is set to satisfy $1/T_s \geq 2B = (1+\alpha)/T_c$ and then set to an integer multiple of the chip rate. That is, $1/T_s = N_s/T_c$ where $N_s = 1 + \lceil \alpha \rceil$. Second, the sampled signal is fed into an FSE with N_{FSE} taps and delay spacings of T_s. Since, as shown in Appendix G.1, the duration of the filter impulse response is $T_g = 3(2M-1)T_c$ (three times the duration of $\tilde{q}(t)$ given in (3.28)), $N_{\text{FSE}} \geq 2BT_g$. The sampled output of the FSE is $y(nT_c)$. And third, $y(nT_c)$ is fed into the despreading filter in the form of a correlator to produce an estimate of the bit $\hat{b}^{(0)}_{\lfloor n/N \rfloor - 1}$.

The design of the training signal and error signal is described next. The training signal d_n is formed in one of two ways depending on the mode of operation. In

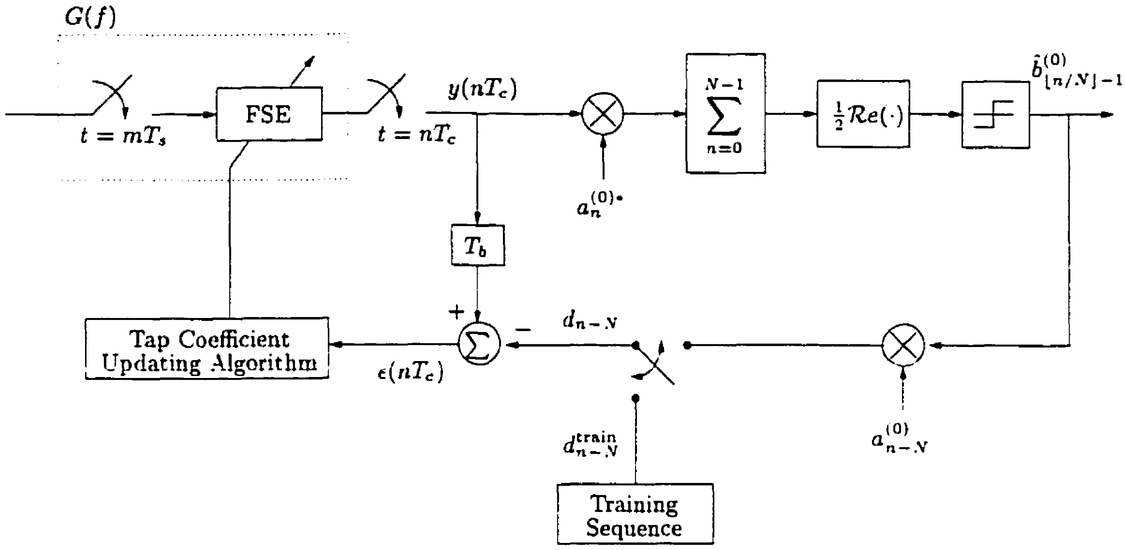

Fig. 6.2 Structure I.

training mode, the training signal is determined by a training sequence d_n^{train} shared by the transmitter and receiver. In decision-directed mode, the training signal is created by spreading the estimated bit with the spreading sequence of the desired user. Consequently,

$$d_n = \begin{cases} d_n^{\text{train}}, & \text{training mode} \\ \hat{b}^{(0)}_{\lfloor n/N \rfloor} a_n^{(0)}, & \text{decision-directed mode.} \end{cases} \tag{6.1}$$

The error signal $\epsilon(nT_c)$ is formed by taking the difference between the expected and actual sampled output such that

$$\epsilon(nT_c) = y\big((n-N)T_c\big) - d_{n-N}. \tag{6.2}$$

The delay term of $T_b = NT_c$ has been introduced to account for the delay incurred by the correlator. The error signal $\epsilon(nT_c)$ is fed into a tap coefficient updating algorithm at the chip rate. The function of the algorithm is to update the tap coefficients in the FSE to minimize the MSE $\mathrm{E}\left[|\epsilon(nT_c)|^2\right]$. A variety of well-known techniques [119, Part 3] such as the least-mean-square (LMS) algorithm [119, Chapter 9] or recursive least-squares (RLS) algorithm [44, pp. 654–660] can be used to implement the updating algorithm.

As mentioned earlier, structure I differs slightly from the structure proposed in [79]. In decision-directed mode of operation, the structure in [79] avoids the delay incurred by the correlator by implementing two FSEs. Since $\hat{b}^{(0)}_{\lfloor n/N \rfloor}$ can assume either 1 or -1 in (6.1), one FSE assumes $\hat{b}^{(0)}_{\lfloor n/N \rfloor} = 1$ in forming the its error signal. The other FSE assumes $\hat{b}^{(0)}_{\lfloor n/N \rfloor} = -1$ in forming the its error signal. Once a bit decision is made, the tap coefficients of the FSE updated using the estimated bit value serve as the starting point for both FSEs to estimate the next bit.

6.2 Structure II — Chip Symbol Adaptive Bandpass Filtering

Structure II is based on a bank of bandpass filters as described in section 4.4.3 and Fig. 4.7. In this case, the adaptive chip filter implementing $G(f)$ in Fig. 6.1 is given in Fig. 6.3. It contains L_H bandpass filters whose outputs are summed to form the

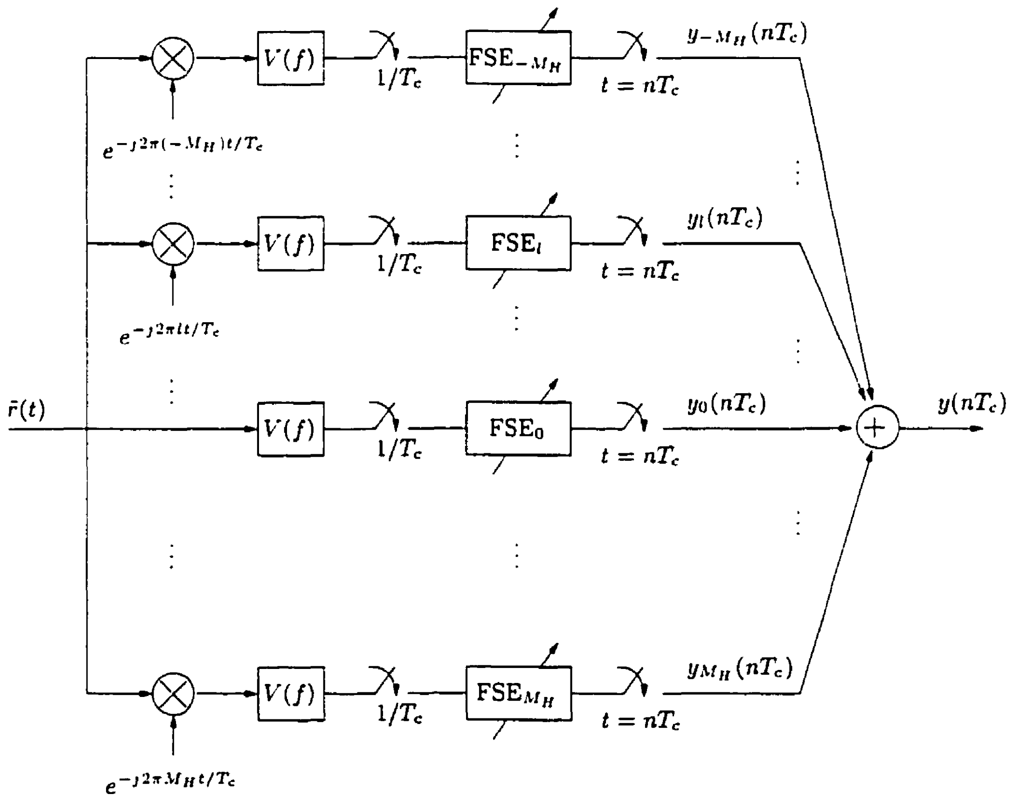

Fig. 6.3 Structure II to implement $G(f)$.

sampled filter output $y(nT_c)$. For example, using (4.39), when the excess bandwidth satisfies $0 < \alpha \leq 200\%$, $M_H = 1$ and the structure consists of $L_H = 3$ bandpass filters.

The lth bandpass filter where $l \in [-M_H, M_H]$ consists of five parts. First, the received signal is frequency shifted by $-l/T_c$ so that the portion of the received signal over $f \in [\frac{l}{T_c} - \frac{1}{2T_c}, \frac{l}{T_c} + \frac{1}{2T_c}]$ is shifted to the baseband region of $f \in [-\frac{1}{2T_c}, \frac{1}{2T_c}]$. Second, the output of the frequency shift operation is input to the ideal lowpass filter $V(f)$ with a bandwidth of $\frac{1}{2T_c}$. Third, the output of $V(f)$ is sampled at a rate of $1/T_s$. Since the signal is bandlimited to $\frac{1}{2T_c}$, $1/T_s = 1/T_c$. Fourth, the sampled output is passed through FSE_l whose design is explained shortly. And fifth, the output of FSE_l is sampled at the chip rate to produce the chip filter output $y_l(nT_c)$ associated with the lth bandpass filter. The modulator $e^{j2\pi lt/T_c}$ at the output has been absorbed by the sampler operating at $t = nT_c$. The summation of the outputs of each bandpass filter forms $y(nT_c) = \sum_l y_l(nT_c)$.

The design of FSE_l is described. As shown in Fig. 6.4, FSE_l is driven by a tap coefficient updating algorithm whose operation is independent of the FSEs in the other bandpass filters. Moreover, each FSE_l is a baseband filter since, it is preceded

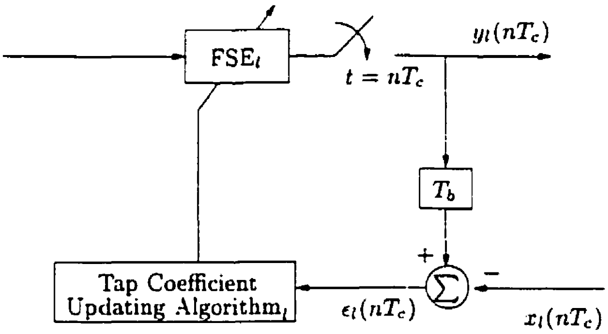

Fig. 6.4 FSE_l in structure II.

by a frequency shift operation (with the exception of FSE_0) and low pass filter $V(f)$ as shown in Fig. 6.3. The error signal used by the Tap Coefficient Updating Algorithm$_l$ is

$$\epsilon_l(nT_c) = y_l\Big((n-N)T_c\Big) - x_l(nT_c). \tag{6.3}$$

The training signal $x_l(nT_c)$ is formed in three steps. First, the training signal $\sum_p d_p \tilde{q}\Big(t-(p+N)T_c\Big)$ is input into Structure II as $\tilde{r}(t)$ in Fig. 6.3 in the absence of MAI and AWGN. The training symbols d_p are defined in (6.1). Second, the output of $V(f)$ in the lth bandpass filter can be expressed $x_l(t) = \Big[\sum_p d_p \tilde{q}_l\Big(t-(p+N)T_c\Big)\Big] \star \Big[v(t)e^{-j2\pi lt/T_c}\Big]$ where $\star$ denotes linear convolution and the inverse Fourier transform of $V(f)$ is $v(t) = \frac{1}{T_c}\text{sinc}\left(\frac{t}{T_c}\right)$. And third, simplification of $x_l(t)$ leads to, at $t = nT_c$,

$$x_l(nT_c) \;=\; \sum_p d_p\, \tilde{q}_l\Big((n - N - p)T_c\Big) \tag{6.4}$$

where $\tilde{q}_l(t)$ is the inverse Fourier transform of the lth HSR component of the chip filter $Q_l(f)$ defined in (4.15). In contrast to the signal symbol d_{n-N} in (6.2), in (6.4), previous and future symbols are required to form the training signal to account for the inter-chip symbol interference introduced by $V(f)$. An example of the design of each training signal is illustrated in Fig. 6.5.

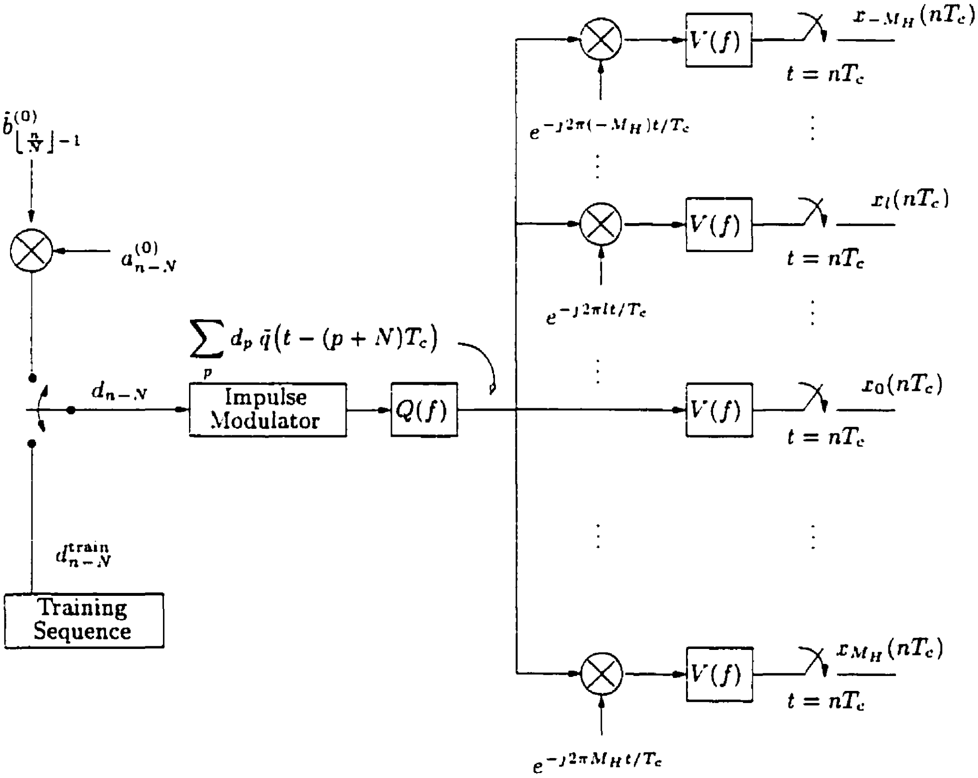

Fig. 6.5 Reference signals $x_l(nT_c)$, $l \in [-M_H, M_H]$ for structure II.

Compared to structure I, structure II increases hardware and computational complexity by a factor of at least L_H. It does, however, offer two advantages. First, as pointed out in section 2.2.3 with respect to the bit symbol frequency domain TDAF, the bandpass structure can improve the rate of convergence of the adaptive filter [76][73, pp. 205–210]. And second, structure II may be particularly useful in applications where narrowband interference exists. For example, narrowband interference may appear in dual-mode cellular systems consisting of cell sites employing either

AMPS or CDMA. It may also appear in overlay CDMA systems in which part of the spectrum is shared with a narrowband system [120, 121]. In such systems, the performance of the adaptive filter in structure I may degrade considerably. Furthermore, the application of a narrowband interference rejection technique such as the adaptive line enhancer (ALE) [122, 123] would come at the expense of introducing some distortion to the desired signal [124]. Further details on other narrowband interference rejection techniques can be found in [124, 125]. In contrast, in structure II, narrowband interference affects the operation of only one of the bandpass filters. The operation of the remaining bandpass filters is unaffected. Consequently, the receiver has the option of either simply cutting the output of the affected bandpass filter or applying a narrowband interference rejection technique to the affected bandpass filter. Moreover, such a technique would introduce some distortion only in the desired signal in one of the bandpass filters. Thus, it is expected that the performance of structure II would exceed that of structure I in the presence of narrowband interference and in terms of rate of convergence.

6.3 Structure III — Two Parallel Adaptive FSEs

Structure III is based on the decomposition of each bandpass filter in structure II into a set of L_H branch filters as described in section 4.4.3 and Fig. 4.8. The resulting filter structure would consist of L_H^2 FSEs. A more cost-effective structure is presented, instead, based on the following observations. As explained in section 4.2.2, when the MAI is WSS (corresponding to rapidly changing chip delays), with respect to the lth bandpass filter, only the $m = l$th branch filter remains where $m \in [-M_H, M_H]$ while the other branch filters ($m \neq l$) disappear. Furthermore, when chip-delay locked interferers are present (corresponding to interferers whose chip delays are fixed or changing very slowly), the $m = l$th filters are only weakly affected by changing chip delays. In contrast, the remaining branch filters $m \neq l$ are strongly affected by changing chip delays. The difference in sensitivity among the branch filters to changes in interferer chip delays T_k for $k \in [1, K]$ is explained next.

As pointed out in section 4.4.3, the frequency response of each branch filter in Fig. 4.8 is affected by T_k through the filter $[\mathbf{R}^{-1}(f)]_{nm}$ for $n, m \in [-M_H, M_H]$. The aim is to show that branch filters with $[\mathbf{R}^{-1}(f)]_{nn}$ are insensitive to changes in T_k whereas those with $[\mathbf{R}^{-1}(f)]_{nm}$ for $m \neq n$ are sensitive to changes in T_k. For the general case of unlocked and chip-delay locked interferers, $\mathbf{R}(f)$ in (4.52) and (4.51) is composed of diagonal terms independent of T_k and non-diagonal terms dependent on T_k. Assuming that the inverse of $\mathbf{R}(f)$ exists (which should be the case when AWGN is present), $\mathbf{R}^{-1}(f) = \mathrm{adj}\,[\mathbf{R}(f)]\,/\det[\mathbf{R}(f)]$ where $\det[\mathbf{R}(f)]$ represents the *determinant* of $\mathbf{R}(f)$ and $\mathrm{adj}\,[\mathbf{R}(f)]$ represents the *adjoint* of $\mathbf{R}(f)$ [126, p. 128]. The $\{\mathrm{adj}\,[\mathbf{R}(f)]\}_{nm}$, for $m \neq n$ branch filters, consists of a sum of terms each containing $[\mathbf{R}(f)]_{nm}$ for $m \neq n$. Hence, the filters $[\mathbf{R}^{-1}(f)]_{nm}$ are adversely affected by changes in chip delays. On the other hand, $\{\mathrm{adj}\,[\mathbf{R}(f)]\}_{nn}$ for $m = n$ branch filters, consists, in addition to a sum of terms affected by T_k, the term $\prod_{l \neq n}[\mathbf{R}(f)]_{ll}$ where $[\mathbf{R}(f)]_{ll} = \frac{N_o}{2} + \left[\frac{\gamma_{CII}}{2T_c} + \sum_k \frac{P_k}{2}\right] |Q_l(f)|^2$ independent of T_k. The presence of this term makes $\{\mathrm{adj}\,[\mathbf{R}(f)]\}_{nn}$ less sensitive to changes in T_k (compared to $\{\mathrm{adj}\,[\mathbf{R}(f)]\}_{nm}$ for $m \neq n$). The same argument for $\{\mathrm{adj}\,[\mathbf{R}(f)]\}_{nn}$ applies to $\det[\mathbf{R}(f)]$ which contains $\prod_l [\mathbf{R}(f)]_{ll}$.

The L_H branch filters satisfying $m = l$ can be categorized as class A filters insensitive to changing chip delays. The remaining $L_H^2 - L_H$ branch filters can be categorized as class B filters sensitive to changing chip delays. By linearly combining the filters of each class into filter A and filter B, it is possible implement the L_H^2 filters as two adaptive filters instead. Based on this decomposition of $G(f)$ into the two filters, the structure of the adaptive chip filter in Fig. 6.1 is given by Fig. 6.6. First, the received signal is sampled at the sampling rate of $1/T_s = N_s/T_c$ where

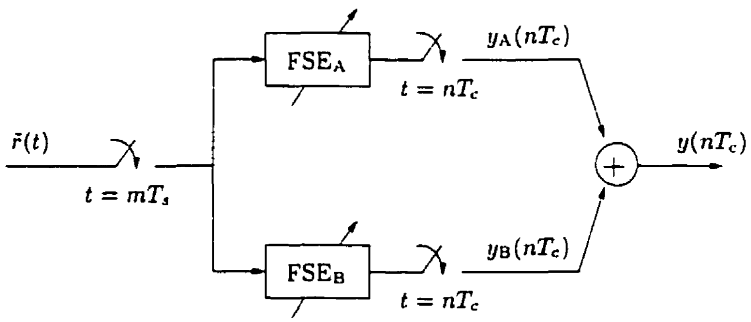

Fig. 6.6 Structure III to implement $G(f)$.

$N_s = 1 + \lceil \alpha \rceil$ as discussed in section 6.1. The samples are input to two adaptive filters FSE$_\mathrm{A}$ and FSE$_\mathrm{B}$ whose outputs are summed to form the sampled filter output $y(nT_c) = y_\mathrm{A}(nT_c) + y_\mathrm{B}(nT_c)$. The FSE$_\mathrm{A}$ is insensitive to changing chip delays while FSE$_\mathrm{B}$ is sensitive to changing chip delays. Furthermore, in the extreme case where the chip delays of all interferers change rapidly, FSE$_\mathrm{A}$ should ideally converge to the combined response of the noise-whitening filter and chip filter while FSE$_\mathrm{B}$ should go to zero.

The design of FSE$_\mathrm{A}$ and FSE$_\mathrm{B}$ is described. As shown in Fig. 6.7, FSE$_\mathrm{A}$ is driven

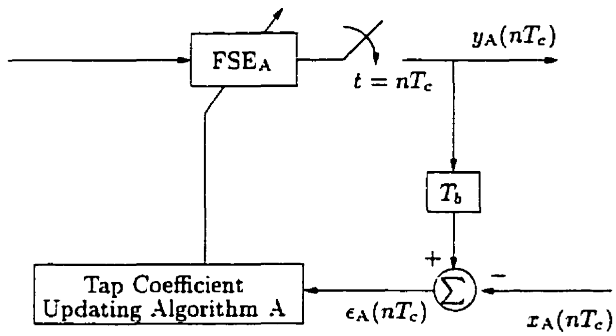

Fig. 6.7 FSE$_A$ in structure III.

by Tap Coefficient Updating Algorithm A whose operation is independent of FSE$_B$. The error signal used by the algorithm is

$$\epsilon_A(nT_c) = y_A\Big((n-N)T_c\Big) - x_A(nT_c). \tag{6.5}$$

The training signal $x_A(nT_c)$ is determined in four steps. First, the training signal $\sum_p d_p\tilde{q}\big(t-(p+N)T_c\big)$ is passed through each of the bandpass filters in Fig. 4.7 indexed by l in the absence of MAI and AWGN. Second, in Fig. 4.8, the positions of the two filters $Q^*_m(f-\frac{l}{T_c})$ and $\big[\mathbf{R}^{-1}(f-\frac{l}{T_c})\big]_{nm}$ for $m \in [-M_H, M_H]$ are switched via linearity. Third, the training signal $\sum_p d_p\tilde{q}\big(t-(p+N)T_c\big)$ is passed through the mth branch filter $Q^*_m(f-\frac{l}{T_c})$ of the lth bandpass filter. The output of $Q^*_m(f-\frac{l}{T_c})$ is $x_{l,m}(t) = \big[\sum_p d_p \sum_l \tilde{q}\big(t-(p+N)T_c\big)\big] \star \big[\tilde{q}_m(-t)e^{j2\pi lt/T_c}\big]$ where $\tilde{q}_m(-t)e^{j2\pi lt/T_c}$ is the inverse Fourier transform of $Q^*_m(f-\frac{l}{T_c})$. And fourth, only the outputs for $m = l$, corresponding to those filters insensitive to chip delay changes, are summed to form the training signal $x_A(t) = \sum_l x_{l,l}(t)$ for FSE$_A$. This leads to

$$x_A(t) = \sum_p d_p \sum_l \tilde{q}\Big(t-(p+N)T_c\Big) \star \Big[\tilde{q}_l(-t)e^{j2\pi lt/T_c}\Big] \tag{6.6}$$

sampled at $t = nT_c$. An example of the design of $x_A(nT_c)$ is illustrated in Fig. 6.8 when $0 < \alpha \leq 200\%$.

FSE$_B$ is illustrated in Fig. 6.9. Although its structure is similar to FSE$_A$, it differs in two aspects. First, the training signal $x_B(nT_c)$ assumes a slightly different form. It is determined in much the same manner as $x_A(t)$ except that in the fourth step, the outputs of $Q^*_m(f-\frac{l}{T_c})$ for $m \neq l$, corresponding to those filters sensitive to chip delay changes, are summed to form the training signal $x_B(t) = \sum_l \sum_{m\neq l} x_{l,m}(t)$ for FSE$_B$.

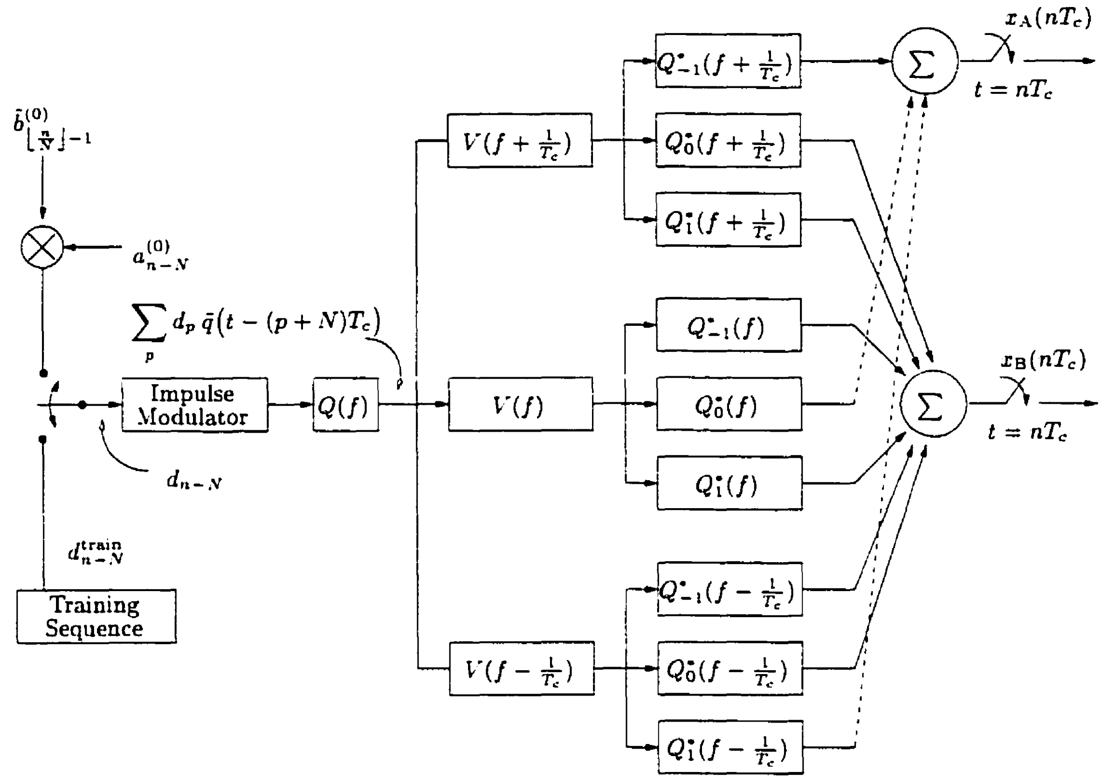

Fig. 6.8 An example of the two reference signals $x_A(nT_c)$ and $x_B(nT_c)$ for structure III when the excess bandwidth satisfies $0 < \alpha \leq 200\%$.

This leads to

$$x_B(t) = \sum_p d_p \sum_l \sum_{m \neq l} \tilde{q}\Big(t-(p+N)T_c\Big) \star \Big[\tilde{q}_m(-t)e^{j2\pi lt/T_c}\Big] \qquad (6.7)$$

sampled at $t = nT_c$. An example of the design of $x_B(nT_c)$ is illustrated in Fig. 6.8 when $0 < \alpha \leq 200\%$. The second distinguishing aspect of FSE$_B$ is its tap coefficient updating algorithm B. Since its filter impulse response is sensitive to changes in chip delays, in applications where chip delays are not fixed, Algorithm B can be designed according to how fast the changes in chip delays need to be tracked.

Compared to structure I, structure III increases hardware and computational complexity by a factor of at least two. The utility of structure III, however, is its ability to discriminate between tap coefficients which are sensitive to changing chip delays and those which are insensitive to changing chip delays. The tap coefficients which are insensitive and sensitive to changing chip delays are contained in, respectively, FSE$_A$ and FSE$_B$. The ability to separate the coefficients into two classes permits the

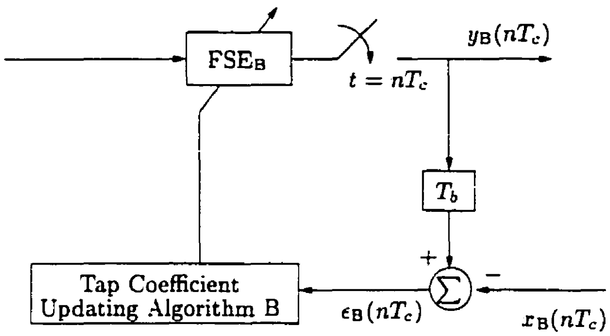

Fig. 6.9 FSE$_B$ in structure III.

misadjustment in at least FSE$_A$ to be reduced under changing chip delay conditions. Misadjustment refers to the amount by which the final value of the MSE differs from the minimum MSE produced by the optimum MSE minimizing linear filter [119, p. 3]. In contrast, structure I does not have this capability. Consequently, when chip delays change, it would be expected that the misadjustment in structure III would be less than that of structure I.

6.4 Summary

This chapter has considered adaptive receiver structures which can realize either the NWMF, CLMF or CUMF. The basic receiver structure was shown to consist of an adaptive chip filter, a sampler at the chip rate and a despreading filter. It resembles the CMF except that the adaptive chip filter replaces the CMF chip filter. The complexity in implementing the adaptive chip filter was found to be independent of the number of interferers and dependent upon the number of tap coefficients in the adaptive chip filter, instead. The minimum number of taps needed to realize the SNR maximizing chip filter was determined to be $N_{\rm FSE} = 2BT_g$ since the minimum duration of the SNR maximizing filter response, T_g, was three times that of the chip filter.

Three adaptive chip filter structures were proposed. Structure I required the least in terms of hardware and computational complexity. It consisted of a single FSE whose tap coefficients are adaptively updated to minimize the MSE formed between the FSE output and training signal. The two remaining structures introduced larger hardware and computational complexity. However, they can provide greater performance depending on the application. The advantage of Structure II, based on a bank of adaptive bandpass filters, appears in systems where narrowband interference may be present or where a faster rate of convergence may be desired. Structure III separated the adaptive filter of structure I into two FSEs: one sensitive to changing chip delays and another insensitive to changing chip delays. Its advantage is its ability to reduce misadjustment in the adaptive filters.

Chapter 7

Conclusions

This thesis has addressed the deficiencies of current receiver designs for DS-CDMA systems based on long sequence spreading. As discussed in Chapter 2, the only low-complexity receivers compatible with long sequence spreading were shown to be the conventional MF (CMF), noise-whitening MF (NWMF) and chip symbol adaptive fractionally-spaced equalizer (FSE) (proposed to realize the NWMF). The problem with these receivers, however, was identified to be their limited performance under power-imbalance conditions. Similar to the CMF, the NWMF was found, in Chapter 5, to have a near-far resistance of zero. In an effort to counter the power-imbalance effect and maintain compatibility with long sequence spreading, the thesis developed the chip-delay locked MF (CLMF) maximizing SNR for bit symbol detection. It required the knowledge of only interferer chip delays and signal powers; knowledge of their spreading sequences was unnecessary.

The design of the CLMF took advantage of the observation that, given the interferer chip delays and signal powers, multiple-access interference (MAI) could be modelled as wide-sense cyclostationary (WSCS) with a period of one chip period. The CLMF was shown to consist of an SNR maximizing chip filter for chip symbol detection and a despreading filter. Its structure was straightforward in that it could be constructed from the CMF, used in current systems, by replacing the CMF chip filter with this new chip filter. Furthermore, its computational complexity per bit symbol was shown to be reasonably low. Analysis revealed that the complexity involved in computing the new chip filter response, required only when an interferer parameter changed, grew linearly with the number of interferers.

In terms of performance, the analysis and numerical results, presented in Chapter 5, clearly demonstrated the improvement achievable by the CLMF, compared to the CMF and NWMF, over multiple-access channels corrupted with additive white Gaussian noise (AWGN). It was established that, unlike the NWMF and CMF, the CLMF could deliver non-zero near-far resistance. Furthermore, under MAI dominated conditions typical of most applications, it was found that the improvement in terms of SNR and BER increased when chip delays of interferers were clustered about a half chip period and as signal powers of interferers increased relative to that of the desired user. In addition, it was demonstrated that further SNR gains could be obtained with the knowledge of interferer phase-offsets. With respect to probability of outage, the amount of improvement offered by the CLMF was shown to grow with increased excess bandwidth and more severe power-imbalance conditions. Moreover, in a dual-rate DS-CDMA system based on the IS-95 pulse and high-rate users with signal powers 9 dB stronger than those of low-rate users at a spreading factor of 64, the use of the CLMF in place of the CMF increased low-rate user capacity by two to three users.

To eliminate the need for interferer signal parameters, adaptive implementations of the CLMF were considered in brief. The basic adaptive receiver structure was shown to consist of an adaptive chip filter to realize the SNR maximizing (or MSE minimizing) chip filter, a sampler operating at the chip rate and a correlator. Three adaptive chip filter structures suited for different applications were proposed. The first structure, equivalent to the chip symbol adaptive FSE, required the least in terms of hardware and computational complexity. The next two structures took advantage of the internal structure of the SNR maximizing chip filter as described in Chapter 4. The second structure consisted of a bank of FSEs to realize a bank of bandpass filters. Such a structure would be effective in reducing the rate of convergence of the adaptive filter and in dealing with narrowband interference in applications such as overlay CDMA. The third structure was composed of two parallel FSEs one sensitive to changes in interferer chip delays and the other less sensitive to such changes. Such a structure would be appropriate in systems with changing chip delays to reduce misadjustment in the adaptive filters. A detailed study of the performance of these adaptive structures was beyond the scope of the thesis and was left as the subject of future research.

And finally, based on the same approach used to synthesize the CLMF, the thesis presented a unifying framework in Chapter 2 which could derive other one-shot linear receivers (referred to as enhanced single-user receivers). Depending on the level of interferer signal parameters available to the receiver, the framework could synthesize, in addition to the CLMF, the NWMF, and the one-shot linear MMSE detector (BLMF). Furthermore, in the limit as the AWGN power spectral density (PSD) level approached zero, the NWMF, CLMF and BLMF were shown to reduce to, respectively, an inverse chip filter followed by a despreading filter (D-NWMF) a decorrelator-type CLMF (D-CLMF) and the one-shot decorrelator (D-BLMF). Similar to the D-BLMF, these structures aimed at completely tuning out MAI while eliminating the need for interferer signal powers. The thesis also examined the effect of interferer phase-offset information, ISI and the presence of both unlocked and chip-delay locked interferers on the design of the MFs.

7.1 Directions for Future Research

Several directions for future research are stated. First, adaptive chip filters appear to show much promise in improving receiver performance in DS-CDMA. The thesis has presented three possible structures to implement the adaptive chip filter. Other structures such as the frequency domain time-dependent adaptive filter (TDAF) or blind adaptive filter may be possible as well. Furthermore, once the structure of the adaptive chip filter has been selected, a number of issues have yet to be investigated to assess its feasibility. These include the selection of a tap coefficient updating algorithm and the analysis of its complexity and performance (in terms of rate of convergence, misadjustment, tracking and robustness). Another important issue which has not been dealt with is the effect of channel coding. Depending on the application, decoding delay may play an important role in the design of the adaptive chip filter.

The second direction relates to the performance of the CLMF. As an initial step, its performance had been assessed for a DS-CDMA system in an AWGN channel with fixed interferer chip delays and signal powers. Its performance remains to be analyzed for channels arising, for example, in fixed or mobile applications where multipaths may exist and where interferer parameters may change. Consequently, the evaluation of performance gains offered by the CLMF under various channel conditions would help justify its development for different applications.

And finally, there exists much on-going research towards the development of interference cancellation (IC) receivers despite their high computational complexity. Similar to the CMF and NWMF, the implementation of the CLMF does not preclude the use of IC receivers. That is, the CLMF can be employed at the front end (in place of the CMF) of an interference cancellation (IC) receiver to improve initial bit estimates and improve IC performance. It may be worthwhile to evaluate the level of improvement the CLMF may offer to IC receivers.

Appendix A

Relationship of the Linear MMSE Filter and MF

The relationship of the LTI filter which minimizes mean square error (MSE) and that which maximizes SNR is investigated. The result of [95, pp. 252-261] is generalized for an observation interval which is not constrained to be infinite and for noise which is not necessarily WSS. Furthermore, an expression which relates minimum MSE and maximum SNR is established. The discussion is divided into two parts. First the LTI filter which minimizes MSE is derived assuming pulse amplitude modulation (PAM). The problem is posed as a one-shot linear estimation of the amplitude of an isolated pulse with a known shape in the presence of noise. Once the solution is established, the equivalence of the MMSE filter and SNR maximizing filter is shown.

The following derivation assumes real signals as opposed to complex baseband signals to maintain clarity. Moreover, the final results can be readily transposed to complex baseband signals. The LTI filter which minimizes MSE is represented as $c(t)$ as shown in Fig. A.1. The filter has an impulse response existing over $t \in [t_1, t_2]$. It

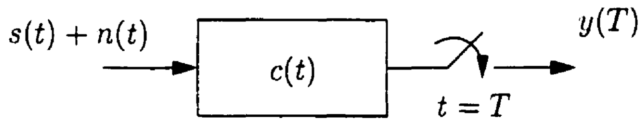

Fig. A.1 One-shot MMSE LTI filter.

is a time interval which contains the signal of interest. Its input consists of a PAM signal $s(t)$ associated with one bit symbol for one-shot detection and noise $n(t)$. The

PAM signal carrying the bit information is defined as

$$s(t) = a\,x(t) \tag{A.1}$$

where a is a discrete random variable which for binary PAM could be ± 1 and where $x(t)$ is the pulse shape normalized to satisfy $\int_{t_1}^{t_2} |x(t)|^2 dt = 1$. Thus, the energy of $s(t)$ is $\overline{a^2} = \mathrm{E}[a^2]$. The output of the filter is sampled at $t = T$ to generate the sample $y(T)$. The sample can be broken into two components:

$$y(T) = aX(T) + N(T) \tag{A.2}$$

where $X(T) = \int_{t_1}^{t_2} x(t)c(T-t)dt$ and $N(T) = \int_{t_1}^{t_2} n(t)c(T-t)dt$. Given that the ideal or expected value of the sample is $y(T) = a$, the error between the two values can be defined as

$$\epsilon = y(T) - a. \tag{A.3}$$

Based on this framework, the objective is to find the filter $c(t)$ which minimizes

$$\mathrm{MSE} = \mathrm{E}[\epsilon^2]. \tag{A.4}$$

Substitution of (A.3) and (A.2) into (A.4) yields

$$\begin{aligned}\mathrm{MSE} = {} & \overline{a^2} + \overline{a^2}\int_{t_1}^{t_2}\int_{t_1}^{t_2} x(t)x(u)c(T-t)c(T-u)du\,dt \\ & - \int_{t_1}^{t_2}\int_{t_1}^{t_2} R_n(t,u)c(T-t)c(T-u)du\,dt \\ & -2\overline{a^2}\int_{t_1}^{t_2} x(t)c(T-t)dt \end{aligned} \tag{A.5}$$

where the noise autocorrelation function is $R_n(t,u) = \mathrm{E}[n(t)n(u)]$. As explained in [80, p. 490], the filter $c(t)$ which minimizes MSE is found by equating the first variation of MSE with respect to $c(t)$ to zero. This leads to

$$\int_{t_1}^{t_2} \left[\overline{a^2}\,x(t)x(u) + R_n(t,u)\right] c(T-u)du = \overline{a^2}\,x(t) \tag{A.6}$$

which is of the same form as [80, p. 490 (7.59)] except that only one pulse in the PAM signal is included and noise is not assumed to be white. At first glance, (A.6) does not appear to have the same form as the integral equation in (2.19) associated with the LTI filter which maximizes SNR. However, (A.6) can be re-arranged with the insight provided by [95, pp. 251-261]. By expanding the left hand side into two integrals and collecting the coefficients of $x(t)$, (A.6) can be expressed as

$$\int_{t_1}^{t_2} R_n(t,u)c(T-u)du \;=\; \overline{a^2}\,x(t)\left[1-\int_{t_1}^{t_2} x(u)c(T-u)du\right]. \tag{A.7}$$

The right hand side consists of $x(t)$ and a multiplicative constant. By defining

$$c(t) \;=\; \alpha\, h(t) \tag{A.8}$$

where α is a scaling factor to be determined shortly, (A.7) can be re-written as

$$\int_{t_1}^{t_2} R_n(t,u)h(T-u)du \;=\; x(t) \tag{A.9}$$

where

$$\alpha \;=\; \frac{\overline{a^2}}{1+\overline{a^2}\int_{t_1}^{t_2} x(u)h(T-u)du}. \tag{A.10}$$

Therefore, the linear MMSE filter $c(t)$ for one-shot detection is obtained by solving for $h(t)$ in the integral equation (A.9) and substituting $h(t)$ and (A.10) into (A.8).

The relationship between the linear MMSE and the MF is shown. Notice that the integral equation in (A.9) is of the same form as that used to derive the SNR maximizing LTI filter in (2.19) and [93, p. 122 (3.23)] for real signals. Thus, the filter $h(t)$ which satisfies (A.9) is the MF. Furthermore, since introducing a scaling factor in front of $h(t)$ does not affect its SNR performance [92, p. 174], $c(t)$ which is simply a scaled version of $h(t)$ delivers maximum SNR as well. On the contrary, introducing a multiplicative constant in front of $c(t)$ does not yield minimum MSE. Consequently, although the linear MMSE filter which minimizes MSE maximizes SNR, the converse is not necessarily so unless the MF impulse response is properly scaled by a multiplicative constant.

Next, the relationship between minimum MSE and maximum SNR is established. When the filter $c(t)$ satisfies (A.9) and (A.8), (A.5) reduces to the minimum MSE. As shown in [80, p. 498 (7.83)], the minimum MSE normalized with respect to $\overline{a^2}$ is given by

$$\mathrm{MMSE}_{\mathrm{norm}} \;=\; 1-\int_{t_1}^{t_2} x(t)c(T-t)dt$$

$$= \frac{1}{1+\overline{a^2}\int_{t_1}^{t_2} x(t)h(T-t)dt} \tag{A.11}$$

where $\text{MMSE}_{\text{norm}} = \text{MMSE}/\overline{a^2}$. The term in the denominator of (A.11) is simply

$$\text{SNR}_{\text{opt}} = \overline{a^2}\int_{t_1}^{t_2} x(t)h(T-t)dt \tag{A.12}$$

for either $c(t)$ or $h(t)$ when $h(t)$ is the MF which satisfies (A.9). Thus, given (A.11) and (A.12), the minimum MSE and maximum SNR values are related by

$$\text{MMSE}_{\text{norm}} = \frac{1}{1+\text{SNR}_{\text{opt}}} \tag{A.13}$$

or, conversely, $\text{SNR}_{\text{opt}} = \frac{1}{\text{MMSE}_{\text{norm}}} - 1$. The relationship in (A.13) is the same as that derived in [62] for the particular case of one-shot linear MMSE detection in DS-CDMA under the condition of short sequence spreading.

Appendix B

Derivation of the MAI Autocorrelation Functions

The autocorrelation and pseudo-autocorrelation functions for the three models of the MAI are derived.

B.1 Autocorrelation Functions for Unlocked Interferers

B.1.1 MAI Autocorrelation Function — NWMF

The autocorrelation function for unlocked MAI is derived. Substitution of the MAI given in (2.10) and (2.6) into (2.17) yields

$$R_{\tilde{I}}^{(U)}(t,u) = \sum_{k=1}^{K} R_{\tilde{s}^{(k)}}(t,u) \tag{B.1}$$

where, the signal of each interferer given in (2.6) has zero-mean and is assumed to be independent of those of other interferers. Since τ_k is uniformly distributed over $\tau_k \in [0, T_b)$, the autocorrelation function of the kth interferer is

$$R_{\tilde{s}^{(k)}}(t,u) = \frac{1}{T_b}\int_0^{T_b} \mathrm{E}[\,\tilde{s}^{(k)}(t)\,\tilde{s}^{(k)*}(u)\,|\,\tau_k\,]\,d\tau_k \tag{B.2}$$

where

$$\mathrm{E}[\,\tilde{s}^{(k)}(t)\,\tilde{s}^{(k)*}(u)\,|\,\tau_k\,] = 2P_k \sum_{n=-\infty}^{\infty} \tilde{q}(t-\tau_k-nT_c)\,\tilde{q}^*(u-\tau_k-nT_c) \tag{B.3}$$

which is conditioned on τ_k. As described in section 2.1.2, the spreading sequence $a_n^{(k)}$ is modelled as a as a discrete WSS random process with $\mathrm{E}[a_n^{(k)}a_m^{(k)*}] = \delta_{nm}$. The phase-offset θ_k disappears regardless of whether it is known or random. Next, by evaluating the integral in (B.2) using (B.3), (B.2) becomes

$$R_{\tilde{s}^{(k)}}(t,u) \;=\; 2P_k \cdot \frac{1}{T_b} \sum_{n=-\infty}^{\infty} \int_0^{T_b} \tilde{q}(t-\tau_k-nT_c)\,\tilde{q}^*(u-\tau_k-nT_c)\,d\tau_k. \quad \text{(B.4)}$$

By letting $y = u - \tau_k - nT_c$, (B.4) becomes

$$R_{\tilde{s}^{(k)}}(t,u) \;=\; 2P_k \cdot \frac{1}{T_c} \int_{-\infty}^{\infty} \tilde{q}(t-u+y)\tilde{q}^*(y)dy. \quad \text{(B.5)}$$

Substitution of (B.5) into (B.1) results in

$$R_{\tilde{I}}^{(U)}(t,u) \;=\; \sum_{k=1}^{K} 2P_k \left[\frac{1}{T_c} \int_{-\infty}^{\infty} \tilde{q}(t-u+y)\tilde{q}^*(y)dy\right] \quad \text{(B.6)}$$

which when re-arranged gives the desired result of (3.9).

B.1.2 MAI Pseudo Autocorrelation Function — NWMF

The pseudo-autocorrelation function for unlocked MAI is shown to be zero. Substitution of the MAI given in (2.10) and (2.6) into (2.18) yields

$$\tilde{R}_{\tilde{I}}(t,u) \;=\; \sum_{k=1}^{K} \tilde{R}_{\tilde{s}^{(k)}}(t,u) \quad \text{(B.7)}$$

where the signal of each interferer given in (2.6) has zero-mean and is assumed to be independent of other interferers. Since τ_k is uniformly distributed over $\tau_k \in [0, T_b)$, the autocorrelation function of the kth interferer is

$$\tilde{R}_{\tilde{s}^{(k)}}(t,u) \;=\; \frac{1}{T_b} \int_0^{T_b} \mathrm{E}[\,\tilde{s}^{(k)}(t)\,\tilde{s}^{(k)}(u)|\,\tau_k\,]\,d\tau_k \quad \text{(B.8)}$$

where

$$\mathrm{E}[\,\tilde{s}^{(k)}(t)\,\tilde{s}^{(k)}(u)\,|\,\tau_k\,] = 2P_k\mathrm{E}[e^{j2\theta_k}] \sum_{n=-\infty}^{\infty} \tilde{q}(t-\tau_k-nT_c)\,\tilde{q}(u-\tau_k-nT_c) \quad \text{(B.9)}$$

which is conditioned on τ_k. If the bit delay τ_k of the kth interferer is uniformly distributed, then its phase-offset is uniformly distributed as well since θ_k is linearly dependent on τ_k. That is, $\theta_k = \psi_k + w_c\tau_k$ where ψ_k is the phase-offset at the transmitter of user k relative to that of the desired user. Thus, the term $\mathrm{E}[e^{j2\theta_k}] = 0$ and, for all t, u,

$$\tilde{R}_{\tilde{I}}(t,u) = 0. \tag{B.10}$$

B.2 Autocorrelation Function for Chip-Delay Locked Interferers

B.2.1 MAI Autocorrelation Function — CLMF

The autocorrelation function for chip-delay locked MAI is derived. Substitution of the MAI given in (2.10) and (2.6) into (2.17) yields

$$R_{\tilde{I}}^{(C)}(t,u) = \sum_{k=1}^{K} R_{\tilde{s}(k)}^{(C)}(t,u) \tag{B.11}$$

where the signal of each interferer given in (2.6) has zero-mean and is assumed to be independent of other interferers. The autocorrelation function of the kth interferer is

$$R_{\tilde{s}(k)}^{(C)}(t,u) = 2P_k \sum_{n=-\infty}^{\infty} \tilde{q}(t-\tau_k-nT_c)\,\tilde{q}^*(u-\tau_k-nT_c) \tag{B.12}$$

where τ_k is modelled as being fixed. The spreading sequence $a_n^{(k)}$ is modelled as a discrete WSS process with $\mathrm{E}[a_n^{(k)}a_m^{(k)*}] = \delta_{nm}$. The phase-offset θ_k disappears regardless of whether it is known or random. Next, by noting that the bit delay can be written as $\tau_k = n_kT_c + T_k$ where $n_k = \lfloor \tau_k/T_c \rfloor$ and letting $l = n + n_k$, (B.12) becomes

$$R_{\tilde{s}(k)}^{(C)}(t,u) = 2P_k \sum_{n=-\infty}^{\infty} \tilde{q}(t-T_k-nT_c)\,\tilde{q}^*(u-T_k-nT_c). \tag{B.13}$$

Thus, (B.13) and (B.11) together give the desired result of (3.26).

B.2.2 MAI Pseudo Autocorrelation Function — CLMF

The pseudo-autocorrelation function for chip-delay locked MAI is derived. Substitution of the MAI given in (2.10) and (2.6) into (2.18) yields

$$\tilde{R}_{\tilde{I}}^{(C)}(t,u) = \sum_{k=1}^{K} \tilde{R}_{\tilde{s}(k)}^{(C)}(t,u) \tag{B.14}$$

where the signal of each interferer given in (2.6) has zero-mean and is assumed to be independent of other interferers. For the same reasons given in Appendix B.2.1, the pseudo-autocorrelation function of the kth interferer is conditioned on T_k instead of τ_k and can be written as

$$\tilde{R}^{(C)}_{\tilde{s}(k)}(t,u) = 2P_k \mathrm{E}[e^{j2\theta_k}] \sum_{n=-\infty}^{\infty} \sum_{m=-\infty}^{\infty} \mathrm{E}[a_n^{(k)} a_m^{(k)}] \tilde{q}(t - T_k - nT_c)\, \tilde{q}(u - T_k - mT_c). \tag{B.15}$$

The pseudo-autocorrelation function $\tilde{R}^{(C)}_{\tilde{s}(k)}(t,u) \equiv 0$ if at least one of the following two conditions is satisfied. The spreading sequence $a_n^{(k)}$ is modelled as a proper, discrete WSS processes with $\mathrm{E}[a_n^{(k)} a_m^{(k)}] = 0$ or the phase-offset θ_k is uniformly distributed over $\theta_k \in [0, 2\pi)$ such that $\mathrm{E}[e^{j2\theta_k}] = 0$. Either case implies that $\tilde{R}^{(C)}_{\tilde{I}}(t,u) \equiv 0$. On the contrary, $\tilde{R}^{(C)}_{\tilde{s}(k)}(t,u) \neq 0$ for all t, u if the following two conditions are satisfied. The spreading sequence $a_n^{(k)}$ is modelled as an improper, discrete WSS process with $\mathrm{E}[a_n^{(k)} a_m^{(k)}] = \delta_{nm}$ and the phase-offsets θ_k are known such that $\mathrm{E}[e^{j2\theta_k}] = e^{j2\theta_k}$. When both of these conditions are satisfied, (B.15) becomes

$$\tilde{R}^{(C)}_{\tilde{s}(k)}(t,u) = 2P_k e^{j2\theta_k} \sum_{n=-\infty}^{\infty} \tilde{q}(t - T_k - nT_c)\, \tilde{q}(u - T_k - nT_c). \tag{B.16}$$

Using the same procedure outlined in section 3.3.2, (B.16) can be expressed in the form the separable kernel

$$\tilde{R}^{(C)}_{\tilde{s}(k)}(t,u) = 2P_k e^{j2\theta_k} \sum_{n=-M}^{N+M-2} \tilde{q}(t - T_k - nT_c)\, \tilde{q}(u - T_k - nT_c) \tag{B.17}$$

for $t, u \in [0, T_b]$. Thus, (B.17) and (B.14) together give the desired result of (3.46).

B.3 Autocorrelation Function for Bit-Delay Locked Interferers

B.3.1 MAI Autocorrelation Function — BLMF

The autocorrelation function for bit-delay locked MAI is derived. Substitution of the MAI given in (2.10) and (2.7) into (2.17) yields

$$R^{(B)}_{\tilde{I}}(t,u) = \sum_{k=1}^{K} R^{(B)}_{\tilde{s}(k)}(t,u) \tag{B.18}$$

where the signal of each interferer given in (2.7) has zero-mean and is assumed to be independent of other interferers. The autocorrelation function of the kth interferer is

$$R_{\tilde{s}(k)}^{(B)}(t,u) \;=\; 2P_k \sum_{i=-\infty}^{\infty} \tilde{a}^{(k)}(t-\tau_k-iT_b)\,\tilde{a}^{(k)*}(u-\tau_k-iT_b) \qquad \text{(B.19)}$$

where τ_k is modelled as being fixed. The bits $b_i^{(k)} \in \{\pm 1\}$ are modelled as a discrete WSS process with $\mathrm{E}[b_i^{(k)} b_j^{(k)}] = \delta_{ij}$. The phase-offset θ_k disappears regardless of whether it is known or random. Equations (B.19) and (B.18) together give the desired result of (3.35).

B.3.2 MAI Pseudo Autocorrelation Function — BLMF

The pseudo-autocorrelation function for bit-delay locked MAI is derived. Substitution of the MAI given in (2.10) and (2.7) into (2.17) yields

$$\tilde{R}_{\tilde{I}}^{(B)}(t,u) \;=\; \sum_{k=1}^{K} \tilde{R}_{\tilde{s}(k)}^{(B)}(t,u) \qquad \text{(B.20)}$$

where the signals of each interferer given in (2.7) have zero-mean and are assumed to be independent. The pseudo-autocorrelation function of the kth interferer is

$$\tilde{R}_{\tilde{s}(k)}^{(B)}(t,u) \;=\; 2P_k \mathrm{E}[e^{j2\theta_k}] \sum_{i=-\infty}^{\infty} \tilde{a}^{(k)}(t-\tau_k-iT_b)\,\tilde{a}^{(k)}(u-\tau_k-iT_b) \qquad \text{(B.21)}$$

where τ_k is modelled as being fixed. The bits $b_i^{(k)} \in \{\pm 1\}$ are modelled as a discrete WSS process with $\mathrm{E}[b_i^{(k)} b_j^{(k)}] = \delta_{ij}$. When the phase-offset θ_k is random and uniformly distributed over $\theta_k \in [0, 2\pi)$, $\mathrm{E}[e^{j2\theta_k}] = 0$ and $\tilde{R}_{\tilde{s}(k)}^{(B)}(t,u) \equiv 0$ which implies that $\tilde{R}_{\tilde{I}}^{(B)}(t,u) \equiv 0$. On the contrary, when the phase-offset is known, $\mathrm{E}[e^{j2\theta_k}] = e^{j2\theta_k}$ and (B.21) becomes

$$\tilde{R}_{\tilde{s}(k)}^{(B)}(t,u) = 2P_k e^{j2\theta_k} \sum_{i=-\infty}^{\infty} \tilde{a}^{(k)}(t-\tau_k-iT_b)\,\tilde{a}^{(k)}(u-\tau_k-iT_b). \qquad \text{(B.22)}$$

Using the same procedure outlined in section 3.4.2, (B.22) can be expressed in the form the separable kernel

$$\tilde{R}_{\tilde{s}(k)}^{(B)}(t,u) = 2P_k e^{j2\theta_k} \sum_{i=-M_1}^{M_2} \tilde{a}^{(k)}(t-\tau_k-iT_b)\,\tilde{a}^{(k)}(u-\tau_k-iT_b) \qquad \text{(B.23)}$$

for $t, u \in [0, T_b]$. Thus, (B.23) and (B.20) together give the desired result of (3.48).

Appendix C

Calculation of Coefficients

This appendix describes the steps involved in deriving the coefficients needed for obtaining the MF impulse response when the observation interval is finite. The derivation of the coefficients proceeds from unlocked, chip-delay locked to bit-delay locked interferers.

C.1 Calculation of the Coefficients $f_j^{(U)}$

Multiply both sides of the integral equation (3.17) by $\phi_i^*(t)$ where $i \in [1, N_U]$. The integration of both sides results in

$$f_i^{(U)*} + \frac{\gamma}{N_o} \sum_j \lambda'_j f_j^{(U)*} \phi_{i,j} = a_i^{(U)*} \tag{C.1}$$

where $a_i^{(U)*}$ is given in (3.20) and $\phi_{i,j} = \int_0^{T_b} \phi_i^*(t)\phi_j(t)dt$. Since Hermitian kernels give rise to orthonormal eigenfunctions, $\phi_{i,j} = \delta_{i,j}$ [101, p.138]. By defining

$$\mathbf{\Lambda} = \begin{bmatrix} \lambda'_1 & \dots & 0 \\ \vdots & & \vdots \\ 0 & \dots & \lambda'_{N_U} \end{bmatrix} \tag{C.2}$$

$$\mathbf{a}^{(U)} = \left[a_1^{(U)}, \dots, a_{N_U}^{(U)}\right] \tag{C.3}$$

and $\mathbf{f}^{(U)} = \left[f_1^{(U)}, \dots, f_{N_U}^{(U)}\right]$, the N_U equations associated with i can be rewritten compactly as

$$\left(\mathbf{I}_{N_U} + \frac{\gamma}{N_o}\mathbf{\Lambda}\right) \mathbf{f}^{(U)^{\mathrm{H}}} = \mathbf{a}^{(U)^{\mathrm{H}}}. \tag{C.4}$$

Since the matrix is diagonal, the coefficients are, therefore,

$$f_i^{(U)} = \frac{a_i^{(U)}}{1 + \frac{\gamma}{N_o}\lambda_i'} \tag{C.5}$$

which is the desired result given in (3.19).

C.2 Calculation of the Coefficients $f_{k,m}^{(C)}$

Multiply both sides of the integral equation (3.30) by $\tilde{q}^*(t - T_i - jT_c)$ where $i \in [1, K]$ and $j \in [-M, N + M - 2]$. The integration of both sides results in

$$f_{i,j}^{(C)*} + \frac{1}{N_o}\left[P_1 \sum_n c_{i,1;j,n} f_{1,n}^{(C)*} + \ldots + P_K \sum_n c_{i,K;j,n} f_{K,n}^{(C)*}\right] = a_{i,j}^{(C)*} \tag{C.6}$$

where $c_{i,k;j,n} = \int_0^{T_b} \tilde{q}^*(t - T_i - jT_c)\tilde{q}(t - T_k - nT_c)dt$ and $a_{i,j}^{(C)} = \int_0^{T_b} \tilde{q}(t - T_i - jT_c)\tilde{a}^{(0)*}(t)dt$. Working towards a compact expression in matrix notation, let $\mathbf{f}_i^{(C)} = \left[f_{i,-M}^{(C)}, \ldots, f_{i,N+M-2}^{(C)}\right]$, $\mathbf{a}_i^{(C)} = \left[a_{i,-M}^{(C)}, \ldots, a_{i,N+M-2}^{(C)}\right]$ and

$$\mathbf{C}_{i,k}^{(C)} = \begin{bmatrix} c_{i,k;-M,-M} & \cdots & c_{i,k;-M,N+M-2} \\ \vdots & & \vdots \\ c_{i,k;N+M-2,-M} & \cdots & c_{i,k;N+M-2,N+M-2} \end{bmatrix}. \tag{C.7}$$

The $N + 2M - 1$ equations associated with i can be rewritten as

$$\mathbf{f}_i^{(C)\mathrm{H}} + \frac{1}{N_o}\left[P_1 \mathbf{C}_{i,1}^{(C)} \mathbf{f}_1^{(C)\mathrm{H}} + \ldots + P_K \mathbf{C}_{i,K}^{(C)} \mathbf{f}_K^{(C)\mathrm{H}}\right] = \mathbf{a}_i^{(C)\mathrm{H}}. \tag{C.8}$$

For $i \in [1, K]$, this then can be written compactly as

$$\left(\mathbf{I}_{K(N+2M-1)} + \frac{1}{N_o}\mathbf{C}^{(C)}\mathbf{P}^{(C)}\right)\mathbf{f}^{(C)\mathrm{H}} = \mathbf{a}^{(C)\mathrm{H}} \tag{C.9}$$

where $\mathbf{f}^{(C)} = \left[\mathbf{f}_1^{(C)} \ldots \mathbf{f}_K^{(C)}\right]$,

$$\mathbf{a}^{(C)} = \left[\mathbf{a}_1^{(C)} \ldots \mathbf{a}_K^{(C)}\right], \tag{C.10}$$

$$\mathbf{C}^{(C)} = \begin{bmatrix} \mathbf{C}_{1,1}^{(C)} & \cdots & \mathbf{C}_{1,K}^{(C)} \\ \vdots & & \vdots \\ \mathbf{C}_{K,1}^{(C)} & \cdots & \mathbf{C}_{K,K}^{(C)} \end{bmatrix}, \tag{C.11}$$

$$\mathbf{P}^{(C)} = \begin{bmatrix} P_1\mathbf{I}_{N+2M-1} & \cdots & \mathbf{O} \\ \mathbf{O} & \ddots & \mathbf{O} \\ \mathbf{O} & \cdots & P_K\mathbf{I}_{N+2M-1} \end{bmatrix} \tag{C.12}$$

and $\mathbf{I}_L$ is the $L \times L$ identity matrix. Thus, the $K(N+2M-1)$ coefficients in $\mathbf{f}^{(C)}$ can be obtained by solving this set of $K(N+2M-1)$ equations.

The matrices and vectors can be interpreted as follows. The vector $\mathbf{a}^{(C)}$ represents the correlation between the desired user's spreading signal $\tilde{a}^{(0)}(t)$ and the $K(N+2M-1)$ basis functions $\{\tilde{q}^*(t-T_k-nT_c)|\ n \in [-M, N+M-2],\ k \in [1,K]\ \}$. The basis function indexed by k and n is the conjugate of the chip waveform $\tilde{q}^*(t)$ delayed by $T_k + nT_c$. The matrix $\mathbf{C}^{(C)}$ is a covariance matrix. It holds information regarding the auto and cross-correlations among the basis functions.

C.3 Calculation of the Coefficients $f_{k,m}^{(B)}$

Multiply both sides of the integral equation (3.38) by $\tilde{a}^{(i)*}(t-\tau_i-jT_b)$ where $i \in [1,K]$ and $j \in [M_1, M_2]$. The integration of both sides results in

$$f_{i,j}^{(B)*} + \frac{1}{N_o}\left[P_1\sum_m \rho_{i,1;j,m} f_{1,m}^{(B)*} + \ldots + P_K \sum_m \rho_{i,K;j,m} f_{K,m}^{(B)*}\right] = a_{i,j}^{(B)*} \tag{C.13}$$

where $\rho_{i,k;j,m} = \int_0^{T_b} \tilde{a}^{(i)*}(t-\tau_i-jT_b)\,\tilde{a}^{(k)}(t-\tau_k-mT_b)dt$ and $a_{i,j}^{(B)} = \int_0^{T_b} \tilde{a}^{(i)}(t-\tau_i-jT_b)\,\tilde{a}^{(0)*}(t)dt$. Note that $a_{i,j}^{(B)} = \rho_{i,0;j,0}$. Working towards a compact expression in matrix form, let $\mathbf{f}_i^{(B)} = \left[f_{i,M_1}^{(B)}, \ldots, f_{i,M_2}^{(B)}\right]$, $\mathbf{a}_i^{(B)} = \left[a_{i,M_1}^{(B)}, \ldots, a_{i,M_2}^{(B)}\right]$ and

$$\mathbf{C}_{i,k}^{(B)} = \begin{bmatrix} \rho_{i,k;M_1,M_1} & \cdots & \rho_{i,k;M_1,M_2} \\ \vdots & & \vdots \\ \rho_{i,k;M_2,M_1} & \cdots & \rho_{i,k;M_2,M_2} \end{bmatrix} \tag{C.14}$$

which is a M_3 by M_3 matrix where $M_3 = M_2 - M_1 + 1$. The M_3 equations associated with i can be rewritten as

$$\mathbf{f}_i^{(B)^{\mathrm{H}}} + \frac{1}{N_o}\left[P_1\mathbf{C}_{i,1}^{(B)}\mathbf{f}_1^{(B)^{\mathrm{H}}} + \ldots + P_K\mathbf{C}_{i,K}^{(B)}\mathbf{f}_K^{(B)^{\mathrm{H}}}\right] = \mathbf{a}_i^{(B)^{\mathrm{H}}}. \tag{C.15}$$

For $i \in [1,K]$, this then can be written compactly as

$$\left(\mathbf{I}_{KM_3} + \frac{1}{N_o}\mathbf{C}^{(B)}\mathbf{P}^{(B)}\right)\mathbf{f}^{(B)^{\mathrm{H}}} = \mathbf{a}^{(B)^{\mathrm{H}}} \tag{C.16}$$

where $\mathbf{f}^{(B)} = \left[\mathbf{f}_1^{(B)} \ldots \mathbf{f}_K^{(B)}\right]$,

$$\mathbf{a}^{(B)} = \left[\mathbf{a}_1^{(B)} \ldots \mathbf{a}_K^{(B)}\right], \tag{C.17}$$

$$\mathbf{C}^{(B)} = \begin{bmatrix} \mathbf{C}_{1,1}^{(B)} & \ldots & \mathbf{C}_{1,K}^{(B)} \\ \vdots & & \vdots \\ \mathbf{C}_{K,1}^{(B)} & \ldots & \mathbf{C}_{K,K}^{(B)} \end{bmatrix}, \tag{C.18}$$

$$\mathbf{P}^{(B)} = \begin{bmatrix} P_1\mathbf{I}_2 & \ldots & \mathbf{O} \\ \mathbf{O} & \ddots & \mathbf{O} \\ \mathbf{O} & \ldots & P_K\mathbf{I}_2 \end{bmatrix}. \tag{C.19}$$

Thus, the KM_3 coefficients in $\mathbf{f}^{(B)}$ can be obtained by solving the set of KM_3 equations in (C.16).

The vectors and matrices can be interpreted as follows. The vector $\mathbf{a}^{(B)}$ represents the correlation between the desired user's spreading signal $\tilde{a}^{(0)}(t)$ and the KM_3 basis functions $\{\tilde{a}^{(k)*}(t - \tau_k - mT_b) | \ n \in [M_1, M_2], \ k \in [1, K] \ \}$. The basis function indexed by k and m is in fact the conjugate of the spreading signal of the kth interferer $\tilde{a}^{(k)*}(t)$ delayed by $\tau_k + mT_b$. The matrix $\mathbf{C}^{(B)}$ is a covariance matrix. It holds information regarding the auto and cross-correlations among the basis functions.

C.4 Calculation of the Coefficients $f_{k,m}^{(C)}$ and $f_j^{(U)}$

This section utilizes many of the expressions developed in Appendix C.2 and C.1. First, multiply both sides of the integral equation (3.44) by $c_{i,j}^*(t)$ where $i \in [1, K_C]$ and $j \in [-M, N + M - 2]$. The integration of both sides results in

$$f_{i,j}^{(C)*} + \frac{1}{N_o}\left[\sum_k P_k \sum_n c_{i,k;j,n} f_{k,n}^{(C)*} + \gamma_{CU} \sum_q \lambda_q' f_q^{(U)*} K_{i;q;j}^*\right] = a_{i,j}^{(C)*} \tag{C.20}$$

where

$$K_{i;q,j} = \int_0^{T_b} \tilde{q}(t - T_i - jT_c)\phi_q^*(t)dt. \tag{C.21}$$

By defining an $N_U \times (N+2M-1)$ matrix

$$\boldsymbol{K}_i = \begin{bmatrix} K_{i;1,-M} & \cdots & K_{i;1,N+2M-1} \\ \vdots & & \vdots \\ K_{i;N_U,-M} & \cdots & K_{i;N_U,N+2M-1} \end{bmatrix}, \tag{C.22}$$

the $N+2M-1$ equations associated with i can be rewritten as

$$\boldsymbol{f}_i^{(C)^{\mathrm{H}}} + \frac{1}{N_o}\left[\sum_k P_k \boldsymbol{C}_{i,k} \boldsymbol{f}_k^{(C)^{\mathrm{H}}} + \gamma_{CU} \boldsymbol{K}_i^{\mathrm{H}} \boldsymbol{\Lambda} \boldsymbol{f}^{(U)^{\mathrm{H}}}\right] = \boldsymbol{a}_i^{(C)^{\mathrm{H}}}. \tag{C.23}$$

For $i \in [1, K_C]$, this becomes

$$\boldsymbol{f}^{(C)^{\mathrm{H}}} + \frac{1}{N_o}\left[\boldsymbol{C}^{(C)} \boldsymbol{P}^{(C)} \boldsymbol{f}^{(C)^{\mathrm{H}}} + \gamma_{CU} \boldsymbol{K}^{\mathrm{H}} \boldsymbol{\Lambda} \boldsymbol{f}^{(U)^{\mathrm{H}}}\right] = \boldsymbol{a}^{(C)^{\mathrm{H}}} \tag{C.24}$$

where

$$\boldsymbol{K} = [\boldsymbol{K}_1, \ldots, \boldsymbol{K}_{K_C}]. \tag{C.25}$$

To obtain $K_C(N+2M-1)+N_U$ equations for the $K_C(N+2M-1)+N_U$ unknown complex coefficients, next, multiply both sides of the integral equation (3.44) by $\phi_p^*(t)$ where $p \in [1, N_U]$. The integration of both sides results in

$$f_p^{(U)*} + \frac{1}{N_o}\left[\sum_k P_k \sum_n K_{k,p;n}^* f_{k,n}^{(C)*} + \gamma_{CU} \sum_q \lambda_q' f_q^{(U)*} \phi_{p,q}\right] = a_p^{(U)*}. \tag{C.26}$$

Then the $N+2M-1$ equations associated with i can be rewritten as

$$\boldsymbol{f}^{(U)^{\mathrm{H}}} + \frac{1}{N_o}\left[\boldsymbol{K} \boldsymbol{P}^{(C)} \boldsymbol{f}^{(C)^{\mathrm{H}}} + \gamma_{CU} \boldsymbol{\Lambda} \boldsymbol{f}^{(U)^{\mathrm{H}}}\right] = \boldsymbol{a}^{(U)^{\mathrm{H}}}. \tag{C.27}$$

Combining the two matrix equations (C.24) and (C.27),

$$\left(\boldsymbol{I}_{K_C(N+2M-1)+N_U} + \frac{1}{N_o} \boldsymbol{C}^{(CU)} \boldsymbol{P}^{(CU)}\right) \boldsymbol{f}^{(CU)^{\mathrm{H}}} = \boldsymbol{a}^{(CU)^{\mathrm{H}}} \tag{C.28}$$

where $\boldsymbol{f}^{(CU)} = \left[\boldsymbol{f}^{(C)} | \boldsymbol{f}^{(U)}\right]$,

$$\boldsymbol{a}^{(CU)} = \left[\boldsymbol{a}^{(C)} | \boldsymbol{a}^{(U)}\right], \tag{C.29}$$

$$C^{(CU)} = \left[\begin{array}{c|c} C^{(C)} & K^{\mathrm{H}} \\ \hline K & I_{N_U} \end{array}\right] \tag{C.30}$$

and

$$P^{(CU)} = \left[\begin{array}{c|c} P^{(C)} & O \\ \hline O & \gamma_{CU}\Lambda \end{array}\right]. \tag{C.31}$$

The vector $f^{(CU)}$ consists of the unknown coefficients needed for the MF solution. The vector $a^{(CU)}$ represents the correlation between the desired user's spreading signal $\tilde{a}_0(t)$ and the basis functions $\{\tilde{q}^*(t-T_k-nT_c)|\; n \in [-M, N+M-2],\, k \in [1, K]\;\}$ and $\{\phi_j^*(t)\}_{j=1}^{N_U}$. The matrix $C^{(CU)}$ is a covariance matrix. It contains all the information regarding the auto and cross-correlations among the basis functions. The matrix $P^{(CU)}$ holds information on the interference power. Each diagonal element represents the power of its corresponding basis function.

Appendix D

Effect of ISI on MF Design

This appendix addresses the effect of ISI on MF design. In section 2.1, the ISI term in the received signal was assumed to be negligible as is the case in most DS-CDMA applications where PG >> 1 [18, p. 339]. For applications where PG may be small, the NWMF, CLMF and BLMF, developed in Chapter 3, are rederived without neglecting ISI.

The appendix is divided into four parts. First, the noise autocorrelation function and integral equation are re-developed by including ISI. Second, the effect of ISI on the MF for unlocked interferers is examined. This is then followed by similar examinations when the interferers are either chip-delay or bit-delay locked.

D.1 The Integral Equation Which Includes ISI

The effect of taking the ISI into account in the derivation of the general MF solution is considered. The ISI term $\tilde{\zeta}(t)$ is defined in (2.14) and shall now be included in the noise expression in (2.13). Assuming that the thermal noise $\tilde{w}(t)$, MAI $\tilde{I}(t)$ and ISI are independent processes, the autocorrelation function of the noise $\tilde{n}(t)$ from (2.13) can be evaluated and written as

$$R_{\tilde{n}}(t,u) = R_{\tilde{w}}(t,u) + R_{\tilde{I}}(t,u) + R_{\tilde{\zeta}}(t,u). \tag{D.1}$$

The noise pseudo-autocorrelation function can be written as

$$\bar{R}_{\tilde{n}}(t,u) = \bar{R}_{\tilde{I}}(t,u) + \bar{R}_{\tilde{\zeta}}(t,u). \tag{D.2}$$

Next, the substitution of (D.1) and (D.2) into (3.1) transforms (3.1) into a Fredholm integral equation of the second kind [100]

$$\tilde{f}^*(u) + \frac{1}{2N_o}\int_0^{T_b}\left[R_{\tilde{I}}(t,u) + R_{\tilde{\zeta}}(t,u)\right]\tilde{f}^*(u) + \left[\tilde{R}_{\tilde{I}}(t,u) + \tilde{R}_{\tilde{\zeta}}(t,u)\right]\tilde{f}(u)du = \tilde{a}^{(0)}(t), \tag{D.3}$$

where $0 \le t \le T_b$. The solution $\tilde{f}(t)$ to the integral equation now depends upon. not only the MAI and AWGN. but also the ISI via its two autocorrelation functions terms: $R_{\tilde{\zeta}}(t,u)$ and $\tilde{R}_{\tilde{\zeta}}(t,u)$ This leads to modifications of the NWMF, CLMF and BLMF to be discussed next.

D.2 Unlocked Interferers and ISI

The ISI autocorrelation function can be evaluated by using (2.14) and the assumption of random spreading sequences. Furthermore, it can be written as a finite sum by using the same arguments presented in section 3.3.2 in order to have a separable kernel. This yields

$$R_{\tilde{\zeta}}(t,u) = 2P_0\left[\sum_{n=-M}^{-1}\tilde{q}(t-nT_c)\tilde{q}^*(u-nT_c) + \sum_{n=N}^{N+M-2}\tilde{q}(t-nT_c)\tilde{q}^*(u-nT_c)\right] \tag{D.4}$$

where $0 \le t, u \le T_b$. Similarly, the ISI pseudo-autocorrelation function can be written as

$$\tilde{R}_{\tilde{\zeta}}(t,u) = 2P_0\left[\sum_{n=-M}^{-1}\tilde{q}(t-nT_c)\tilde{q}(u-nT_c) + \sum_{n=N}^{N+M-2}\tilde{q}(t-nT_c)\tilde{q}(u-nT_c)\right] \tag{D.5}$$

where $0 \le t, u \le T_b$.

To derive the MF for unlocked interferers via the separable kernel method, (3.16), (D.4), (D.5), $R_{\tilde{I}}(t,u) = R_{\tilde{I}}^{(U)}(t,u)$ and $\tilde{R}_{\tilde{I}}(t,u) = \tilde{R}_{\tilde{I}}^{(U)}(t,u) = 0$ from (B.10) are substituted into the integral equation of (D.3). With some simplifications, this leads to the modified NWMF solution

$$\begin{aligned}\tilde{f}(t) &= \tilde{a}_0^*(t) - \frac{\gamma}{N_o}\sum_{j=1}^{N_U}\lambda_j' f_j^{(U)}\phi_j^*(t)\\ &\quad -\frac{2P_0}{N_o}\left[\sum_{n=-M}^{-1} f_n^{(U,\zeta)}\tilde{q}^*(t-nT_c) + \sum_{m=N}^{N+M-2} f_n^{(U,\zeta)}\tilde{q}^*(t-nT_c)\right]\end{aligned} \tag{D.6}$$

where $0 \leq t \leq T_b$. The term $f_j^{(U)}$ has been defined in (3.18) whereas

$$f_n^{(U,\zeta)} = \mathcal{R}e\left[\int_0^{T_b} \tilde{q}^*(t - nT_c)\tilde{f}(u)du\right] \quad \text{(D.7)}$$

which is real. This follows since the ISI is completely in-phase with the desired signal which also explains why the factor of 2 appears in front of the P_0 term for the ISI component in (D.6). Basically, the ISI can be interpreted as an in-phase, chip-synchronous, equal-powered interferer whose signal portion associated with the bit modulated chip symbols $b_{\lfloor n/N \rfloor}^{(0)} a_n^{(0)}$ from $n \in [0, N-1]$ are removed. The MF assumes an impulse response which now balances the suppression of ISI in addition to the MAI and AWGN.

D.3 Chip-delay Locked Interferers and ISI

The CLMF solution which takes ISI into account can be derived in the same fashion as the NWMF discussed in the previous section. This is because the two ISI autocorrelation functions in the chip-delay locked case are identical to those of the unlocked case in (D.4) and (D.5). For clarity in presentation, the pseudo-autocorrelation function is dropped by assuming $\tilde{R}_{\tilde{I}}(t, u) = \tilde{R}_{\tilde{I}}^{(C)}(t, u) = 0$. The derivation which follows can be readily repeated with the MAI pseudo-autocorrelation function re-instated. The substitution of (3.26), (3.29), (D.4), (D.5) and $R_{\tilde{I}}(t, u) = R_{\tilde{I}}^{(U)}(t, u)$ into the integral equation of (D.3) yields with some simplifications the modified CLMF solution

$$\begin{aligned} \hat{f}(t) &= \tilde{a}_0^*(t) - \sum_{k=1}^{K} \frac{P_k}{N_o} \sum_{n=-M}^{N+M-2} f_{k,n}^{(C)} \tilde{q}^*(t - T_k - nT_c) \\ &\quad - \frac{2P_0}{N_o}\left[\sum_{n=-M}^{-1} f_n^{(C,\zeta)} \tilde{q}^*(t - nT_c) + \sum_{m=N}^{N+M-2} f_n^{(C,\zeta)} \tilde{q}^*(t - nT_c)\right] \end{aligned} \quad \text{(D.8)}$$

for $0 \leq t \leq T_b$. The coefficient $f_{k,m}^{(C)}$ has been defined in (3.31) whereas

$$f_n^{(C,\zeta)} = \mathcal{R}e\left[\int_0^{T_b} \tilde{q}(t - nT_c)\tilde{f}(u)du\right]. \quad \text{(D.9)}$$

D.4 Bit-delay Locked Interferers and ISI

When the interferers are bit-delay locked, the two ISI autocorrelation functions can be written as, for $m \in [-M_1, M_2]$,

$$R_{\zeta}^{(B)}(t,u) = 2P_0 \sum_{m \neq 0} \tilde{a}^{(0)}(t - mT_c)\tilde{a}^{(0)*}(u - mT_c) \tag{D.10}$$

and

$$\tilde{R}_{\zeta}^{(B)}(t,u) = 2P_0 \sum_{m \neq 0} \tilde{a}^{(0)}(t - mT_b)\tilde{a}^{(0)}(u - mT_b) \tag{D.11}$$

where $0 \leq t, u \leq T_b$. The substitution of (3.37), (D.10), (D.11) and $R_{\tilde{I}}(t,u) = R_{\tilde{I}}^{(B)}(t,u)$ into the integral equation of (D.3) yields, with some simplifications, the modified BLMF solution

$$\begin{aligned} \hat{f}(t) = {} & \tilde{a}_0^*(t) - \frac{1}{N_o}\sum_{k=1}^{K} P_k \sum_{m=-M_1}^{M_2} f_{k,m}^{(B)}\tilde{a}^{(k)*}(t - \tau_k - mT_b) \\ & - \frac{2P_0}{N_o}\sum_{m \neq 0} f_m^{(B,\zeta)}\tilde{a}^{(0)*}(t - mT_b) \end{aligned} \tag{D.12}$$

where $0 \leq t \leq T_b$. The coefficient $f_{k,m}^{(B)}$ has been defined in (3.39) whereas

$$f_m^{(B,\zeta)} = \mathcal{R}e\left[\int_0^{T_b} \tilde{a}^{(0)}(u - mT_b)\hat{f}(u)du\right]. \tag{D.13}$$

This solution removes the ISI from the signal portion associated with bit symbols for $b_m^{(0)}$ where $m \neq 0$.

In summary, when taking the ISI into account, the form of the MF solutions is slightly modified since there are now three sources of noise: the ISI, MAI and AWGN. The MF assumes an impulse response which balances its rejection of ISI, MAI and AWGN.

Appendix E

Derivation of the MAI Covariance Matrix $\mathrm{E}[\vec{I}\vec{I}^{\mathrm{H}}]$

E.1 $\mathrm{E}[\vec{I}\vec{I}^{\mathrm{H}}]$ for Unlocked Interferers

From (2.10) and (2.6), the signal space representation of $\tilde{I}(t)$ can be expressed as $\vec{I} = \sum_{k=1}^{K} \sqrt{2P_k} e^{j\theta_k} \sum_{n=-\infty}^{\infty} b_{\lfloor n/N \rfloor}^{(k)} a_n^{(k)} \vec{q}_{k,n}$. Its substitution into $\mathrm{E}[\vec{I}\vec{I}^{\mathrm{H}} \mid \{T_k\}_{k=1}^{K}]$ leads to $\mathrm{E}[\vec{I}\vec{I}^{\mathrm{H}} \mid \{T_k\}_{k=1}^{K}] = \sum_{k=1}^{K} 2P_k \sum_{n=-\infty}^{\infty} \vec{q}_{k,n}\vec{q}_{k,n}^{\mathrm{H}}$ since $\mathrm{E}[a_n^{(k)} a_m^{(i)*}] = \delta_{ki}\delta_{nm}$. Examining the l,mth component of $\mathrm{E}[\vec{I}\vec{I}^{\mathrm{H}}] = \left(\frac{1}{T_c}\right)^{K} \int_0^{T_c} \cdots \int_0^{T_c} \mathrm{E}[\vec{I}\vec{I}^{\mathrm{H}} \mid \{T_k\}_{k=1}^{K}]\, dT_1 \ldots dT_K$,

$$
\begin{aligned}
\left\{ \mathrm{E}[\vec{I}\vec{I}^{\mathrm{H}}] \right\}_{l,m} &= \sum_{k=1}^{K} 2P_k \sum_{n=-\infty}^{\infty} \int_0^{T_c} \left[\int_0^{T_b} \tilde{q}(t - T_k - nT_c)\psi_l(t)dt \right. \\
&\qquad \left. \int_0^{T_b} \tilde{q}^*(u - T_k - nT_c)\psi_m^*(u)du \right] dT_k \\
&= \int_0^{T_b} \int_0^{T_b} \psi_l(t)\psi_m^*(u) \left[\sum_{k=1}^{K} 2P_k \int_{-\infty}^{\infty} \tilde{q}(t-u+y)\tilde{q}^*(y)dy \right] dtdu
\end{aligned}
\tag{E.1}
$$

where $\{\psi_l(t)\}$ represents an arbitrary complete orthonormal set of functions in $L_2[0, T_b]$. Using (3.9) and (3.11), (E.1) becomes $\{ \mathrm{E}[\vec{I}\vec{I}^{\mathrm{H}}] \}_{l,m} = \int_0^{T_b} \int_0^{T_b} \psi_l(t)\psi_m^*(u) R_{\tilde{I}}^{(U)}(t,u)dtdu$. Substitution of (3.16) yields $\{ \mathrm{E}[\vec{I}\vec{I}^{\mathrm{H}}] \}_{l,m} = 2\gamma \sum_{i=1}^{N_U} \lambda_i' \int_0^{T_b} \int_0^{T_b} \psi_l(t)\psi_m^*(u)\phi_i(t)\phi_i^*(u)\, dtdu = 2\gamma \sum_{i=1}^{N_U} \lambda_i' [\vec{\phi}_i]_l\, [\vec{\phi}_i]_m^*$ and

$$
\mathrm{E}[\vec{I}\vec{I}^{\mathrm{H}}] = 2\gamma \sum_{i=1}^{N_U} \lambda_i' \vec{\phi}_i \vec{\phi}_i^{\mathrm{H}}. \tag{E.2}
$$

E.2 $\mathrm{E}[\vec{I}\vec{I}^{\mathrm{H}}]$ for Chip-delay Locked Interferers

From (2.10) and (2.6), the signal space representation of $\tilde{I}(t)$ can be expressed as $\vec{I} = \sum_{k=1}^{K} \sqrt{2P_k} e^{j\theta_k} \sum_{n=-M}^{N+M-2} b_{\lfloor n/N \rfloor}^{(k)} a_n^{(k)} \vec{q}_{k,n}$. Its substitution into $\mathrm{E}[\vec{I}\vec{I}^{\mathrm{H}}]$ leads to $\mathrm{E}[\vec{I}\vec{I}^{\mathrm{H}}] = \sum_{k=1}^{K} \sum_{i=1}^{K} \sqrt{2P_k}\sqrt{2P_i} \mathrm{E}[e^{j(\theta_k-\theta_i)}] \sum_{n=-M}^{N+M-2} \sum_{l=-M}^{N+M-2} \mathrm{E}[b_{\lfloor n/N \rfloor}^{(k)} b_{\lfloor l/N \rfloor}^{(i)*}] \mathrm{E}[a_n^{(k)} a_l^{(i)*}] \vec{q}_{k,n} \vec{q}_{i,l}^{\mathrm{H}}$. Since $\mathrm{E}[a_n^{(k)} a_m^{(i)*}] = \delta_{ki}\delta_{nm}$, hence,

$$\mathrm{E}[\vec{I}\vec{I}^{\mathrm{H}}] = \sum_{k=1}^{K} 2P_k \sum_{n=-M}^{N+M-2} \vec{q}_{k,n}\vec{q}_{k,n}^{\mathrm{H}}. \tag{E.3}$$

E.3 $\mathrm{E}[\vec{I}\vec{I}^{\mathrm{H}}]$ for Bit-delay Locked Interferers

From (2.10) and (2.7), the signal space representation of $\tilde{I}(t)$ can be expressed as $\vec{I} = \sum_{k=1}^{K} \sqrt{2P_k} e^{j\theta_k} \sum_{m=M_1}^{M_2} b_m^{(k)} \vec{a}_{k,m}$. Its substitution into $\mathrm{E}[\vec{I}\vec{I}^{\mathrm{H}}]$ leads to $\mathrm{E}[\vec{I}\vec{I}^{\mathrm{H}}] = \sum_{k=1}^{K} \sum_{i=1}^{K} \sqrt{2P_k}\sqrt{2P_i} \mathrm{E}[e^{j(\theta_k-\theta_i)}] \sum_{m=M_1}^{M_2} \sum_{l=M_1}^{M_2} \mathrm{E}[b_m^{(k)} b_l^{(i)*}] \vec{a}_{k,m} \vec{a}_{i,l}^{\mathrm{H}}$. Since $\mathrm{E}[b_m^{(k)} b_l^{(i)*}] = \delta_{ki}\delta_{ml}$, hence,

$$\mathrm{E}[\vec{I}\vec{I}^{\mathrm{H}}] = \sum_{k=1}^{K} 2P_k \sum_{m=M_1}^{M_2} \vec{a}_{k,m}\vec{a}_{k,m}^{\mathrm{H}}. \tag{E.4}$$

Appendix F

Derivation of the PSD and CSD of the MAI

The expressions for the power spectral density (PSD) of the unlocked MAI, the cross spectral density (CSD) of the chip-delay locked MAI and the CSD of the bit-delay locked MAI are derived.

F.1 PSD of the Unlocked MAI

The expression of the PSD for unlocked MAI can be obtained by taking the Fourier transform of $R_{\tilde{I}}^{(U)}(\tau)$ in (3.9) where $\tau = t - u$. This yields

$$\begin{aligned} S_{\tilde{I}}^{(U)}(f) &= \frac{2\gamma}{T_c}\int_{-\infty}^{\infty}\tilde{q}^*(y)\int_{-\infty}^{\infty}\tilde{q}(y+\tau)e^{-j2\pi f\tau}d\tau dy \\ &= \frac{2\gamma}{T_c}Q(f)\int_{-\infty}^{\infty}\tilde{q}^*(y)e^{j2\pi fy}dy \\ &= \frac{2\gamma}{T_c}Q(f)Q^*(f). \end{aligned} \tag{F.1}$$

F.2 CSD of WSCS MAI

The CSD $R_{nm}^{(\tilde{I})}(f)$ is the Fourier transform of $r_{nm}^{(\tilde{I})}(t-u)$ as described in (4.8). Consequently, the first step in the derivation of the CSD requires the derivation of $r_{nm}^{(\tilde{I})}(t-u)$ defined in (4.7). Based on the HSR of signals explained in section 4.1.3 and $\tilde{I}(t)$ from (2.10),

$$r_{nm}^{(\tilde{I})}(t-u) = \sum_{k=1}^{K} r_{nm}^{(\tilde{s}^{(k)})}(t-u) \tag{F.2}$$

where

$$r_{nm}^{(\tilde{s}^{(k)})}(t-u) = \mathrm{E}\left[\tilde{s}_n^{(k)}(t)\tilde{s}_m^{(k)*}(u)\right]. \tag{F.3}$$

The $\tilde{s}_n^{(k)}(t)$ is the nth HSR component of $\tilde{s}^{(k)}(t)$. Its Fourier transform is $S_n^{(k)}(f) = V(f)S^{(k)}(f+\frac{n}{T})$ where $S^{(k)}(f) = \mathcal{F}\{\tilde{s}^{(k)}(t)\}$. Using these relationships and the inverse Fourier transform, (F.3) can be expressed as

$$r_{nm}^{(\tilde{s}^{(k)})}(t-u) = \int_{-\infty}^{\infty}\int_{-\infty}^{\infty} \mathrm{E}\left[S_n^{(k)}(f)S_m^{(k)*}(\lambda)\right] e^{j2\pi(ft-\lambda u)} df\, d\lambda. \tag{F.4}$$

The next step requires deriving

$$\mathrm{E}\left[S_n^{(k)}(f)S_m^{(k)*}(\lambda)\right] \tag{F.5}$$

inside (F.4). Its expression depends on the method of spreading which can be either short sequence spreading associated with chip-delay locked MAI or long sequence spreading associated with bit-delay locked MAI. Once the expression for (F.5) is obtained, it is inserted into (F.4) to obtain $r_{nm}^{(\tilde{s}^{(k)})}(t-u)$. Taking the Fourier transform of (F.2) yields the CSD of the MAI

$$R_{nm}^{(\tilde{I})}(f) = \sum_{k=1}^{K} R_{nm}^{(\tilde{s}^{(k)})}(f) \tag{F.6}$$

in terms of the CSD of the kth interferer's signal $R_{nm}^{(\tilde{s}^{(k)})}(f)$ which is the Fourier transform of $r_{nm}^{(\tilde{s}^{(k)})}(t-u)$. The CSD for chip-delay locked MAI is derived in section F.2.1 while the CSD for bit-delay locked MAI is derived in section F.2.2.

F.2.1 CSD of the Chip-Delay Locked MAI

In order to evaluate $\mathrm{E}\left[S_n^{(k)}(f)S_m^{(k)*}(\lambda)\right]$ in (F.5), the expression for $S_n^{(k)}(f)$ is needed for the chip-delay locked case. Using (2.6) and $S_n^{(k)}(f) = V(f)S^{(k)}(f+\frac{n}{T_c})$,

$$S_n^{(k)}(f) = \sqrt{2P_k}e^{j\theta_k}Q_n(f)e^{-j2\pi(f+\frac{n}{T_c})T_k}\sum_{p=-\infty}^{\infty} b_{\lfloor p/N\rfloor}^{(k)}a_p^{(k)}e^{-j2\pi fpT_c} \tag{F.7}$$

where $Q_n(f)$ is given by (4.15). Substitution of (F.7) into (F.5) results in

$$\mathrm{E}\left[S_n^{(k)}(f)S_m^{(k)*}(\lambda)\right] = \frac{2P_k}{T_c}Q_n(f)Q_m^*(f)e^{-j2\pi(f+\frac{n}{T_c})T_k}e^{j2\pi(\lambda+\frac{m}{T_c})T_k}\sum_{p=-\infty}^{\infty}\delta(\lambda-f-\frac{p}{T_c}).$$

(F.8)

Substitution of (F.8) into (F.4) leads to

$$r_{nm}^{(\tilde{s}^{(k)})}(t-u) = \frac{2P_k}{T_c} e^{-j2\pi(n-m)T_k/T_c} \int_{-\infty}^{\infty} Q_n(f) Q_m^*(f) e^{j2\pi f(t-u)}\, df. \quad \text{(F.9)}$$

Taking the Fourier transform of (F.9) returns the CSD of the kth interferer's signal

$$R_{nm}^{(\tilde{s}^{(k)})}(f) = \frac{2P_k}{T_c} e^{-j2\pi(n-m)T_k/T_c} Q_n(f) Q_m^*(f). \quad \text{(F.10)}$$

Substituting (F.10) into (F.6) yields the desired result

$$R_{nm}^{(\tilde{I})}(f) = \sum_{k=1}^{K} \frac{2P_k}{T_c} e^{-j2\pi(n-m)T_k/T_c} Q_n(f) Q_m^*(f) \quad \text{(F.11)}$$

which when re-arranged returns (4.35).

F.2.2 CSD of the Bit-Delay Locked MAI

The method of deriving the CSD for the bit-delay locked MAI closely follows that of the previous section for chip-delay locked MAI. In order to evaluate $\mathrm{E}\left[S_n^{(k)}(f) S_m^{(k)*}(\lambda)\right]$ in (F.5), the expression for $S_n^{(k)}(f)$ is needed for the bit-delay locked case. Using (2.7) and $S_n^{(k)}(f) = V(f) S^{(k)}(f + \frac{n}{T_b})$,

$$S_n^{(k)}(f) = \sqrt{2P_k} e^{j\theta_k} A_n^{(k)}(f) e^{-j2\pi(f+\frac{n}{T_b})\tau_k} \sum_{p=-\infty}^{\infty} b_p^{(k)} e^{-j2\pi f p T_b} \quad \text{(F.12)}$$

where $A_n^{(k)}(f)$ is given by (4.11). Substitution of (F.12) into (F.5) results in

$$\mathrm{E}\left[S_n^{(k)}(f) S_m^{(k)*}(\lambda)\right] = \frac{2P_k}{T_b} A_n^{(k)}(f) A_m^{(k)*}(f) e^{-j2\pi(f+\frac{n}{T_b})\tau_k} e^{j2\pi(\lambda+\frac{m}{T_b})\tau_k} \sum_{p=-\infty}^{\infty} \delta(\lambda - f - \frac{p}{T_b}). \quad \text{(F.13)}$$

Substitution of (F.13) into (F.4) leads to

$$r_{nm}^{(\tilde{s}^{(k)})}(t-u) = \frac{2P_k}{T_b} e^{-j2\pi(n-m)\tau_k/T_b} \int_{-\infty}^{\infty} A_n^{(k)}(f) A_m^{(k)*}(f) e^{j2\pi f(t-u)}\, df. \quad \text{(F.14)}$$

Taking the Fourier transform of (F.14) returns the CSD of the kth interferer's signal

$$R_{nm}^{(\tilde{s}^{(k)})}(f) = \frac{2P_k}{T_b} e^{-j2\pi(n-m)\tau_k/T_b} A_n^{(k)}(f) A_m^{(k)*}(f). \tag{F.15}$$

Substitution of (4.14) and (F.15) into (F.6) yields the desired result

$$R_{nm}^{(\tilde{I})}(f) = \sum_{k=1}^{K} \frac{2P_k}{T_b} e^{-j2\pi(n-m)\tau_k/T_b} Q_n(f) Q_m^*(f) \mathcal{A}^{(k)}(e^{j2\pi(f+\frac{n}{T_b})T_c}) \mathcal{A}^{(k)*}(e^{j2\pi(f+\frac{m}{T_b})T_c}) \tag{F.16}$$

which when re-arranged returns (4.46).

Appendix G

Complexity in Computing the SNR Maximizing Chip Filter

The computational complexity in computing the SNR maximizing chip filter $G^{(C)}(f)$ and its impulse response $\tilde{g}^{(C)}(t)$ is analyzed. The impulse response is computed by sampling $G^{(C)}(f)$ in the frequency domain and evaluating its inverse discrete Fourier transform (DFT) to obtain a sampled version of $\tilde{g}^{(C)}(t)$. First, $\mathbf{G}^{(C)}(f)$ where $f \in [-B, B]$ must be solved to obtain the HSR components $G_n^{(C)}(f)$ for $n \in [-M_H, M_H]$ which form the frequency response $G^{(C)}(f) = \sum_{n=-M_H}^{M_H} G_n^{(C)}(f - \frac{n}{T_c})$. The $G^{(C)}(f)$ can be obtained by solving for $\mathbf{G}^{(C)}(f)$ in (4.42) at the samples $f = f_i$ where $f_i = i\,\Delta f$ where $i = \left[-\left\lfloor\frac{B}{\Delta f}\right\rfloor, \left\lfloor\frac{B}{\Delta f}\right\rfloor\right]$ and $\Delta f \geq 1/T_g$ where $f \in [-B, B]$. When the frequency spacing is set to its minimum $\Delta f = 1/T_g$, the total number of samples required to represent the impulse response with bandwidth B and time duration T_g is approximately $N_g = \lceil 2BT_g \rceil$. As shown in section G.1, $\tilde{g}^{(C)}(t)$ exists over $t \in [(-3M+2)T_c, (3M-1)T_c]$ such that its time duration is $T_g = 3(2M-1)T_c$ where M is described in (3.28).

The next step involves obtaining $\mathbf{G}^{(C)}(f_i)$ by solving the set of $L_H = 2M_H + 1$ linear equations $\mathbf{R}(f_i)\mathbf{G}^{(C)}(f_i) = \mathbf{Q}(f_i)\,\mathbf{u}$ obtained by re-arranging (4.42). The right hand side, $\mathbf{Q}(f_i)\,\mathbf{u}$, can be pre-computed and saved in advance. The computation of $\mathbf{R}(f_i)$ requires evaluating (4.38). The only part of the expression, affected by changing chip delays or signal powers, is $\mathbf{P}_g = \sum_{k=1}^{K} \mathbf{P}_k^{(C)} \mathbf{P}_k^{(C)^{\mathrm{H}}}$ which is independent of f_i. As shown in (4.35), $[\mathbf{P}_g]_{nm} = \sum_{k=1}^{K} 2P_k e^{-j2\pi(n-m)T_k/T_c}$ which requires roughly K multiplications and K summations. Moreover, due to the structure of $\mathbf{P}_g$, only the elements of one row need to be computed to determine the elements of the remaining rows. Consequently, $2KL_H$ operations are required to obtain $\mathbf{P}_g$. And since $\mathbf{I}_{L_H}$ and

$\mathbf{Q}(f_i)$ are diagonal matrices, $\mathbf{R}(f_i)$ for all i requires $KL_H + 2L_H^2 N_g$ multiplications and $KL_H + L_H N_g$ additions.

To solve for L_H linear equations with L_H unknowns in $\mathbf{G}^{(C)}(f_i)$ for all i requires $N_g\left(\frac{L_H^3}{3} + L_H^2 - \frac{L_H}{3}\right)$ multiplications and $N_g\left(\frac{L_H(L_H-1)(2L_H+5)}{6}\right)$ additions [63, p. 514]. Approximations for large L_H are not used since L_H tends to be small for bandwidth efficient chip pulses. Thus, the samples $G^{(C)}(f_i)$ for all i are obtained at a cost of roughly $KL_H + N_g\left(\frac{L_H^3}{3} + 2L_H^2 - \frac{L_H}{3}\right)$ multiplications and $KL_H + N_g\left(L_H + \frac{L_H(L_H-1)(2L_H+5)}{6}\right)$ additions. An example is given for the square root raised cosine pulse (Sqrt-RC), defined in (H.1), with $\alpha = 100\%$. In this case, $M_H = 1$, $L_H = 3$. $M = 3$ (to ensure 99.99% of the energy is contained in the truncated pulse). $T_g = 15T_c$ and $N_g = 2 \cdot [(1+\alpha)/(2T_c)] \cdot T_g = 32$. Consequently, $3K + 1408$ multiplications and $3K + 448$ additions are required to compute $\mathbf{G}^{(C)}(f_i)$ for all i.

The final step requires an inverse DFT operation which can be performed using the Fast Fourier Transform (FFT) requiring roughly another $\frac{N_g}{2}\log_2 N_g$ multiplications and $N_g \log_2 N_g$ additions [127, p. 717]. For the Sqrt-RC 100% pulse, since $N_g = 2^5$, the FFT requires 80 multiplications and 160 additions.

In summary, the computation of the sampled impulse response $g^{(C)}(t)$ requires

$$KL_H + N_g\left(\frac{L_H^3}{3} + 2L_H^2 - \frac{L_H}{3}\right) + \frac{N_g}{2}\log_2 N_g \text{ multiplications,} \tag{G.1}$$

$$KL_H + N_g\left(L_H + \frac{L_H(L_H-1)(2L_H+5)}{6}\right) + N_g \log_2 N_g \text{ additions.} \tag{G.2}$$

Consequently, the Sqrt-RC 100% pulse would roughly require a total of $3K + 1488$ multiplications and $3K + 608$ additions.

G.1 Time Duration of the SNR Maximizing Chip Filter Impulse Response

The time duration of the SNR maximizing chip filter impulse response $g^{(C)}(t)$ is evaluated. By letting $\tau = u - t$, $R_{\tilde{I}}^{(C)}(t,u)$ in (3.26) can be re-written as $R_{\tilde{I}}^{(C)}(t, t+\tau) = \sum_{k=1}^{K} 2P_k \sum_{n=-\infty}^{\infty} \tilde{q}(t - T_k - nT_c)\tilde{q}^*(t + \tau - T_k - nT_c)$. In this form, it can be seen that, for $\tilde{q}(t)$ as defined in (3.28), $R_{\tilde{I}}^{(C)}(t, t+\tau) = 0$ for $|\tau| \geq (2M-1)T_c$. This implies that, for a given t, when $|t-u| \geq (2M-1)T_c$, $R_{\tilde{I}}^{(C)}(t,u) = 0$. Next, by examining the integral equation in (4.45), since $\tilde{q}(t)$ exists over $t \in [-(M-1)T_c, MT_c]$, as defined in (3.28), therefore, the solution $\tilde{g}^{(C)}(t)$ exists over $t \in [(-3M+2)T_c, (3M-1)T_c]$. This indicates that noise outside this interval is uncorrelated with noise inside the interval. Hence, the time duration of $\tilde{g}^{(C)}(t)$ is $T_g = 3(2M - 1)T_c$. Furthermore, since the time duration of $\tilde{q}(t)$ is $(2M - 1)T_c$, T_g is three times larger than the duration of $\tilde{q}(t)$.

Appendix H

Chip Waveforms

H.1 Power Spectral Density of the Rectangular Pulse

The power spectral density (PSD) of the rectangular pulse defined in (3.7) is $\frac{1}{T}|Q(f)|^2 = T\text{sinc}^2(fT)$ [128, pp. 260–261]. A plot of the normalized PSD is given in in Fig. H.1. Based on a −40 dB rule, the bandwidth of the rectangular pulse is $B = 32.5/T$.

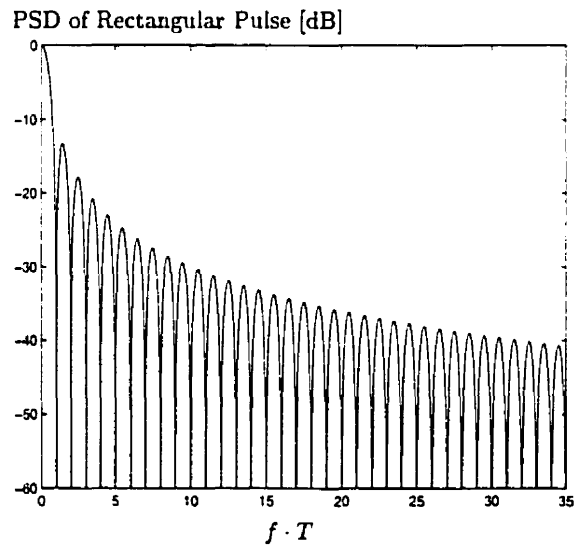

Fig. H.1 The normalized PSD of the rectangular pulse of width T. Using a −40 dB rule, bandwidth is $B = 32.5/T$.

H.2 Square-Root Raised Cosine Pulse

The expression of the sqrt-RC pulse in the time-domain is given in [18, (6.105) p. 228] and reproduced here for reference

$$\tilde{q}(t) = \frac{4\alpha}{\pi\sqrt{T}} \cdot \frac{\cos\left(\frac{(1+\alpha)\pi t}{T}\right) + T \cdot \sin\left(\frac{(1-\alpha)\pi t}{T}\right)/4\alpha t}{1-\left(\frac{4\alpha t}{T}\right)^2} \tag{H.1}$$

where T and α represent, respectively, the symbol period set to $T = T_c$ and excess bandwidth (or roll-off factor) which satisfies $0 \leq \alpha \leq 100\%$.

H.3 Power Spectral Density of the IS-95 System Chip Filter

The power spectral density (PSD) of the chip waveform used in the IS-95 system is given in Fig. H.2. The chip waveform is given by the impulse response of the chip

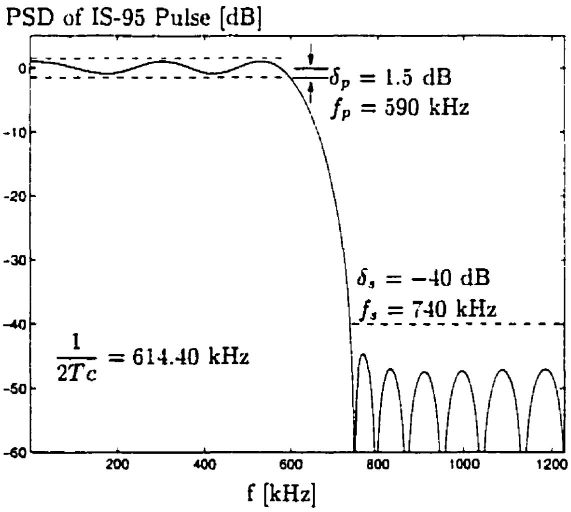

Fig. H.2 Power Spectral Density (PSD) of the chip waveform defined in the IS-95 standard [1, Section 6.1.3.1.10 on pp. 6-28 to 6-30]. Excess bandwidth is $\alpha = 20.44\%$ using a −40 dB rule.

filter defined in the IS-95 standard [1, Section 6.1.3.1.10 on pp. 6-28 to 6-30]. The filter specifications δ_p, f_p, δ_s and f_s as shown in Fig. H.2 represent, respectively, the ripple in the passband, passband edge frequency, attenuation in the stopband and stopband edge frequency [127, p. 593]. By re-arranging (2.4), the excess bandwidth can be expressed as $\alpha = 2BT_c - 1$. Since $\frac{1}{2T_c} = 614.4$ kHz and $B = f_s = 740$ kHz based on the −40 dB rule for bandwidth, the excess bandwidth of the IS-95 pulse is $\alpha = 20.44\%$.

Appendix I

Analysis of Near-far Resistance for the NWMF

The near-far resistance of the NWMF is analyzed by evaluating the asymptotic efficiency of the NWMF in (5.12) and (5.11) by deriving D, $\rho_{k,m}(\tau_k)$ and $\sqrt{E_h}$. For clarity and insight, the following analysis is based on the NWMF obtained over the infinite observation interval. Since the performance of the NWMF can only improve with the extension of the observation interval [93, p. 121], the following results represent upper limits to the near-far resistance achievable by the NWMF derived over the finite observation interval.

First, the desired component D is evaluated by extending the interval $t \in [0, T_b]$ to $t \in (-\infty, \infty)$ in (5.9). This gives $D = \mathcal{R}e\left[\int_{-\infty}^{\infty} \tilde{a}^{(0)}(t)\tilde{h}(T_b - t)dt\right]$. By writing $\tilde{a}^{(0)}(t)$ and $\tilde{h}(T_b - t)$ in terms of their corresponding Fourier transforms, $D = \mathcal{R}e\left[\int_{-\infty}^{\infty} A^{(0)}(f)H(f)e^{j2\pi fT_b}df\right]$. Assuming that the inverse chip filter $1/Q(f)$ exists over $f \in [-B, B]$ where the bandwidth B of the chip filter $Q(f)$ is given by (2.4), substitution of (4.12) and (4.34) into D yields $D = \int_{-B}^{B} |\mathcal{A}^{(0)}(e^{j2\pi fT_c})|^2 df$. Using (4.13), $D = \sum_{p=0}^{N-1}\sum_{q=0}^{N-1} a_p^{(0)}a_q^{(0)*} \int_{-B}^{B} e^{-j2\pi f(p-q)T_c}df$. Since $\int_{-B}^{B} e^{-j2\pi ft}df = 2B\,\mathrm{sinc}(2Bt)$,

$$D \;=\; 2B\sum_{p=0}^{N-1}\sum_{q=0}^{N-1} a_p^{(0)}a_q^{(0)*}\,\mathrm{sinc}\left[2B(p-q)T_c\right]. \qquad \text{(I.1)}$$

A peculiar feature of (I.1) is that, in the limit as $B \to \infty$, $D \to \sum_{p=0}^{N-1} |a_p^{(0)}|^2\,\delta(0) = N\,\delta(0)$. Such a result is not possible in practice since it implies infinite energy in D. Furthermore, as noted in [113], an inverse filter over $f \in (-\infty, \infty)$ is, in general, physically unrealizable.

Next, $\rho_{k,m}(\tau_k)$ is evaluated by extending the interval $t \in [0, T_b]$ to $t \in (-\infty, \infty)$ in

(5.10). Following the same procedure used to derive D, $\rho_{k,m}(\tau_k) = \mathcal{R}e\Big[\int_{-\infty}^{\infty} \tilde{a}^{(k)}(t-\tau_k-mT_b)\tilde{h}(T_b-t)dt\Big] = \mathcal{R}e\Big[\int_{-\infty}^{\infty} A^{(k)}(f)e^{-j2\pi f(\tau_k+mT_b)}H(f)e^{j2\pi fT_b}df\Big] = \mathcal{R}e\Big[\int_{-B}^{B} \mathcal{A}^{(k)}(e^{j2\pi fT_c})\,\mathcal{A}^{(0)*}(e^{j2\pi fT_c})\, e^{-j2\pi f(\tau_k+mT_b)}df\Big] = \sum_{p=0}^{N-1}\sum_{q=0}^{N-1} a_p^{(k)}a_q^{(0)*}\int_{-B}^{B} e^{-j2\pi f[(p-q)T_c+\tau_k+mT_b]}df$. This simplifies to

$$\rho_{k,m}(\tau_k) \;=\; 2B\sum_{p=0}^{N-1}\sum_{q=0}^{N-1} a_p^{(k)}a_q^{(0)*}\,\mathrm{sinc}\left[2B\left((p-q)T_c+\tau_k+mT_b\right)\right]. \qquad \text{(I.2)}$$

In contrast to the D-CLMF and D-BLMF, as $\sigma \rightarrow 0$ for the limiting form of the NWMF, the $\rho_{k,m}(\tau_k)$ in (I.2) is, in general, non-zero for $B < \infty$. The presence of a non-zero $\rho_{k,m}(\tau_k)$ in $\lim_{\sigma\to 0} z_0(\sigma)$ in (5.11) indicates that, although the asymptotic efficiency η_0 in (5.12) may be non-zero, near-far resistance of the NWMF is zero.

A non-zero near-far resistance may theoretically be possible by letting $B \rightarrow \infty$, in (I.2). This leads to $\rho_{k,m}(\tau_k) \rightarrow \sum_{p=0}^{N-1}\sum_{q=0}^{N-1} a_p^{(k)}a_q^{(0)*}\,\delta\left((p-q)T_c+\tau_k+mT_b\right)$. As long as $\left(\,p-q+\frac{\tau_k}{T_c}+mN\,\right)T_c \neq 0$, $\rho_{k,m}(\tau_k) = 0$. This is ensured when the chip delay $\tau_k \neq 0$ since m, p, q are integers. Consequently, if both $Q(f)$ and $1/Q(f)$ did exist over $f \in (-\infty, \infty)$, only then would it be possible for the NWMF to have a non-zero near-far resistance.

Finally, for completeness, E_h is evaluated by extending the interval $t \in [0, T_b]$ to $t \in (-\infty, \infty)$ in (5.8). Following the same procedure used to derive D and $\rho_{k,m}(\tau_k)$, (5.8) can be expressed as $E_h = \int_{-\infty}^{\infty}\left|\tilde{h}(T_b-t)\right|^2 dt = \int_{-\infty}^{\infty}\left|H(f)e^{j2\pi fT_b}\right|^2 df$. Consequently,

$$E_h \;=\; \int_{-B}^{B}\left|\frac{1}{Q(f)}\mathcal{A}^{(0)}(e^{j2\pi fT_c})\right|^2 dt \qquad \text{(I.3)}$$

which is, in general, finite. Even in the limit as $B \rightarrow \infty$ $E_h < \infty$. This follows by noting that the integrand in (I.3) satisfies $\left|\frac{1}{Q(f)}\mathcal{A}^{(0)}(e^{j2\pi fT_c})\right|^2 = \left|\frac{1}{Q(f)}\right|^2\left|\mathcal{A}^{(0)}(e^{j2\pi fT_c})\right|^2 \leq \left|\frac{1}{Q(f)}\right|^2 N^2$. Thus, $E_h \leq N^2\int_{-\infty}^{\infty}\left|\frac{1}{Q(f)}\right|^2 dt < \infty$ for an inverse filter with finite energy.

An interesting result can be obtained if an inverse filter $1/Q(f)$ did exist over $f \in (-\infty, \infty)$ and if $\tau_k \neq 0$. Since, as $B \rightarrow \infty$, E_h remains finite, $D \rightarrow \infty$ and $\rho_{k,m}(\tau_k) \rightarrow 0$, this would imply that $\eta_0 \rightarrow \infty$ in (5.12) is unbounded and that the NWMF achieves the maximum near-far resistance of 1. Note, however, that the asymptotic efficiency must satisfy $0 \leq \eta_0 \leq 1$ [60]. The contradiction arises since the energy of the inverse filter $\int_{-\infty}^{\infty}\left|\frac{1}{Q(f)}\right|^2 dt$, if it did exist, would have to be infinite making E_h no longer finite.

Appendix J

Modifications to the Characteristic Function Expressions for $P_{e,0}$

To compute the bit error rate (BER) $P_{e,0}$ for a receiver using a real MF $\tilde{h}(t)$ in a DS-BPSK system, some modifications to the expressions in [114] are required. The full BER expression for the desired user based on [114] is given by

$$P_{e,0} = Q\left(\sqrt{\frac{1}{\sigma_w^2}}\right) + \frac{1}{\pi}\int_0^\infty \frac{\sin u}{u}\phi_2(u)\left[1-\phi_1(u)\right] du. \tag{J.1}$$

The functions in (J.1) shall now be defined. The Q function is $Q(x) = \int_x^\infty \frac{1}{\sqrt{2\pi}} e^{-y^2/2} dy$. Using (5.8) and (5.9), the normalized thermal noise variance is

$$\sigma_w^2 = \frac{E_h T_b}{2D^2 E_b / N_o} \tag{J.2}$$

where E_h and D are defined in (5.8) (5.9), respectively. The characteristic function of the thermal noise is $\phi_2(u) = \exp\left(-\frac{1}{2}\sigma_w^2 u^2\right)$. The characteristic function of the MAI

$$\phi_1(u) = \prod_{k=1}^{K_C} \phi_{1,k}^{(C)}(u) \prod_{k=K_C+1}^{K_C+K_U} \phi_{1,k}^{(U)}(u) \tag{J.3}$$

is the product of the characteristic function of the locked MAI

$$\begin{aligned}\phi_{1,k}^{(C)}(u) = \frac{1}{4\pi}\int_0^{2\pi} & \cos\left[\frac{u\sqrt{\beta_k}}{D}\cos\theta_k\left(\rho_{k,-1}(\tau_k)+\rho_{k,0}(\tau_k)\right)\right] \\ & +\cos\left[\frac{u\sqrt{\beta_k}}{D}\cos\theta_k\left(\rho_{k,-1}(\tau_k)+\rho_{k,0}(\tau_k)\right)\right] d\theta_k\end{aligned} \tag{J.4}$$

and the characteristic function of the unlocked MAI

$$\begin{aligned}\phi_{1,k}^{(U)}(u) &= \frac{1}{4\pi T_b}\int_0^{2\pi}\int_0^{T_b}\cos\left[\frac{u\sqrt{\beta_k}}{D}\cos\theta_k\left(\rho_{k,-1}(\tau_k)+\rho_{k,0}(\tau_k)\right)\right] \\ &\quad +\cos\left[\frac{u\sqrt{\beta_k}}{D}\cos\theta_k\left(\rho_{k,-1}(\tau_k)+\rho_{k,0}(\tau_k)\right)\right] d\tau_k d\theta_k. \qquad (J.5)\end{aligned}$$

Considerable reduction in computation time can be achieved by pre-calculating and storing the partial correlation functions $\rho_{k,m}(\tau)$, defined in (5.10), at uniformly spaced points over $\tau \in [0, T_b]$.

Appendix K

Computation of Probability of Outage

K.1 Modified Monte Carlo Method for Computing Probability of Outage

The algorithm which applies the Modified Monte Carlo method described in [117] to the computation of probability of outage is outlined. The parameters K, N, E_b/N_o and signal powers $\mathbf{P}$ are assumed to be constant during the computation of the outage probability. The algorithm to be explained can be modified to handle the situation where signal powers can change and need to be biased as well. The two remaining set of parameters to sample consist of the spreading sequence of the desired user $\mathbf{a}^{(0)}$ and the interferers' chip delays in $\mathbf{T}$. The samples of the desired user's spreading sequence are not biased. Only the chip delay samples used to form $\mathbf{T}$ are biased. Thus, the SNR expression in (5.2) summarized in (5.3) reduces to a function of two random vectors $\text{SNR}(\mathbf{a}^{(0)}, \mathbf{T})$. When N_a independent samples of $\mathbf{a}^{(0)}$ and N_T independent samples of $\mathbf{T}$ are substituted into $\text{SNR}(\mathbf{a}^{(0)}, \mathbf{T})$, a total of $N_S = N_a N_T$ independent SNR samples is produced.

The algorithm used to generate the nth SNR sample SNR_n is summarized as follows:

1. Initialize the sample counter for spreading sequences $l = 1$.

2. Generate a random spreading sequence vector $\mathbf{a}_l^{(0)}$ indexed by l.

3. Initialize the sample counter for chip delays $m = 1$.

4. Generate K interferer chip delays $\{T_k^{(m)}\}_{k=1}^{K}$ indexed by m and the chip delay vector
$\mathbf{T}_m = [T_1^{(m)}, T_2^{(m)}, \ldots, T_K^{(m)}]$ by taking K independent samples from a Beta distributed random number generator.

   (a) The Beta distributed random number generator produces independent samples of $T_k^{(m)}/T_c$ with the Beta probability density function (PDF) [129, p. 28]

$$f_{a,b}^{\mathrm{Beta}}(x) = \frac{x^{a-1}(1-x)^{b-1}}{\int_0^1 x^{a-1}(1-x)^{b-1}dx} \tag{K.1}$$

where $x \in [0, 1]$. The two parameters a and b affect the the shape of the Beta PDF. Furthermore, the parameters satisfy $b = a$ and $0 < a \leq 1$ to maintain a symmetrical distribution about $x = 0.5$. The parameter a is the only adjustable parameter. Under this constraint, a parameterizes the Beta PDF. For $0 < a < 1$, the PDF is a curve which is concave upwards with its maximum value at the end points $x = 0, 1$ and its minimum value in the middle at $x = 0.5$. An example of the Beta PDF is given in Fig. K.1 where $a = 0.4$. The probability of selecting an x close to 0 or 1 is much

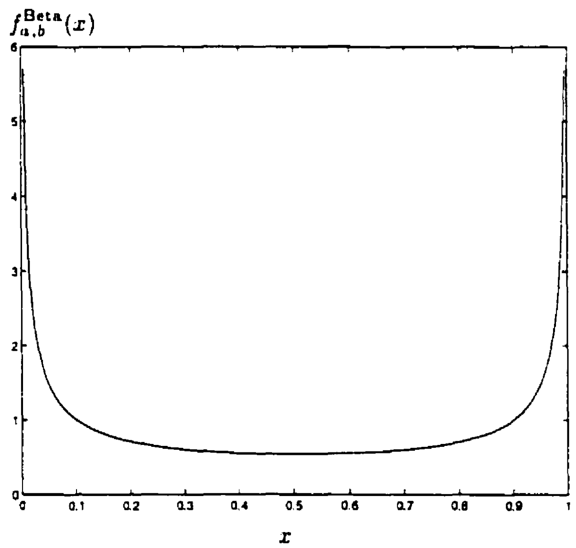

Fig. K.1 The Beta PDF $f_{a,b}^{\mathrm{Beta}}(x)$ where $a = b = 0.4$.

greater than that of selecting an x close to 0.5. By using the relationship $T_k = xT_c$ and the Beta distributed random number generator, the chip delay samples can then be biased towards either 0 or T_c. As $a \to 1$, the

Beta PDF approaches the Uniform PDF of $f^{\text{Unif}}(x) = 1$ for $0 \le x < 1$ and $f^{\text{Unif}}(x) = 0$, otherwise. This is the original distribution of the chip delays. As $a \to 0$, the Beta PDF approaches the two impulse functions $\delta(x)$ and $\delta(x-1)$. That is, as $a \to 0$, the random number generator produces samples which are either very close to 0 or 1. This is precisely what is needed to bias the SNR sample towards its minimum value which occurs in the chip synchronous case when the $T_k/T_c \to 0$ or $T_k/T_c \to 1$. The steps required to construct a Beta distributed random generator are outlined in [129, pp. 427–429].

5. Compute the weighting factor w_n associated with $\mathbf{T}_m$ and $\mathbf{a}_l^{(0)}$ where $n = (l-1)N_a + m$. This is done in the following two steps.

   (a) For each of the K chip delays, calculate the bias factor $B(T_k^{(m)})$ defined as

   $$B_{\text{bias}}(x) = \frac{f_{a,a}^{\text{Beta}}(x)}{f^{\text{Unif}}(x)}. \tag{K.2}$$

   (b) Calculate the weighting factor

   $$w_m = \frac{1}{\prod_{k=1}^{K} B_{\text{bias}}(T_k^{(m)})} \tag{K.3}$$

6. Compute $\text{SNR}_n = \text{SNR}(\mathbf{a}_l^{(0)}, \mathbf{T}_m)$

7. Store both: w_n and SNR_n.

8. If $m < N_T$, increment m by 1 and go to step 4. Otherwise, continue to the next step.

9. If $l < N_a$, increment l by 1 and go to step 2. Otherwise, continue to the next step.

10. At this point, N_S values of w_n and SNR_n have been generated and stored. Compute the unbiased probability of outage

    $$P_{\text{out}} = w_{\text{avg}} \frac{N_{\text{out}}}{N_S} \tag{K.4}$$

    where the number of outage events N_{out} has been defined in (5.17). The average of only those weighting factors associated with outage events is defined as

$$w_{\text{avg}} = \frac{1}{N_{\text{out}}} \sum_{n=1}^{N_S} w_n \, \mathrm{I}_{\text{ind}} \left(\mathrm{SNR}_n - \mathrm{SNR}_{\min} \right) \tag{K.5}$$

where the indicator function $\mathrm{I}_{\text{ind}}(x)$ has been defined in (5.18).

K.2 Method of Computing Confidence Intervals

The steps for computing the confidence interval $[P_{\text{out,low}}, P_{\text{out,upp}}]$ are reproduced here using the procedure outlined in [116, pp. 244 - 248]. Given the confidence coefficient $\gamma_{\text{out}} \in [0, 1)$ and the M_{out} samples of $P_{\text{out,m}}$ where $m \in [1, M_{\text{out}}]$:

1. Compute the mean of the samples $\overline{P}_{\text{out}} = \frac{1}{M_{\text{out}}} \sum_{m=1}^{M_{\text{out}}} P_{\text{out,m}}$.
2. Compute the standard deviation of the samples $\sigma_{\text{out}} = \sqrt{\frac{1}{M_{\text{out}} - 1} \sum_{m=1}^{M_{\text{out}}} (P_{\text{out,m}} - \overline{P}_{\text{out}})^2}$.
3. Set $u = \frac{1 + \gamma_{\text{out}}}{2}$.
4. Convert u to z_u using the conversion table in [116, Table 9-1, p 247] or by using the relation $u = \frac{1}{\sqrt{2\pi}} \int_{-\infty}^{z_u} e^{-z^2/2} dz$. For instance, when $\gamma_{\text{out}} = 99\%$, $u = 0.995$ and $z_u = 2.576$.
5. Compute $P_{\text{out,low}} = \overline{P}_{\text{out}} - z_u \sigma_{\text{out}} / \sqrt{M_{out}}$.
6. Compute $P_{\text{out,upp}} = \overline{P}_{\text{out}} + z_u \sigma_{\text{out}} / \sqrt{M_{out}}$.

Bibliography

[1] TIA/EIA/IS-95, "Mobile station – base station compatability standard for dual-mode wideband spread spectrum cellular system," tech. rep., TIA/EIA, July 1993.

[2] D. V. Sarwate and M. B. Pursley, "Crosscorrelation properties of pseudorandom and related sequences," *Proc. of IEEE*, vol. 68, pp. 593–619, May 1980.

[3] J. E. Padgett, C. G. Gunther, and T. Hattori, "Overview of wireless personal communications," *IEEE Communications Magazine*, vol. 33, pp. 28–41, Jan. 1995.

[4] T. S. Rappaport, *Wireless Communications.* IEEE Press, 1996.

[5] P. G. Flikkema, "Spread-spectrum techniques for wireless communication," *IEEE Signal Processing Magazine*, vol. 14, pp. 26–36, May 1997.

[6] M. K. Simon and *et al.*, *Spread Spectrum Communications, Volumes I-III.* Computer Science Press, 1985.

[7] R. L. Pickholtz, D. L. Schilling, and L. Milstein, "Theory of spread-spectrum communications – a tutorial," *IEEE Trans. Communications*, vol. 30, pp. 129–158, May 1982.

[8] R. C. Dixon, "Why spread spectrum?," *IEEE Communications Magazine*, vol. 13, pp. 21–25, July 1975.

[9] A. J. Viterbi, *CDMA: Principles of Spread Spectrum Communication.* Addison-Wesley Publishing Co., 1995.

[10] R. F. Ziemer and R. L. Peterson, *Digital Communications and Spread Spectrum Sysetms.* MacMillan, 1985.

[11] M. B. Pursley, "Spread-spectrum multiple-access communications," in *Multi-User Communication Systems* (G. Longo, ed.), pp. 139–199, Springer-Verlag, 1981.

[12] W. C. Y. Lee, "Overview of cellular CDMA," *IEEE Trans. Vehicular Tech.*, vol. 40, pp. 291–302, May 1991.

[13] R. Meidan, "To spread or not to spread, this is the question," *Proc. IEEE Vehicular Technology Conf.* (Stockholm, Sweden), pp. 56–59, June 8 – 10, 1994.

[14] A. J. Viterbi, "When not to spread spectrum – a sequel," *IEEE Communications Magazine*, vol. 23, pp. 12–17, Apr. 1985.

[15] K. S. Gilhousen, I. M. Jacobs, R. Padovani, A. J. Viterbi, J. L. A. Weaver, and C. E. W. III, "On the capacity of a cellular CDMA system," *IEEE Trans. Vehicular Tech.*, vol. 40, pp. 303–312, May 1991.

[16] G. L. Turin, "Introduction to spread-spectrum antimultipath techniques and their application to urban digital radio," *Proc. of IEEE*, vol. 68, pp. 328–353, Mar. 1980.

[17] R. Padovani, "Reverse link performance of IS-95 based cellular system," *IEEE Personal Communications Magazine*, vol. 1, pp. 28–34, 3rd quarter 1994.

[18] E. A. Lee and D. G. Messerschmitt, *Digital Communication*. Kluwer Academic Publishers, 2nd ed., 1994.

[19] P. Mermelstein, A. Jalali, and H. Leib, "Integrated services on wireless multiple access networks," *Proc. IEEE Intl. Conf. Communications* (Geneva, Switzerland), pp. 863–867, May 23-26, 1993.

[20] V. K. Paulrajan and J. A. Roberts, "Capacity of a CDMA cellular system with variable user data rates," *Proc. IEEE Globecomm Conf.* (London, U.K.), pp. 1458–1462, Nov. 18 – 22, 1996.

[21] S. Ariyavisitakul and L. F. Chang, "Signal and interference statistics of a CDMA system with feedback power control," *IEEE Trans. Communications*, vol. 41, pp. 1626–1634, Nov. 1993.

[22] C. F. Kou and H. Leib, "Power imbalance effects on packet CDMA," *IEEE J. Select. Areas Communications*, vol. 9, pp. 1830–1840, Dec. 1996.

[23] D. D. Falconer, F. Adachi, and B. Gudmundson, "Time division multiple access methods for wireless personal communications," *IEEE Communications Magazine*, vol. 33, pp. 50–57, Jan. 1995.

[24] V. K. Garg and E. L. Sneed, "Digital wireless local loop system," *IEEE Communications Magazine*, vol. 34, pp. 112–115, Oct. 1996.

[25] B. D. Bollinger, "CDMA fixed wireless application," *Proc. 1st CDMA International Conf.* (Seoul, S. Korea), Nov. 12 – 15, 1996.

[26] N. Sharp, "A CDMA approach to wireless fixed access," *Proc. 1st CDMA International Conf.* (Seoul, S. Korea), Nov. 12 – 15, 1996.

[27] T. Ojanpera, "Overview of research activities for third generation mobile communication," in *Wireless Communication TDMA versus CDMA* (S. G. Glisic and P. A. Leppanen, eds.), pp. 415–446, Kluwer Academic Publishers, 1997.

[28] P.-G. Andermo and L.-M. Ewerbring, "A CDMA-based radio access design for UMTS," *IEEE Personal Communications Magazine*, vol. 2, pp. 48–53, Feb. 1995.

[29] F. Adachi, K. Ohno, A. Higashi, T. Dohi, and Y. Okumura, "Coherent multicode DS-CDMA mobile radio access," *IEICE Trans. Communications*, vol. E79B, pp. 1316–1325, Sept. 1996.

[30] T. Dohi, Y. Okumura, A. Higashi, K. Ohno, and F. Adachi, "Experiments on coherent multicode DS-CDMA," *IEICE Trans. Communications*, vol. E79B, pp. 1326–1332, Sept. 1996.

[31] A. Fukasawa, T. Sato, Y. Takizawa, T. Kato, M. Kawabe, and R. E. Fisher, "Wideband CDMA system for personal radio communications," *IEEE Communications Magazine*, vol. 34, pp. 116–123, Oct. 1996.

[32] K. S. Gilhousen, I. M. Jacobs, R. Padovani, and J. L. A. Weaver, "Increased capacity using CDMA for mobile satellite communication," *IEEE J. Select. Areas Communications*, vol. 8, pp. 503–514, May 1990.

[33] L. P. Seidman, "Satellites for wideband access," *IEEE Communications Magazine*, vol. 34, pp. 108–111, Oct. 1996.

[34] S. G. Glisic, J. . Talvite, T. Kumpumaki, M. Latva-aho, J. H. Iinatti, and T. J. Poutanen, "Design study for a CDMA-based LEO satellite netowrk: Downlink system level parameters," *IEEE J. Select. Areas Communications*, vol. 14, pp. 1796–1808, Dec. 1996.

[35] R. D. Gaudenzi, C. Elia, and R. Viola, "Bandlimited quasi-synchronous CDMA: A novel satellite access technique for mobile and personal communication systems," *IEEE J. Select. Areas Communications*, vol. 10, pp. 328–343, Feb. 1992.

[36] J. S. Thompson, P. M. Grant, and B. Mulgrew, "Performance of antenna array receiver algorithms for CDMA," *Proc. IEEE Globecomm Conf.* (London), pp. 570–574, Nov. 18 - 22, 1996.

[37] Y. C. Yoon and H. Leib, "Matched filters with interference suppression capabilities for DS-CDMA," *IEEE J. Select. Areas Communications*, vol. 14, pp. 1510–1521, Oct. 1996.

[38] Y. C. Yoon and H. Leib, "Maximizing SNR in improper complex noise and applications to CDMA," *IEEE Communication Letters*, vol. 1, pp. 5–8, Jan. 1997.

[39] S. Vembu and A. J. Viterbi, "Two different philosophies in CDMA - a comparison," *Proc. IEEE Vehicular Technology Conf.* (Atlanta, GA, USA), pp. 869–873, Apr. 18 to May 1, 1996.

[40] F. Ling, "Coherent detection with reference-symbol based channel estimation for direct sequence CDMA uplink communications," *Proc. IEEE Vehicular Technology Conf.* (Secaucus, NJ, USA), pp. 400–403, May 18 - 20, 1993.

[41] F. Ling, E. Brucket, and T. A. Sexton, "Analysis of performance and capacity of coherent DS-CDMA reverse link communications," *Proc. IEEE Vehicular Technology Conf.* (Chicago, USA), pp. 912–916, July 25–28, 1995.

[42] G. Brismark, M. Ewerbring, T. Sandin, and P. Teder, "A coherent detection scheme for the uplink channel in a CDMA system,," *Proc. IEEE Vehicular Technology Conf.* (Stockholm, Sweden), pp. 729–732, June 8 - 10, 1994.

[43] K. J. Kim, S. Y. Kwon, S. H. Hwang, C. H. Pak, and K. Whang, "Comparison of coherent and noncoherent CDMA system in time-varying fading channel," *Proc. IEEE Vehicular Technology Conf.* (Atlanta, Georgia, USA), pp. 884–888, April 28 - May 1, 1996.

[44] J. G. Proakis, *Digital Communications.* McGraw-Hill, 3nd ed., 1995.

[45] L. E. Franks, "Synchronization subsystems: Analysis and design," in *Digital Communications Satellite/Earth Station Engineering* (K. Feher, ed.), pp. 294–335, Prentice-Hall, 1981.

[46] J. R. K. Morrow and J. S. Lehnert, "Bit-to-bit error dependence in slotted DS/SSMA packet systems with random signature sequences," *IEEE Trans. Communications*, vol. 37, pp. 1052–1061, Oct. 1989.

[47] F. D. Neeser and J. L. Massey, "Proper complex random processes with applications to information theory," *IEEE Trans. Inform. Theory*, vol. 39, pp. 1293–1302, July 1993.

[48] J. D. Laster and J. H. Reed, "Interference rejection in digital wireless communications," *IEEE Signal Processing Magazine*, vol. 14, pp. 37–62, May 1997.

[49] S. Moshavi, "Multi-user detection for DS-CDMA communications," *IEEE Communications Magazine*, vol. 34, pp. 124–136, Oct. 1996.

[50] A. Duel-Hallen, J. Holtzman, and Z. Zvonar, "Multiuser detection for CDMA systems," *IEEE Personal Communications Magazine*, vol. 2, pp. 46–58, Apr. 1995.

[51] S. Verdu, "Recent progress in multiuser detection," in *Multiple Access Communications* (N. Abramson, ed.), pp. 164–175, IEEE Press, 1993.

[52] S. Verdu, "Minimum probability of error for asynchronous gaussian multiple access channels," *IEEE Trans. Inform. Theory*, vol. 32, pp. 85–96, Jan. 1986.

[53] J. M. Holtzman, "DS/CDMA successive interference cancellation," *Proc. Intl. Symposium on Spread Spectrum Techniques and Applications* (Oulu, Finland), pp. 69–78, Jul. 4 - 6, 1994.

[54] A. J. Viterbi, "Very low rate convolutional codes for maximum theoretical performance of spread-spectrum multiple-access channels," *IEEE J. Select. Areas Communications*, vol. 8, pp. 641–649, May 1990.

[55] D. Divsalar, M. Simon, and D. Raphaeli, "A new approach to parallel interference cancellation for CDMA," *Proc. IEEE Globecomm Conf.* (London), pp. 1452–1457, Nov. 18 - 22, 1996.

[56] M. K. Varanasi and B. Aazhang, "Multistage detection in asynchronous code-division multiple-access communications," *IEEE Trans. Communications*, vol. 38, pp. 509–519, Apr. 1990.

[57] Y. C. Yoon, R. Kohno, and H. Imai, "A spread-spectrum multi-access system with co-channel interference cancellation for multipath fading channels," *IEEE J. Select. Areas Communications*, vol. 11, pp. 1067–1075, Sept. 1993.

[58] A. Duel-Hallen, "A family of multiuser decision-feedback detectors for asynchronous code-division multiple-access channels," *IEEE Trans. Communications*, vol. 43, pp. 421–434, Feb/Mar/Apr 1995.

[59] B. Aazhang, B.-P. Paris, and G. C. Orsak, "Neural networks for multiuser detection in code-division multiple-access communications," *IEEE Trans. Communications*, vol. 40, pp. 1212–1222, July 1992.

[60] R. Lupas and S. Verdu, "Near-far resistance of multiuser detectors in asynchronous channels," *IEEE Trans. Communications*, vol. 38, pp. 496–508, Apr. 1990.

[61] Z. Xie, R. T. Short, and C. T. Rushforth, "A family of suboptimum detectors for coherent multiuser communications," *IEEE J. Select. Areas Communications*, vol. 8, pp. 683–690, May 1990.

[62] U. Madhow and M. L. Honig, "MMSE interference suppression for direct-sequence spread-spectrum CDMA," *IEEE Trans. Communications*, vol. 42, pp. 3178–3188, Dec. 1994.

[63] K. E. Atkinson, *An Introduction to Numerical Analysis*. John Wiley & Sons, 1989.

[64] H. V. Poor and S. Verdu, "Single-user detectors for multiuser channels," *IEEE Trans. Communications*, vol. 36, pp. 50–60, Jan. 1988.

[65] S. Verdu, "Adaptive multiuser detection," *Proc. Intl. Symposium on Spread Spectrum Techniques and Applications* (Oulu, Finland), pp. 43–50, July 4 – 6, 1994.

[66] S. U. H. Qureshi, "Adaptive equalization," *Proc. of IEEE*, vol. 73, pp. 1349–1387, Sept. 1985.

[67] P. B. Rapajic and B. S. Vucetic, "Adaptive receiver structures for asynchronous CDMA systems," *IEEE J. Select. Areas Communications*, vol. 12, pp. 685–697, May 1994.

[68] V. Aue and J. H. Reed, "An interference robust CDMA demodulator that uses sp ectral correlation properties," *Proc. IEEE Vehicular Technology Conf.* (Stockholm, Sweden), pp. 563–567, June 8 – 10, 1994.

[69] S. L. Miller, "An adaptive direct-sequence code-division multiple-access receiver for multiuser interference rejection," *IEEE Trans. Communications*, vol. 43, pp. 1746–1755, Feb/Mar/Apr 1995.

[70] W. A. Gardner and W. A. Brown, "Frequency-shift filtering theory for adaptive co-channel interference removal," *Proc. Asilomar Conf. on Signals, Systems and Computers* (Pacific Grove, California), pp. 562–567, Oct 30 – Nov 1, 1989.

[71] W. A. Gardner, "An introduction to cyclostationary signals," in *Cyclostationarity in Communications and Signal Processing* (W. A. Gardner, ed.), pp. 1–90, IEEE Press, 1994.

[72] J. E. A. Ferrara, "Frequency-domain adaptive filtering," in *Adaptive Filters* (C. F. N. Cowan and P. M. Grant, eds.), pp. 145–179, Prentice-Hall, 1985.

[73] J. R. Treichler, *Theory and Design of Adaptive Filters.* John Wiley & Sons, 1987.

[74] J. H. Reed, N. M. Yuen, and T. C. Hsia, "An optimal receiver using a time-dependent adaptive filter," *IEEE Trans. Communications*, vol. 43, pp. 187–190, Feb/Mar/Apr 1995.

[75] C. D. Greene, J. H. Reed, and T. C. Hsia, "An optimal receiver using a time-dependent adaptive filter," *Proc. IEEE Military Communications Conf.* (Boston, Mass.), pp. 650–656, Oct 15 – 18, 1989.

[76] J. H. Reed, A. A. Quilici, and T. C. Hsia, "A frequency domain time-dependent adaptive filter for interference rejection," *Proc. IEEE Military Communications Conf.* (San Diego, California), pp. 391–397, Oct 23 – 26, 1988.

[77] M. Honig, U. Madhow, and S. Verdu, "Blind adaptive multiuser detection," *IEEE Trans. Inform. Theory*, vol. 41, pp. 944–960, July 1995.

[78] M. K. Tsatsanis, "Inverse filtering criteria for CDMA systems," *IEEE Trans. Acoustics, Speech and Signal Processing*, vol. 45, pp. 102–112, Jan. 1997.

[79] M. Davis, A. M. Monk, and L. B. Milstein, "A noise-whitening approach to multiple access noise rejection – part II: Implementation issues," *IEEE J. Select. Areas Communications*, vol. 14, pp. 1488–1499, Oct. 1996.

[80] R. D. Gitlin, J. F. Hayes, and S. B. Weinstein, *Data Communications Principles.* Plenum Press, 1992.

[81] M. Abdulrahman, A. U. H. Sheikh, and D. D. Falconer, "Decision feedback equalization for CDMA in indoor wireless communications," *IEEE J. Select. Areas Communications*, vol. 12, pp. 698–706, May 1994.

[82] B. R. Petersen and D. D. Falconer, "Minimum mean square equalization in cyclostationary and stationary interference – analysis and subscriber line calculations," *IEEE J. Select. Areas Communications*, vol. 6, pp. 931–940, Aug. 1991.

[83] U. Mitra and H. V. Poor, "Neural network techniques for adaptive multiuser demodulation," *IEEE J. Select. Areas Communications*, vol. 12, pp. 1460–1470, Dec. 1994.

[84] S. Haykin, "Neural networks expand SP's horizons," *IEEE Signal Processing Magazine*, vol. 13, pp. 24–49, Mar. 1996.

[85] B. Mulgrew, "Applying radial basis functions," *IEEE Signal Processing Magazine*, vol. 13, pp. 50–65, Mar. 1996.

[86] A. M. Monk, M. Davis, L. B. Milstein, and C. W. Helstrom, "A noise-whitening approach to multiple access noise rejection – part I: Theory and background," *IEEE J. Select. Areas Communications*, vol. 12, pp. 817–827, June 1994.

[87] Y. Huang and T.-S. Ng, "Performance of coherent receiver with weighted despreading sequence for DS-CDMA," *IEE Electronic Letters*, vol. 33, pp. 23–25, Jan. 1997.

[88] J. Chaib, "Chip shaping and channel coding for CDMA," Master's thesis, McGill University, 1996.

[89] M. Rupf, *Coding for CDMA Channels and Capacity.* PhD thesis, Technische Hochschule, 1994. Hartung-Gorre Verlag Konstanz.

[90] H. L. V. Trees, *Detection, Estimation, and Modulation Theory, Part I.* John Wiley & Sons, 1968.

[91] J. B. Thomas, *Statistical Communication Theory.* John Wiley & Sons, 1969. Chapter 5.

[92] A. D. Whalen, *Detection of Signals in Noise.* Academic Press, 1971. Chapter 6.

[93] C. W. Helstrom, *Statistical Theory of Signal Detection.* Pergamon Press, 2nd ed., 1968. Chapter 4.

[94] A. Ansari and R. Viswanathan, "On SNR as a measure of performance for narrowband interference rejection in direct sequence spread spectrum systems," *IEEE Trans. Communications*, vol. 43, pp. 1318–1322, Feb/Mar/Apr 1995.

[95] L. Franks, *Signal Theory.* Prentice-Hall, 1969.

[96] H. Urkowitz, *Signal Theory and Random Processes.* Artech House, 1983. Chapter 13.

[97] Y. C. Yoon and H. Leib, "Matched filtering in improper complex noise and applications to DS-CDMA," *Proc. IEEE Intl. Symposium on Personal, Indoor and Mobile Radio Communications* (Toronto, Canada), pp. 701–705, Sept. 27–29, 1995.

[98] W. A. Gardner and L. E. Franks, "Characterization of cyclostationary random signal processes," *IEEE Trans. Inform. Theory*, vol. 21, pp. 4–14, Jan. 1975.

[99] B. J. Skinner, F. M. Ingels, and J. P. Donohoe, "Stationary and cyclostationary random process models," *Proc. IEEE SOUTHEASTCON* (Miami, Florida), pp. 450–454, Apr 10 - 13, 1994.

[100] F. G. Tricomi, *Integral Equations.* Interscience Publishers, 1965.

[101] A. J. Jerri, *Introduction to Integral Equations with Applications.* Marcel Dekker, 1985.

[102] J. A. Cochran, *The Analysis of Linear Integral Equations.* McGraw-Hill, 1972.

[103] D. Middleton, *An Introduction to Statistical Communication Theory.* IEEE Press, 1996.

[104] J. W. B. Davenport and W. L. Root, *An Introduction to the Theory of Random Signals and Noise.* IEEE Press, 1987.

[105] D. C. Youla, "The use of the method of maximum likelihood in estimating continuous-modulated intelligence which has been corrupted by noise," *IRE Trans. Inform. Theory*, vol. PGIT-3, pp. 90–105, Mar. 1954.

[106] M. Abdulrahman and D. D. Falconer, "Cyclostationary crosstalk suppression by decision feedback equalization on digital subscriber loops," *IEEE J. Select. Areas Communications*, vol. 10, pp. 640–649, Apr. 1992.

[107] R. N. McDonough and A. D. Whalen, *Detection of Signals in Noise, 2nd ed.* Academic Press, 1995. Chapter 6.

[108] L. L. Scharf, *Statistical Signal Processing: Detection, Estimation, and Time Series Analysis.* Addison-Wesley, 1991.

[109] L. E. Franks, "Polyperiodic linear filtering," in *Cyclostationarity in Communications and Signal Processing* (W. A. Gardner, ed.), pp. 240–266, IEEE Press, 1994.

[110] J. V. DiFranco and W. L. Rubin, *Radar Detection.* Prentice-Hall, 1968.

[111] H. Urkowitz, "Filters for detection of small radar signals in clutter," *J. Appl. Physics*, vol. 24, pp. 1024–1031, Aug. 1953.

[112] S. Verdu, "Optimum multiuser asymptotic efficiency," *IEEE Trans. Communications*, vol. 34, pp. 890–897, Sept. 1986.

[113] E. E. Newhall, S. U. H. Qureshi, and C. F. Simone, "A technique for finding approximate inverse systems and its application to equalization," *IEEE Trans. Communications*, vol. 19, pp. 1116–1127, Dec. 1971.

[114] E. A. Geraniotis and M. B. Pursley, "Error probability for direct-sequence spread-spectrum multi-access communications – part ii: Approximations," *IEEE Trans. Communications*, vol. 30, pp. 985–995, May 1982.

[115] R. Kohno, R. Meidan, and L. B. Milstein, "Spread spectrum access methods for wireless communications," *IEEE Communications Magazine*, vol. 33, pp. 58–67, Jan. 1995.

[116] A. Papoulis, *Probability, Random Variables, and Stochastic Processes.* McGraw-Hill, 3rd ed., 1991.

[117] K. S. Shanmugan and P. Balaban, "A modified monte-carlo simulation technique for the evaluation of error rate in digital communication systems," *IEEE Trans. Communications*, vol. 28, pp. 1916–1924, Nov. 1980.

[118] M. L. Honig and D. G. Messerschmitt, *Adaptive Filters: Structures, Algorithms, and Applications.* Kluwer Academic Publishers, 1984.

[119] S. Haykin, *Adaptive Filter Theory.* Prentice-Hall, 3rd ed., 1996.

[120] L. B. Milstein and *et al.*, "On the feasibility of a CDMA overlay for personal communications networks," *IEEE J. Select. Areas Communications*, vol. 10, pp. 655–668, May 1992.

[121] J. Wang and L. B. Milstein, "CDMA overlay situations for microcellular mobile communications," *IEEE Trans. Communications*, vol. 43, pp. 603–614, Feb/Mar/Apr 1995.

[122] N. J. Bershad, "Error probabilities for DS spread spectrum systems using an ALE for narrowband interference rejection," *IEEE Trans. Communications*, vol. 36, pp. 586–595, May 1988.

[123] H. Leib, M. Eizenman, S. Pasupathy, and J. Krolik, "Adaptive lattice filter for multiple sinusoids in white noise," *IEEE Trans. Acoustics, Speech and Signal Processing*, vol. 35, pp. 1015–1023, July 1987.

[124] J. W. Ketchum and J. G. Proakis, "Adaptive algorithms for estimating and suppressing narrow-band interference in PN spread-spectrum systems," *IEEE Trans. Communications*, vol. 30, pp. 913–924, May 1982.

[125] L. B. Milstein, "Interference rejection techniques in spread spectrum communications," *Proc. of IEEE*, vol. 76, pp. 657–671, June 1988.

[126] W. K. Nicholson, *Elementary Linear Algebra with Applications*. PWS-KENT, 1986.

[127] J. G. Proakis and D. G. Manolakis, *Digital Signal Processing*. Macmillan Publi. Co., 2nd ed., 1992.

[128] S. Haykin, *Communication Systems*. John Wiley & Sons, 2nd ed., 1983.

[129] L. Devroye, *Non-Uniform Random Univariate Generation*. Springer-Verlag, 1986.